Assessing Byproduct Mining and Metal Recycling as Indicators of Material Criticality

by

Xinkai Fu

B.S. Physics, Nanjing University (2014)

Submitted to the Department of Materials Science and Engineering
in Partial Fulfillment of the Requirements for the Degree of

Doctor of Philosophy
at the
MASSACHUSETTS INSTITUTE OF TECHNOLOGY

~~February 2020~~ [September 2019]

Signature redacted

Signature of Author:_____
Department of Materials Science and Engineering
August 30, 2019

Signature redacted

Certified by:_____
Elsa A. Olivetti
Atlantic Richfield Associate Professor of Energy Studies
Thesis Supervisor

Signature redacted

Accepted by:_____
Donald R. Sadoway
John F. Elliott Professor of Materials Chemistry
Chair, Departmental Committee on Graduate Students

Assessing Byproduct Mining and Metal Recycling as Indicators of Material Criticality

by

Xinkai Fu

Submitted to the Department of Materials Science and Engineering
On August 30, 2019 in Partial Fulfillment of the Requirements
for the Degree of Doctor of Philosophy in Materials Science

ABSTRACT

The development of advanced technologies relies on using a broader suite of elements from the periodic table, and many agree that the future availability of a set of 'critical materials' is an issue of global concern. However, assessments of material criticality are often overly general, leading to excessive concerns by policy makers and market participants. A quantitative and detailed investigation for supply risk indicators is necessary to further understand the risk associated with specific materials. This thesis investigates two aspects related to material criticality: 1) the status of a metal being produced as a byproduct; 2) The market impact of increased metal recycling.

To identify the type of major risks associated with a byproduct metal, a techno-economic analysis is performed on 42 carrier-byproduct metal pairs, by employing cluster analysis and econometric modelling. Contrary to conventional view, it is found in several case studies that the availability of a byproduct metal is not directly limited by carrier supply, but rather limited by the lack of incentive to improve recovery efficiencies. Therefore, developing alternative extraction processes with high recovery rate is proposed as a mitigation strategy for byproduct metals. The economic feasibility of such processes is examined, first in a screening assessment and then in a detailed case study for extracting indium as byproduct of zinc. It is demonstrated that an alternative process could significantly increase byproduct supply, by up to 10% in the case of indium.

A bottom-up copper market simulation system is developed by modeling the behaviors of market participants, to estimate the market impact of increased metal recycling. Results from the simulation demonstrates the existence of various rebound effects for primary copper production. Depending on the size and duration of secondary supply shocks, these rebound effects can offset 50% to 90% of the environmental benefits of recycling. In terms of carrier recycling impacting byproduct supply, it is shown that recycling as carrier metal supply risk mitigation strategy would not significantly hurt the availability of byproduct metal.

Thesis Supervisor: Elsa A. Olivetti
Title: Atlantic Richfield Associate Professor of Energy Studies

Acknowledgement

I wish to express my deepest gratitude to my advisor Professor Elsa Olivetti at the beginning of this thesis. Five years ago, you led me into an exciting research area that I, a clueless new college grad, had never heard of. I could not imagine how I would have spent these five years without your unwavering support, both academically and mentally. Thank you for the countless hours you spent on guiding and motivating me, without which this thesis would not be possible. You are more than the best advisor I could ever ask for.

I would like to extend my thanks to Professor Donald Sadoway and Professor Antoine Allanore, the other two members of my thesis committee. They have provided critical and insightful feedback along the way, which helped me greatly improve this thesis. In particular, discussions with Professor Allanore on metal extraction processes have enabled the development of Chapter 4 of this thesis. Although not listed as a committee member, Dr. Richard Roth played an important role in the completion of this thesis. His profound knowledge and deep insights of the copper industry have helped me refine the copper market simulation model introduced in Chapter 5.

Many other individuals have helped with the development of this thesis. In the limited space here, I would like to thank Dr. Randolph Kirchain, Dr. Frank Field, Dr. Omar Swei, Dr. Jingshu Zhang, and Karan Bhuwalka from the Materials Systems Laboratory at MIT; And Dr. Stian Ueland, Dr. Jiyoun Chang, Dr. Jonathan Krones, John Ryter, Adriano Polli and Nagisa Tadjfar from the Olivetti Group. Many of my friends both from and out of MIT have provided me tremendous mental support, particularly my lab mates in the Olivetti Group and friends from the MIT Chinese Entrepreneurs Association. I would also like to thank Kathrine Simons and Terra Cholfin for providing logistical support during my years as a PhD student. Also, this thesis is impossible without the financial support from the National Science Foundation.

I am forever indebted to my parents. Without their support, I couldn't have pursued studies in a foreign country in the first place. Their encouragement and understanding have also given me courage and motivation at moments of frustration.

Last but not least, not a single word can express my feelings for my life partner, my 'bwado', Yidan. Meeting you was the best thing that happened to me in my time at MIT, and I could not imagine what life would be without you. Thank you for all the time you stood by me, and for all the joy you brought to my life. The completion of this thesis marked an important chapter in my life, and I dedicate it to you. I can't wait to open a new life chapter together with you.

Table of Contents

Abstract 3

Acknowledgement 4

List of Figures 7

List of Tables 10

Chapter 1: Introduction 12

- Increasing use of materials and availability concerns 12
  - Long term concerns 14
  - Short term concerns 15
- Supply risk mitigation strategies 17
  - Primary supply strategies 17
  - Secondary supply strategies 18
  - Demand side strategies 20
- Thesis overview 20

Chapter 2: Literature Review 23

- A brief overview of material criticality 23
- Material criticality and byproduct metals 27
- Risk mitigation, recycling and displacement 28
- Research gaps and thesis contributions 31

Chapter 3: Quantifying Availability Risk for By-Product Metals from Primary Production 32

- Classification of Carrier-Byproduct Systems 32
  - Methodology 32
  - Data analysis and results 37
- Developing criticality indicators 39
  - Price elasticity of supply 39
  - Supply potential 43
  - Case study on the zinc-indium system 43
  - Case study on the copper-selenium system 47
  - Case study on the zinc/coal-germanium system 51
  - Using supply potential as a screening tool 54
- Conclusions 55

Chapter 4: Feasibility of Alternative Extraction Process, Case Study on Indium 56

Motivation for alternative process 56
Screening assessment for economic feasibility 57
Case study on indium 60
Description of alternative extraction process 64
Cost model for alternative process 68
Deposit level analysis 73
Conclusions 76
Chapter 5: Displacement Potential and Market Impact of Metal Recycling, Case Study on Copper 78
Background and Motivation 78
Methodology for displacement estimation 79
Introduction of framework 79
Primary supply module 81
Scrap supply module 100
Demand module 108
Refinery module 112
Semis module 118
Price formation module 124
System evolution 136
Results from baseline scenario 139
Prices 139
Production and consumption 142
Estimating displacement 145
Sensitivity of displacement rate to baseline system parameters 152
Impact on byproducts 156
Impact on cobalt 156
Impact on selenium and tellurium 160
Conclusion 164
Chapter 6: Concluding Remarks 167
Conclusions and contributions 167
Limitations and future work 169
References 170
Appendices 185

List of Figures

Figure 1. 1 The growth of elements required in computer chips in the two decades from 1980 to 2000, reproduced from (U.S. National Research Council, 2008) 13
Figure 1. 2 Inflation adjusted metal prices (2017 constant USD/t) for copper, lead, zinc (left figure), aluminum, nickel and tin (right figure) during 1900 to 2015 15
Figure 1. 3 Common byproducts of major metals including tin, aluminum, zinc, lead, copper, platinum and nickel (adapted from (Hagelüken & Meskers, 2010)) 17
Figure 1. 4 Estimates for global average EOL-RR for 60 elements. Reproduced from (Reck and Graedel, 2012) 19
Figure 1. 5 Visualization of thesis structure (Chapter 3 to Chapter 5) 21

Figure 2. 1 The 'criticality matrix' for 13 metals, reproduced from (U.S. National Research Council, 2008) 24

Figure 3. 1 Flowchart of methods for classification and econometric assessment 33
Figure 3. 2 Classification results of carrier-byproduct pairs. Each big shaded ellipse represents a different cluster, and each small ellipse reflects the uncertainty with respect to byproduct fraction and value ratio of each pair. Size of the circles represents 2015 production size of the byproduct metal. The byproduct metals marked in green are important metals for the energy industry. 38
Figure 3. 3 Flowchart for the econometric assessment 40
Figure 3. 4 Illustration of supply shifter in supply and demand model 42
Figure 3. 5 Times series of indium supply (SIn), indium price (PIn) and upper/lower limit of supply potential from zinc ($SPZn, u/l$). Values of supply and supply potential are in metric tonnes (left axis) and values of prices are in USD/kg (right axis). 45
Figure 3. 6 Value of metal content in ore for 71 deposits, in dollars per ton. Ore grade data is primarily based on Werner et al. (Werner et al., 2017). Data from two other studies for the Huari Huari deposit (Ishihara, Murakami, & Marquez-Zavalia, 2011), the Dulong deposit and the Dachang deposit (Ishihara, Murakami, & Li, 2011) are also used. 46
Figure 3. 7 Times series of selenium supply (SSe), selenium price (PSe) and supply potential from copper ($SPCu$). Values of supply and supply potential are in metric tonnes (left axis) and values of prices are in USD/kg (right axis). 50
Figure 3. 8 Times series of selenium supply (SGe), selenium price (PGe) and supply potential from coal ($SPCoal$) and zinc ($SPZn$). Values of supply and supply potential are in metric tonnes (left axis) and values of prices are in USD/kg (right axis). All values are shown in logarithmic scales. 52
Figure 3. 9 Comparison of actual byproduct metal supply ($Sbyproduct$) represented by green curves and supply potential from carrier ($SPcarrier$) represented by shaded regions, for 6 byproduct metal (9 carrier-byproduct pairs) in the intermediate-byproduct clusters. (a) Lead-bismuth and tungsten-bismuth; (b) Copper-rhenium; (c) Copper-tellurium; (d) Copper-molybdenum; (e) Niobium-tantalum and tin-tantalum; (f) Nickel-cobalt and Copper-cobalt. 54

Figure 4. 1 Violin plot of the distribution of economic feasibility indicators, for six byproduct metals. Y-axis is represented in logarithmic scales..... 59
Figure 4. 2 Simplified flowchart of current indium extraction process as byproduct from zinc production. Yellow boxes are used for materials, blue box for processing steps and green boxes for processing facilities 61
Figure 4. 3 Kellogg diagram of the Zn-S-O and the In-S-O systems, at constant temperature 1300K. Zinc phase are separated by black solid lines and indium phases by dashed blue lines. The red dashed line represents the relationship $PSO2 + PO2 = 0.21\ atm.$ 63
Figure 4. 4 Simplified flowchart of alternative indium extraction process. Yellow boxes are used for materials, blue box for processing steps and green boxes for processing facilities..... 65
Figure 4. 5 Standard Gibbs free energy of reaction for the direct carbothermic reduction reaction: MS + CaO +C = M + CaS + CO. Reaction at 900K is highlighted with a red dashed line..... 67
Figure 4. 6 Total cash margin and fraction of revenue from indium under the proposed alternative process, for 69 indium deposits from Werner et al. (Werner et al., 2017) 74

Figure 5. 1 Framework of the simulation system. Semis = semi-finished products 80
Figure 5. 2 (a) Simulated cash flow and (b) Mining production in Maya's mine life 92
Figure 5. 3 Sensitivity of mine life IRR to long term copper price forecast. The blue dashed line represents the 15% cutoff..... 93
Figure 5. 4 Historical mining production and future simulated production..... 96
Figure 5. 5 Historical copper cathode price (black line) and future price scenarios, in 2017 constant USD/t 97
Figure 5. 6 Historical average ore grade (black solid line) and simulated future ore grade under five price scenarios shown in Figure 5.5..... 98
Figure 5. 7 Historical copper mining production (black solid line) and simulated future mining production under five price scenarios shown in Figure 5.5. 99
Figure 5. 8 Structure of the global copper flow model reproduced from (Glöser et al., 2013) 101
Figure 5. 9 Historical old scrap supply by waste type, calculated based on Equations 5.12 to 5.15 104
Figure 5. 10 Historical total scrap supply and consumption 107
Figure 5. 11 Historical copper mining production and demand, and future simulated values under five price scenarios shown in Figure 5.5..... 112
Figure 5. 12 World refinery capacity and production from 1992 to 2016 from SNL (S&P Global Market Intelligence, 2019b) 113
Figure 5. 13 Historical cathode production and consumption data..... 120
Figure 5. 14 World copper inventory from ICSG and its seasonal decomposition..... 126
Figure 5. 15 Simplified old scrap supply chain structure. Small yards are highlighted because it is believed to be the bottleneck for old scrap supply..... 130
Figure 5. 16 Historical prices of copper cathode, Barley and Birch..... 132
Figure 5. 17 Historical spread calculated as difference between nominal value and consumer buying price, for four grades of alloyed scrap..... 135
Figure 5. 18 Historical and simulated copper cathode price in 2017 constant USD/t 140
Figure 5. 19 Historical and simulated annual TCRC price in 2017 constant USD/t..... 141
Figure 5. 20 Historical and simulated Birch spread in 2017 constant USD/t..... 142
Figure 5. 21 Historical and simulated copper mining production and consumption in kt 143

Figure 5. 22 Historical and simulated copper cathode production and consumption in kt 143
Figure 5. 23 Historical and simulated copper scrap supply and consumption in kt 144
Figure 5. 24 Simulated direct melt scrap consumption breakdown in kt 145
Figure 5. 25 Displacement rate under different duration of marginal shocks 147
Figure 5. 26 Displacement rate under different size of shocks 149
Figure 5. 27 Cathode price evolution under different size of temporary shocks (2019 only) 149
Figure 5. 28 Mining production reduction from the baseline, for different size of temporary shocks (2019 only) 150
Figure 5. 29 Mining production reduction from the baseline, for different size of permanent shocks (2019 only) 151
Figure 5. 30 Sensitivity of displacement rate to MPE 153
Figure 5. 31 Sensitivity of displacement rate to SREs 154
Figure 5. 32 Sensitivity of displacement rate to DEs 155
Figure 5. 33 Sensitivity of displacement rate to SSDE 155
Figure 5. 34 Modeled cobalt mining production between 2015 and 2030 by primary metals, reproduced from (Beatty et al., 2019) 157
Figure 5. 35 Cobalt mining production reduction from the baseline, under four different scenarios described in Figure 5.29 159
Figure 5. 36 Copper cathode price evolution under different size of permanent shocks 160
Figure 5. 37 Primary copper refined production reduction from the baseline, for different size of permanent shocks 161
Figure 5. 38 Selenium production and supply potential history and future scenarios 163
Figure 5. 39 Tellurium production and supply potential history and future scenarios 163

List of Tables

Table 2. 1 Country-level supply risk indicators used in 25 criticality studies between 2006 and 2018, and their frequencies of use. Studies prior to 2011 are based on (Achzet & Helbig, 2013) 25

Table 3. 1 Metrics for assigning uncertainty scores to value ratios of carrier-byproduct pairs 36
Table 3. 2 ARDL model results for zinc-indium case study 44
Table 3. 3 Summary of key statistics of 71 indium deposits. Ore grade data is primarily based on Werner et al. (Werner et al., 2017) 47
Table 3. 4 ARDL model results for copper-selenium case study 48
Table 3. 5 OLS model results for zinc/coal-germanium case study 51
Table 3. 6 Summary of supply elasticities for three case studies 53

Table 4. 1 Sources and methods for obtaining/calculating distribution of metal concentration in ore, for six byproduct metals 58
Table 4. 2 Melting point and boiling point of metal elements in the sphalerite. Cells highlighted in light yellow color indicate metals that melts at 900K, the proposed reaction temperature. 67
Table 4. 3 Description of variables used in Equation 4.4 to 4.7 70
Table 4. 4 Sensitivity analysis results on the amount of indium (kt) in economically feasible deposits 75

Table 5. 1 Description and values of operating characteristics for a hypothetical mine 82
Table 5. 2 Summary statistics for regression in Equation 5.11 89
Table 5. 3 Sensitivity of mine closure related mine properties to long term copper price forecasts 93
Table 5. 4 Variables and parameters used in the scrap supply module, their symbols, timeframe and sources of data 101
Table 5. 5 Technical recycling efficiency and collection rate by waste type 103
Table 5. 6 Demand volume indicators for each end-use sector and respective data sources 108
Table 5. 7 Mean and standard deviation of intercepts and elasticities estimated from Bayesian regression models 110
Table 5. 8 Projection methods for demand volume indicators for each end-use sector 111
Table 5. 9 Data used in the refinery module, time frame and data sources 114
Table 5. 10 Summary statistics for regression in Equation 5.24 115
Table 5. 11 Summary statistics for regression in Equation 5.25 115
Table 5. 12 Summary statistics for regression in Equation 5.26 116
Table 5. 13 Semis classified based on ICA classification, by fabricator and alloyed/unalloyed 118
Table 5. 14 Description of variables used in the blending optimization model 123
Table 5. 15 Summary statistics for regression in Equation 5.40 126
Table 5. 16 Summary statistics for regression in Equation 5.41 129
Table 5. 17 Summary statistics for regression in Equation 5.45 133
Table 5. 18 Summary statistics for regression in Equation 5.46 133
Table 5. 19 Summary statistics for regression in Equation 5.47 135
Table 5. 20 Description of all variables and functions used in the evolution of the system 138

Table 5. 21 Opportunity for increase in old scrap supply by waste type 148
Table 5. 22 Comparison of cumulative scrap supply increase, cumulative mining production reduction and displacement rate at 2040 for shocks with different durations and sizes..... 151
Table 5. 23 Comparison of cumulative scrap supply increase, cumulative mining production/primary refined production reduction and displacement rate at 2040 for permanent shocks with different sizes 162
Table 5. 24 Example system parameters and their respective direct impacts on the system if the initial values are higher than baseline 165

Chapter 1: Introduction

Acknowledgement: Portions of this chapter are based on 1) A 2017 publication by Fu et al. in Journal of Industrial Ecology, titled *High-Resolution Insight into Materials Criticality: Quantifying Risk for By-Product Metals from Primary Production* (Fu, Polli, & Olivetti, 2018); 2) A work by Fu et al. submitted to Environmental Science and Techonology in 2019, titled *Supply Perspectives on Cobalt in the Face of Changing Demand* (Fu et al., 2019)

Given advanced technologies dependence on a broad suite of materials, we must develop measures to quantify the supply risk associated with that reliance, so that robust strategies can be developed to mitigate that risk.

Increasing use of materials and availability concerns

The development of human civilization is marked by increasingly sophisticated metals use. Copper is the first metal to be discovered and has been used in human societies since 9000 BC (Copper Development Association, 2019b). It is one of the few metals that occur in its native metallic form in nature, making it possible to be worked into other shapes without being smelted. Copper smelting and alloying innovation marked the end of the *Stone Age* and the beginning of *Bronze Age* around 3300 BC (Von Erdberg, 1993). The Bronze Age was followed by the *Iron Age* around 1200 BC, during which tools and weapons made with iron and steel outperformed their bronze counterparts (Milisauskas, 2002). In addition to copper and iron, there are five other *metals of* antiquity that have been discovered and widely used by humans in prehistoric times, including lead, tin, mercury, silver and gold (Smith & Forbes, 1957). These were the only seven elemental metals found until the discovery of arsenic in the 13th century (Smith & Forbes, 1957).

The 19th and 20th centuries brought an explosion of metal development and use. Metals have become indispensable components in engineering applications, such as automobiles, electrical appliances, and building construction (Gramatyka, Nowosielski, & Sakiewicz, 2007; Kapur & Graedel, 2006; Shinjoh, 2006). To meet increased demand due to population growth, industrialization and urbanization, the extraction of metal minerals increased nearly 19-fold from 1900 to 2005 (Krausmann et al., 2009). This increase has been driven by the need for not only larger quantities of the same materials, but **also the need for a larger fraction of metal elements in the periodic table** (T. E. Graedel & Cao, 2010). For example, based on a report from the U.S. National Research Council ((U.S. National Research Council, 2008), see Figure 1.1), the growth of computer chip technology has led to a dramatic increase in the number of elements needed in the two decades from 1980 to 2000 from 12 elements to 60 two decades later.

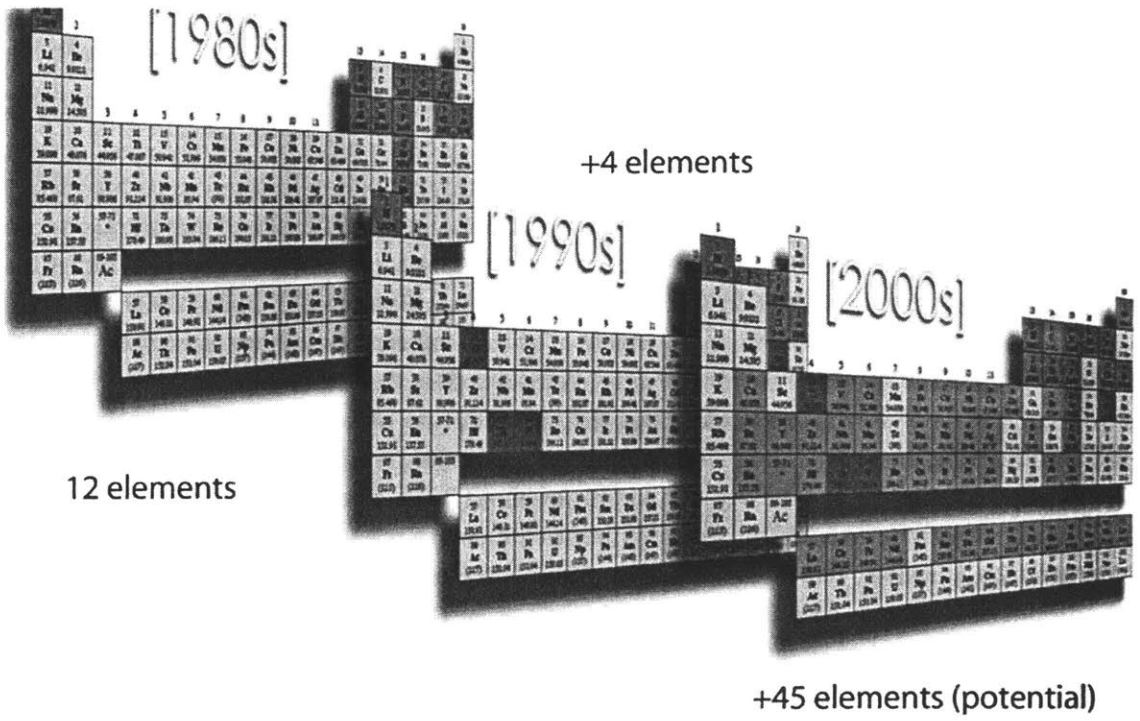

Figure 1. 1 The growth of elements required in computer chips in the two decades from 1980 to 2000, reproduced from (U.S. National Research Council, 2008)

Due to the fast growth of metal demand in terms of both quantity required and the variety of elements required, there has been an increasing attention to resource availability in the last two decades. Governments, resource economists, geologists, manufacturers, and other metal market participants have raised concerns about whether future metal supply would meet expectations for demand (Duclos, Otto, & Konitzer, 2010; Prior, Giurco, Mudd, Mason, & Behrisch, 2012; U.S. National Research Council, 2008; Yaksic & Tilton, 2009). Factors contributing to these availability concerns have been systematically studied in the field of *material criticality*, which will be reviewed in detail in Chapter 2. However, frequently these studies are overly general leading to unnecessary hype and overreaction by actors in the system. Instead assessing materials availability requires nuanced appreciation of supply chain dynamics and meticulous treatment of technology opportunities and social actors in the system. This thesis aims to provide a reasoned approach to understanding two aspects of materials availability: whether a metal is mined as a byproduct of a more major metal, and what are the market impacts of increased recycling activities. One important illustration of the need for more nuanced treatment of availability is that these concerns have temporal dimension, and they could either be long-term concerns or short-term concerns. Long-term concerns are about the ultimate depletion of metals from the earth's crust if more is needed than available. The remaining metal resources would be that currently circulating in the anthrosphere, such as metals recovered from end-of-life sources.

Long term concerns

Researchers and geologists have used the *static depletion index* to quantify how fast the mineral resources of a metal might be depleted in the future. This index is often calculated as the ratio between reserves and the current annual primary production. For many metals, this index is calculated to be less than 50 years (Alonso, 2010), indicating that metal reserves might be depleted fairly soon if current production trend continues. However, this metric is limited because reserves are a function of economics, rather than an absolute geologic constraint: based on the definition from U.S. Geological Survey (USGS), reserve is *'that portion of an identified resource from which a usable mineral or energy commodity can be economically and legally extracted at the time of determination.'* (U.S. Geological Survey, 1980) Therefore, changes in metal prices and extraction costs, and the identification of new resources can significantly change the amount of reserves estimated. For example, the estimated world copper reserve is 340 million tonnes (Mt) in 1998, leading to a static depletion index of about 30 years at a primary production rate of 11.4 Mt/y (U.S. Geological Survey, 2000). This number might create the perception that copper reserve will run out by 2028. However, two decades later in 2018, while production rate almost doubles to 21.0 Mt/y, the amount of reserve is now 830 Mt (U.S. Geological Survey, 2019c), and the static depletion is increased to 40 years instead of linearly decreasing to 10 years. While primary production did speed up due to rise in copper consumption, the increase of reserve offsets that perceived scarcity, possibly through one or more of the factors below: 1) more copper enters reserve due to rise in copper price; 2) more copper enters reserve due to decrease in extraction costs; or 3) discovery of new resources due to rise in demand. Therefore, those who believe in the long-term effectiveness of the market would probably wonder: should we ever fear the depletion of metals, since the market will act in our favor to alleviate scarcity?

While the future of resource depletion and metal scarcity remains uncertain, one finds some indication from historic trends. The extraction of metals has been accompanied by a decline of the metal content in ore, or ore grade decline. Ore grade decline has been viewed as one possible indicator for metal scarcity (Northey, Mohr, Mudd, Weng, & Giurco, 2014). Deposits that are rich in metals, or richer parts of the deposits usually get extracted first because of the potential for better profits, therefore the remaining deposits have lesser quality. From a long-term perspective, the ore grade of many metals have been consistently declining, including lead, zinc (Mudd, Jowitt, & Werner, 2017), copper (Northey et al., 2014), gold (Mudd, 2007), platinum group metals (Mudd, 2012) and uranium (Mudd, 2014). Ore grade decline can translate directly into an increase in mining cost per unit of metal extracted. On an industry level, a consistent rise in mining cost means that less metal can be extracted at the same margin. This would cause supply to be in deficit and drive price to rise. In Figure 1.2, the historical prices for six base metals are shown between 1900 to 2015. All prices are inflation adjusted and shown in 2017 constant United States Dollars per tonne (USD/t). None of the six metals has shown trends of linear price growth in the last century, even though ore grades have declined by a factor of 3-4, based on the literature above. This indicates that the extraction cost must have decreased over time, which offsets the decrease in ore grade. This is most apparent for the price of aluminum, whose current price is only 10% of its 1900 level. In fact, when aluminum was first produced, its price exceeded even gold (Venetski, 1969). It was only after the development of a large scale production method by French engineer, Paul Heroult, American engineer, Charles Martin Hall, and Austrian chemist, Carl Joseph Bayer (Drozdov, 2007) that the price of aluminum dropped and become widely used.

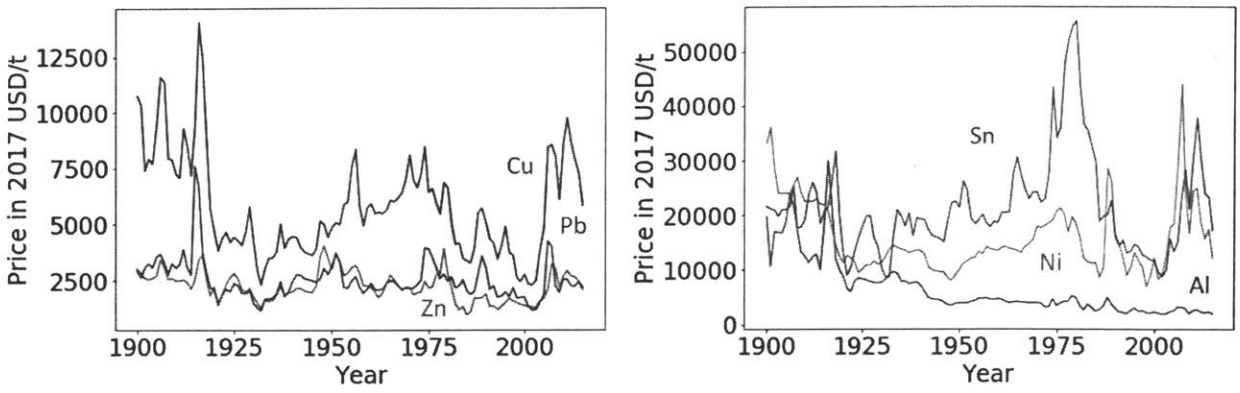

Figure 1. 2 Inflation adjusted metal prices (2017 constant USD/t) for copper, lead, zinc (left figure), aluminum, nickel and tin (right figure) during 1900 to 2015.

Given the above observations of metal prices, it seems that these metals have not become more scarce with increasing production. In the long-term, if the market perceives the scarcity of a metal, it should be followed by a rise in the metal's price, which further causes a cascade of results including, 1) metal suppliers to extract and produce more of that metal; 2) more efficient and cost saving extraction methods to be developed; 3) more resources to be discovered, identified and deposits being explored; and 4) consumers of the metal use more substitute materials. All these results will act contrary to the rise in price, and bring supply and demand to a new balance. If the market is efficient enough in the long term, demand should not exceed supply for a very long period, as suppliers and consumers will find ways to increase supply or decrease demand. The result is that the possible metal depletion indicated by a depletion index will be at least delayed, if not completely avoided.

Short term concerns

Compared to the long-term concern for metal depletion, short term concerns over lack of supply might be more critical and immediate. These concerns can originate either from the demand side or the supply side. On the demand side, significant increase in metal consumption, or the expectation for future metal consumption, can cause supply deficit in the short term. For example, demand for cobalt in electric vehicles is expected to grow exponentially after 2020, causing the availability of cobalt to be questioned towards 2030 (Fu et al., 2019). A consequence of this significant demand increase is the jump in its price: cobalt metal price on the London Metal Exchange (LME) has grown from 22000 USD/t in the mid-2016 to 94000 USD/t in the beginning of 2018 ("London Metal Exchange: LME Cobalt," n.d.). While demand can increase fairly quickly once a material demanding new technology is adopted, increase in primary metal production can be very slow, often taking 10 years or more. In order for a deposit to turn into an operating mine, owner of the deposit has to carefully assess the technical, economic, environmental and regulatory feasibilities, and the whole process can take years (Fu et al., 2019). This is followed by mine construction, which will take another one to five years depending on the metal and the deposit (S&P Global Market Intelligence, 2019b). The consequence of this slow response is that growth in metal production cannot catch up with growth in consumption, and the perceived scarcity leads to speculative behaviors that cause

high metal price, delaying technology adoption. Another risk on the demand side is the lack of substitutability. On a corporate level, substitutability can be described semi-quantitatively by substitute performance, substitute availability, price ratio and environmental impact ratio (T. E. Graedel et al., 2012). If price a metal has jumped up and substitutability of that metal is bad in the short term, its consumers either have to rely on it and pay the high price, or switch to a cheaper option by sacrificing performance.

On the supply side, there are also quite a few factors that can cause a metal to be conceived as critical or risky. Among the many factors that have been discussed in literature, country-level production concentration and governance risk are the most frequently used indicator of supply risk (M. Frenzel, Kullik, Reuter, & Gutzmer, 2017). Highly concentrated supply in countries with poor governance is an indicator that consumer countries with high import reliance might not be able to obtain stable metal supply. Another critical supply-side risk factor is the byproduct status of many metals, the focus on this research. For many metals, their values in ore are so small that they cannot be economically extracted on their own. Rather, these metals are mined and produced together with other metals that have relatively higher values in ore, so the supply of these byproducts is contingent on the dynamics of their carrier materials. Such contingencies have been viewed as significant sources of supply risk in many criticality studies (M. Frenzel et al., 2017). The hypothesis for byproduct metals' supply being riskier is as follows. For metals that are mostly mined as primary products, their production can respond to changes in demand and price, although possibly with long delays mentioned above; For the production of a byproduct metal, however, it will only follow the production of its carrier metal rather than the demand of the byproduct. This is because the value of a byproduct in ore is usually very small compared to the carrier metal, so the miner will not likely increase its production just due to price increase of the byproduct. The byproduct status also has other implications on a metal: a group of researchers (Max Frenzel, Ketris, & Gutzmer, 2014; Max Frenzel, Ketris, Seifert, & Gutzmer, 2016; Max Frenzel, Tolosana-Delgado, & Gutzmer, 2015) argued that the maximum potential production, or supply potential of a byproduct, is limited by the production of the carrier; Redlinger and Eggert found that the prices of common byproduct metals have typically been more volatile than metals that are produced as primary products (Redlinger & Eggert, 2016).

Some common examples of byproduct connections are shown in Figure 1.3, which includes many key metals in low-carbon technologies. For example, cobalt is used for electric vehicles, cadmium, indium, gallium, tellurium and selenium for thin-film solar cells, germanium for electric grids and transmissions, and REEs for wind energy (Buchholz & Brandenburg, 2018). If these technologies became widely adapted, it means that growing demand will meet with less supply, creating gaps to clean energy application manufacturers and potentially impacting the transition to a low-carbon future.

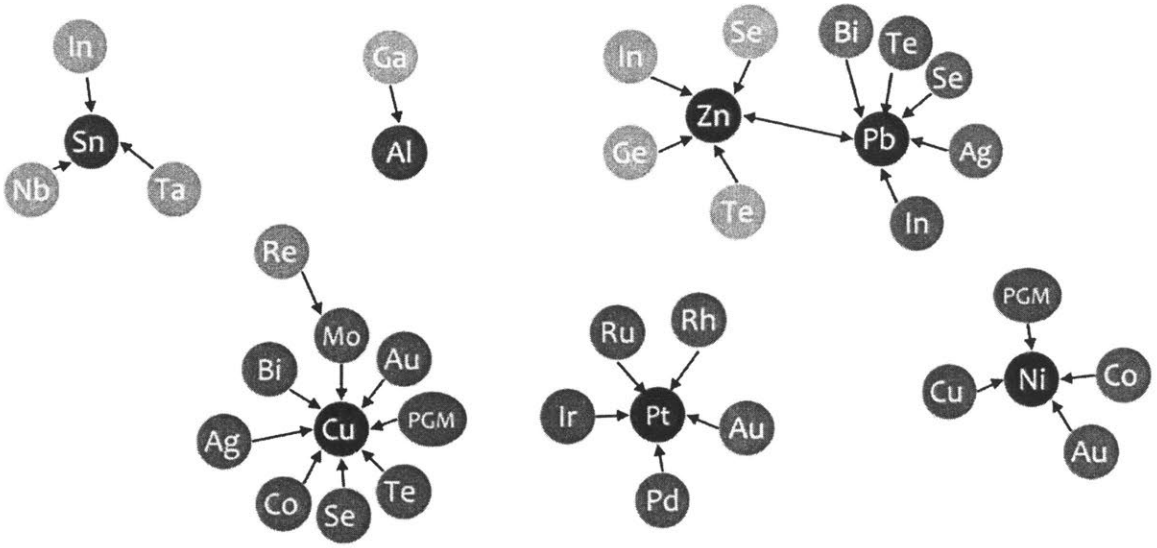

Figure 1. 3 Common byproducts of major metals including tin, aluminum, zinc, lead, copper, platinum and nickel (adapted from (Hagelüken & Meskers, 2010))

In this thesis I hypothesize that all byproduct metals are not created equal. The relationship of a pair of carrier-byproduct metals is unique, as the mineral containing both metals, the extraction process, the market and end-use applications are different for each metal. For example, while indium is extracted almost entirely as byproduct of zinc, cobalt can be produced as byproduct of copper, nickel, PGMs and also as a primary commodity. Therefore, it is the primary goal of this thesis to understand the detailed implications of the byproduct status on the supply risk of a metal. With this more detailed understanding, strategies to address availability can be better prioritized and motivated. On one hand, it is necessary to systematically understand the carrier-byproduct relationship for carrier-byproduct metal pairs with different characteristics; On the other hand, it is also crucial to investigate approaches to mitigate supply risks, if such risks do exist for byproduct metals. In what follows, a few common supply risk mitigation strategies are discussed.

Supply risk mitigation strategies

Approaches to mitigate metal supply risk can be classified into three categories, depending on the target of the approach: 1) those that aim to increase the primary supply of the metal; 2) those that aim to increase the secondary supply of the metal; and 3) those that aim to reduce the demand of the metal.

Primary supply strategies

On the primary supply side, several approaches can increase the amount of metal supplied to the market. For metal processors such as miners, smelters and refineries, short term approaches can be taken to temporarily increase metal production, without adding new capacity or using new extraction processes. For example, short run production can be raised by either raising the capacity utilization rate, or increasing the recovery efficiency. However, the marginal cost of producing one more unit of metal is usually an

increasing function with production beyond some threshold (Baumol & Blinder, 2015), so these short run improvements are usually done only when metal prices are high enough.

In order to improve metal supply in the long run, more metal in deposits must be made economically available, through 1) the identification of new resources and/or 2) more identified resources being turned into reserves. As an example of 1), cobalt is currently only being extracted from terrestrial deposits and the identified total world terrestrial cobalt resources are 15 Mt in 2008 (U.S. Geological Survey, 2009). A decade later, while identified terrestrial cobalt resources grow to 25 Mt (U.S. Geological Survey, 2019b), another 120 Mt of cobalt resources have been identified on the sea floors of the Atlantic, Indian, and Pacific Oceans. If these deep sea resources can be made economically viable under cost-effective seabed mining technologies, concerns over the availability of cobalt should be greatly alleviated. As for 2), improvement in extraction technologies may enable more resources to be considered as reserves. For example, the solvent extraction and electrowinning (SX-EW) process for copper production has been widely applied globally since 1960, due to its cost advantage for low grade oxide ores compared to the conventional pyrometallurgical process (International Copper Study Group, 2019b). The share of SX-EW in global copper mining production has grown from 0 in 1960 to about 20% in 2017 (International Copper Study Group, 2019b). Without the SX-EW process, the treatment of some low grade oxide ores would be difficult and probably uneconomical, and it is reasonable to assume that cumulative world copper mining production during the last five decades would be less than that of the current. More recently, a molten electrolysis method has been proposed to extract copper from sulfide minerals (Sahu, Chmielowiec, & Allanore, 2017). These method is cost-effective as well as environmentally friendly, eliminating toxic byproducts such as sulfur dioxide produced in a conventional pyrometallurgical process. If stricter environmental regulations on sulfur oxide emissions are carried out, some deposits might be uneconomical under that pyrometallurgical process due to high environmental cost, while the alternative process could avoid that issue.

The improvement of extraction technology is particularly important for metals extracted as byproducts, as the overall recovery rate for many byproduct metals are very low. These recovery rates are low because metal extraction processes are usually optimized for the primary metals to increase the profit for metal processors, while the recovery of byproduct metals are less critical from an economical sense. For example, for primary copper refineries that extract selenium and tellurium from copper anode slimes in the electrolytic copper refining process, the extraction efficiency for selenium and tellurium can be as low as 30%, while recovery efficiency for copper is usually greater than 99% (Jensen, 1985). The recovery efficiency of extracting germanium as byproduct of coal and indium as byproduct of zinc are also estimated to be less than 30% (Max Frenzel et al., 2014; Lokanc, Eggert, & Redlinger, 2015). If these current extraction processes can be improved, supply of many byproduct metals can be improved not only in the short run due to recovery rate increase, but also in the long run because more amount of these byproducts can be extracted economically. In this thesis I examine the economic feasibility of such improvements, first in a general screening assessment and then in a detailed case study for indium.

Secondary supply strategies

Increasing secondary metal supply, or supply from metal recycling, is one of the most widely discussed supply risk mitigation strategies. The critical role of secondary supply has been well recognized for many metals with important industrial applications, as metals from recycling provides a buffer to mitigate the imbalance between demand and primary supply (Reck & Graedel, 2012). Besides providing additional

supply, metal recycling is also generally much more energy-efficient and environmentally-friendly than mining (Robert U. Ayres, 1997; Reck & Graedel, 2012; Worrell & Reuter, 2014). For example, it is estimated that production of austenitic stainless steel from scrap would cut energy use by 67% and CO2 emission by 70% compared to virgin-based production (J. Johnson, Reck, Wang, & Graedel, 2008).

For many metals, recycling still presents significant challenges despite its many benefits. The end-of-life recycling rate (EOL-RR) is currently quite low for many metals. A study of the EOL-RR for 60 elements (T. E. Graedel et al., 2011a) shows that the commonly-used base metals such as iron, copper, zinc and aluminum are recycled in large quantities and fraction (EOL-RR > 50%) because of the scale of their economic values. Precious metals like gold and silver are also recycled at high rates due to their high unit values. However, over half of the elements have an EOL-RR lower than 1%, most of them being minor metals that are utilized by emerging technologies (See Figure 1.4). Many common byproduct metals fall in this category, such as gallium, germanium, selenium, tellurium and indium. The main reason for their low recycling rates is that modern technologies usually require extensive mixing of elements to enhance performance for products, and this has created challenges for separation technology (Reck & Graedel, 2012). While increasing the recycling rates for byproduct metals would directly increase their availability, it is not explored as a mitigation strategy in this thesis. The intention of this thesis is to explore some significant but indirect consequences of recycling.

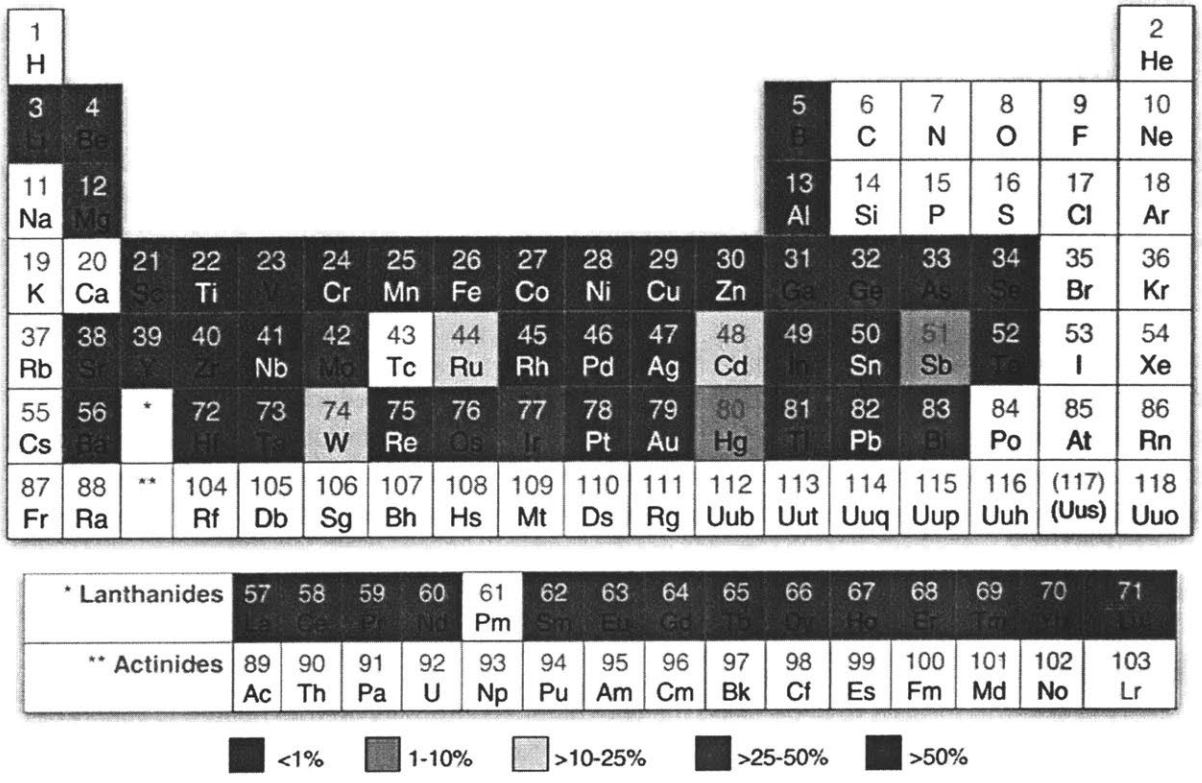

Figure 1. 4 Estimates for global average EOL-RR for 60 elements. Reproduced from (Reck and Graedel, 2012)

In addition to the low recycling rate, challenges for metal recycling also exist from a market perspective. The energy and environmental benefits of recycling can only be realized if the increase in secondary supply leads to reduced extraction of virgin ores. The proportion of primary material production prevented by recycling was termed the *displacement rate* in previous studies (Zink, Geyer, & Startz, 2016, 2018). If displacement rate of a metal is low, the environmental benefits from recycling can be undermined. The logic of displacement is as follows: when recycling activities increase and more metal scraps become available to the market, prices of metal scraps should decrease. More intermediate metal consumers and end consumers, such as smelters, refineries and manufacturers would then substitute metal scraps for metal and intermediate materials made from primary production. As the consumption for primary materials decreases, prices of those materials would drop, and primary producers such as miners would eventually reduce production because of lower profit level.

Due to the interconnection between the supply of a carrier metal and its byproduct, recycling activities for the carrier metal have been hypothesized to cause changes in the byproduct metal's own cycle. Many byproduct metals only accompany the primary production of their carriers but not the secondary production: For example, while tellurium and selenium can be extracted from anode slimes during the primary electrolytic refining of copper anode, the refining of copper scrap does not lead to these two byproducts being recovered. This is because tellurium and selenium are considered impurities in the primary production process and are separated from copper during primary production. End-use of copper cathode in final products require little or no impurities, so recovering copper from final products are usually not accompanied by byproduct production. This observation has important implications to the availability of byproduct metals: while increase in recycling for the carrier metal alleviates its supply risk, the potential to produce byproduct metals might be negatively impacted, if primary production of the carrier is reduced due to increased recycling. Therefore, it is crucial to managing the trade-off between two metal systems in the context of the carrier-byproduct relationship. An analytical tool is built in this thesis to quantitatively understand the impact of carrier recycling on its own primary production, and the impact on its byproduct.

Demand side strategies

Demand side strategies aim to mitigate material availability risk by reducing material demand in manufacturing and use. Just to name a few, some common strategies include material substitution, product lifetime extension, product re-use, dematerialization and so on. These strategies are outside the scope. While these are also important mitigation strategies, they are not explicitly explored in this thesis. The focus of this thesis is on the supply side.

Thesis overview

The primary goal of this thesis is to understand the two materials criticality metrics related to supply risk: 1) the status of a metal produced as a byproduct; 2) the market impact of increased metal recycling. The structure of this thesis (Chapter 3 to Chapter 5) is visualized in Figure 1.5.

Figure 1. 5 Visualization of thesis structure (Chapter 3 to Chapter 5)

A literature review on material criticality studies is provided in Chapter 2, which provides motivation for why these the above two metrics should be investigated in this thesis. For the first metric, byproduct metal status, the following research question is posed:

For which cases and under what contexts will the byproduct status be a significant criticality indicator?

An attempt is made to answer this question, which will be presented in the third chapter of the thesis. In Chapter 3, a classification of carrier-byproduct metal systems is performed, based on the distinct market characteristics and dynamics of each pair. Results from this classification allows me to identify groups of byproduct metals with high criticality status. In addition, two criticality indicators specific to byproduct metals are developed in this chapter, including price elasticity of supply and supply potential. These two indicators are applied to three carrier-byproduct metal systems to provide high-resolution analysis to the

supply risks of the byproduct metals. Furthermore, supply potential is also used as a screening tool to investigate the risk status of byproduct metal systems with intermediate criticality concerns.

Following the risk diagnosis in Chapter 3, the next two chapters further investigate the impact of two specific mitigation strategies. This part aims to answer the second research question posed in this thesis:

What are the impacts of supply risk mitigation strategies on the availability of metals?

Chapter 4 will examine the impact of developing alternative extraction processes to mitigate supply risk specifically for byproduct metals. Such processes are motivated by the results of Chapter 3, where it is found that low recovery efficiency has limited the supply for a few byproduct metals. Therefore, it is the goal of Chapter 4 to investigate whether alternative extraction processes could improve these low recovery rates in economically feasible manners. A screening assessment for economic feasibility is first performed on byproduct metals of copper and zinc, which allows indium to be identified as the metal of interest. In this chapter, an extraction process is developed specifically for indium, which is shown to be thermodynamically feasible. A cost model is further developed for the process, and applied to global indium containing deposits. This application provides mine-level insights to the concept of economic feasibility.

Metal recycling is the supply risk mitigation strategy studied in Chapter 5. As a specific aspect, this chapter aims to quantify the primary production market impact of increased recycling activities. A bottom-up copper market simulation model is developed to provide an estimate for how much copper primary production is offset by increased copper recycling. This is then linked to the subsequent influence on the availability of byproduct of copper, namely selenium, tellurium and cobalt. To mimic the market dynamics in reality, the supply and demand of major copper related commodities are modeled in detail based on historical data and industry expert opinions. A particular effort is spent on modeling the formation of prices, which in turn drives producers and consumers' decision making.

Chapter 2: Literature Review

Acknowledgement: Portions of this chapter are based on a 2017 publication by Fu et al. in Journal of Industrial Ecology, titled *High-Resolution Insight into Materials Criticality: Quantifying Risk for By-Product Metals from Primary Production* (Fu et al., 2018)

The first chapter provided an overview to the thesis, the goal of which was to provide more thorough understanding on two aspects of material criticality: the status of a metal produced as a byproduct, and the market impacts of increased recycling activities. In this chapter, I review literature related to these topics and present the research gaps that motivate the development of this thesis. An overview of general materials criticality studies is presented, from which I find that byproduct dependency and metal recyclability are the two criticality indicators that require more quantitative attention. Following this observation, studies investigating specific byproduct metals and challenges in metal recycling are reviewed in detail, which provide further motivation for specific focuses on the two criticality indicators.

It is worth mentioning that only studies that provide overall motivation to this thesis are reviewed in this chapter. Other studies that provide data and specific backgrounds for case studies, or insights to methodologies are reviewed in each topic chapter following Chapter 2.

A brief overview of material criticality

The growing demand for many elements in terms of both quantity and variety has brought concerns over the availability of raw materials. This has motivated research focus on *material criticality*, which aims to identify metals that have significant *importance* to the sustainable development of human society and metals whose future *availability* might be in doubt. The first widely accepted publication that defines material criticality is a 2008 report titled *Minerals, Critical Minerals and the U.S. economy* written by the United States National Research Council (US NRC) (U.S. National Research Council, 2008). In this report, US NRC defined the criticality of minerals as a function of two variables: a variable that embodies the idea of *importance* in use and represents the impact of supply restriction; Another variable that embodies the idea of *availability* and represents the supply risk. Such a two variable determination can be visually represented by a two-dimensional 'criticality matrix', shown in Figure 2.1. According to this framework, metals located at the upper right corner of the figure have the highest level of criticality, while metals located at the lower left corner are less critical.

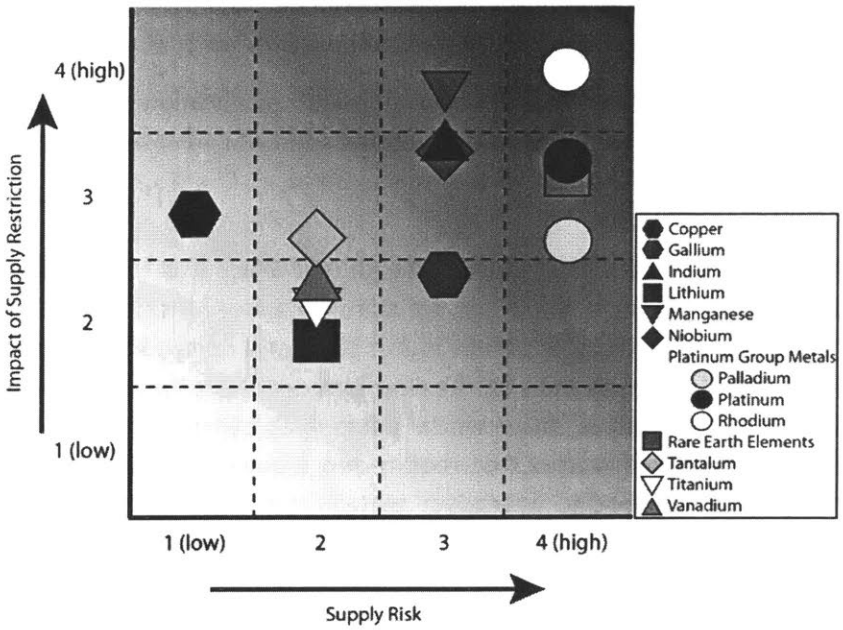

Figure 2. 1 The 'criticality matrix' for 13 metals, reproduced from (U.S. National Research Council, 2008)

Following US NRC's research in 2008, a number of criticality studies have been carried out by manufacturing companies (Duclos et al., 2010), government agencies (Bauer et al., 2010, 2011; British Geological Survey, 2011; British Geological Survey, 2012; British Geological Survey, 2015), research institutes (Glöser, Tercero Espinoza, Gandenberger, & Faulstich, 2015; T. E. Graedel et al., 2012; T. E. Graedel, Harper, Nassar, Nuss, & Reck, 2015) and international organizations (Arrobas, Hund, Mccormick, Ningthoujam, & Drexhage, 2017; European Commission, 2014). While the geological focus, time horizon, material focus, and assessment dimensions vary across these studies, all considered supply risk to be an important component for material criticality. In addition, most of these investigations considered the economic importance of materials, although the specific indicators used varies. These two aspects are analogous to the two variables of US NRC's criticality matrix, *availability risk* and *important of use*. The studies by Graedel et al. (T. E. Graedel et al., 2012) also introduced a third variable for environmental concerns.

There are some key differences across supply indicators across the studies mentioned above. In a 2013 review paper (Achzet & Helbig, 2013), Achzet and Helbig reviewed the differences of supply risk evaluation in 15 criticality assessments published between 2006 and 2011. They found that among the many supply risk indicators used, country level production concentration represented by Herfindahl-Hirschman index (HHI) is the most frequently used, followed by country governance, depletion time, and by-product dependency. Below I expand this analysis, by including ten more studies published between 2011 to 2018. The results of this analysis is shown in Table 2.1. Only indicators included in at least two criticality studies are presented.

Table 2. 1 Country-level supply risk indicators used in 25 criticality studies between 2006 and 2018, and their frequencies of use. Studies prior to 2011 are based on (Achzet & Helbig, 2013)

Study	Supply risk indicators												
	Country concentration of production	Country governance	Depletion time	Byproduct dependency	Recyclability	Demand growth	Substitutability	Company concentration in mining corporations	Import reliance	Country concentration of reserve/ reserve base	Abundance in earth's crust	Volatility of commodity prices	Temporary scarcity
(Frondel et al., 2007)	√	√							√				
(Behrendt et al., 2007)	√		√					√				√	
(U.S. National Research Council, 2008)			√	√	√				√				
(Morley & Eatherley, 2008)	√	√	√										
(Duclos et al., 2010)	√	√		√		√	√				√	√	
(Angerer et al., 2009)						√							
(Rosenau-Tornow, Buchholz, Riemann, & Wagner, 2009)	√	√	√					√					
(Buchert, Schüler, & Bleher, 2009)	√		√	√									√
(Reller, 2009)	√	√	√			√	√	√					
(European Commission, 2010; European Commission, 2014)	√	√			√		√						
(Thomason et al., 2010)									√				
(Bauer et al., 2010, 2011)	√	√	√	√	√	√		√					
(Moss, Tzimas, Kara, Willis, & Kooroshy, 2011; Moss et al., 2013)	√	√		√		√							
(Erdmann, Behrendt, & Feil, 2011)	√	√	√	√	√			√					√
(British Geological Survey, 2011)	√	√								√	√		
(British Geological Survey, 2012)	√	√			√		√			√	√		
(British Geological Survey, 2015)	√	√		√	√		√			√			
(T. E. Graedel et al., 2012)	√	√	√	√									
(Hatayama & Tahara, 2015)	√		√						√	√			
(National Science and Technology Council, 2016)	√	√											
(European Commission, 2017)	√	√			√		√		√				

(Fortier et al., 2016)	√	√		√					√				
Total counts	22	19	11	11	9	7	7	6	6	4	3	2	2

The top five supply risk indicators used in these 25 studies are country level concentration of production, country governance, depletion time, byproduct dependency and recyclability. It is worth briefly reviewing how these indicators are quantified in these criticality studies:

1. **Country level concentration of production.** In most studies, this was quantified either using HHI, or the production fraction of the top one to three producing countries. HHI is a commonly accepted measure of market concentration, and it is calculated by summing the of squares of each competing entity's percentage share. The idea behind using HHI as a supply risk indicator is that, if the production of a metal is concentrated in just one or a few countries, then all the other net-importing countries have to rely only on the supply of those few countries. If supply disruption events such as export restrictions are carried out in these producing countries, then only domestic metal consumers will still have access to that metal supply, while all other foreign consumers will be affected. A high supply concentration can be found for many minor metals, such as indium, germanium, niobium and most of the rare earth elements, just to name a few (N. T. Nassar, Graedel, & Harper, 2015).

2. **Country governance.** A high country-level concentration can be further exacerbated if the major producing countries are geopolitically unstable. This metric can be quantified by using composite indices published by international organizations, such as the Worldwide Governance Indicators developed by the World Bank (D. Kaufmann, Kraay, & Mastruzzi, 2011) and the Human Development Index developed by the United Nations Environment Programme ("Human Development Reports," 2019). In most studies, these indices were then averaged for top producing countries to obtain the risk indicator for a material. Taking cobalt as an example, close to 60% of 2018 cobalt mining production is concentrated in the Democratic Republic of Congo (DRC), and the HHI was around 4000 in 2018 (Fu et al., 2019). According to the World Governance Indicators, DRC has consistently ranked in the lowest 10 percentile among all countries it investigates, in terms of political stability, government effectiveness, rule of law and control of corruption. The geopolitical risk associated with DRC had significant impacts on the cobalt market: In the late 1970s, an invasion of the copper-cobalt mining region in the former Zaire was a major reason for the 'cobalt crisis' that led to a five-time price increase from 1977 to 1979 (T. D. Kelly & Matos, 2015). The first and the second Congo War also led to substantial volatility in the cobalt market in the mid-1990s.

3. **Byproduct dependency.** In the 11 studies that include byproduct dependency as criticality indicator, 4 of them quantified it by the byproduct fraction, i.e., the fraction of a material produced as a byproduct in its global total production (British Geological Survey, 2015; Erdmann et al., 2011; T. E. Graedel et al., 2012; U.S. National Research Council, 2008). However, in the rest 7 studies either a score was assigned qualitatively, or the exact measure for byproduct dependency was unclear.

4. **Recyclability.** In the 9 studies that include recyclability as criticality indicator, four studies used end-of-life recycling input rate (EOL RIR) (European Commission, 2010; European Commission,

2014; European Commission, 2017; U.S. National Research Council, 2008), three studies used end-of-life recycling rate (EOL RR) (British Geological Survey, 2011; British Geological Survey, 2012; British Geological Survey, 2015), and the rest two studies only described recyclability qualitatively. While EOL RIR and EOL RR sounded a lot alike, these two rates are measured by very different material flows as denominators: EOL RIR is the ratio between old scrap recovered and total consumption of a material, while EOL RR is the ratio between old scrap recovered and old scrap generated. For example, in a study that estimated recycling indicators for copper, it was estimated that the global EOL RR for copper is higher than two times of its EOL RIR between 2000 to 2010 (Glöser, Soulier, & Tercero Espinoza, 2013).

Based on the investigation of supply risk indicators above, I can conclude the following: while the material criticality field has widely recognized the role of byproduct dependency and material recyclability as important criticality indicators, the understanding of these two indicators is not quantitative enough, and also lacks consistency across studies, in the case of recyclability. These are major research gaps and important motivation for the development of this thesis.

Material criticality and byproduct metals

While most studies that included byproduct dependency in lacks quantitative detail for this indicator, even those that did use quantitative indicators (such as byproduct fraction) still missed important aspects. Although the use of this indicator to date has provided a useful screening tool, two essential aspects specific to the byproduct metal problem were understated. First, the use of byproduct fraction overlooks the fact that the carrier-byproduct dynamics are based on one-to-one (or many-to-one) connections. For example, while gallium and germanium are both extracted almost 100% as byproduct of other materials, around 98% of gallium produced is byproduct of aluminum (bauxite) and germanium is associated with both zinc (60% of germanium production) and coal (40% of germanium production) (U.S. Geological Survey, 2019d; U.S. Geological Survey, 2019e). The upper limit of gallium supply, which only depends on bauxite production, is clearly different in nature from the case of germanium. Secondly, the use of this indicator has thus far neglected the economic aspect of byproduct metals. Metals are produced as byproducts not because the physics prohibits them from being produced as primary products, but rather that the cost of doing so cannot be covered by the value of those metals alone (there may also be legislative or environmental considerations that influence the economics). Moreover, whether that cost can be covered is also driven by the geology of the ore deposits, which determines the metal concentrations in an ore. These two limitations call for the development of other byproduct specific criticality indicators, in order to provide high-resolution insights into byproduct metal systems so that we might more effectively understand and mitigate any limited availability.

These methodologies to determine material criticality are typically applied to a wide range of elements in the periodic table, and other non-elemental raw materials. Following the identification of a set of critical materials, there is another set of literature that focuses on specific critical materials. These studies provide deeper analysis of the supply and demand for these critical materials, and identify mitigation strategies to reduce supply risk. Many such studies have been carried out for a variety of byproduct metals, which often focus on the stocks and flows of metal elements in the anthroposphere. To quantify physical flows of metals in their entire life cycles, diagnostic tools such as material flow analysis (MFA) have been employed in the assessment of a wide variety of byproduct metals. Løvik et al. (Løvik, Restrepo, & Müller,

2016) investigated the carrier-byproduct metal linkage for the case of aluminum-gallium, and projected gallium supply potential as function of aluminum production scenarios. Licht et al. (Licht, Peiró, & Villalba, 2015) quantified the stocks and flows of gallium, germanium and indium and illustrated significant potential for improvement in extraction processes and recovery rates. Nakajima et al. (Nakajima, Yokoyama, Nakano, & Nagasaka, 2007) provided a substance flow analysis (SFA) for indium used for flat panel displays in Japan, while Yoshimura et al. (Yoshimura, Daigo, & Matsuno, 2013) expanded the SFA for indium to a global level. For byproduct metals of copper, two studies (Kavlak & Graedel, 2013a, 2013b) focusing on tellurium and selenium were performed and published consecutively by two authors. Bustamante and Gaustad (Bustamante & Gaustad, 2014) investigated the copper-tellurium linkage in detail and showed the impacts from several mitigation strategies. There were also studies in which a group of byproduct metals are assessed for specific applications, such as for wind power generation (Nedal T. Nassar, Wilburn, & Goonan, 2016), for light-emitting diodes (Wilburn, 2012) and for solar cells (Blewais, 2010; Nedal T. Nassar et al., 2016) These studies argued that the supply of certain byproduct metals might be inadequate under rapid development of these technologies, and suggested increase in recycling rate, improvement in primary production recovery and material substitution as important mitigation strategies.

Aspects related to the price of byproduct metals have also been discussed in various studies, in which researchers found that byproduct metal prices are volatile in general. For example, the high volatility of indium, cadmium, selenium and tellurium have been noted in several studies (Green, 2006; Naumov & Grinberg, 2009). Redlinger and Eggert (Redlinger & Eggert, 2016) made a more general argument that the price volatility of byproduct metals has been typically higher than that of common carrier metals. Fizaine and Florian further discussed the high price volatility from a theoretical perspective, and used statistical tests to assess the long term equilibrium between the markets of a carrier metal and a byproduct (Fizaine, 2013). One point they argued is that the byproduct content in carrier metal minerals is usually so small that the value of the extracted byproduct metals is negligible compared to their carrier metals. Therefore, mining companies will not increase production capacity just to extract more byproduct content even when prices of certain byproduct metals are higher. Based on these authors, the supply of byproduct metals should be relatively inelastic to its price, which may lead to high price volatility.

These byproduct metal specific studies presented above can be linked through their markets: stocks and flows of a metal are ultimately determined by the evolution of its supply and demand, which are in one part driven by price of the metal, and in another part driven by the supply and demand of its carrier metal. Therefore, a successful candidate for the byproduct specific criticality indicator should reflect the supply and demand dynamics of the byproduct, and its linkage with the carrier metal.

Risk mitigation, recycling and displacement

Various supply risk mitigation strategies have been developed and discussed in literature. Many studies focused on strategies to reduce material demand. For example, developing material substitution options is a useful approach, which has been shown to be beneficial from both the resource supply (T. E Graedel, 2002) and the environmental impact (J. C. Kelly, Sullivan, Burnham, & Elgowainy, 2015) perspectives. These substitution options are usually developed at the manufacturer's level, where multiple materials options can be designed for a certain product. During periods when the metal originally used was in supply deficit, the substitute material with price and availability advantages could be used instead of the original metal. This would cause a temporary demand decrease of the original metal, which could further help

supply and demand to equilibrate. Another set of approaches aim to reduce materials demand through increasing material efficiency, including product lifetime extension, remanufacturing, component re-use and dematerialization (Allwood, Ashby, Gutowski, & Worrell, 2011). The extension of product lifetime has been studied for products such as electronic products (Nes, Cramer, & Stevels, 1999), mobile phones (Wilhelm, 2012) and automobiles (Kagawa, Tasaki, & Moriguchi, 2006). The extension of product lifetime could help reduce the demand of that product because consumers of the product can use it for longer period of time, therefore demanding less new products. Remanufacturing, component re-use and dematerialization on the other hand, take place at the manufacturers. The hope of these strategies is to use less new material or just less material in the manufacturing stage, therefore reducing overall material demand.

The importance of recycling as a supply risk mitigation strategy has been thoroughly discussed in many criticality studies. Metal recyclability is an important supply risk indicator, because increased recycling of a metal could bring additional metal supply to the market. The European Commission's 2010 *Critical Raw Materials for the EU* Report (European Commission, 2010) claimed that 'The higher the import dependence on an individual metal, then the more important recycling becomes, especially if the possibilities for material substitution and savings in manufacturing are limited.' Two other supply risk mitigation strategies were mentioned here, namely substitution and dematerialization in manufacturing. While these two strategies may require product redesign that are long and expensive (K. J. Huang, Li, & Olivetti, 2018), improvements in recycling can be achieved through policy interventions. For example, the report mentioned above (European Commission, 2010) recommended 'preventing illegal exports of end-of-life (EOL) products containing critical raw materials' and 'mobilizing EOL products with critical raw materials for proper collection' as two policy actions to make recycling more efficient. The 2017 version of this report (European Commission, 2017), further argued that the role of recycling is particularly important for consumer countries, as the availability from EOL products does not have to rely on producing countries.

The challenges of metal recycling have been reviewed by Graedel and Reck (Reck & Graedel, 2012) in a 2012 article. Some of these are technological challenges. For example, recycling efficiency is limited by the thermodynamics in the processing stage. Several Japanese studies have analyzed the ability to remove impurity elements in the metallurgical processing of base metals (Hiraki et al., 2011; Nakajima, Takeda, Miki, Matsubae, & Nagasaka, 2011; Nakajima et al., 2010). Results have shown that impurity elements may end up in the recovered metal in gas, slag or metal phase, depending on several parameters including the Gibbs free energy of the impurity reaction, the activity coefficient of the oxidation product, etc. If impurity elements remain in the metal phase, removal will be difficult. This problem is a big challenge for aluminum recycling, as most impurity elements occur as troublesome tramp elements (Nakajima et al., 2010). Optimization of recycling processes and redesigning scrap types and alloy compositions are possible solutions to the increase recyclability of aluminum (Gaustad, Li, & Kirchain, 2007; Olivetti, Gaustad, Field, & Kirchain, 2011). On the other hand, many challenges in metal recycling are related to social behavior and economics in nature. The greatest potential to improve metal recycling lies in collection rate (T. E. Graedel et al., 2011a), which is especially important for metals identified to be critical in the above mentioned criticality studies. These metals are usually used in small quantities for products high mixed with a variety of elements. The low collection rate of these metals is mostly an issue of behavioral habits (Reck & Graedel, 2012), which can be improved through education on recycling and policy incentives. From the economical perspective, the value of metals in end-of-life products is the main driver for recycling (Dahmus & Gutowski, 2007). However, recent trends show that metal prices are highly volatile (Naumov & Grinberg, 2009), and price volatility transmits between primary metal and secondary

metal markets (Xiarchos & Fletcher, 2009). This can cause troubles for collectors and processors of metal scrap, as their revenue is closely tied to metal scrap prices.

There is also another broader challenge in the recycling system, which is not directly related to recycling rate. As mentioned in Chapter 1, the energy and environmental benefits of recycling can only be realized if the increase in recycling leads to significant reduction of primary production. Understanding and estimating secondary production displacement of primary production is crucial for correctly accounting the benefits from recycling. It has been recognized in several studies that displacement might not take place on a one-to-one basis (Ekvall, 2000; Frees, 2007; J. X. Johnson, McMillan, & Keoleian, 2013; McMillan, Skerlos, & Keoleian, 2012; Thomas, 2003; Weidema, 2003). However, it is still often implicitly assumed in life cycle assessments (LCAs) that displacement takes place one-to-one, such as for metals (Atherton, 2007), building materials (Zabalza Bribián, Valero Capilla, & Aranda Usón, 2011), steel (Yellishetty, Mudd, Ranjith, & Tharumarajah, 2011) and battery (Dewulf et al., 2010). A few other studies explicitly assumed 0% or 50% displacement without providing quantitative evidence for why these rates are assumed (Ekvall & Weidema, 2004; Klöpffer, 1996). In order to understand the drivers of displacement and accurately estimate displacement rate, Zink and colleagues have developed a methodology based on partial equilibrium modeling (Zink et al., 2016), and applied the methodology to estimating displacement for aluminum in the U.S. market (Zink et al., 2018). While these two studies were useful attempts towards accurately estimating displacement, their methodology and application suffers from three major drawbacks:

1. On the primary aluminum side, this framework does not differentiate different primary aluminum commodities. Extraction of primary aluminum starts from mining production, where the commodity produced is bauxite; Bauxite is then processed through the Bayer process to produce alumina in smelters; Alumina can then be converted to aluminum metal in the Hall-Heroult process. The market of bauxite, alumina and aluminum metal are independent, and the price of bauxite and alumina are not simply linearly dependent on aluminum metal. Therefore, the use of bauxite production aluminum metal price data created mismatch between different commodities that could bring bias to the estimated coefficients. It is important to differentiate at what production level (mining vs smelting vs refining) the displacement is estimated, as results might vary greatly depending on the level.
2. On the secondary aluminum side, the authors oversimplified the price and supply network of aluminum scrap. While the Institute of Scrap Recycling Industries (ISRI) recognizes more than 40 grades of aluminum scraps, the authors only used a single aluminum scrap price in their study by averaging price five secondary **aluminum alloys**. Again, aluminum alloys are different commodities from aluminum metal. Also, although the authors mention that scrap dealers may hold stockpiles in response to price changes, this aspect is neglected in the model.
3. The methodology is applied to the aluminum market in the U.S., a country which almost entirely depend on import for bauxite consumption. In this case, estimated displacement for primary mining production can be deceptively small. In addition, modern base metal markets are globally connected, and price changes in one country can affect prices all over the world. To accurately estimate the full potential of secondary production displacing primary production, one has to consider a global perspective.

These drawbacks call for the improvement of displacement estimation methodologies. Moreover, accurately estimating displacement allows one to quantify the impact of carrier recycling on its byproduct, which is also not well understood in current literature. Most studies focusing on carrier-byproduct linkages have not investigated impact from carrier recycling; For the studies that attempted to quantify this impact, they made simplistic assumptions without studying displacement in detail. For example,

Bustamante and Gaustad (Bustamante & Gaustad, 2014) attempted investigated tellurium supply sensitivity to secondary copper growth rate, for years up to 2060, but they simply made assumptions on constant recycling growth; Løvik et al. (Løvik et al., 2016) assessed gallium supply potential under two aluminum recycling scenarios, but these aluminum recycling and primary production scenarios are simply based on results from another MFA study (Liu, Bangs, & Müller, 2013).

Research gaps and thesis contributions

Here I summarize major research gaps based on the literature review presented above, and how this thesis has attempted to bridge these gaps.

First, I assert that byproduct dependency, a frequently used supply risk indicator in material criticality studies, is poorly understood and quantified. In this thesis, a byproduct specific criticality assessment is performed based on characteristics essential to byproduct metals, including physical concentration, market value of metals, and extraction technology efficiency. Over 40 carrier-byproduct pairs are analyzed, allowing the identification of five 'high-byproduct' pairs. It is further suggested that price elasticity of supply and supply potential from carrier metal be used as byproduct specific criticality indicators, which may allow one to further identify availability risks associated with byproduct metals. As a complement to other quantitative methods developed for material systems, such as material flow analysis (MFA), an essential techno-economic analysis of byproduct metals problem is provided, by employing cluster analysis and econometric modelling. These approaches provide insight into supply risk mitigation strategies related to extraction efficiency and supply chain structure.

Second, the feasibility of alternative extraction process provides another byproduct specific criticality indicator. Although several studies pointed out the potential to improve recovery rate for byproduct metal extraction, the feasibility of such improvements have not been addressed. Improvement of recovery rate is investigated under the context of alternative extraction processes, and a case study focusing on indium is performed, which assesses the deposit level cost perspectives of an alternative extraction process in detail. I demonstrate that improvement in extraction processes may benefit metal producers, and mitigate byproduct metal supply risk at the same time. Such an assessment provides new insights to supply risk mitigation strategies, and points out future directions for future supply side strategies.

Third, while the important role of displacement for assessing environmental benefits has been recognized in literature, most studies have not quantitatively estimated displacement rate. To estimate displacement, a bottom-up global copper market simulation tool is built to mimic the behavior of major market participants. Production and consumption of different copper commodities (concentrate, cathode and copper scraps) from these participants/agents are modeled as function of copper prices. With more than 100 system parameters corresponding to the decision making of different agents, this high granularity model not only allows the estimation of displacement, but also enables various supply and demand scenarios to be explored. As a case study, the impact of carrier recycling on byproduct supply is estimated with this model. To the best of my knowledge, this is the first time such an impact has been modeled under the consideration of primary and secondary market interaction.

Chapter 3: Quantifying Availability Risk for By-Product Metals from Primary Production

Acknowledgement: Portions of this chapter are based on a 2017 publication by Fu et al. in Journal of Industrial Ecology, titled *High-Resolution Insight into Materials Criticality: Quantifying Risk for By-Product Metals from Primary Production* (Fu et al., 2018)

Classification of Carrier-Byproduct Systems

In order to study the carrier-byproduct relationship systematically, the first step is to classify different carrier-byproduct systems into groups with distinct market characteristics and dynamics. Also, the characteristics/variables used in the classification should address essential aspects of the carrier-byproduct relationship. Several important aspects are currently missing in literature, which have been discussed in Chapter 2. As a recapitulation, there are two major limitations of criticality indicators currently used. The first is that indicators such as byproduct dependency or companionality overlook the fact that the carrier-byproduct dynamic is based on one-to-one (or many-to-one) connection. A 100% byproduct dependency has very different implications for different metals: it could be a byproduct metal that is 100% connected to a single carrier, or it could be a byproduct of five carriers, each accounting for 20% of total production. Supply risk from the latter should be lower because supply of byproduct is more spread out. The second is that current criticality indicators usually do not take into account the market price of metals. Price is a fundamental to the decision making of metal producers, as miners, smelters and refineries seek to maximize profit/return of metal production. Moreover, whether a metal is considered to be the primary product, co-product or byproduct of a project is not just a function of metal contents in ore, but also dependent on price expectations for each product that is produced from the project.

The above two aspects of the carrier-byproduct relationship are critical for understanding the availability of byproduct metals. In what follows, carrier-byproduct systems are classified into groups with distinct market characteristics and dynamics, and a clustering analysis is performed on byproduct-carrier pairs based on metrics of byproduct and value fraction. In this way I present a comprehensive quantitative assessment of materials criticality based on a metal's byproduct status, and provide economic analyses of byproduct behavior, which serve as complements of other quantitative methods, such as MFA.

Methodology

As byproduct status is essentially an interaction between a byproduct and a carrier, this analysis is based on properties related to specific carrier-byproduct pairs, rather than single byproduct metals. The analysis starts with identifying carrier-byproduct pairs and the properties of a pair that is hypothesized to be most relevant to their economic behavior. Based on data availability and quality, the majority of the carrier-byproduct pairs discussed in current literature are included. Rare earth elements (REEs) are excluded, as the main concern with REEs has been geopolitical risk rather than a concern based on byproduct status (Massari & Ruberti, 2013; Nedal T. Nassar, Du, & Graedel, 2015). Platinum group metals (PGMs) are also excluded because they have been investigated in detail previously by others (Alonso, 2010; N. T. Nassar et al., 2015). Other elements have been excluded based on data quality, such as zirconium and hafnium.

I also excluded molybdenum-rhenium because it does not fit into the carrier-byproduct framework[1]. 42 carrier-byproduct pairs are examined, and classified by employing both qualitative assessment of their market behavior and quantitative clustering including an uncertainty analysis. This classification enables the identification of carrier-byproduct pairs where the byproduct's supply may be strongly limited by its status as a byproduct metal (as opposed to other considerations). The steps and methods used in this chapter are presented as a flow chart in Figure 3.1 and the details are described in what follows.

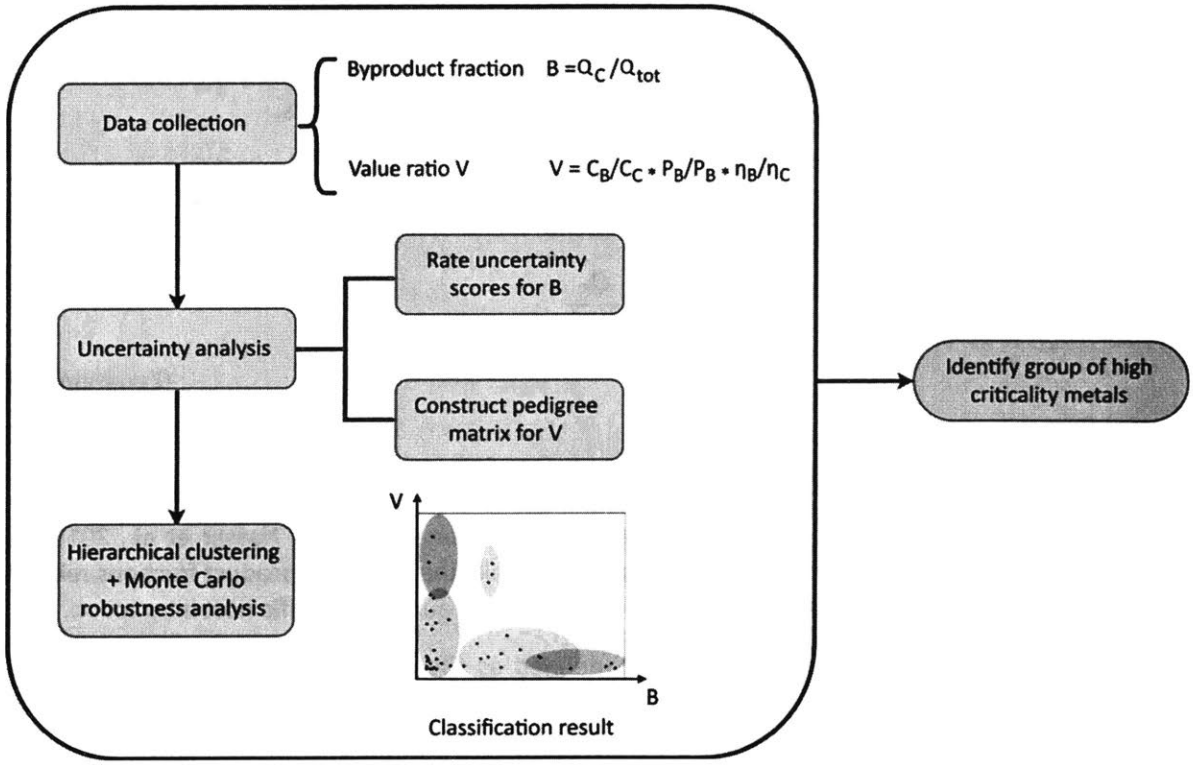

Figure 3. 1 Flowchart of methods for classification and econometric assessment

Market-related indicators for classification

A first step in classifying a carrier-byproduct pair (shown in Figure 3.1) is the quantification of related economic properties. The supply for carrier metals and byproduct metals are connected by the causal relationships between physical processes and market information. On one hand, a carrier metal affects a

[1] From the description in Ullmann's Encyclopedia of Industrial Chemistry (Nadler & Starck, 2012), there are two sources for primary rhenium: The first is copper concentrates, which accounts for 29% of Rhenium production (N. T. Nassar, Graedel, & Harper, 2015) and I have included this copper-Rhenium system in the byproduct classification; The second is from copper-molybdenum porphyry ores, where the sulfides of copper and molybdenum are first separated, and then Rhenium is separated from the MoS_2 concentrates. These copper-molybdenum porphyry ores contain 0.3 – 1.6% and 0.01 – 0.05% molybdenum, and on average the value of copper content is ~10 times higher than the value of molybdenum content, based on 2015 metal price. Therefore, copper is still the actual carrier in the so-called molybdenum-Rhenium system, but Rhenium is extracted from molybdenum production process. This does not fit into my carrier-byroduct pair classification framework, and I have therefore not added another copper-Rhenium system in my byproduct classification.

byproduct metal through a physical connection: the production of a carrier, the percentage of byproduct production associated with that carrier, and the relative concentration of a byproduct with respect to a carrier determine the production of byproduct. On the other hand, a byproduct metal affects the production of its carriers through its monetary value in production: the higher the value of a byproduct with respect to a carrier, the more likely a producer will be driven to extract more mineral due to the value of the byproduct. Therefore, two main characteristics are inferred from these causal relationships: the *byproduct fraction* associated with a carrier, and the *value fraction* of a byproduct compared to a carrier. While I acknowledge the existence of other metal criticality indicators used in previous studies, such as substitution performance (Thomas E. Graedel et al., 2012), recyclability (Buchert et al., 2009) and geographic concentration (N. T. Nassar et al., 2015), I intentionally choose only the above two indicators for classification, because of their direct relevance to carrier-byproduct dynamics.

Byproduct fraction, B, is defined as

$$B = \frac{Q_C}{Q_{tot}}$$

(Equation 3.1)

where Q_C is the production quantity related to a specific carrier and Q_{tot} is its total global production quantity. Previous literature uses a similar concept of 'companionality' (N. T. Nassar et al., 2015) or 'byproduct share' (Redlinger & Eggert, 2016) which are essentially the sum of byproduct fractions related to all possible carriers, but I specifically differentiate carriers to account for specific host interaction.

The second indicator of interest is 'value ratio', V, defined as the global average ratio between the monetary value of a byproduct B and a carrier C in all the mines which produce B as byproduct of C. Value ratio is calculated using the following formula,

$$V = \frac{C_B}{C_C} \times \frac{P_B}{P_C} \times \frac{\eta_B}{\eta_C}$$

(Equation 3.2)

where the three terms on the right hand side correspond to the average ratio between mineral concentration, C , unit price, P, and extraction efficiency, η, respectively. The extraction efficiency used here refers to the overall recovery rate in the metal extraction process. Byproduct and carrier materials are subscripted by B and C, respectively.

Data for byproduct fraction and value ratio are collected from different sources of varying quality, including journal articles, scientific encyclopedias, reports from mining companies, consulting companies and industry associations, government scientific agencies.

Clustering Analysis

A clustering analysis of the 42 carrier-byproduct pairs is performed, based on byproduct fraction and value ratio. The method used is hierarchical clustering based on an average linkage agglomerative clustering algorithm. (Friedman, Hastie, & Tibshirani, 2008)

This algorithm starts with each N observation representing its own cluster. At each subsequent step, the algorithm merges the closest two clusters based on the average dissimilarity between clusters. The average dissimilarity between cluster A and cluster B can be expressed as

$$d_{AB} = \frac{1}{N_A N_B} \times \sum_{i_A \in A} \sum_{i_B \in B} d_{i_A i_B}$$

(Equation 3.3)

where N_A and N_B are the number of observations in cluster A and cluster B, respectively, and

$$d_{ij} = \sqrt{(B_i - B_j)^2 + (V_i - V_j)^2}$$

(Equation 3.4)

is the Euclidean distance between observation i and j. B_i and V_i are the byproduct fraction and the value ratio of observation i respectively. The result of hierarchical clustering at M-th step is N-M clusters where the values of byproduct fraction and value ratio are similar within each cluster.

Uncertainty analysis

As highly disaggregated data is collected from different sources, there are some potential limitations with the reliability and representativeness of data. An attempt is made to address these issues in part with a semi-quantitative uncertainty analysis. The uncertainty analysis is based on approaches used in MFA (Laner, Rechberger, & Astrup, 2014). Because byproduct fraction and value ratio are collected and calculated differently, two different approaches are developed for uncertainty evaluation, based on the concept of uncertainty ratings and pedigree matrix, which are described as follows. Both these approaches reflect the hypothesis that the level of uncertainty is proportionate to the actual estimated value. Using these values of uncertainty, a Monte Carlo simulation is performed with the clustering analysis to test the consistency of the clusters.

For byproduct fraction, data are collected from narratives within industry and government reports where the major sources of uncertainty include variation over time, approximation and linguistic imprecision. Therefore, a semi-quantitative approach id used based on uncertainty ratings. The method is adapted from a multilevel study of the anthropogenic copper cycle by Graedel et al. (T. E. Graedel et al., 2004).

Four different uncertainty levels are assigned to each different carrier-byproduct pair, namely very low (±0), low (±5%), medium (±10%) and high (±20%). It is assumed that byproduct fraction for each pair follows a symmetric triangular distribution where the minimum and maximum are symmetric around the measured value and the range corresponds to the uncertainty level.

For value ratio, the pedigree matrix method is used to assess data quality and uncertainty. The pedigree matrix method is often used in life-cycle assessment studies to quantitatively characterize uncertainty based on a qualitative description (Lloyd & Ries, 2007). It consists of multiple independent data quality indicators which can then be directly transferred into probability distributions (Weidema & Wesnæs, 1996). In this case, four data quality indicators are used to generate the parameters for probability distribution. They are temporal correlation, sample size, data source consistency and reliability of efficiency ratio. Since metal price data are well recorded in various data sources and reports, it is assumed that data uncertainty do not arise from the price ratio term in Equation 3.2.

Each indicator reflects one source of uncertainty with respect to quantities used in calculating value ratio, and uncertainty scores are assigned to the indicators according to Table 3.1, and the resulting scores are shown in Table 3.2. The uncertainty scores are then transferred to uncertainty ranges using the formula below

$$R = R_b \times exp\left(\sqrt{[\ln(U_1)]^2 + [\ln(U_2)]^2 + [\ln(U_3)]^2 + [\ln(U_4)]^2}\right)$$

(Equation 3.5)

where $R_b = 5\%$ is the basic uncertainty factor and U_1 to U_4 are the four uncertainty scores respectively. For example, if all four data quality indicators are assigned the lowest score of 1, then $R = R_b = 5\%$. Similar to byproduct fraction, R is used as the range parameter in symmetric triangular distribution. These parameters of probability distribution are then used in a Monte Carlo simulation to test the robustness of hierarchical clustering. The algorithm of the simulation is described as follows:

1. For each pair, a random value of byproduct fraction and value ratio are generated from a joint symmetric triangular distribution, which parameters are determined from the original measured value and the uncertainty analysis. All the other observations are fixed at their original values;
2. Average linkage agglomerative hierarchical clustering is performed for this new dataset that includes one new observation whose position is changed;
3. Step 1 and 2 are repeated 10,000 times. Clustering results from each time is recorded.

If a pair is within different clusters across the simulations, it means that clustering result is sensitive to changes of its values and this should raise concern on how the carrier-byproduct interaction should be considered in the subsequent analysis. These pairs are represented in Figure 3.2 as the overlap between different clusters.

Table 3. 1 Metrics for assigning uncertainty scores to value ratios of carrier-byproduct pairs

	Uncertainty scores and metrics			
Temporal Correlation	1	1.5		2
	Data source later than 2010	Data source between 2000 to 2010		Data source older than 2000
Sample Size	1	1.5	2	3
	Data collected from >20 mines	Data collected from 5 to 20 mines	Data collected from 1 to 5 mines	Data collected from only 1 mine
Data Source Consistency	1		2	
	If there is only one data source involved in calculation or all data sources agree with each other		If there is inconsistency or disagreement in multiple data sources	
Reliability of Efficiency Ratio	1	1.2		1.5
	If no efficiency ratio is collected and set to a default value of 1	If data source for efficiency ratio is reliable based on subjective judgement		If data source for efficiency ratio is unreliable based on subjective judgement

Data analysis and results

Based on the classification of carrier-byproduct pairs, I identify a cluster of metal pairs that is believed to have high criticality concerns. These metal pairs share similar characteristics of high byproduct fraction and low value ratio. In what follows, the classification results are shown along with the supply elasticity assessments for the zinc-indium, copper-selenium and zinc/coal-germanium systems. An assessment based on supply potential is also presented, for metals systems that are found to be of intermediate criticality concern.

Results from the hierarchical clustering with five clusters are shown in Figure 3.2, where each large shaded ellipse represents a different cluster. The sizes of the outlined circles for each metal pair are proportional to the 2015 production of the byproduct metal (the second element listed for each pair). Byproduct metals most relevant to energy technologies are highlighted in green. It can be observed that bigger circles tend to lie on the left of the x-axis while smaller circles lie on the right. This is an indication that smaller production volumes relate to the degree to which a metal is a byproduct of another carrier metal.

A semi-quantitative uncertainty analysis is also plotted in Figure 3.2, where each small ellipse reflects the uncertainty with respect to byproduct fraction and value ratio of each pair. The overlapping regions

between different clusters represent the cluster consistency from the Monte Carlo simulation. Pairs in these overlapping areas are classified to different clusters in different simulation runs.

Seven pairs are classified in the high-byproduct cluster, including copper-selenium, zinc-cadmium, zinc-indium, aluminium-gallium, copper-tellurium, copper-molybdenum and zinc-germanium. This cluster is characterized by high byproduct fraction (0.6-1) and low value ratio (0-0.1), and the byproduct metals in this cluster have important applications in energy related applications such as photovoltaic (PV) cells, batteries, and thin film coating (Blewais, 2010). The byproduct-carrier pairs within the high-byproduct cluster are similar to qualitative assessments that have identified availability concerns for these elements (N. T. Nassar et al., 2015).

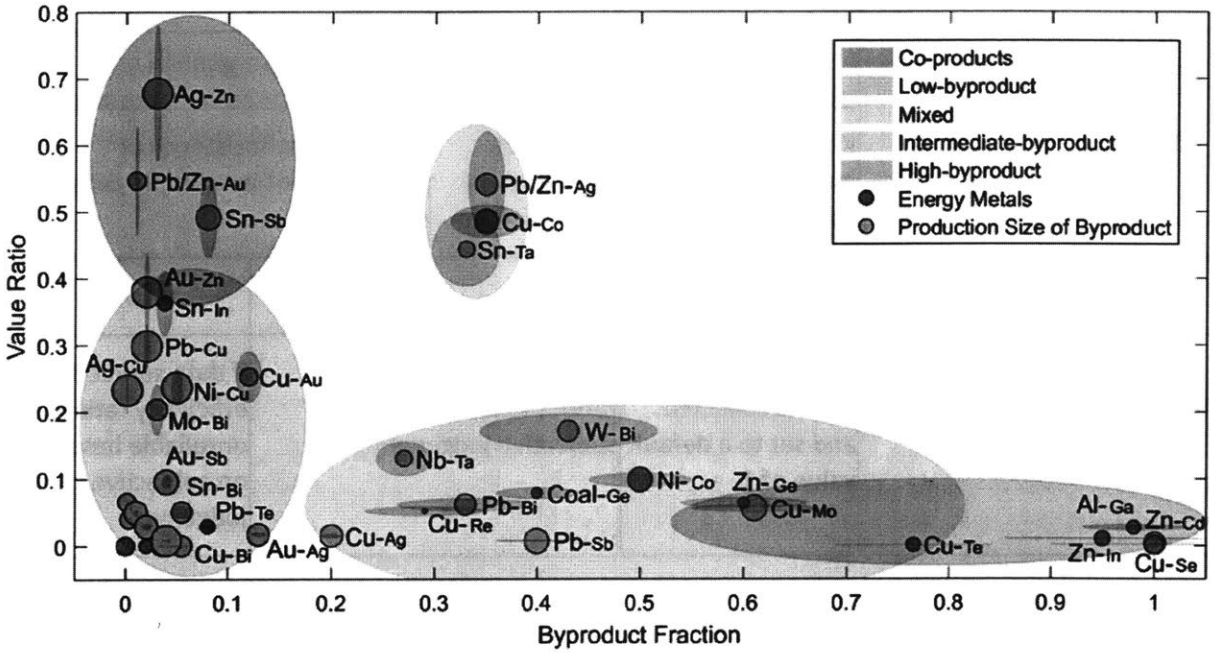

Figure 3. 2 Classification results of carrier-byproduct pairs. Each big shaded ellipse represents a different cluster, and each small ellipse reflects the uncertainty with respect to byproduct fraction and value ratio of each pair. Size of the circles represents 2015 production size of the byproduct metal. The byproduct metals marked in green are important metals for the energy industry.

The intermediate-byproduct cluster has eleven metal pairs, and it is characterized by relatively high byproduct fraction (0.2-0.8) and low value ratio (0-0.2). Different from the high-byproduct cluster, the sources of supply for byproduct metals in this cluster are split between two or more carrier metals and primary production of the byproduct itself. For example, germanium supply comes from two carriers (zinc 60% and coal 40%) and bismuth supply comes from five carriers (tungsten 43%, lead 33%, tin 5.5%, zinc 3.5%, and molybdenum 3%) plus primary bismuth production (as the main product) (12%). In this cluster, byproduct metal supply is neither dominated nor limited by any one carrier, but the total byproduct fraction from multiple carriers are usually greater than 50%. Therefore, while byproduct production is still the major source of supply for these metals, they are not necessarily limited by any one carrier, and

compared to the high-byproduct cluster the risk of availability is mitigated by having a larger fraction of primary production.

The low-byproduct cluster is located on the lower-left corner of the classification figure, with low byproduct fraction (0-0.15) and relatively low value ratio (0-0.4). A wide variety of metal pairs are located in the low-byproduct cluster. On one hand, due to the low byproduct fraction, carriers in this cluster are not significant sources of supply for byproduct metals. On the other hand, due to the low value ratio, producers will not be driven to increase byproduct production even when high demand is expected. Therefore, the markets of the carrier and the byproduct act relatively independently, and the byproduct connections are usually not of much interest either to consumers or producers. However, if significant changes in market conditions and extraction technologies take place, these metal pairs will shift to other clusters where corresponding criticality concerns should be raised.

On the upper part of Figure 3.2, four pairs are classified in a 'co-products' cluster and three to a mixed cluster. The general characteristics of the co-products cluster are low byproduct fraction (0-0.1) and high value ratio (0.38-0.7). Similar to the low-byproduct cluster, the supply of lower value co-product metals is not limited by higher value co-product metals because of low byproduct fraction. In addition, high value ratios would drive producers to consider both metals in the pair as important sources of revenue, and the economic nature of byproducts essentially shifts to co-products. Economic theories pertaining to co-production (or joint production) are well-developed (Baumol & Blinder, 2015). Detailed cost-model development for the co-producing mining companies would help explain the resulting decisions of a company from market or policy changes. Finally, the three metal pairs in the mixed cluster have both relatively high byproduct fraction (0.3-0.4) and high value ratio (0.4-0.6). Thus, the mixed cluster has shared characteristics from the intermediate-byproduct cluster and the co-products cluster. The connection between a carrier and a byproduct in this cluster is not only important for the co-producing mining company, but also for the consumers of that byproduct who would act to secure their supply.

In addition, metal pairs located at the edges of a cluster or the overlaps between two clusters should raise some concern, as technology improvements or changes in metal prices might shift a metal pair to another cluster. If such changes are expected, then the modelling strategies and decisions should change correspondingly.

Developing criticality indicators

In what follows, a deeper dive is took for the high-criticality and the intermediate-criticality groups of carrier-byproduct systems. Two byproduct specific criticality indicators are developed, namely price elasticity of supply and supply potential, to diagnose availability risk with carrier-byproduct pairs in these two groups. These two indicators are used to answer two questions regarding the level of a carrier limiting byproduct supply: 1) Is the supply of byproduct elastic to changes in market price? 2) If the answer is no, is the carrier limiting byproduct supply a major reason for this inelasticity?

Price elasticity of supply

I am interested in whether or not byproduct metal supply responds to changes in price, because a lack of price response could lead to high price volatility (Redlinger & Eggert, 2016) and may increase risk to manufacturers across the supply chain. In economic terms, the responsiveness of the quantity supplied

to a change in its price is called price elasticity of supply, or simply supply elasticity[2]. If a metal's supply is inelastic, the amount produced would not be responsive to changes in the metal's price caused by a perturbation in demand. Using econometric models, researchers have found that the long-run supply elasticities for base metals such as steel, copper, and aluminum in the United States are 1.2 (Barnett & Crandall, 2002), 1.67 (F. M. Fisher, Cootner, & Baily, 1972) and 1.50 (L. A. Fisher & Owen, 1981) respectively, all exhibiting elastic behavior. For byproduct metals, however, while the research community generally agrees that supply is inelastic, there has been little quantitative validation of this argument to date. It is worth mentioning that many byproduct metal trades are based on long-term contracts that are not publicly reported, and price information are not always available. It is assumed that price data used for developing criticality indicators here, such as free market price, producer price and dealer's price, still reflect the average of all market prices. However, limited visibility into these contracts implies that specific quantitative findings are incomplete.

A linear model is constructed to estimate supply elasticity of byproduct metals as describe in Figure 3.3. The model is based on well-developed econometric theories of supply and demand (Baumol & Blinder, 2015; Stock & Watson, 2003).

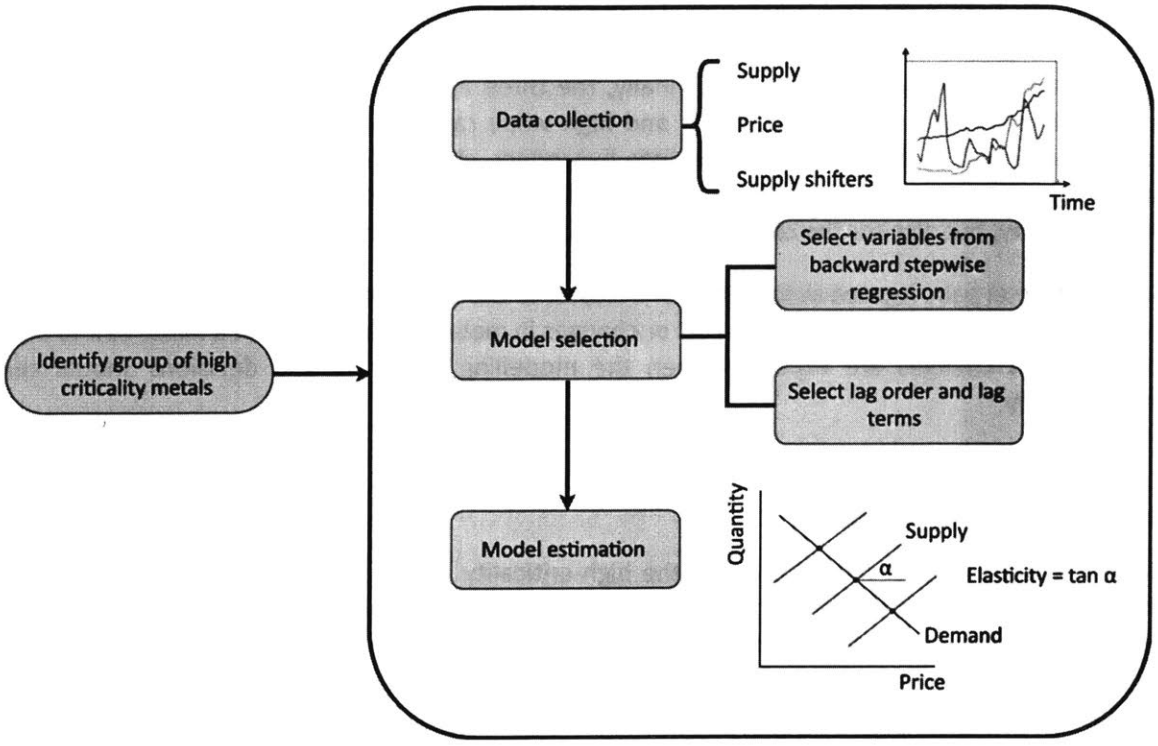

Figure 3. 3 Flowchart for the econometric assessment

[2] Mathematically, I assume that quantity of supply Q can be expressed in Cobb-Douglas form (Cobb & Douglas, 1928) such that $Q \propto P^e$ where P is price of the material, and the power index e is the value of supply elasticity. The good is said to be elastic when $e > 1$ and inelastic when $e < 1$; $e = 0$ is called perfectly inelastic.

The relationships between supply and the covariates are modelled using an autoregressive distributed lag (ARDL) model (Equation 3).

$$Q_t = C + \sum_{\tau=0}^{t_1} \gamma_\tau Q_{t-\tau} + \sum_{\tau=0}^{t_2} \alpha_\tau P_{t-\tau} + \sum_{i=1}^{k} \sum_{\tau=0}^{t_i} \beta_{i,\tau} W_{i,t-\tau} + \varepsilon_t$$

(Equation 3.6)

The variable Q_t represents world production of a byproduct metal in year t, P_t represents the price of the same metal at year t, and $\{W_{i,t}\}_{i=1}^{k}$ is a set of control variables representing various supply shifters, C a constant, ε_t represents the error term, and k is the number of different supply shifters included. I normalize the variables by taking the logarithms of variables that represent prices, production quantities and values, so that the elasticities can be compared across different case studies. ARDL models also include lag terms of the dependent variable and the independent variables to characterize time dependencies between variables. For example, $Q_{t-\tau}$, which is the τth lag of Q_t, represents the world production of a byproduct metal in year $t - \tau$. Other lag terms can be defined similarly. The upper limit of summations, t_1, t_2 and t_i's represent number of lags included for production Q, price P and supply shifters W_i's. Lastly, α, β and γ's represent regression coefficients to estimate.

The role of supply shifters is crucial to the econometric analysis, and the concept is briefly introduced here. According to theory of economic equilibrium, the quantity supplied and demanded will vary until the two equal, leading to an economic equilibrium at which the price of a good is determined. In Figure 3.4 for example, the equilibrium points are the intersections between the blue supply curves, S_1 to S_3, and the red demand curve, D. Price elasticity of supply is represented by the slope of the supply curve. Note that the position of supply curves could be shifted in ways that are uncorrelated to the demand so that the equilibrium points fall on the same demand curve. For example, an industry-wide increase in production costs would shift the supply curve to the right. The factors that shift supply curves in such ways are called supply shifters. In reality, only the equilibrium points on different supply curves can be observed, so supply shifters are included in the model to correctly estimate supply elasticities on the same supply curve.

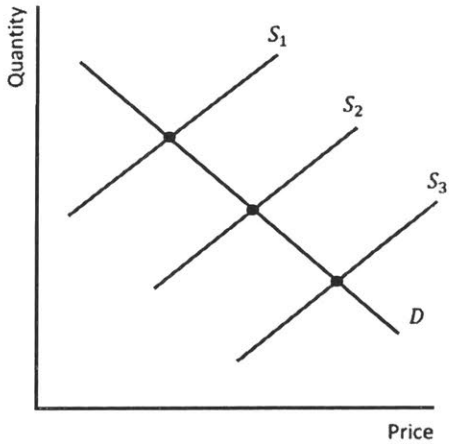

Figure 3. 4 Illustration of supply shifter in supply and demand model

The selection of supply shifters is based on a literature survey and three variables are chosen to reflect general metal supply-related factors, namely interest rate, industrial production, and time. First, supply of non-renewable resources follows Hotelling's rule which states that lower interest rate lead to higher metal production. According to Hotelling's rule of exhaustible resources (Hotelling, 1931), owners of natural resources would be more likely to extract and sell if this action yields more value than other financial instruments such as interest bearing securities. Second, supply of metals are influenced by industrial production activities, and researchers have used industrial production indices to explain drivers of natural resource production such as oil (Herrera, Lagalo, & Wada, 2011) and base metals (Walter C. Labys, Achouch, & Terraza, 1999). Third, a variable that describes advancements in metal extraction technologies should be included in the supply model. A linear time trend provides a proxy for such advancements. Finally, in the context of byproduct metal supply, the primary supply of carrier metal is also included as a supply shifter.

Model selection is then performed, which includes selection of supply shifters, lag orders and lag terms. To select the best performing model, I start with an ordinary least squares (OLS) model backward stepwise regression, in order to select the most statistically significant supply shifters. The goodness-of-fit metric used in the stepwise regression is Bayesian Information Criterion (BIC).

The next step is to determine which lag order terms to be included. BIC of the vector autoregressive (VAR) model is also used to select the optimal lag order, l. In the following case studies, the VAR model is used as a special ARDL model that has all its variable lag orders equal to l. In other words, $Q = P = W = l$ in Equation 3.6. Then I vary each lag order from 0 to l and compare the adjusted R squared of all $(k+2)^{l+1}$ models. Coefficients are estimated from the model with the best adjusted R squared.

After the estimation of coefficients in Equation 3.5, long run supply elasticity e can be calculated as

$$e = \frac{\sum_{p=0}^{P} \alpha_{t-p}}{1 - \sum_{q=1}^{Q} \gamma_{t-q}}$$

(Equation 3.7)

with variables defined as above. Here the long-run elasticity is estimated as the ratio between the sum of all price coefficients (including lags) and the net sum of coefficient for supply, in order to account for the impact of past prices on current supply. The approach of long-run supply elasticity estimation follows the standard approach of previous studies (Cooper, 2003; F. M. Fisher et al., 1972; Madlener, Bernstein, & González, 2011). Data for the variables are collected from multiple databases and reports such as USGS historical statistics (U. S. Geological Survey, 2016) and US Board of Governors of the Federal Reserve System (Federal Reserve Bank of St. Louis, 2016).

The selection of time series data is based on data availability from several data sources. I intentionally excluded data after 2011 for indium and germanium although recent data are available. This is due to a huge financial fraud by the Fanya Metal Exchange in China, which involved around 6 billion US dollars of investment from over 200,000 investors.

Supply potential

To further understand the role of byproduct status limiting supply, supply potential is introduced as a metric to investigate the cause of the inelastic supply. A byproduct metal's supply potential from carrier is defined as the maximum amount of metal content accompanied with the primary production of the carrier. Since primary production data can be found as time series, supply potential is also presented as a time series.

In what follows, econometric models are developed to estimate supply elasticities of three byproduct metals, namely indium, selenium and germanium. These metals are selected due to their high byproduct status and their significant roles in clean energy applications. Supply potential of each byproduct is estimated in order to investigate the level of carrier metal limiting byproduct. The three cases are chosen to demonstrate the econometric model development, but this methodology could be easily applied to the other metal systems.

Case study on the zinc-indium system

According to industry estimates (Tolcin, 2016), 95% of global indium primary production is in the form of byproduct of zinc ores, 4% is associated with tin production and 1% is from copper production. Indium is predominantly extracted from zinc production dust and then further refined by electrolysis (Chagnon, 1995). In 2015, China and South Korea accounted for around 50% and 20% of global indium refinery production (750 tons, from (Tolcin, 2016)) respectively. The other leading producing countries include Japan and Canada, each producing about 70 tons of refined indium. On the demand side, production of indium tin oxide (ITO) has been estimated to account for 55% to 85% of global indium demand (Tolcin, 2016). ITO coatings are used mainly for the production of flat-panel displays such as liquid crystal displays.

Indium supply elasticity is investigated using 40 years of annual data (1972-2011) and the model introduced in Equation 3.6. Data after 2011 are excluded due to the Fanya scam. Indium was in fact the most affected metal by the scam: by the time Fanya collapsed, its indium inventory had reached 3,600 tons, which is more than five times global indium production in 2010. According to an anonymous industry expert, it might take more than 10 years for this inventory to be sold. The initial set of supply shifters include zinc mining production, Industrial Production Index of OECD countries (OECD IP), China GDP in Mining, Manufacturing and Utilities (China MMU), United States 10-Year Treasury Constant Maturity Rate (US10) and time. The presence of carrier supply, interest rate, and time as variables is explained above in the method section, while China MMU and OECD IP are selected as these variables represent industrial production activities of the major producing countries.

The OLS results show that zinc mining production and China MMU are not significant regressors (α=0.05) and they are eliminated in the backward stepwise regression. The ARDL model further includes in three more lag terms, and the final model is expressed as

$$Q_t = C + \gamma Q_{t-1} + \alpha P_t + \sum_{w=0}^{1} \beta_{1,w} US10_{t-w} + \sum_{w=0}^{1} \beta_{2,w} OECDIP_{t-w} + \beta_3 t + \varepsilon_t$$

(Equation 3.8)

Estimated parameters for the ARDL model are shown in Table 3.2. Based on Equation 3.7, the long-run supply elasticity is estimated to be 0.10, with the 95% confidence interval (-0.08, 0.29). Therefore, the hypothesis that supply of indium is inelastic is accepted at a significance level of α=0.05.

Table 3. 2 ARDL model results for zinc-indium case study

	Dependent variable: Q_t (Indium supply)
Constant	-5.741
	(33.039)
Q_{t-1}	0.464***
	(0.118)
P_t (Indium price)	0.056
	(0.056)
$US10_t$	-0.004
	(0.034)
$US10_{t-1}$	-0.053
	(0.037)
$OECDIP_t$	0.006
	(0.012)
$OECDIP_{t-1}$	0.016
	(0.013)
t (Year)	0.004
	(0.017)
Observations	40
Adjusted R2	0.968
F statistic	162.646***
Notes:	*p<0.1; **p<0.05; ***p<0.01

The supply potential of indium from zinc is presented in Figure 3.5. Because data on indium content in zinc ores is highly uncertain (See data from (Werner, Mudd, & Jowitt, 2017)), there have been different assumptions about its average value in the literature: many studies assume ~50 grams of indium per ton of zinc content in ores (Jorgenson & George, 2005; Polinares, 2012; Roskill, 2010). However, a report prepared by the US National Renewable Energy Laboratory believes that 50 grams is a significant underestimate, because this value underestimated losses during the recovery process (Lokanc et al., 2015).

Based on their estimate of 2130-5870 potential tons of indium mined in 2011, and 2011 zinc mining production of 12500 kt (Tolcin, 2017), I calculated indium content to be 171 grams to 470 grams per ton zinc content in ore. This range still exhibits significant uncertainty, so indium supply potential is also presented as a range in Figure 3.5, and compared with the actual primary refined indium production. The upper and lower limit of the range are represented by $SP_{Zn,u}$ and $SP_{Zn,l}$ respectively. The changes in indium ore grade over time is not considered due to data limitation.

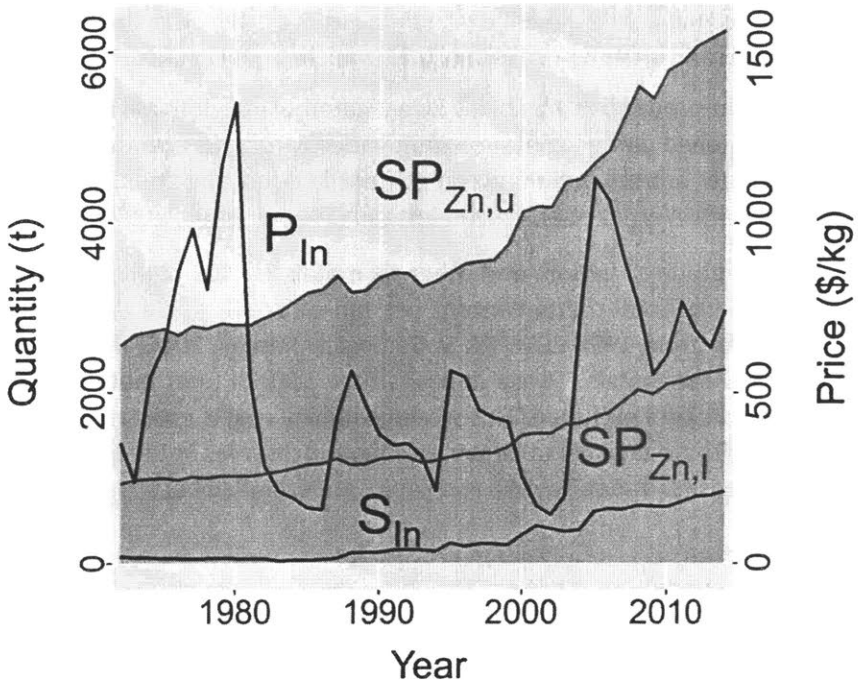

Figure 3. 5 Times series of indium supply (S_{In}), indium price (P_{In}) and upper/lower limit of supply potential from zinc ($SP_{Zn,u/l}$). Values of supply and supply potential are in metric tonnes (left axis) and values of prices are in USD/kg (right axis).

In Figure 3.5, it can be seen that even the lower estimate of supply potential is still much higher than the actual indium primary production, indicating significant loss during recovery. To be more specific, Lokanc et al. described four sources of loss in the indium recovery process (Lokanc et al., 2015):

a. During zinc mining and processing, 30%-50% of indium is lost to mine tailings and the rest ends up in zinc concentrate;
b. About 30% of indium-bearing zinc concentrate are not sent to indium capable smelters;
c. Of the concentrates that are sent to indium capable smelters, about 50% indium is lost in smelter wastes;
d. Finally, loss of indium in refineries is about 20%.

The overall recovery efficiency is therefore 14% to 20%. However, loss from a, b and c take place at zinc mining sites and zinc smelters, where zinc is still the main product. Zinc miners and smelters are not likely to be driven by changes in indium price. On the other hand, indium refineries produce indium as their main products, so they may be more likely to increase recovery rates given higher indium price. Given

that current recovery rate for refiners already averages 80%, there is at most 25% potential of increase. Therefore, the responsiveness of indium refinery production to price is very limited. Indeed, while price increased 8-fold from 2002 to 2005 (real price from 142 USD/kg to 1129 USD/kg), primary refined production only increased modestly from 400 tons to 600 tons (See Figure 3a). Also, zinc mining production does not show up as a significant supply shifter in the ARDL model, which suggests a lack of co-movement between primary zinc and primary indium production trends. The fluctuation of the ratio between indium refinery production and zinc mining production (indium/zinc ratio) is caused by changes in indium content per unit zinc content in ore, and changes in overall indium recovery efficiency. However, indium/zinc ratio is not significantly driven by indium price either: The linear correlation coefficient between indium/zinc ratio and indium price is only 0.21, which is not significant at significance level α=0.1.

So far, the primary indium production has been investigated using global average values of indium ore grade. However, as mentioned earlier, metal content varies across different mines and deposits. To the best of my knowledge, data around indium metal content in operating mines are not publicly available, so indium deposit data from Werner et al. is used instead (Werner et al., 2017).

This dataset includes ore grade of indium and other six metals for 101 deposits which have reported to contain indium. The value of total metal content per ton of ore in these deposits is calculated, using average annual metal price from 1996-2015 (U. S. Geological Survey, 2016) in 2015 constant USD as the long term unit price of these metals. Those deposits that contain total metal value less than average mining cost (33 USD/t of ore) are excluded. This average mining cost is estimated by Lokanc et al. (Lokanc et al., 2015). These deposits are unlikely to become economic reserves in the short term due to low metal values. Another three deposits (Isabel, Toyoha and Ikuno) are excluded because they only reported indium content.

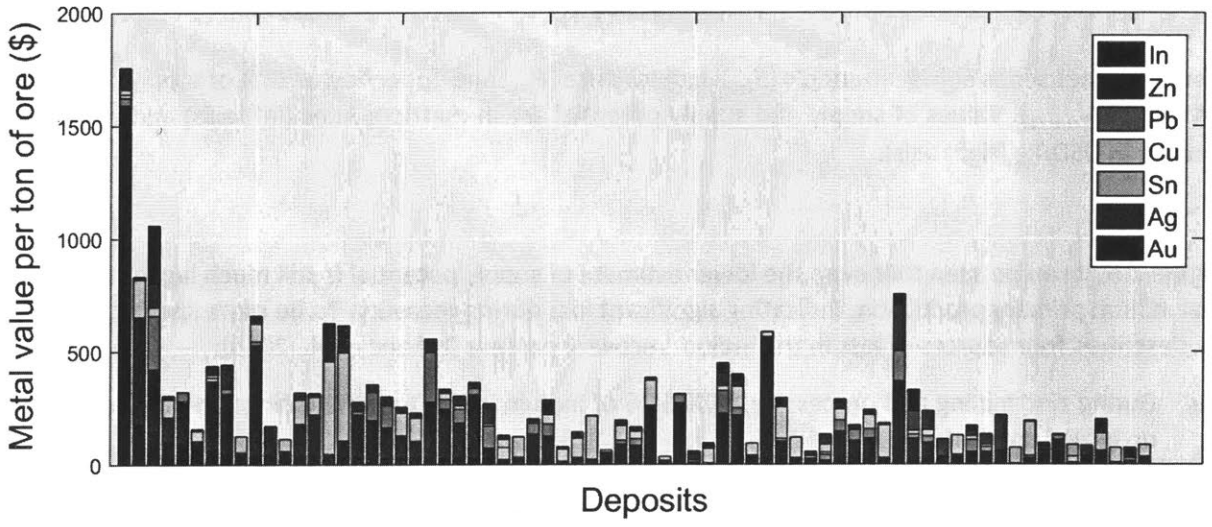

Figure 3. 6 Value of metal content in ore for 71 deposits, in dollars per ton. Ore grade data is primarily based on Werner et al. (Werner et al., 2017). Data from two other studies for the Huari Huari deposit (Ishihara, Murakami, & Marquez-Zavalia, 2011), the Dulong deposit and the Dachang deposit (Ishihara, Murakami, & Li, 2011) are also used.

Table 3. 3 Summary of key statistics of 71 indium deposits. Ore grade data is primarily based on Werner et al. (Werner et al., 2017)

Carrier	Contained In (t)	Percentage of contained In in total	Value ratio	Average indium grade in parts per million (ppm)
Zn	29215	49.94%	0.026	29.65
Pb	10	0.02%	0.046	47.90
Cu	15902	27.18%	0.015	17.23
Sn	5242	8.96%	0.049	29.90
Ag	219	0.37%	0.0054	2.94
Au	3	0.01%	0.0001	0.05
In	7911	13.52%	NA	429.95
Total	58502	100.00%	NA	

The value of the metal in the remaining 71 deposits is shown in Figure 3.6, ranked by indium content. A summary of important statistics is shown in Table 3.3. For each deposit the metal with the highest total value is assigned to be the carrier. Then, the value ratio of indium to that carrier is calculated as the ratio between total value of indium and total value of carrier, multiplied by overall recovery efficiency. It is assumed that overall recovery efficiency is 17% for all deposits, which is the median of the 14%-20% overall recovery efficiency range mentioned earlier for indium produced as byproduct from zinc. From the analysis on deposits, it can be seen that zinc is still the largest carrier by fraction in the deposits considered, accounting for ~50% of total indium content in deposits. However, different from current primary production where other carriers of indium only accounts for 5% in total production, there is significant amount of indium that could be recovered as byproduct of copper (27%) and tin (9%). The average value ratio is still low (<0.05) across all six carriers, indicating that indium will be produced as byproduct rather than coproduct, if metal prices do not deviate too much from the 20-year average real prices. Around 10% of indium could be potentially produced as the main product, due to the very high indium grade in ore (~430 ppm). Therefore, a significant amount of indium can be recovered as the main product if mines on these deposits start to operate, and this part of production will not be limited by zinc primary production.

Here I briefly summarize findings on the zinc-indium system case study. It is found that the indium's price elasticity of supply is indeed very low, and the main cause of this inelasticity is zinc miner and producer's lack of incentive for improving indium recovery efficiency. Moreover, from the analysis of metal content on 71 indium-bearing deposits around the world, it is found that about half of the indium content contained in deposits can be produced as main product or byproduct of metals other than zinc. Therefore, the future primary production of indium may be less limited by production of zinc.

Case study on the copper-selenium system

Copper-selenium is one of the most discussed carrier-byproduct systems in literature because of selenium's wide application in photovoltaic systems. Selenium, together with tellurium and other byproducts, can be obtained from the anode slimes of copper refineries (Andersson, 2000). Selenium is

now produced entirely as a byproduct of copper (R. U. Ayres & Peiro, 2013). The leading producing countries in 2015 were China, Japan, Germany, US, and Belgium. Supply data from several countries are not published in common metal survey reports, so I compared different data sources and made additional assumptions in order to arrive at an estimate for world selenium supply. On the demand side, selenium is not dominated by any one application, and the estimates for world consumption in 2015 (C. S. Anderson, 2015) are as follows: metallurgy, 40%; glass manufacturing, 25%; agriculture, 10%; chemicals and pigments, 10%; electronics, 10%; and other uses, 5%.

The selenium supply elasticity is investigated using 1967 to 2012 data with annual frequency using the model introduced in Equation 3.6. The initial set of supply shifters include copper mining production (QCU), Industrial Production Index of European OECD countries (OECDE IP), United States 1-Year Treasury Constant Maturity Rate (US1) and time. For QCU, copper mining production from the solvent extraction and electrowining (SX-EW) process is excluded, as this hydrometallurgical process does not yield selenium (Bustamante & Gaustad, 2014). OECDE IP is selected because of its representativeness of recent industrial production activities of the major producing countries and data availability.

All the selected regressors are included for the ARDL model. After lag term and lag order selection, the final form of the model is

$$Q_t = C + \gamma Q_{t-1} + \alpha P_t + \sum_{w=0}^{1} \beta_{1,w} US1_{t-w} + \sum_{w=0}^{1} \beta_{2,w} QCU_{t-w} + \beta_3 OECDEIP_t + \beta_4 t + \varepsilon_t$$

(Equation 3.9)

Estimated parameters for the ARDL model are shown in Table 3.4.

Table 3. 4 ARDL model results for copper-selenium case study

	Dependent variable: Q_t (Selenium supply)
Constant	-36.809**
	(15.476)
Q_{t-1}	0.276*
	(0.149)
P_t (Selenium price)	0.024
	(0.019)
$US1_t$	0.010
	(0.010)
$US1_{t-1}$	-0.019*
	(0.011)

QCU_t	0.573
	(0.583)
QCU_{t-1}	-0.584
	(0.481)
$OECDEIP_t$	-0.001
	(0.005)
t (Year)	0.021**
	(0.010)
Observations	46
Adjusted R2	0.939
F statistic	86.005***
Notes:	*p<0.1; **p<0.05; ***p<0.01

Based on Equation 3.7, the supply elasticity is calculated to be 0.03, with the 95% confidence interval (-0.03, 0.09). Similar to the case study on zinc-indium, this value can also be clearly seen as statistical evidence of inelastic supply of selenium.

The cause of inelastic supply is similar to that described for indium. Again, selenium primary production supply potential from copper is calculated, assuming that the material availability of selenium from copper anode slimes is 400 grams of selenium per ton of copper anode (nominal 99.3% purity). This value represents a weighted average from a survey of copper refineries worldwide (Green, 2006).The comparison of primary selenium production and selenium supply potential is shown in Figure 3.7.

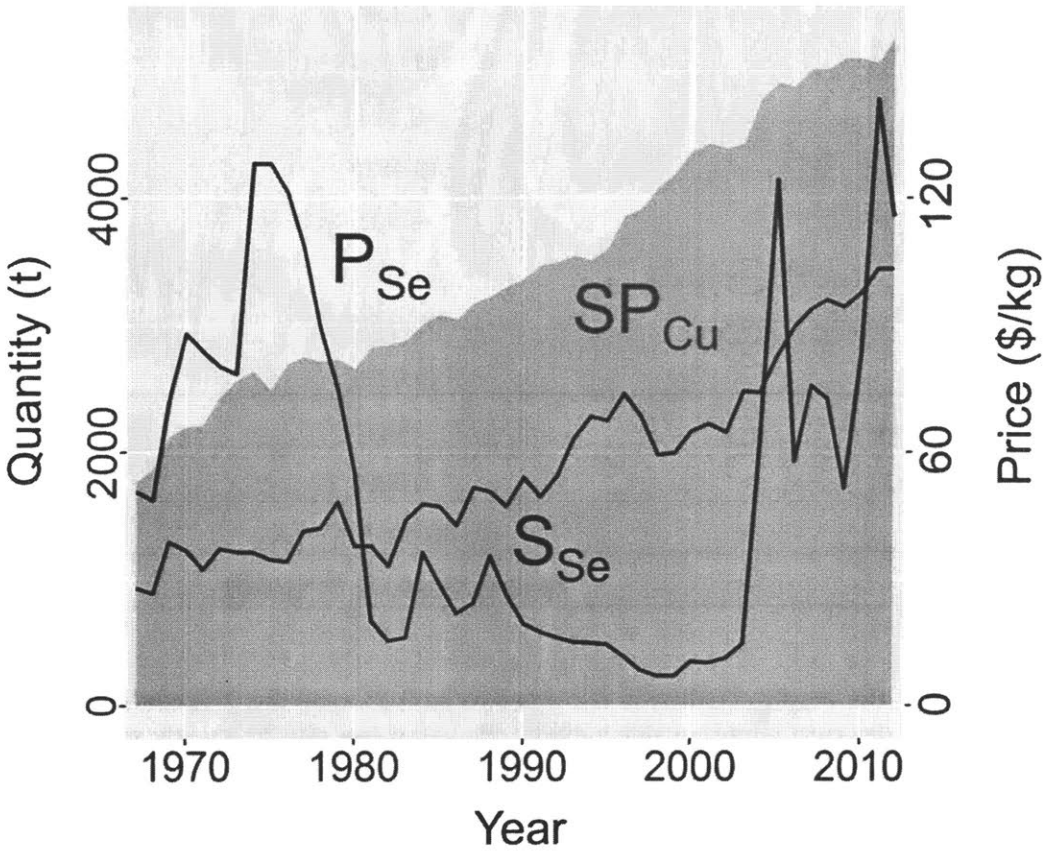

Figure 3. 7 Times series of selenium supply (S_{Se}), selenium price (P_{Se}) and supply potential from copper (SP_{Cu}). Values of supply and supply potential are in metric tonnes (left axis) and values of prices are in USD/kg (right axis).

Under the assumed values of concentration, the supply potential from copper is consistently higher than actual supply by about 1000 tons. This means that there is still considerable amount of selenium lost during recovery process. Historically, selenium recovery efficiency from anode slimes at refineries is estimated to be 30%-80% (Jensen, 1985). Therefore, the cause of inelastic supply could be that recovery efficiency has little response to price changes.

Furthermore, while recovery efficiency cannot be higher than 100% and selenium supply potential have increased rather steadily during the period under investigation, price is much more volatile which has changed by over an order of magnitude. As is the case for many minor metals, there is no global price-setting agency such as the London Metal Exchange (LME), and the selenium price used in this study is the price from a New York dealer only. The supply and demand relationships of base metals such as copper and zinc are well reflected by the LME, but not for selenium. The New York dealer price might be dominated just by a few consumers and producers, and thus exhibits high volatility (this volatility is seen frequently for byproduct metals). It is conversely possible that these dealer prices stay artificially constant due to lack of trades.

Technological limits might also translate to potential availability risk of selenium in the future. One important application of selenium is in PV, and the amount of selenium required is expected to increase as that sector grows (C. S. Anderson, 2017). However, even if increase in selenium price may increase its

recovery rates from anode slimes (George, 2004), part of that increase may have been offset by an increasing fraction of refined copper coming from the hydrometallurgical copper extraction process, a process which does not provide the recovery of selenium (International Copper Study Group, 2019b). These factors from both the supply and demand side may close the gap between selenium supply and supply potential in the near future.

Case study on the zinc/coal-germanium system

As a third case study, the zinc/coal-germanium systems from the intermediate-byproduct cluster is investigated. It is estimated that 60% of germanium extraction is originated from zinc and 40% from coal fly ash (N. T. Nassar et al., 2015). In 2015 China accounted for over 70% of global germanium refinery production (120 tons, from (Guberman, 2016)), but other major producing countries include Russia, Belgium, Canada and Germany make up the rest. The worldwide demand breakdown for germanium is estimated to be the following: fiber optics, 30%; infrared optics, 20%; polymerization catalysts, 20%; electronics and solar applications, 15%; and other uses, 15%.

Germanium supply elasticity is investigated using 45 years of annual data (1967-2011) and the model introduced in Equation 3.6. The initial set of supply shifters include world zinc mining production (QZN), world coal production, OECDE IP, United States 5-Year Treasury Constant Maturity Rate (US5) and time.

The OLS results show that OECDE IP is not a significant regressor (α=0.05) and it is eliminated in the backward stepwise regression. While coal as a carrier does account for 40% of germanium production, it does not appear to be a significant regressor as well so it is also removed. Different from the first two case studies, it is found that the OLS residuals do not exhibit significant autocorrelation, so no lag variables are included in the final model. The model can be expressed as

$$Q_t = C + \alpha P_t + \beta_1 QZN_t + \beta_2 US5_t + \beta_3 t + \varepsilon_t$$

(Equation 3.10)

Estimated parameters for the model are shown in Table 3.5.

Table 3. 5 OLS model results for zinc/coal-germanium case study

	Dependent variable: Q_t (Germanium supply)
Constant	59.789***
	(11.670)
P_t (Germanium price)	0.022
	(0.105)
QZN_t	3.918***
	(0.513)

$US5_t$	0.092***
	(0.018)
t (Year)	-0.059***
	(0.010)
Observations	45
Adjusted R2	0.607
F statistic	17.57***
Notes:	*p<0.1; **p<0.05; ***p<0.01

Based on Equation 3.7, the supply elasticity is calculated to be 0.02, with the 95% confidence interval (-0.31, 0.36). This result, which is similar to the other two case studies, can also be seen as the statistical evidence of inelastic supply of germanium.

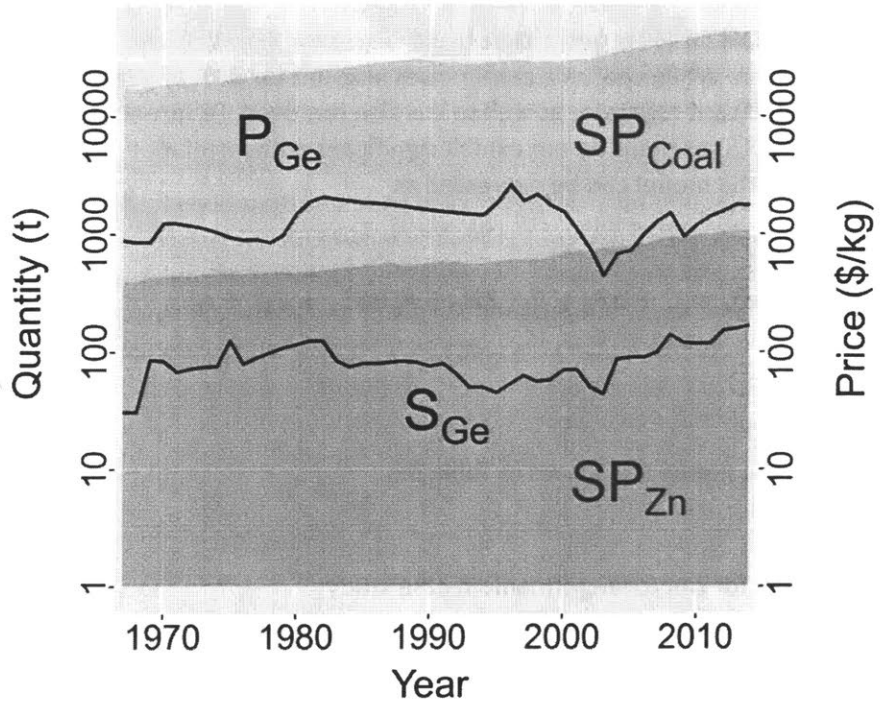

Figure 3. 8 Times series of selenium supply (S_{Ge}), selenium price (P_{Ge}) and supply potential from coal (SP_{Coal}) and zinc (SP_{Zn}). Values of supply and supply potential are in metric tonnes (left axis) and values of prices are in USD/kg (right axis). All values are shown in logarithmic scales.

Germanium primary production and supply potential are presented in Figure 3.8, and it can be seen that current germanium production is far from reaching the supply potential. Supply potential from zinc alone is more than five times that of germanium production, and supply potential from coal is about two orders

of magnitudes higher than that from zinc. Therefore, it does not appear that the byproduct status plays a significant role in limiting supply, but rather that most germanium in the carriers' minerals do not reach the refining stage. This observation agrees with a global substance flow analysis on germanium, in which most germanium available is found to end up in carriers' residues (Licht et al., 2015). Thus, germanium refiners should be able to increase their production by purchasing more raw materials to catch up with increase in demand. In that case, why is germanium's supply elasticity still very low? Similar to the selenium case that have been discussed, this might still be attributed to lack of global price-setting agencies. Moreover, according to an anonymous industry source, China's State Reserve Bureau has been purchasing significant amount of germanium from Chinese domestic producers for its national strategic stockpile, and the price is much higher than free market price. This has apparently made Chinese producers less responsive to changes in free market price since the national stockpiling serves as a long-term contract, which helps them avoid risks from price fluctuations.

The interaction between coal-germanium and zinc-germanium also presents an interesting phenomenon. Germanium production has been expected to rise due to increasing demand from optics, electronics and solar cells. Although there is a much greater potential to extract more germanium as byproduct of coal than zinc, coal production is already beginning to saturate (Tadeusz W. Patzek & Croft, 2010; Rutledge, 2011), while there is still no sign of zinc production saturation. In addition, if demand for zinc and coal are not highly correlated in the future, the existence of these two carriers might have stabilized germanium production and price volatility.

To summarize, it is found that for all three byproduct systems under investigation, price elasticity of supply is low (see summary in Table 3.6). However, the cause of inelasticity is not that primary production of byproduct is limited by available metal contents in the carrier's ores. For indium and selenium, a likely reason is that only refiners are responsive to price changes, but the potential to increase recovery efficiency is limited. For germanium, current primary production is far from reaching potential amount from coal mining and zinc mining, but national strategic stockpiling disrupts producers' responsiveness to market prices. In addition, lack of a global price-setting mechanism makes metal prices very volatile, but primary supply would not be able to adjust to these dramatic changes in prices.

Table 3. 6 Summary of supply elasticities for three case studies

System	Supply elasticity 95% CI	Causes of inelasticity	
Zinc-indium	(-0.08, 0.29)	Limit of recovery efficiency (~17%)	Lack of market liquidity and global price setting mechanism
Copper-selenium	(-0.03, 0.09)	Supply limit of carrier; Limit of recovery efficiency (~50%)	
Zinc/Coal-Germanium	(-0.31, 0.36)	National stockpiling strategy	

Using supply potential as a screening tool

The comparison between current supply and supply potential is used here as an additional criticality metric for the intermediate-byproduct cluster. A comparison is shown in Figure 3.9, for the annual production and supply potential for 6 byproduct metals (9 carrier-byproduct pairs) in the intermediate-byproduct cluster. All recovery efficiencies are assumed to be 100% in the supply potential calculation. From the copper-selenium case study, it can be seen that byproduct production can be close to the supply potential. In the intermediate-byproduct cluster, however, byproduct production is usually far from reaching supply potential for most pairs (lead-bismuth, tungsten-bismuth, copper-tellurium and copper-rhenium). In other cases where the difference is smaller (copper-molybdenum, niobium-tantalum and nickel-cobalt), although increased byproduct production might be limited by one specific carrier, it does not necessarily lead to a supply constraint, since byproduct fraction from that one carrier is relatively low. Additional byproduct demand can be met from coproduction with other metals (tin-tantalum and copper-cobalt) or primary production.

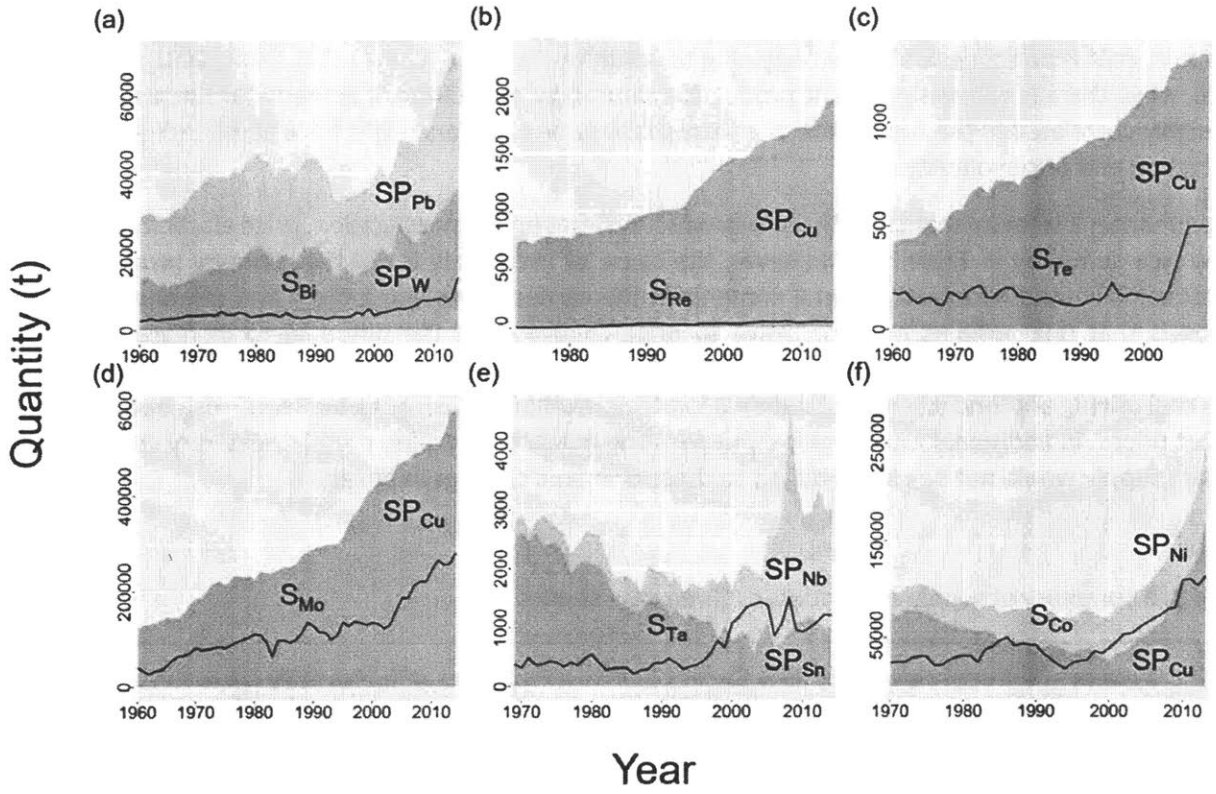

Figure 3. 9 Comparison of actual byproduct metal supply ($S_{byproduct}$) represented by green curves and supply potential from carrier ($SP_{carrier}$) represented by shaded regions, for 6 byproduct metal (9 carrier-byproduct pairs) in the intermediate-byproduct clusters. (a) Lead-bismuth and tungsten-bismuth; (b) Copper-rhenium; (c) Copper-tellurium; (d) Copper-molybdenum; (e) Niobium-tantalum and tin-tantalum; (f) Nickel-cobalt and Copper-cobalt.

Based on this comparison, the concern around whether byproduct metals in the intermediate-byproduct cluster will be available in the future should be less than those metals in the high-byproduct cluster. However, the above observation only indicates that the supply of these byproduct metals are not limited

by their 'byproduct status', but it does not guarantee low supply risk. As mentioned in previous case studies, many disrupting forces specific to the minor metals market might still bring challenges for these byproduct metals.

Conclusions

Compared to previous material criticality assessments, which only include byproduct dependency as the sole byproduct specific criticality indicator, the work presented in here provides detailed assessments focusing on the economic characteristics of byproduct metals. Several recent papers have developed quantitative methods around critical metals, which focused on metal value in scrap (Bandara, Darcy, Apelian, & Emmert, 2014), risk of mining (Nansai et al., 2014), future demand (Zhang et al., 2016) and life cycle impact of critical metals (Vieira, Goedkoop, Storm, & Huijbregts, 2012). In this chapter I made similar attempts, by employing cluster analysis to divide carrier-byproduct pairs into groups with different criticality concerns. By matching the carrier-byproduct metal system of interest to a cluster in Figure 3.2, decision makers will be able to identify different types of risk.

As described throughout this chapter, data availability restricts how quantitative my conclusions can be. In order to compare the value ratios across different carrier-byproduct pairs, highly disaggregated data and information are compiled regarding mineral concentration and extraction efficiencies. First, many of the data regarding mineral concentrations are found in USGS reports, peer-reviewed articles, and scientific encyclopedias. Data from these sources represent global average concentrations from different deposits and mining projects. However, in some cases, when such sources are not available, estimates are made based on one or few mineral reserves only. For example, in order to find the concentration ratio of tin-niobium system, the mineral resources estimate of a Malaysian tin mine is used. Secondly, the extraction efficiencies used in the study often represent efficiency from a single extraction process for a certain carrier-byproduct pair, while in reality different extraction processes are used in industrial production.

In the absence of more reliable data, an attempt is made to address the lack of representativeness in the uncertainty analysis. Higher uncertainty scores are assigned to those mineral concentration data estimated from a smaller sample of mines and deposits. For extraction efficiencies, higher uncertainty scores are assigned to those data believed to be less reliable. Nevertheless, I recognize that the estimated results of the value suffer from a lack of a larger sample of more reliable data.

Furthermore, although econometric modelling does take into account fluctuations in various economic conditions, it is inherently designed to select independent variables which capture the most variance in the dependent variables from a statistical aspect. For example, in my case studies, treasury rates of different time length are selected based on which variable gives the highest correlation with metal supply. While this might not be a problem for estimation of supply elasticity because treasury rates themselves are highly correlated, a more careful investigation would be required to determine whether these different variables differentially inform the drivers of metal supply. Furthermore, this work only provides an economic perspective on the material criticality problem; I acknowledge that full understanding of this problem requires collaboration of scientists and engineers from all related fields, such as economists, material scientists, environmental scientists, mining engineers and so on. Future work of criticality assessments could, for example, focus on the thermodynamic properties of minerals in extraction processes or the impacts of declining ore grade on material availability.

Chapter 4: Feasibility of Alternative Extraction Process, Case Study on Indium

Acknowledgement: Portions of this chapter are based on a 2017 class project report (MIT Course 3.19 Sustainable Chemical Metallurgy, taught by Professor Antoine Allanore) by Xinkai Fu, Jordan Ladd, Rachel Osmundsen, Jennifer A. Glerum, titled *'Indium Extraction as a Byproduct of Zinc'.* (Fu, Ladd, Osmundsen, & Glerum, 2017)

Motivation for alternative process

In Chapter 3, I have discussed in detail the implication of carrier metal limiting the supply of byproduct metals. There are two major limiting factors that are related to the current production processes of the byproduct metals:

1. The recovery rates for some byproduct metals are low. Metal extraction processes are usually designed and optimized for the primary metals, as they are the major sources of revenue for processors. For example, for primary copper refineries that extract selenium and tellurium from copper anode slimes in the electrolytic copper refining process, while recovery efficiency for copper is usually greater than 99%, efficiency for selenium and tellurium can be as low as 30% to 80% (Jensen, 1985).
2. Intermediate material (e.g. concentrate, matte, blister) containing the byproduct metals are sent to processors that are not capable of extracting them. The extraction of metal from ore minerals to final refined metals can often take place in multiple metal processors, such as miners, smelters, refineries and so on, while the separation of byproduct from the primary metal often take place in downstream processors. The value of the byproduct metal is not always accounted for, and is up to negotiation between the buyer and the seller of the intermediate material. Depending on the metal, if significant amount of byproduct metals occurs in an intermediate material, a premium might be added so that sellers are credited for the value of the byproducts. For example, copper concentrate can be priced for the gold/silver content, subject to a deduction of one/thirty grams of gold/silver in per dry metric tonne of concentrate (Söderström, 2008). However, other less valuable minor metals, such as selenium and tellurium in copper concentrate, are often not credited for their value. Even if 100% of their value is accounted for, the value would still be much less than the primary metal: based on data collected in Chapter 3, the value of selenium and tellurium are about 40 USD and 10 USD for per tonne of copper content, while price of copper is around 6500 USD/t. Therefore, from an economic perspective, the sellers of copper concentrate would not be incentivized to just selling their concentrate to downstream refineries that are capable of extracting the byproduct.

For many metal systems, further improvement of the byproduct production is difficult under the current supply chain structure and the existing extraction processes, based on reasons described above. In what follows, an attempt is made to investigate if such improvements are possible under alternative extraction processes. An economic screening analysis is first performed on multiple byproduct metals, allowing the identification of metals of interest.

Screening assessment for economic feasibility

The purpose of this screening assessment is to find carrier-byproduct metal systems that should be prioritized to develop alternative extraction processes. Results from this assessment indicate only the relative favorability of metal systems, rather than the absolute feasibility. From both technical and economic perspectives, an alternative extraction process to improve byproduct production should satisfy the requirements below:

1. The process should allow higher overall extraction efficiency of the byproduct metal.
2. The process should allow byproduct metals to be separated from the primary product at earlier processing stages.
3. Compared to current extraction processes, there should be enough economic advantage from the alternative process so that metal processors can be incentivized to adopt the new process.

While the first two requirements are related to the technical aspects of metal extraction, the third requirement is an economic one, and can be quantified using monetary values. Therefore, an *economic feasibility indicator* is developed following Equation 4.1, as the ratio between the value of metal B in ore and minesite cost, both in USD/t of ore treated. Metal B indicates the metal of interest and is not necessarily the byproduct of a specific project.

$$F = \frac{Value\ of\ metal\ B\ in\ ore}{Minesite\ cost}$$

(Equation 4.1)

The rationale of this indicator is explained below. This indicator is developed from a miner's perspective, because the first stage in the extraction process for all metals is the mining stage and it is the preferable venue for byproduct separation from carrier (Assumption 2). Miners incur different costs in metal extraction processes, including operational costs such as minesite cost, treatment and refining charge, freight cost, royalty and fixed costs such as development expenditure. Minesite cost, including mining and milling costs, is the first component of operational cost that must be incurred before any other further activities of metal extraction and transaction. This cost is based on per tonne of ore treated in Equation 4.1, and unrelated to the amount of metal value in ore. If the value of metal B in the ore is much smaller than the mining cost, i.e., $F \ll 1$, then it is unlikely that metal B becomes the primary product, or even the co-product of a mine. Therefore, it is assumed in this case that there would be little incentive for a miner or the owner of a potential mining project to adopt a new extraction process that is optimized for that metal.

Following Equation 4.1, the economic feasibility indicator is applied to six metals: cadmium, germanium, indium, rhenium, selenium and tellurium. These six metals are chosen because of their high-byproduct status from the classification in Chapter 3. Cadmium, germanium and indium are mainly byproducts from zinc production while rhenium, selenium and tellurium are mainly byproducts from copper production. The value ratio of all six carrier-byproduct pairs are smaller than 0.1 (see Figure 3.2). For each of these metals, the value in per tonne of ore varies across different deposits. Therefore, instead of presenting the economic feasibility indicator as an average value for each metal, the distribution of the indicator is calculated, which is proportionate to the distribution of metal concentration:

$$pdf(F) = pdf(metal\ concentration\ of\ B\ in\ ore) \cdot \frac{Unit\ price\ of\ metal\ B}{Minesite\ cost}$$

(Equation 4.2)

In Equation 4.2, $pdf(F)$ and $pdf(metal\ concentration\ of\ B)$ are the probability density function of the economic feasibility indicator F and the metal concentration of B, respectively. Distribution of metal concentration is obtained directly or calculated based values reported in literature, as shown in Table 4.1.

Table 4. 1 Sources and methods for obtaining/calculating distribution of metal concentration in ore, for six byproduct metals

Byproduct metal element	Distribution of metal concentration
Te	Calculated, based on tellurium/selenium concentration per tonne of copper anode from refineries data, and adjusted for copper ore grade, concentration and smelting efficiency (Green, 2006; Andersson, 2000; Glöser et al., 2013; S&P Global Market Intelligence, 2019b)
Se	
Re	Calculated, based on Re content in Cu concentrates from selected mines, adjusted for Cu content in ore and concentrate (Nadler, 2000; Jiang, Wang, Zou, Zhang, & Liu, 2012; S&P Global Market Intelligence, 2019b)
Ge	Directly obtained from a study that surveys Ge content in ore, in more than 300 deposits worldwide (Max Frenzel et al., 2014)
Cd	Directly obtained from several estimates of Cd content in ore/concentrate, represented in ranges (Andersson, 2000; Schulte-Schrepping & Piscator, 2000; U.S. Geological Survey, 2019a)
In	Directly obtained from worldwide deposit level data (Werner et al., 2017)

For each byproduct metal, the minesite cost used in the Equation 4.2 is the cost for its major carrier metal (zinc or copper). These costs are calculated from the weight average of mine level cost data reported by

SNL Mine Economics in 2018 (S&P Global Market Intelligence, 2019b). For rhenium, selenium and tellurium, only the copper concentrate mines are included as these byproduct metals are not produced in SX-EW mines. Minesite cost is calculated to be 18.9 USD/t of ore treated for byproducts of copper, and 32.6 USD/t for byproducts of zinc.

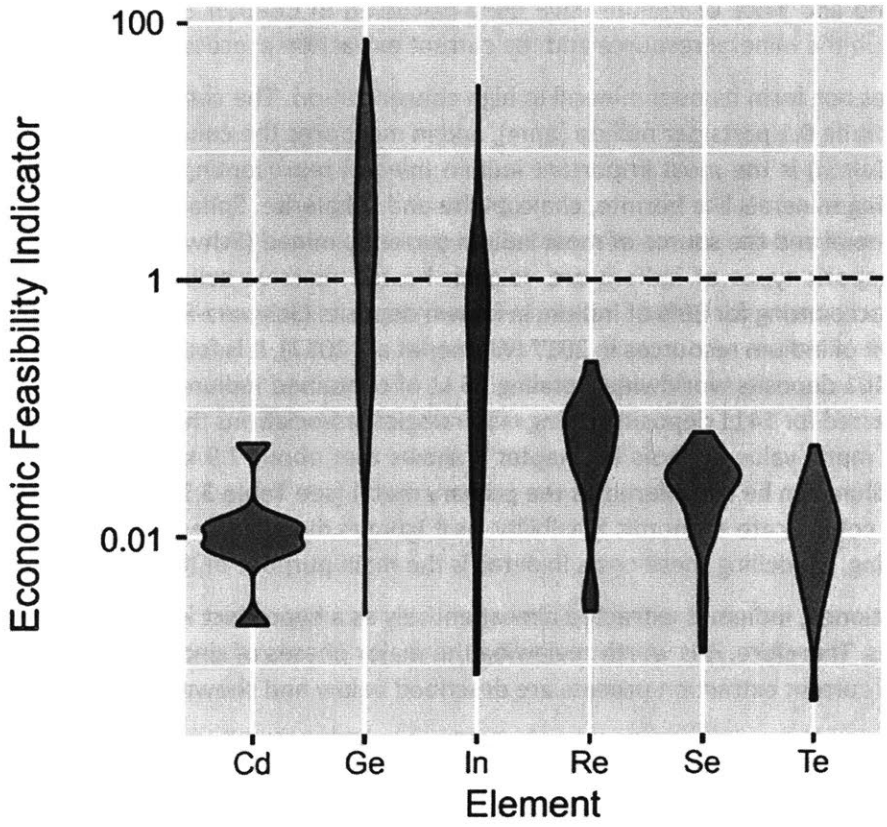

Figure 4. 1 Violin plot of the distribution of economic feasibility indicators, for six byproduct metals. Y-axis is represented in logarithmic scales.

The results on $pdf(F)$ are shown in Figure 4.1 in violin plots, where each shape (violin) represents the smoothed probability density corresponding to an element and the total size of each shape is a constant. The y-axis is shown in logarithmic scales, as distribution of indicators expand over several orders of magnitude. It can be seen that, for cadmium, selenium and tellurium, even the highest values of economic feasibility indicators are still smaller than 0.1, indicating little economic feasibility for alternative extraction processes. The same is true for rhenium, although the highest value is slightly higher at 0.23. For indium and germanium, however, significant portions of their $pdf(F)$ are above 1, indicating the possibility for some deposits to produce these two metals as primary products or co-products if alternative processes are applied.

In what follows, detailed case study is performed on indium. An alternative extraction process is proposed for indium and a cost model is built for the process, allowing further investigation of the economic

feasibility on a deposit level. Indium is chosen over germanium mainly due to deposit level data availability, but the extraction process proposed can be easily extended to germanium.

Case study on indium

The supply, demand and price of indium have been discussed in Chapter 3. Here, a brief overview is provided focusing on the mineral resource and the current extraction process of indium.

Indium usually does not form its own mineral in high concentration. The content of indium in the earth crust is estimated to be 0.1 parts per million (ppm), and in most ores the concentration of indium is 1-50 ppm. Roquesite ($CuInS_2$) is the most important indium mineral representing a trace component in the principal ore-forming minerals like bornite, chalcopyrite and sphalerite. Sphalerite is the most important indium bearing mineral and the source of most indium currently mined (Schwarz-Schampera, 2013). Two most important deposit types of indium are volcanic-hosted massive sulphide and sediment-hosted massive sulphide, accounting for 80% of indium in known deposits (Schwarz-Schampera, 2013). Based on a global assessment of indium resources in 2017 (Werner et al., 2017), it is found that indium content has been reported in 101 deposits worldwide, totaling 76 kt of contained indium. Another 280 kt of indium content can be inferred for 1411 deposits having mineralogical associations that indicate they are indium-bearing. The brief metal value analysis in Chapter 3 shows that about 7.9 kt of indium is contained in deposits where indium can be considered as the primary metal (see Table 3.3). However, this analysis of metal values does not indicate economic feasibility, as it ignores many processing costs in reality such as smelting and refining. Modelling these costs in detail is the main purpose of this case study.

As previously mentioned, indium is extracted almost entirely as a byproduct in zinc production processes in current practices. Therefore, it is worth reviewing the major phases of zinc and indium recovery here. The major steps of current extraction process are described below and shown in Figure 4.2.

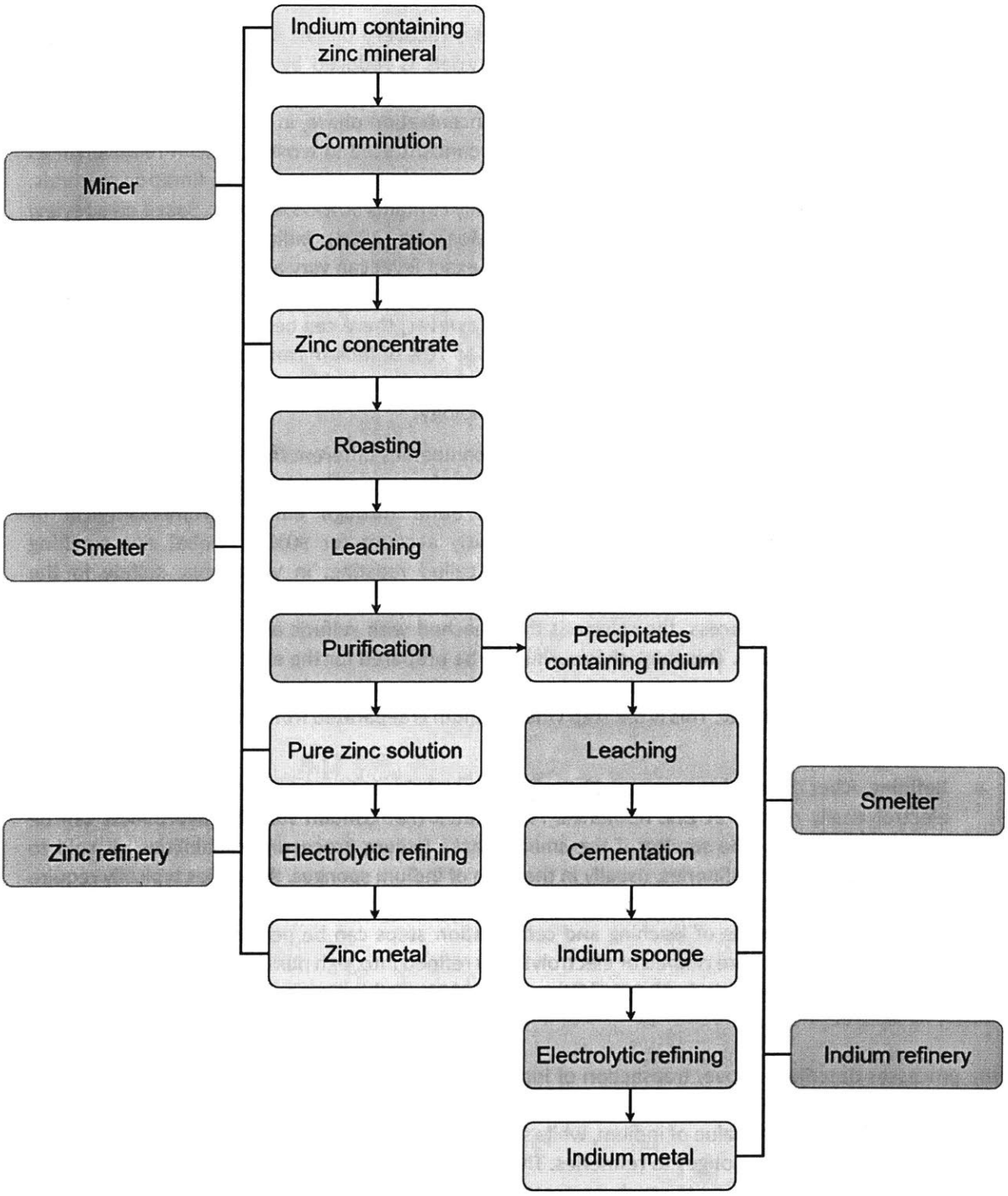

Figure 4. 2 Simplified flowchart of current indium extraction process as byproduct from zinc production. Yellow boxes are used for materials, blue box for processing steps and green boxes for processing facilities

1. **Comminution**. Similar to most base metals, metal recovery of zinc starts with a phase called comminution, in which the size of mineral materials is reduced by crushing and grinding at minesites or in mills.
2. **Concentration**. Comminution is followed by a concentration phase, in which valuable mineral is separated from the waste mineral (gangue) and concentrated to a material with relatively high metal content. In the case of zinc sulfide ores, concentration is usually done by flotation methods. After this step, the resulting zinc concentrate usually contains 50%-55% of zinc. Based on a review of indium processing technology (Alfantazi & Moskalyk, 2003), indium concentration in zinc concentrate is typically around 150 ppm, but the exact level can vary a lot by deposit. It is worth mentioning that, the majority of indium content in ore is not separated from other metals in both the comminution and the concentration steps. However, there can be significant loss of indium content. As mentioned in Chapter 3, around 50% to 70% of indium contained in the ore ends up in the concentrate and the rest ends up in mine tailings and waste. This percentage presents significant space for improvement in mining technology.
3. **Smelting.** In many cases, smelters are owned by companies different from the mines, so the zinc concentrate is sold from miners to smelters. Therefore, smelting can take place at locations distant from the minesite. Smelting can be done through either pyrometallurgical or hydrometallurgical processes. The latter currently account for 90% of global zinc smelting production. Both processes start with a step called roasting, in which zinc sulfide in the concentrate is oxidized to produce a calcine of zinc oxide. Following roasting in the hydrometallurgical process, the calcine is then leached with sulfuric acid to produce a solution containing zinc sulfate. This solution is purified to be prepared for the electrolytic refining of zinc. Impurities in the solution is precipitated out, containing various minor metals including indium, gallium, germanium, etc. This is the step where indium is separated from the primary metal in the ore.
4. **Refining**. After the smelting process, the primary metal zinc is separated from its byproducts, and electrolytically refined at zinc refineries. Precipitates that contain valuable byproducts can be either discarded by the smelter if the smelter lacks indium processing capabilities, or sold to downstream indium refineries, usually in the form of indium sponges. Refineries typically require a minimum 95% indium content in the sponge (Lokanc et al., 2015) In order to reach that level of metal content, a series of leaching and cementation steps can be performed, and the indium sponge can be either fire refined or electrolytically refined into high purity indium metal. Standard indium metal grades include 99.99% (4N) to 99.99999% (7N) indium purity.

In the processes described above, transaction of intermediate materials take place between miner and smelter, and between smelter and refinery. When miners sell zinc concentrate to smelters, they are credited only partially for the value of indium, while smelters can receive a much larger fraction of indium value when they sell indium sponges to refineries. This is because downstream processors usually charge the upstream for processing costs, such as treatment charge, refining charge and other possible deductions. The closer a processor is to the final market of the metal, the more value it can get. Based on the technical report from a zinc-indium-tin coproducing mine in Mount Pleasant, Canada (Thibault, McKeen, Scott, Boyd, & Hara, 2010), it can be calculated that sellers of zinc concentrate only get 15% of indium metal's market value, while sellers of indium sponge can get 71% of indium metal's market value. This gap represents significant opportunity for extra profit, if miners can separate indium from zinc minerals and process it onsite.

However, earlier separation of indium is thermodynamically challenging under current zinc extraction processes. The bottleneck lies in the roasting step, in which metal sulfides react with oxygen to produce metal oxides. To examine the possibility of phase separating indium, the Kellogg diagram of the Zn-S-O and the In-S-O systems is shown in Figure 4.3.

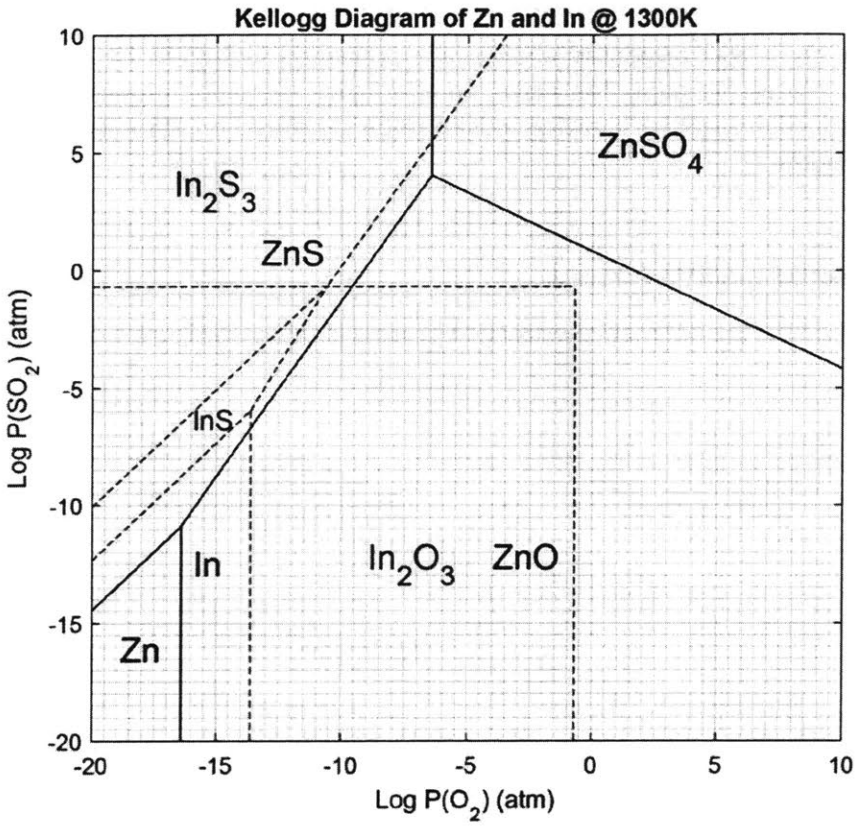

Figure 4. 3 Kellogg diagram of the Zn-S-O and the In-S-O systems, at constant temperature 1300K. Zinc phase are separated by black solid lines and indium phases by dashed blue lines. The red dashed line represents the relationship $P(SO_2) + P(O_2) = 0.21\ atm$.

Kellogg diagram is a useful tool for investigating the various phases that can occur during the roasting process (Habashi, 2017). The phase relationship in a metal-oxygen-sulfur ternary system can be described in a two dimensional space where the logarithmic value of partial pressures $log\ P(SO_2)$ and $log\ P(O_2)$ are usually chosen as the two coordinates. The equilibrium of condensed phases are represented by lines, and areas in the diagram represent phases that are stable under the specified partial pressures. Temperature is fixed in Kellogg diagrams to reduce one degree of freedom in the system. Details of constructing Kellogg diagrams can be found in metallurgy textbooks for the interested readers (Habashi, 2017).

In Figure 4.3, temperature is fixed at 1300K. By comparison, the roasting of sulfide reaction is usually carried out at and above 1100K (Shamsuddin, 2016). If the roasting is operated in air, reaction should follow the red dashed line from upper left to lower right where $P(SO_2) + P(O_2) = 0.21\ atm$. One common way to separate metals in the sulfides is selective oxidation, which is used in copper smelting to

selectively oxidize iron sulfides. However, in the case here, it can be seen that indium sulfides will be first oxidized and then followed by zinc oxidation. Both indium oxide and zinc oxide have very high melting temperatures (2180K and 2250K), so phase separating indium by selective oxidation is infeasible during roasting. Another possibility for phase separation is in the lower left regions in Figure 4.3 where the hope is to stabilize indium metal under the presence of zinc oxide. However, this is also practically infeasible because it requires roasting to be operated under very low oxygen partial pressure.

The thermodynamic challenges presented above have prevented indium to be separated from zinc concentrate in early processing steps. Therefore, an alternative extraction process is proposed below based on a direct reduction reaction, allowing indium to be separated on the minesite. This process is described in details below.

Description of alternative extraction process

The simplified flowchart for the alternative extraction process is shown in Figure 4.4.

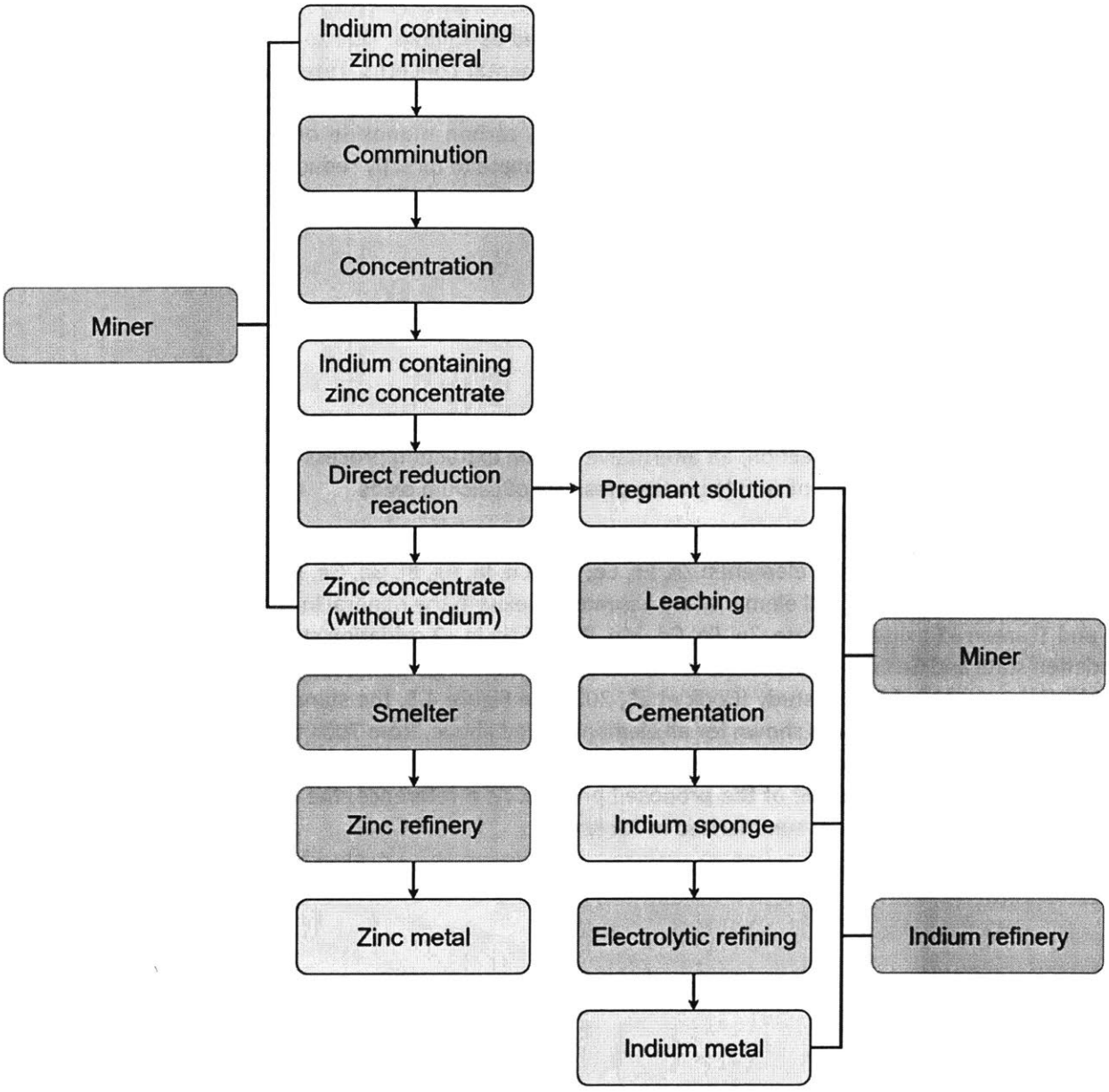

Figure 4. 4 Simplified flowchart of alternative indium extraction process. Yellow boxes are used for materials, blue box for processing steps and green boxes for processing facilities.

Compared to the current process shown in Figure 4.2, the key difference in the alternative process is that indium is separated from zinc concentrate in a direct reduction reaction right after the concentration step, instead of being separated after roasting, leaching and purification. This key step allows indium to be separated at the miner's location instead of at the smelter's location. Following the separation, zinc concentrate (without indium) can be sold to smelters and zinc refineries and for further recovery, similar to conventional processes. The indium containing pregnant solution also be recovered onsite, with the addition of a processing facility for leaching and cementation.

The details of this direct reduction reaction is introduced as follows. Due to the large amount of SO_2 emission from sulfide roasting and associated environmental concerns, researchers have looked into processes that fix sulfur content in the sulfide ores (C. H. Huang, Lin, & Chen, 2005; Rao & El-Rahaiby, 1985). One way is to use a reductant (such as carbon, carbon monoxide or hydrogen) along with a scavenging agent such as lime, limestone or sodium carbonate to directly reduce metal sulfides into pure metal. For example, the use of carbon as reductant and calcium oxide as sulfur fixing agent lead to the following reaction:

$$MS + CaO + C = M + CaS + CO$$

The metal M in the above reaction is in +2 oxidation state, but this can be easily extended to +3 oxidation state as well. Following this reaction, an alternative indium extraction process is proposed based on the direct carbothermic reduction of sulfides in the presence of calcium oxide.

Based on sphalerite mineral composition from literature (Cook et al., 2009), it is assumed that the original mineral contains the following elements: Zn, Fe, Cd, Mn, Cu, In, Ag, Bi, Ga, Ge, Pb, Sb, Sn and Tl (element symbols used for simplicity). All elements are assumed to exist in the mineral in sulfide phases, where Cu, Ag and Tl are in +1 oxidation state, Zn, Fe, Cd, Mn, Pb and Ga in +2 oxidation state, In, Bi, Sb and Sn in +3 oxidation state and Ge in +4 oxidation state. The determination of oxidation states is based on substitution mechanisms proposed in this study (Cook et al., 2009). In Figure 4.5, the standard Gibbs free energy of the direct reduction reaction is shown for all elements listed above, from 700K to 1300K. Calculations are based on standard thermodynamic tables (Barin, 1995) and the red dotted line represents reaction at 900K, the reaction temperature of the proposed process. As a reference, the melting point and boiling point of involved elements are summarized in Table 4.2.

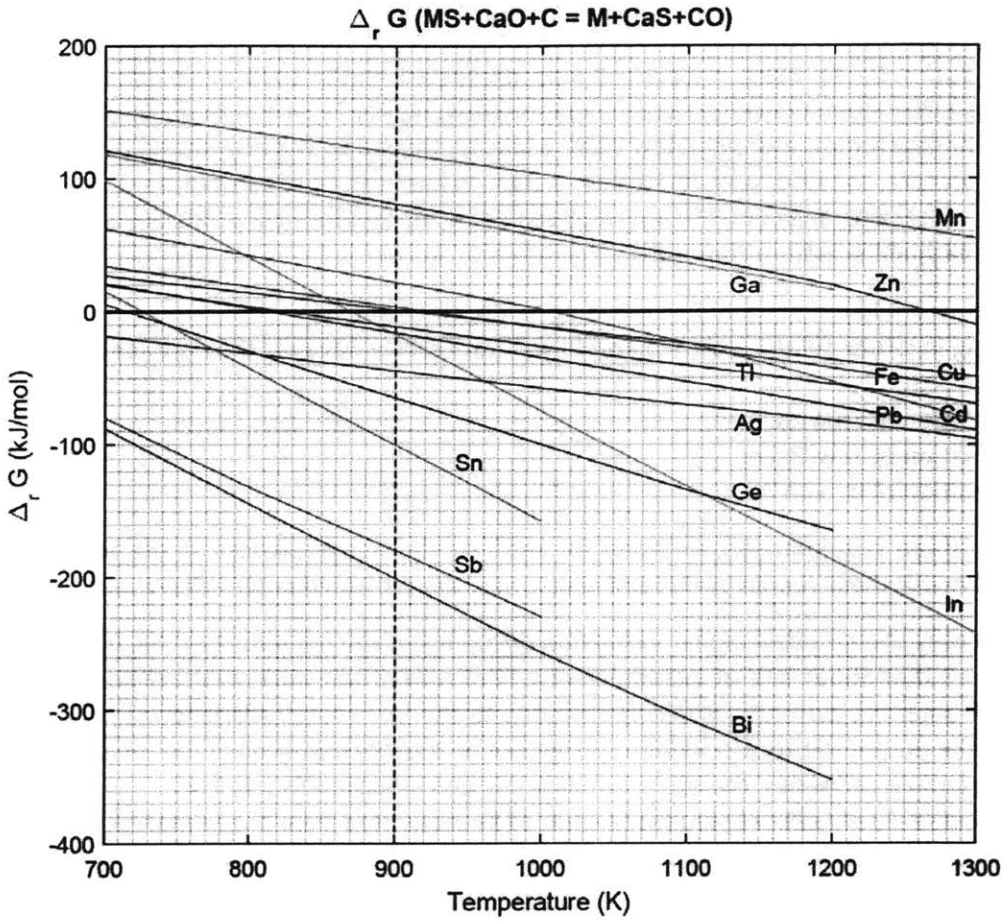

Figure 4. 5 Standard Gibbs free energy of reaction for the direct carbothermic reduction reaction: MS + CaO +C = M + CaS + CO. Reaction at 900K is highlighted with a red dashed line.

Table 4. 2 Melting point and boiling point of metal elements in the sphalerite. Cells highlighted in light yellow color indicate metals that melts at 900K, the proposed reaction temperature.

Element	Melting point (K)	Boiling point (K)	Element	Melting point (K)	Boiling point (K)
Zn	693	1180	Ag	1235	2435
Fe	1811	3134	Bi	545	1837
In	430	2345	Ga	303	2673
Cu	1358	2835	Ge	1211	3106
Cd	594	1040	Sb	904	1908
Mn	1519	2334	Sn	505	2875
Pb	601	2022	Tl	577	1746

It can be seen from Figure 4.5 that, at 900K, the reactions for Mn, Zn, Fe, Cu, Cd and Ga are not spontaneous ($\Delta_r G < 0$) so these metals will stay unreacted in the solid sulfide phases. The direct reduction for all other elements will proceed spontaneously. In, Pb, Tl, Sn and Bi will be reduced to liquid phase as their melting temperature is below 900K, while Ag, Ge and Sb will be reduced to solid metals the solid phase. Therefore, together with four other metals, indium can be separated from zinc in the liquid phase. A series of leaching and cementation steps can be further performed, producing a final product of indium sponge with >95% indium content:

1. Cool down liquid metal solution containing In, Pb, Tl, Sn and Bi;
2. Leaching in dilute sulfuric acid. Pb and Bi will not resolve because they are resistant to sulfuric acid;
3. Cementation of Sn with In;
4. Cementation of Tl with Zn;
5. Cementation of In with Al.

As a reminder, three requirements are listed for such an alternative process at the beginning of this chapter. Here I revisit these requirements and assess how the proposed process have met them:

1. ***The process should allow higher extraction efficiency of the byproduct metal.*** It is mentioned in Chapter 3 that about 30% of indium-bearing zinc concentrate worldwide are not sent to indium capable smelters currently, which contributed to the low overall efficiency of indium recovery. Under the proposed process, indium sponge can be directly produced at the miners' location and sent to indium refineries, therefore avoiding this loss at incapable smelters.
2. ***The process should allow byproduct metals to be separated from the primary product at earlier processing stages.*** Indium separation takes place at minesite instead of at the smelter, under the proposed process.
3. ***Compared to current extraction processes, there should be enough economic advantage from the alternative process so that metal processors can be incentivized to adopt the new process.*** As mentioned earlier, there is a significant gap between indium content credited in concentrate and that in indium sponge, which is an opportunity for revenue. If the extra revenue is larger than the extra cost of direct reduction, leaching and smelting, adopting the new process would be beneficial, at least from an operating margin perspective.

The last requirement above depends on characteristics of the mine, such as indium grade and zinc grade in ore, mining cost, etc. In the next section, a detailed cost model is built in order to further assess the benefit and the economic feasibility of the alternative process, at a deposit level.

Cost model for alternative process

The direct reduction reaction discussed above is the key step in the proposed alternative process. To model the cost associated with this reaction, a hypothetical zinc concentrate is considered, with chemical compositions listed below: 54%Zn, 8%Fe, 2%Cd, 2%Mn, 0.5% Cu, 0.5% Pb, 100ppm In, and 1ppm for Ag, Bi, Ga, Ge, Sb, Sn and Tl. 54% of zinc is a typical zinc content in zinc concentrate, based on industry standards (Nyrstar, 2009; Schwartz, 2015). Contents of other metal elements are obtained by first rounding up the median metal contents across sphalerite samples in literature (Cook et al., 2009), and assume that all elements are enriched by a similar factor from mineral to concentrate. While the concentration of all these elements above may vary by two orders of magnitude depending on deposit, the above composition represents that of a typical zinc concentrate. The cost model developed here will also be applied to indium deposits later, to explore the variation of different ore compositions.

It is further assumed that all elements in this hypothetical concentrate are in sulfide phases, and the direct reduction is performed under 900K and 1atm. The total enthalpy change in the system is used as a proxy for energy consumed in the reaction. It can be calculated as the sum of two components: 1) the enthalpy change to heat the reactants (sulfides, carbon and lime) from room temperature (298K) to 900K; 2) the enthalpy change of reaction at 900K. This can be described by Equation 4.3:

$$\Delta H_{concentrate} = \sum_{R} n_R \cdot (H_R^{900K} - H_R^{298K}) + \sum_{MS} n_{MS} \cdot \Delta H_{r,MS}^{900K}$$

(Equation 4.3)

The first term on the right hand side corresponds to the first component, where the sum is over all reactants and $H_R^{900K} - H_R^{298K}$ is the per mole enthalpy change of reactant R in its standard state. Note that we use R to represent all components in the ore, including those that do not participate in the reduction reaction. The second term is summed over all sulfides that participate in the direct reduction reaction MS + CaO +C = M + CaS + CO. n_{MS} is the chemical amount of sulfide metal M in mole, and $\Delta H_{r,MS}^{900K}$ is the standard enthalpy change of reaction for the direct reduction reaction.

To calculate the value of $\Delta H_{concentrate}$ per tonne of concentrate, the enthalpy change corresponding to elements with 1ppm concentration is neglected due to their insignificance. Also, it can be seen from Figure 4.5 that out of the major elements in the concentrate, sulfides of Zn, Fe, Cd, Mn and Cu do not react spontaneously. Therefore, only the enthalpy change to heat these sulfides are included in Equation 4.3, while the enthalpy change of reaction is calculated for Pb and In only. Based on standard thermodynamic tables (Barin, 1995), $\Delta H_{concentrate}$ is calculated to be 743.3 MJ/t for the hypothetical concentrate. It is assumed that there is no loss of heat, and that coal is used to provide heat to the system. This is equivalent to using 31kg of coal per tonne of concentrate (heating value of coal is 24 MJ/kg (Tad W. Patzek, 2004)). Based on an average coal price of 101.5 USD/t from the last ten years (International Monetary Fund, 2019), the cost of coal used in reduction reaction per tonne of concentrate is about 3.14 USD. The cost of energy is usually only a fraction of total minesite cost, while other costs such as labor and reagents are also important. Based on the cost data for operating primary zinc mines in 2018 (S&P Global Market Intelligence, 2019b), it can be calculated that the fraction of energy cost in total minesite cost is 22.4% on average. Therefore, assuming that the cost structure for the direct reduction reaction is similar to currently operating mines, the total cost for the reaction process should be 14.05 USD/t of concentrate.

In addition to minesite cost (costs for mining, milling and direct reduction), the total cash cost for a miner also includes treatment charge for zinc concentrate, refining charge of indium sponge, offsite transportation cost and royalty. Adding in these costs, the total cash cost per tonne of ore processed, C_{tot}, can be calculated based on Equation 4.4 to 4.6. The miner's revenue comes from selling zinc concentrate to zinc smelters and indium sponge to indium refinery, and the calculation of total revenue is expressed in Equation 4.7.

$$PM_{Zn} = x_{Zn,Ore}\eta_{O2C}\rho_{Zn}$$

$$PM_{In} = x_{In,Ore}\eta_{O2C}\eta_{C2S}\rho_{In}$$

$$C_{tot} = C_{M\&M} + C_{DR}\frac{x_{Zn,Ore}}{x_{Zn,Conc}} + (C_{TC,Zn} + C_{OS} + C_R)PM_{Zn} + C_{RC,In}PM_{In}$$

$$R_{tot} = PM_{Zn}P_{Zn} + PM_{In}P_{In}$$

$$CM_{tot} = R_{tot} - C_{tot}$$

(Equation 4.4 to 4.8)

Table 4. 3 Description of variables used in Equation 4.4 to 4.7

Symbol	Value	Description	Unit	Data source
PM_{Zn}	71.64	Payable amount of zinc in the concentrate	Kilogram of zinc metal per tonne of ore treated	Calculated from Equation 4.4
PM_{In}	11.80	Payable amount of indium in the sponge	Gram of indium metal per tonne of ore treated	Calculated from Equation 4.5
C_{tot}	94.56	Total cash cost	USD per tonne of ore treated	Calculated from Equation 4.6
R_{tot}	174.44	Total revenue from zinc and indium	USD per tonne of ore treated	Calculated from Equation 4.7
CM_{tot}	79.89	Total cash margin	USD per tonne of ore treated	Calculated from Equation 4.8
$x_{Zn,Ore}$	10	Zinc content in ore	%	Typical zinc content in ore, based on literature (Cook et al., 2009)
$x_{In,Ore}$	20	Indium content in ore	ppm	Assumed value
$x_{Zn,Conc}$	54	Zinc content in concentrate	%	Typical zinc content in concentrate, based on industry standard (Nyrstar, 2009; Schwartz, 2015)
η_{O2C}	84.28	Recovery efficiency from ore to concentrate	%	Weighted average from zinc primary mine costs in 2018
ρ_{Zn}	85	Payable fraction of zinc in the concentrate	%	Typical value based on industry standard (Nyrstar, 2009; Schwartz, 2015)
η_{C2S}	80	Indium recovery efficiency from concentrate to sponge	%	Assumed value

ρ_{In}	87.50	Payable fraction of indium in the sponge	%	Typical value based on industry standard (Thibault et al., 2010)
$C_{M\&M}$	25.58	Mining and milling cost	USD per tonne of ore treated	Weighted average from zinc primary mine costs in 2018 (S&P Global Market Intelligence, 2019b)
C_{DR}	14.05	Direct reduction reaction cost, based on 54% Zn in concentrate	USD per tonne of concentrate treated	Calculated based enthalpy change of system, and coal price of 101.5 USD/t
$C_{TC,Zn}$	589.75	Treatment charge of zinc concentrate, paid to smelter	USD per tonne of paid zinc in concentrate	Weighted average from zinc primary mine costs in 2018
$C_{RC,In}$	73930	Refining charge for indium sponge, paid to refinery	USD per tonne of paid indium in sponge	Based on cost from Mount Pleasant mine technical report (Thibault et al., 2010)
C_{OS}	164.65	Offsite cost	USD per tonne of paid zinc in concentrate	Weighted average from zinc primary mine costs in 2018 (S&P Global Market Intelligence, 2019b)
C_R	132.00	Royalty	USD per tonne of paid zinc in concentrate	Weighted average from zinc primary mine costs in 2018 (S&P Global Market Intelligence, 2019b)
P_{Zn}	2343.52	Price of zinc metal	USD per tonne	2008-2017 annual average price (U.S. Geological Survey, 2019g)
P_{In}	555.37	Price of indium metal	USD per kilogram	2008-2017 annual average price (U.S. Geological Survey, 2019f)

It is mentioned earlier that a zinc miner gets paid only 15% of the value of indium in the conventional under the conventional extraction process. The cash margin under the conventional process can be therefore calculated as

$$PM_{Zn} = x_{Zn,Ore}\eta_{O2C}\rho_{Zn}$$

$$PM_{In,0} = x_{In,Ore}\eta_{O2C}\rho_{In,0}$$

$$C_{tot,0} = C_{M\&M} + (C_{TC,Zn} + C_{OS} + C_R)PM_{Zn}$$

$$R_{tot,0} = PM_{Zn}P_{Zn} + PM_{In,0}P_{In}$$

$$CM_{tot,0} = R_{tot,0} - C_{tot,0}$$

(Equation 4.9 to 4.13)

where the subscript 0 indicates the conventional extraction process, and $\rho_{In,0} = 0.15$. The difference in total cash margin is

$$\Delta CM_{tot} = CM_{tot} - CM_{tot,0} = (PM_{In} - PM_{In,0})P_{In} - C_{DR}\frac{x_{Zn,Ore}}{x_{Zn,Conc}} - C_{RC,In}PM_{In}$$

$$= x_{In,Ore}\eta_{O2C}[P_{In}(\eta_{C2S}\rho_{In} - \rho_{In,0}) - C_{RC,In}\eta_{C2S}\rho_{In}] - C_{DR}\frac{x_{Zn,Ore}}{x_{Zn,Conc}}$$

(Equation 4.14)

Plugging in values from Table 4.2, this difference can be expressed numerically as

$$\Delta CM_{tot} = 0.214x_{In,Ore} - 0.260x_{Zn,Ore}$$

(Equation 4.15)

Where $x_{In,Ore}$ is expressed in ppm and $x_{Zn,Ore}$ is expressed in percentage. Therefore, as long as $\frac{x_{In,Ore}}{x_{Zn,Ore}} > 0.822$, the alternative process is more profitable from a total cash margin perspective. Using an average zinc ore grade 4.4% (S&P Global Market Intelligence, 2019b), this means that as long as indium content in ore is greater than 3.6ppm in an average zinc mine, the alternative process would be more profitable. Based on indium deposit data (Werner et al., 2017), the weighted average indium content in all indium reporting deposits is 24.3ppm, much higher than the cutoff requirement. Therefore, the alternative process should lead to higher operating profit for most zinc mines containing indium.

The alternative process is highly favorable from a total cash cost perspective due to two reasons. First, indium is a relatively expensive metal, so the gap between selling indium in concentrate and selling indium as a sponge presents a great opportunity for profit. Second, the proposed direct reduction reaction is not energy intensive, and the total cost for reaction plus refining charge for indium can be well covered by the extra profit from indium.

Moreover, there is also significant improvement from the alternative process in terms of the overall recovery efficiency: while the conventional extraction process leads to 15% to 20% overall recovery efficiency (Lokanc et al., 2015), the proposed alternative process leads to ~55% overall recovery efficiency, if refining efficiency is similar to current industry average. This improvement mainly stems from two aspects. The first is that the ore to concentrate recovery efficiency from the alternative process (~85%) is significantly higher than that of the current extraction process (50% to 70%), because miners are more aware of the value of indium under the alternative process. Such an improvement is totally possible:

according to Lokanc et al. (Lokanc et al., 2015), the ore to concentrate recovery efficiency for indium at an indium primary mine Toyoha is 96%, which is the same with its zinc recovery efficiency. Secondly, while 30% of indium in zinc concentrate is currently lost due to being sent to smelters not capable of extracting them, this loss is avoidable under the alternative process because the production of indium sponge is directly performed at minesite. Therefore, there could be significant improvement in indium supply under the alternative process.

In what follows, a deposit level cost analysis is performed on the indium deposit dataset from Werner et al. (Werner et al., 2017). The cost model developed in this section is applied to each deposit, allowing the economic feasibility of the alternative process to be investigated under a more realistic setting.

Deposit level analysis

The deposit level dataset from Werner et al. (Werner et al., 2017) includes 101 deposits that have reported indium content, totaling 76 kt of contained indium. Data from these deposits are used in the analysis here. While another 280 kt of indium content can be inferred for 1411 deposits, these deposits are not included in the analysis due to their high uncertainty in metal concentrations. Only the metal content of Zn, Sn, Ag, Au, Pb and Cu are reported in this dataset. Because the focus of the alternative process is on miners producing zinc concentrate, tin, gold and lead are not considered in the cost analysis. Silver is considered because silver content in zinc concentrate is commonly credited in industry standards (Nyrstar, 2009; Schwartz, 2015). Future work could explore the cost/profit indication of co-producing zinc concentrate with copper and tin concentrates.

69 out of the 101 deposits reported zinc content, ranging from 0.05% to 27.3%. The rest 32 deposits do not report zinc content, so it is assumed that they do not contain zinc in minerals. Consider a mining and milling cost of 25.58 USD/t (see Table 4.3), and assume that mining and milling cost account for 48% of total cash cost (calculated weighted average from zinc primary mines in 2018, based on data from SNL), this means that revenue from metals have to be at least 53.34 USD/t in order to maintain a positive operating margin. In the 32 deposits that do not contain zinc, the highest indium content is 140ppm, equivalent to 45.87 USD/t using indium price from Table 4.3. This means that revenue from indium alone cannot cover operating costs even considering 100% recovery efficiency, 100% payable fraction and zero refining charge. Therefore, these 32 deposits are considered economically infeasible under the alternative process proposed. 7 deposits out of these 32 can potentially be profitable if producing tin, copper, silver or gold as primary metal under other extraction processes. Together these 7 deposits contain about 500t of indium resources.

Next, the cost model described by Equation 4.4 to 4.8 is applied to 69 deposits containing zinc. As mentioned previously, silver credit in the zinc concentrate is included to calculate the total cash margin. The resulting margin curve is shown in Figure 4.6. Along the x-axis, each bar and each horizontal segment of the red line corresponds to an indium deposit, and the width of the bar and the segment shows the amount of indium contained in each deposit. The height of the red line corresponds to scales on the left y-axis, and represents the total cash margin in USD per tonne of ore (pto) processed. The 69 deposits are plotted from left to right in descending order of margin. The height of bars corresponds to percentages on the right y-axis, and represents the fraction of revenue from indium for each deposit under the proposed alternative extraction process.

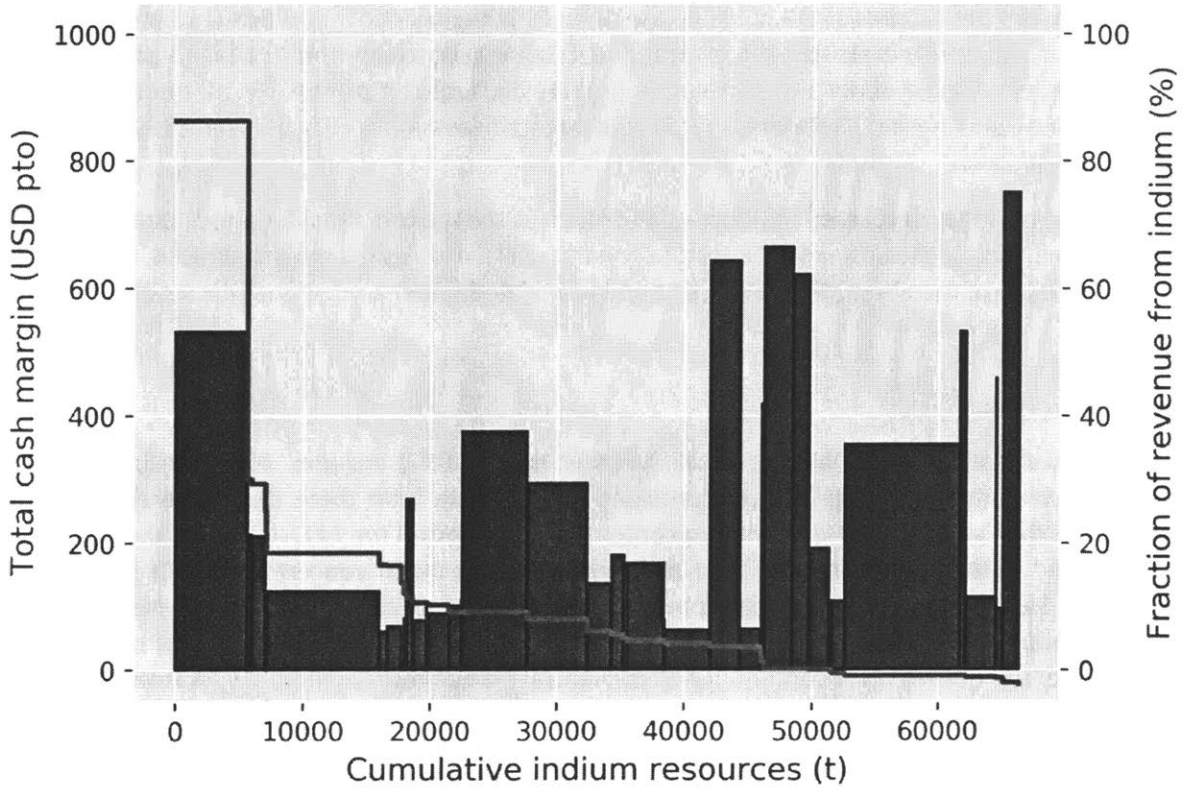

Figure 4. 6 Total cash margin and fraction of revenue from indium under the proposed alternative process, for 69 indium deposits from Werner et al. (Werner et al., 2017)

In the beginning of this chapter, three requirements are described for an alternative extraction process. To expand the third economic requirement, I further define three criteria for the economic feasibility of the alternative process:

1. **The total cash margin must be greater than zero**. This is the minimal requirement that all operating mines must meet in order to ensure a positive cash flow.
2. **The alternative process should lead to greater total cash margin than the conventional process.** Although the alternative process will always lead to higher indium recovery, miners are essentially driven by profitability. Therefore, it is assumed that miners will only consider adopting the alternative process if it is more profitable. This criterion can be expressed as $\Delta CM_{tot} > 0$ and calculated based on Equation 4.15.
3. **The fraction of revenue from indium should be significant enough**. Miners who are likely to adopt the alternative process should be those who are more 'indium aware' because indium is a significant portion of their revenue and can be produced as a coproduct with zinc rather than a byproduct.

In a total of 66.3 kt contained indium from the 69 deposits, the amount of indium coming from deposits meeting criterion 1 and criterion 2 are 51.3 kt and 65.6 kt, respectively. 99% of indium in these deposits satisfy criterion 2, which reflects the universal favorability of the alternative process from a total cash

margin perspective. The amount meeting both criteria is 50.6 kt. The third criterion is a function of the cutoff fraction. Under cutoffs of 20%, 30%, 40%, the amount of indium from deposits meeting all three criteria is 23.3 kt, 16.7 kt, and 11.6 kt, respectively. The indication is that, about 17% to 35% of indium contained in global indium deposits could be produced as co-product of zinc rather than byproduct. Compared to the current production where about 95% of indium is produced globally as byproduct of zinc, the proposed process is a significant improvement in terms of relaxing the potential byproduct supply limitation of indium.

The results above on deposit level economic feasibility are calculated with a set of baseline costs, prices and recovery rates. Here a sensitivity analysis is performed to explore the impact of changing some of these parameters. Results in Table 4.4 show the amount of indium (kt) in deposits that are economically feasible under the alternative process extraction, as function of varying parameters. The cutoff fraction in criterion 3 is presented in three scenarios of 20%, 30% and 40% as well.

Table 4. 4 Sensitivity analysis results on the amount of indium (kt) in economically feasible deposits

Scenarios	Values used	Cutoff fraction for criterion 3		
		20%	30%	40%
Baseline	Baseline values in Table 4.2	23.3	16.7	11.6
Low C_{DR}	$C_{DR} = 70.24$, 500% of the baseline	23.3	16.7	11.6
High C_{DR}	$C_{DR} = 70.24$, 20% of the baseline	23.3	16.7	11.6
Low P_{Zn}	$P_{Zn} = 1061$, lowest price since 2001	34.4	19.6	18.3
High P_{Zn}	$P_{Zn} = 3981$, highest price since 2001	16.7	11.6	11.4
Low P_{In}	$P_{In} = 132$, lowest price since 2001	5.6	0.0	0.0
High P_{In}	$P_{In} = 1206$, highest price since 2001	49.1	38.4	31.4
Low η_{C2S}	$\eta_{C2S} = 70\%$	18.3	13.2	7.9
High η_{C2S}	$\eta_{C2S} = 90\%$	25.0	21.4	16.7

First, it can be seen that the cost of direct reduction, C_{DR}, has no impact on the amount of economically feasible indium even if varied up or down by five times. This means that the cost related to the direct reduction reaction is relatively insignificant compared to the extra profit from recovering more indium. Secondly, price of both zinc and indium metals have significant impact on the result. A higher zinc price or lower indium price means that revenue fraction from indium is lower. It also indicates a decrease in ΔCM_{tot}, the net gain in total cash margin from the alternative process. These two factors contribute to the lower amount of indium from economically feasible deposits, compared to the baseline. On the contrary, a lower zinc price or higher indium price will lead to the opposite. The results are more sensitive to changes in indium price compared to changes in zinc price, due to higher historical volatility of indium

price. Lastly, the recovery efficiency from indium in concentrate to indium in sponge, η_{C2S}, also has an important impact on the result. Therefore, miners operating under the alternative process should consider further increasing that efficiency to gain more benefit from the value of indium.

Conclusions

In this chapter, the feasibility of alternative extraction processes is investigated in detail, for a few byproduct metal systems. Using the ratio between byproduct metal value in ore and ore based minesite cost as a screening indicator, indium and germanium have been found to be the metals of interest. While I only investigated six metals (Cd, Ge, In, Re, Se, Te) that are mainly byproduct of zinc and copper, such a screening assessment can be easily extended to other byproducts metals. While an attempt is made to look for the global distribution of ore grade for these byproduct metals, the values used in this assessment are still incomplete and only represent a fraction of their global resources. As actual deposit level data is often limited for many byproduct metals, future work could explore how to better represent ore grade distribution of a metal statistically, given limited information.

Following the screening assessment, an alternative extraction process is proposed for indium based on a direct reduction reaction of sulfides, and the feasibility of the process is investigated from both thermodynamic and economic perspectives. The proposed reduction reaction can be used to phase separate indium from its carrier metal zinc at minesites, and a series of hydrometallurgical steps can be done to further recovery indium to metal. It is worth noting that, although the thermodynamic feasibility is confirmed in the analysis, other aspects such as kinetics, ore morphology and the yield of the reaction should be further examined through experimental approaches. Such experiments could also be used to better understand the cost, reagent and equipment requirements of the proposed process.

For the deposits level cost analysis, there are also a few limitations and observations that are worth further discussion. First, the cost model developed here only focuses on total cash costs, while the cost components such as development and sustaining expenditure, reclamation costs and corporate taxes are not included in this model. These costs are likely function of production scale, and they important for understanding the net present value (NPV) and the internal rate of return (IRR) for a mining project, which are two critical indicators for determining the profitability and economic feasibility in reality. While it is not the goal of this thesis to develop complete feasibility studies for all indium deposits investigated, a more thorough quantitative investigation on these other cost components could help one better interpret the cost analysis results. Such an investigation is used to model copper production in the next chapter. A second limitation is that I have only modeled cost and revenue for producing zinc concentrate and indium sponges under the proposed extraction process, while the value of other metals such as tin, copper, gold is neglected. Similar alternative processes can be examined for producing indium as coproducts with other metals, and the total economically feasible amount could be further expanded from the values in this analysis.

Results from the deposits level cost analysis show that 17% to 35% of indium in global indium deposits could be potentially produced as coproduct of zinc rather than byproduct in the baseline scenario. Moreover, the overall recovery efficiency could increase from 15%~20% to 55% under the alternative process. Assuming the distribution of ore grade in currently operating indium producing mines is similar to that in these deposits, that means global indium production could increase for 6% to 14%, if all economically feasible mines switch to the alternative process. This represents a potentially large global supply shock, and its implication on indium price and demand should be further investigated. The implication on indium price is particularly important, because it was shown in the sensitivity analysis that

the deposit level economic feasibility is most sensitive to indium price changes (See Table 4.4). In fact, if indium price stays low at the 132 USD/kg level, very little economic feasibility can be found in indium deposits globally. Given the high historical volatility of indium price, producers of indium including miners and refineries should consider better risk management approaches, such as signing long term indium selling contracts, short hedging indium on futures market and diversify revenue sources from a company level. Such approaches will not only help the producing companies to reduce risks, but also stabilize global indium supply.

Chapter 5: Displacement Potential and Market Impact of Metal Recycling, Case Study on Copper

Acknowledgement: The simulation model developed in this chapter has been tested, validated and improved by many industry experts, through in-depth interviews. I would like to appreciate the below interviewees for providing critical feedback: Mr. Shen, General Manager from Ningbo Jintian Refinery; Ms. Ding, Business Manager from Ningbo Jintian Import & Export Company; Wenhao Wang from Zhangjiagang United Copper; Zhenzhong Hu, General Manager from Nanjing Walsin; Adam Estelle, Director for Rod and Bar from Copper Development Association; David Wagger and Joe Pickard from Institute of Scrap Recycling Industries; And many other interviewees who wish to remain anonymous.

Background and Motivation

The amount and fraction of primary production displacing secondary production is recognized as an important variable for the accounting of environmental benefit. A set of literature looking at this problem has been reviewed in Chapter 2. It is found that most studies only implicitly assumed one-to-one displacement, or using heuristics to assume 0% or 50% displacement. Zink et al. (Zink et al., 2016, 2018) have attempted to estimate displacement rate under partial equilibrium analysis, but their methodologies have major drawbacks that bring significant biases to their estimation. Therefore, it is the primary goal of this chapter to develop a methodology that enables better estimation of displacement, and to understand the underlying factors that contribute to a high or low displacement rate.

Without any quantitative estimation, one might wonder: why would secondary production displace primary production? The qualitative answer to this question follows a long chain of market interactions: when the amount of material recycled increases, more scrap will be made available to the market, and the price of scrap should decrease accordingly based on microeconomics theory (Baumol & Blinder, 2015). If secondary material from scrap can substitute primary materials, the price of primary materials should also decrease. Suppliers of primary materials respond to price changes, and as a result decrease the amount of primary materials produced. To estimate the overall effect following an increase in recycling, each link on this chain has to be understood and quantified.

The global copper market is investigated as a case study. Copper is an excellent candidate material for the following reasons: 1) Data on production, consumption and prices are readily available from various scientific literature and industry reports; 2) The size of secondary copper market is comparable to the primary market. As a comparison, global consumption of secondary copper in 2017 is about 9 kt in total while consumption of primary copper is around 20 kt (International Copper Study Group, 2019b); 3) Copper is a common carrier metal for many byproduct metals that have important clean energy applications, such as cobalt, selenium and tellurium.

Here I provide a briefly overview to global copper market, including its primary production process, secondary production and its usage. In terms of primary production, the extraction of copper starts from mining copper ores, which is currently done using either surface mining, underground mining or leaching. Open-pit surface mining is by far the most common mining method for copper. Miners then convert copper ores to copper concentrates which contains about 30% copper content, by crushing, grinding and flotation. Copper concentrate is a commodity that is traded on the market, and the pricing of copper concentrate is up to the negotiation between sellers (miners) and buyers (smelters). Smelters then

perform a series of pyrometallurgical processing steps to first convert copper concentrate to copper matte that contains 50% to 70% copper, and then to blister copper which contains about 98% copper. Finally, blister can be fire refined to produce copper anode, and then electrolytically refined to copper cathode which is often more than 99.99% pure copper. Alternatively, copper recovery can be done through the hydrometallurgical process, in which ore is first leached and then electrowinned. This process is also known as the SX-EW process, which account for about 16% global copper refined production in 2017 (International Copper Study Group, 2019b).

In addition to primary production, secondary copper can be recovered from either pre-consumer scrap (new scrap) or post-consumer scrap (old scrap). New scrap can be obtained from the manufacturing waste of semi-finished product fabricators and final product manufacturers, while old scrap is collected from end-of-life sources. Both old and new scrap can be recovered by fabricators, smelters and refineries. The portion of copper scrap that can be directly utilized by fabricators is called direct melt scrap, as this portion can directly enter the melt of raw materials due to their relatively high quality; The rest has to be refined first before entering use, and is therefore called the refined scrap. Various grades of copper scraps are also commodities, which are purchased and sold between scrap collectors, dealers and scrap consumers.

On the demand/usage side, copper cathode is consumed by fabricators to form semi-finished products in different shapes, such as wires, rods, sheets, plates and tubes. These products are then further manufactured by downstream industries for end-use in different sectors, such as building construction, consumer electronics, communication and transportation.

Methodology for displacement estimation

Introduction of framework

In the following section, the framework and methodology for estimating displacement rate of copper are presented in details. The full simulation model, which includes different types of agents on the global copper supply chain, can be broken down into sub-systems or modules looking at the supply and demand (S&D) of specific commodities.

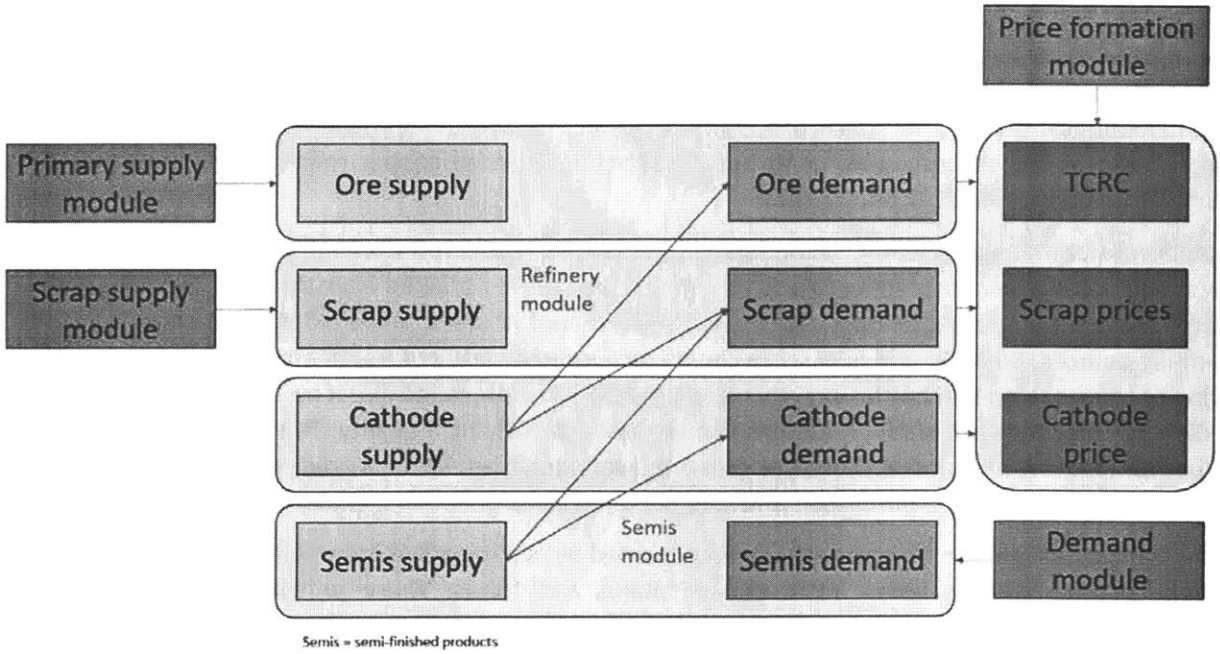

Figure 5. 1 Framework of the simulation system. Semis = semi-finished products

This framework is illustrated in Figure 5.1, where the major modeling components are presented by boxes with different colors. All the major market agents and participants reviewed in the last section are reflected by one or more modules in the full model. There are six major functional modules in the system: 1) Primary supply module; 2) Scrap supply module; 3) Demand module; 4) Refinery module; 5) Semi-finished product fabricator module (semis module); and 6) Price formation module. The boxes marked in yellow and blue represent the S&D of copper related commodities, and the purple boxes represent prices and costs related to those S&D.

Ore S&D: The supply of copper ore is determined by the **primary supply module**, and the total amount of primary mining production is mainly a function of copper cathode price and various mining costs. On the other hand, the demand of copper ore and concentrates is the output of the **refinery module**. Refineries and smelters produce copper cathode from either copper scrap or copper concentrates, and therefore their demand for ore and concentrates is directly a function of primary refined production.

Scrap S&D: The supply of copper scrap is determined by the **scrap supply module**. There are two major sources of copper scrap supply: 1) post-consumer scrap, also known as end-of-life scrap and old scrap; and 2) pre-consumer scrap, or new scrap. The supply of both types of scrap is dependent on many variables such as amount of material flows by end-use sectors, scrap collection rates, technical recycling efficiencies, fabrication efficiencies, etc. However, unlike mining supply, they are not explicitly dependent on prices of copper scrap or copper cathode. Consumption of copper scrap can also be broken down into two categories: 1) refined scrap, which is used by refineries to produce cathodes; 2) direct melt scrap, which is used directly by semi-finished product (semis) fabricators. The amount of refined scrap consumption and direct melt scrap consumption can be estimated from the **refinery module** and the **semis module**.

Cathode S&D: The **refinery module** determines the supply of cathode and the demand for concentrate and refined scrap. It is dependent on both treatment charge and refining charge (TCRC) and scrap prices,

which will be discussed in details in the section for refinery module. Cathode demand, on the other hand, is determined by the **semis module**. Semis fabricators use as both copper cathode and various grades of copper scrap as raw materials, and the amount of particular grades of scrap demanded is also function of the scrap prices.

Semis S&D: Semis demand is the output of **demand module**. This module estimates total copper demand by end use sectors and regions, as function of copper cathode price and various other growth drivers, such as regional per capita GDP. These total copper demand values are then transformed into demand of copper by specific products, in order for the **semis module** to calculate cathode and scrap demand. It is assumed that semis fabricators do not change the stock of semis, and therefore semis production always equals semis consumption.

TCRC, scrap prices and cathode price: The production and consumption (P&C) imbalance of a commodity is an indicator for its market tightness. According to microeconomics theory (Baumol & Blinder, 2015), If there is more production than consumption during a particular period, it indicates that the current price level is beyond equilibrium price and the price of the commodity is expected to drop. On the opposite, if there is supply deficit, price is expected to rise. In the **price formation module**, the P&C imbalance of copper concentrate, copper scrap and copper cathode are drivers of TCRC, scrap prices and cathode price, respectively.

Together, these six modules form a dynamic simulation system. Various scenarios around the copper market can be simulated by changing the initial conditions of the system, or by introducing system shocks. Copper recycling displacement of copper mining production can be estimated by calculating the system response in mining production under a specific copper recycling scenario.

This framework has been tested, validated and improved by industry experts, through more than 20 in-depth interviews. The institutions/companies of these interviewees cover most of the copper supply chain from miners, smelters, refineries, semis fabricators to scrap yard owners and dealers. I have also conducted interviews to more general copper industry participants, such as traders, market analysts and scientists in copper industry and scrap industry associations. These interviews greatly enhanced the validity and accuracy of this simulation model.

In what follows, the details for each module and how they are connected with each other to form the simulation system are discussed.

Primary supply module

The function of the primary supply module is to model the response of copper mining production to varying copper cathode prices. On a high level, cathode price can affect copper mining production through three different mechanisms: A) through changing ore production of operating projects in the short run; B) through changing the incentives of exploration projects and thus changing mine opening decisions; and C) through affecting the remaining net present value (NPV) of operating projects and thus changing mine closure time. A bottom-up mine life simulation model is developed, which captures all three mechanisms described above. This model and the three mechanisms are introduced below.

Mine life simulation model

In the lifetime of a typical mining project, it will go through four stages in general:

1. **Exploration stage**. In this stage, exploration companies will need to perform feasibility studies on behalf of deposits owners, in order to determine the economic, legal, political, and environmental viability of turning deposits into mines. The key economic indicator to determine the possibility of mine opening is the internal rate of return, which will be discussed in details later;
2. **Development stage**. If a deposit is determined to be turned into an operating mine, the necessary processing, transportation, power facilities will be constructed, which takes 2-5 years on average;
3. **Production stage**. Once development and construction is completed, mining production will start. This stage typically involves a ramp up/ramp down period in the beginning/last few years. One important phenomenon during the life of mines is ore grade decline. This is usually due to miners start with richer part of the deposits and then gradually work their way to minerals with lower ore grade;
4. **Closure stage**. After the reserves of a mine have been depleted, a mine will enter the last stage of its life. Closure of a mine typically includes removal of all mining facilities/equipment and building demolition. Another important activity in this stage is mine reclamation, which is the process of restoring the land of mine back to its original natural state. Mine reclamation is an essential part of mining practice for many major mining companies, but it is not yet practiced for all mine sites in the world, unfortunately. Many historical mines have been abandoned without any reclamation, which may cause serious environmental consequences.

The mine life simulation model developed in this thesis captures all four stages described above. Below I will describe the details of this model with the example of a hypothetical deposit. This deposit is being assessed for the feasibility of turning into an operating mine. If feasible, it will turn into an open-pit mine that produces copper from the pyrometallurgical process, and copper will be the only metal to be produced. The operating characteristics of this hypothetical mine is listed in Table 5.1:

Table 5. 1 Description and values of operating characteristics for a hypothetical mine

Mine characteristics	**Values**
Name	Maya
Annual ore capacity (kt)	398.07
Reserves (kt)	48.86
Ore grade (%)	1.29
Recovery rate (%)	99.77
Payable percent (%)	97.00
Minesite cost (US cents/lb)	106.21
Transport and offsite cost (US cents/lb)	6.46
Treatment and refining cost (US cents/lb)	27.67
Royalty (US cents/lb)	32.10
Overhead cost (USD, annual)	707000
Development capital expenditure (USD, annual)	8551000
Sustaining capital expenditure (USD, annual)	273000

Reclamation cost (USD, total)	433000

Here I provide a brief summary of the terms in this table. These terms are mostly consistent with SNL Mine Economics methodology, and the interested readers can refer to (S&P Global Market Intelligence, 2019b) for a more detailed explanation.

All the costs are reported in 2017 constant US dollars. *Minesite cost, transport and offsite cost, treatment and refining cost* (TCRC), and *royalty* are components of the *total cash cost*. The difference between realized metal price (company selling price adjusted for hedging profits and losses) and total cash cost is called *total cash margin* (TCM). According to SNL Mine Economics methodology (S&P Global Market Intelligence, 2019a), total cash cost/margin is 'the most useful measure of short term minesite profitability'. For this reason, TCM will be used instead of cathode price as the independent variable in the regression model for **Mechanism A**.

It is important to note that these total cash cost components shown in Table 5.1 are reported on a *paid metal* basis, i.e., unit costs=total costs/paid metal production. The formula to calculate paid metal production can be expressed as:

Paid metal production = ore capacity * capacity utilization * ore grade * recovery rate * payable amount

(Equation 5.1)

It is assumed that this hypothetical mine, Maya, is constrained by its milling capacity. *Ore capacity* here represents the maximum amount of ore that could be treated by the mill, *ore grade* is the average metal content in ore entering the mill, *recovery rate* represents the yield rate of the mill. Lastly, the *payable amount* is the amount of metal get paid when a miner sells its concentrate to a smelter. Historically, the payable amount has been set around 97% if the copper concentrate sold meets a minimum copper content of 30% (Schwartz, 2015). This value incentivizes smelters to run at a recovery rate higher than 97%, so that they can earn extra profit from the 'free metal'. On the other hand, mines that use solvent extraction and electrowinning (SX-EW) process to extract copper do not incur the process of selling its concentrate, so the equivalent payable amount is 100%.

Based on the values provided in Table 5.1 and assuming 80% ore capacity utilization (CU), the amount of paid metal production is

Paid metal production = 398.07 kt * 80% * 1.29% * 99.77% * 97% = 3.98 kt

(Equation 5.2)

Overhead cost and sustaining capital expenditure (capex) are components of the *all-in-sustaining cost*. These are the necessary costs to sustain the mining production. As they are not linearly dependent on the amount of metal produced, they are reported as annual costs in dollars rather than on a paid metal basis. Development capex is a non-sustaining capex, as it is assumed to be only spent during the development stage of the mine. The same is true for reclamation cost, which is spent after mine closure. Development capex and reclamation cost can also be seen as the opening and closing costs of a mine.

The costs components above can be used to calculate the expected cash flow during a year, assuming cathode price is known. Assume that owners of Maya have made the decision to turn the deposit into the mine, the cash flow during a year of operation can be calculated as

Cash flow = paid metal production * (cathode price – total cash cost) – overhead cost – sustaining capex

(Equation 5.3)

where paid metal production can be calculated from Equation 5.2 and total cash cost is the sum of four components:

Total cash cost = Minesite cost + transport and offsite cost + TCRC + royalty

= 172.44 US cents/lb = 3802 USD/t

(Equation 5.4)

Assume that the miner of Maya is able to sell its concentrate at the 2018 average LME cathode price of 6372 USD/t, the TCM is then 2570 USD/t. As a comparison, the median 2018 TCM is 2316 USD/t, so Maya's TCM is about 10% higher than the industry average. Cash flow for 2018 is

Cash flow = 3.98 kt * 2570 USD/t – 707000 USD – 273000 USD = 9.265 Million USD

(Equation 5.5)

This amount represents cash flow net of corporate income tax payable to the state. For each operating year, a cash flow amount can be calculated following Equation 5.2 to 5.5. These cash flow values can then be used to calculate other useful metrics, such as NPV and internal rate of return (IRR). All the mine characteristics can be considered as exogenous variables, except for CU, TCRC and ore grade, which are determined by the simulation endogenously. Their functional form and evolution over time are discussed below.

Functional form of CU

In the next section for **Mechanism A** it will be discussed in detail that ore production responds weakly to TCM. Assuming that ore capacity remains constant throughout the mine life, this is equivalent to CU being responsive to TCM. In the mine life simulation model, the formula for calculating CU can be expressed as:

$$Mine\ Capcity\ Utilization = \begin{cases} 0.4,\ if\ in\ ramp\ up\ or\ ramp\ down \\ 0.75,\ if\ not\ in\ ramp\ and\ TCM < 0 \\ CU_0 * \left(\frac{TCM}{TCM_0}\right)^{prod.elas},\ else \end{cases}$$

(Equation 5.6)

First, CU is fixed at 40% if the mine is in the ramp up or ramp down period. Second, if the mine is not in the ramp up/down period but the TCM is negative, the CU is fixed at 75%. This reflects the fact that mines are not likely to shut down or operate with very low capacity before the depletion of reserves. Even when profits are bad, mining companies could still operate under negative TCM and sometimes stockpile their concentrates in expectation of rising price in the future. Putting the mine on 'care and maintenance' for a long period of time is another activity sometimes practiced under negative TCM, but it is not modeled under this simulation framework, due to its limited occurrence in our data set. Thirdly, when the mine is operating normally with above zero TCM, CU is calculated based on the Cobb-Douglas form where CU_0 and TCM_0 are two tuning parameters. The value on the power term is the production elasticity that will be estimated in the section for **Mechanism A**.

Ore grade evolution

The other important mine characteristic that evolves over time is ore grade. Ore grade decline is a phenomenon that has been well studied over the last few decades, by resource economists and ore geologists (Northey et al., 2014; Yaksic & Tilton, 2009). The speed of ore grade decline is first modeled by Samuel Lasky in his 1950 publication *How tonnage and grade relationships help predict ore reserves* (Lasky, 1950), in which he predicts that the cumulative amount of ore extracted can be used to predict the grade of the next increment of ore. However, this method is not compatible with the model developed here, in which the focus is to estimate annual ore grade evolution at a deposit level. Therefore, the log-log relationship between ore grade and cumulative ore extracted is used here, as suggested by Cargill et al. (Cargill, Root, & Bailey, 1980, 1981). This relationship can be described by

$$Log(ore\ grade)=\alpha+\beta \cdot Log(\frac{cumulative\ ore\ extracted}{ore\ capacity})$$

(Equation 5.7)

where α and β are two parameters reflecting the initial ore grade and the speed of ore grade decline. The original form of this relationship has been adjusted, by normalizing cumulative ore extracted with ore capacity. β is the ore grade elasticity parameter that needs to be tuned on a mine by mine basis, and this tuning process will be discussed in detail in a later section.

It is worth pointing out that, ore grade changes continuously with each infinitesimal amount of ore extracted, in the above formula. However, mining production in the simulation is discretized on an annual basis. Therefore, ore grade calculated from this formula is used as the average ore grade of annual production, instead of the marginal ore grade of an infinitesimal incremental amount. Furthermore, at the start of mine life, cumulative ore extracted is zero, which leads to an infinite term on the right hand side of Equation 5.7. This issue is avoided by setting the 'initial' ore grade to be the average ore grade of the first year mining production.

Mine closure decision making

A time series of cash flow can be calculated based on the initial mine characteristics and their evolution described above. These cash flow amounts can then be used to calculate the NPV of the mining project. NPV is one of the most important financial concepts in mine planning and it is closely related to the decision making of mine opening and closure (Asad & Topal, 2011; Nieto, 2007; Rendu, 2014). Conceptually, NPV is the sum of expected cash flow generated from a project, in today's cash equivalent. Future cash flow are discounted at some rate, assuming that cash can always be invested on alternative projects to earn interests. The mathematical formula for calculating NPV is

$$NPV_d = \sum_{t=0}^{T} \frac{C_t}{(1+d)^t}$$

(Equation 5.8)

where d is the discount rate, t=0,1,...T is the index for year, and C_t is the undiscounted cash flow (positive or negative) generated in year t. t=0 corresponds to the first year in which NPV is calculated, and it is assumed that the first year cash flow is not discounted.

Considerable research in the field of mining economics is dedicated to developing analytical solutions and computer algorithms to maximizing NPV (Asad, 2007; He, Zhu, Gao, Liu, & Li, 2009; Ahmadi, 2018). In practice, management of a mining project can review their production plans under expected market conditions throughout the life of mine, and change production schedules based on the objective of maximizing NPV. The decision of whether a mine should close is based on this objective in the simulation model. The two examples below can be considered to get a better idea of how mine closure is decided based on maximizing NPV.

For the first example, consider the simplest case towards the end of a mine's life. As production cumulates, minesite cost on a paid metal basis will increase as ore grade declines. Assume that cathode price is expected to stay constant, cash flow will eventually turn negative if production continues. If there is no reclamation cost, then a mine should close in the first year when negative cash flow is expected. The NPV at that point is negative, and will keep dropping if production continues. Therefore, the decision based on maximizing NPV is mine closure in the first year of expected negative cash flow.

As a more sophisticated example, consider the case of Maya towards its end-of-life. Different from the first example, there is a reclamation cost of 433000 USD, which is expected to be spent after mine closure. It is also assumed that the mine will go through a ramp down stage of one year in which CU is fixed at 40%, before it could entirely cease production. When the miner decides whether or not Maya should be closed at year t, two scenarios should be considered: 1). Ramp down the mine at year t, and incur the reclamation cost at year (t+1); 2). Continue production normally at year t, ramp down at year (t+1) and incur the reclamation cost at year (t+2). If scenario 2 leads to a higher NPV, then the mine should continue production. These two scenarios are compared throughout the mine life, until scenario 1 leads to a higher NPV and the mine should start the ramp down process.

Mine opening decision making

The decision on whether a deposit should turn into an operating mine, or mine opening, is a much more complicated one than the decision on mine closure. A miner would need to consider aspects including legal, political, and environmental feasibility on top of economic feasibility in order to make the decision of mine opening. In this simulation model, only the economic feasibility is investigated, and the other aspects are assumed not to be bottlenecks to mine opening.

An important economic indicator that is commonly used by mining companies to assess potential mining projects is IRR (Runge, 1998). IRR can be used to demonstrate the expected profitability of an investment. To calculate IRR, one has to solve the equation below:

$$NPV_r = \sum_{t=0}^{T} \frac{C_t}{(1+r)^t} = 0$$

(Equation 5.9)

The value of r that solves the equation is the IRR of the investment. It has been reported in literature that a value of 15% has been used as a guideline to assess new mining projects (Ramboll IMS Ingenieurgesellschaft mbH, 2016; Runge, 1998; Summers, 1987). This value will be used as a baseline cutoff value for mine opening in the simulation model. For a deposit under consideration of opening, one can first assume that the deposit will open, and then calculate the IRR given 1) the development capex; 2) the cash flow time series in the mine operation period; and 3) reclamation and closure cost. If the calculated IRR is greater than the cutoff, then opening decision should be made.

To summarize, the mine life simulation model developed here captures essential cost and production characteristics in a mine's life, all the way from the development stage to the closure stage. The three mechanisms of cathode price affecting a mine's production in its lifetime is explained in the following.

Mechanism A: price effect on short run production

The first mechanism is price affecting *short run* production. By the definition of traditional micro-economics (Baumol & Blinder, 2015), mining companies cannot change their production capacity in the short run. Therefore, capacity expansion, new mine development and closure are not considered in this period. Under fixed mining capacity, miners can still adjust production levels based on price trends, by adjusting capacity utilization rate. The CU of a mine during a certain period is defined as the ratio between ore production and ore capacity. Historically, global average CU of copper mines have been fluctuating around 75-90% (International Copper Study Group, 2018a).

In order to estimate the response of short run ore production to cathode price, the dynamic panel regression model is used. In the case of one exogenous variable, the standard model form can be expressed as follow,

$$y_{it} = \alpha + \rho y_{i,t-1} + \beta x_{i,t} + \mu_i + \lambda_t + \varepsilon_{i,t}$$

(Equation 5.10)

where i is the index for individual and t is the index for time. y_{it} is the dependent variable, y_{it-1} is the first lag of y_{it}, and x_{it} is the independent variable. The first lag term is included to capture the dynamic feature of the dependent variable, i.e. that the future evolution of y_{it} depend on its own history. α is an intercept term, and there are three separate error terms. μ_i is specific to the individual i and is assumed to be time-invariant. λ_t, the individual-invariant error term, is symmetric to μ_i. These two terms are also called the *unobserved effect* terms. The third term ε_{it} is an idiosyncratic error.

Due to the inclusion of an auto-regressive term, the unobserved effect terms are correlated with the regressors in general, which is also known as lack of strict exogeneity (Stock & Watson, 2003). In such a case, the ordinary least squares (OLS) estimation will no longer be consistent. This can be dealt with by using the generalized method of moments (GMM) framework, which is a standard practice for estimating dynamic panel models. The details of GMM is beyond the scope of this thesis, and therefore not elaborated here. The interested readers can refer to (Arellano & Bond, 1991; Holtz-Eakin, Newey, & Rosen, 1988) for further details.

In the case of modeling short run mining production, the panel model is expressed as

$$log(OP_{i,t}) = \alpha + \rho log(OP_{i,t-1}) + \beta log(TCM_{i,t}) + \mu_i + \varepsilon_{i,t}$$

(Equation 5.11)

where i=1,2,...n is index of the mine, t=1991, 1992, ... 2018 is the time index by year. $OP_{i,t}$ is the ore production by gross weight, and TCM_{it} is the total cash margin, which is the difference between realized copper price and total cash costs. As I mentioned previously, TCM is used here instead of price, because it deducts the mine and time specific total cash cost component, and is a better indicator of short run profitability than cathode price. As a standard practice in econometrics, the logarithmic of $S_{i,t}$ and $TCM_{i,t}$ terms are taken.

The historical production and cost related data use are obtained from SNL (S&P Global Market Intelligence, 2019b). This data set is cleaned and processed through several layers of filters, described below:

1. **Non-continuous production:** Mines that experienced temporary shutdowns in their lives will show non-continuous production patterns. Temporary shutdowns might indicate environmental/ regulatory/ financial challenges outside the forces of price, and are not consistent with the model specification described above. Therefore, mines with such patterns are removed from the data set;
2. **Ramp up/ramp down**: As mentioned earlier, changes in production capacity should not be considered in the short run. However, during the first few/last few years of a mine's life, a mine will go through a ramp up/ramp down period, in order to gradually reach full production capacity/reduce production capacity to zero. These periods are identified and removed from the panel data;
3. **Byproduct mines**: For the most part, copper is the produced as the primary commodity of mining projects in the data set. However, less than 10% of mines (by copper production) produce copper as byproducts. The copper production of these mines should respond more to the prices of their primary commodity (if there is any response) instead of copper. These byproduct mines are therefore removed from the data set;
4. **Supply disruption**: Supply disruption events, such as labor strike, mine site accidents and extreme weather conditions, will affect mine production regardless of copper prices. After identifying the

years and mines under impact of such disruption events, production during these periods is adjusted by removing the years under impact and replace the production by linear interpolation;

5. **Large production swings**: Mine capacity expansion/reduction beyond the ramp up/ramp down period should also be accounted for. If a mine's production has deviated more than 50% from its average production levels, this mine is believed to have experienced capacity changes, and will be removed from the dataset.

After the data cleaning and processing steps described above, the dynamic panel regression model can finally be estimated on the clean dataset. This is implemented through the plm package in R (Croissant & Millo, 2008). Estimated coefficients and their standard deviations are shown in Table 5.2:

Table 5. 2 Summary statistics for regression in Equation 5.11

	Dependent variable: $log(OP_{i,t})$
$log(OP_{i,t-1})$	0.652***
	(0.045)
$log(TCM_{i,t})$	0.008***
	(0.004)
Observations	n=142, T=28, N=1602
Notes:	*p<0.1; **p<0.05; ***p<0.01

In the estimation of standard deviations, a heteroscedasticity and autocorrelation-consistent covariance matrix is used. The coefficients on the first lag of log ore production, and on log TCM, are both significant under a significance level of 0.05.

Following the long run elasticity formula in Equation 3.7 in Chapter 3, it can be calculated that the long run elasticity of ore production on TCM is 0.024, and this coefficient will be used in the mine life simulation model, instead of the short run elasticity of 0.008. The reason is that annual production of a mine in the simulation model does not explicitly depend on its own history, and I would like to choose a coefficient that captures the full effect on ore production. It is worth pointing out that this *long run* coefficient is in an econometrics sense, but it should still be interpreted as *short run* in the sense that capacity changes are filtered out from the data cleaning process.

To get a better sense of the size of price effect through **Mechanism A**, if TCM doubles, ore production will increase by $(2^{0.024} - 1) \times 100\% = 1.68\%$. This represents a very low short run supply elasticity of copper ore production on average.

Mechanisms B: price effect on mine opening

The cathode price of copper in a mine's lifetime will affect its cash flow amounts. Therefore, the IRR of any potential mining project is also a function of cathode price. In mining project exploration, the *long-term price* of copper is often used as a proxy for future price in the potential mine's life time. Here the inflation adjusted 10-year trailing average price is used as the long-term price estimate. For example, if a deposit is being economically assessed in 2019, then the inflation adjusted 2010-2019 average price

becomes the long-term price estimate in the simulation. If the IRR is greater than the cutoff of 15%, then the deposit will proceed to opening in the simulation model.

Therefore, the long-term trailing average price trend will affect the amount of mines opening in a particular year. A high price at one year might not have a significant impact on this amount immediately, since the decision of mine opening is determined by 10-year trailing average price instead of just current price. On the other hand, price at year t can also change the opening decision at year t+9. Therefore, the impact of price on mine opening is lagged but long-lasting.

Mechanisms C: price effect on mine closure

One consequence from the mine closure criterion mentioned earlier is that cathode price towards end-of-life plays a very significant role in determining the year of closure. Miners also need some future cathode price forecasts to calculate the expected cash flow close to the end-of-life, similar to when opening is decided. However, it is assumed that miners only refer to a closer price history for closure decision, and the inflation adjusted 5-year trailing maximum price is used instead of the 10-year average in **Mechanisms B**. The rationale for using a 5-year trailing price rather than a 10-year one is that, at the time when closure is seriously being considered, the remaining mine life should already be relatively short. Also, it is assumed that miners maintain optimistic price expectations towards the mine closing decision: If historical cathode price (last five years) has been high, then a high copper price is also expected in the future; If historical price has been low, then price is expected to recover at least to the 5-year trailing maximum level. If the expected price is not high enough so that a positive cash flow could be maintained, the mine should be closed in the current year.

Another interesting aspect worth mentioning is that the reclamation cost can play a role in delaying mine closure. Since the objective for mine closure decision making is maximizing NPV, then negative cash flows should be preferred to be delayed, other things being equal. A very large reclamation cost would decay to zero if it is delayed for an infinite amount of time. Therefore, towards the end-of-life, mining production could still continue even if it incurs a negative cash flow, as long as that negative amount could be compensated by the discounted amount of reclamation cost. The delay in mine closure should be most significant when the reclamation cost is large relative to the size of metal production.

Model calibration

As I mentioned earlier, there are three important hyper-parameters in the simulation model that needs to tuned in order to mimic the reality. This is done by calibrating mine characteristics obtained from the simulation with that from the historical data.

For calibration of the two parameters in Equation 5.6, TCM_0 is set at 2316 USD/t, the 2018 median TCM of operating mines mentioned in an earlier section. The value of CU_0 is tuned so that the 2018 average CU in the simulation equals to the 2018 global average CU reported by International Copper Study Group (ICSG), (International Copper Study Group, 2018a). The calibrated CU_0 is 87.3%.

The calibration of the ore grade elasticity (OGE) β is done at a mine by mine basis, for each operating mine in the mine characteristics dataset. This parameter essentially reflects the speed of ore grade decline which is different across individual mines. The OGE calibration is done through the following process, for each operating mine:

1. Assume price stays constant at 2018 level, simulate the mine life going forward as a function of an initial OGE. Record a) the cumulative metal production since 2018 to end-of-life and b) the last year of positive cash flow generation;
2. Whenever reserves are reported, compare a) with the 2017 yearend contained copper reserves estimate. If reserves are not reported, compare b) with SNL's projected year of closure;
3. Adjust the value of OGE up if a) is greater than reported reserves, or if b) is later than SNL projected closure year. Adjust the value of OGE down if the opposite is true;
4. Iterate the process until a) is within ±5% of reported reserves, or if b) equals projected closure year. The current value of OGE will be the calibrated value.

The mine life of Maya

Here the result from the mine simulation model is summarized, using the hypothetical deposit Maya as an example. As a reminder, the operating characteristics of Maya are reported in Table 5.1. Using the reserves as a benchmark, the calibrated OGE value is -0.242.

Assume that Maya is being assessed for opening at year 2018, when the average LME cathode price is 6372 USD/t and the inflation adjusted 10-year trailing average price is 7055 USD/t. Using the latter as the long-term price forecast, the mine is expected to generate an IRR of 20.32%, which is above the cutoff of 15%. Therefore, Maya should proceed to open, and it is assumed that the mine will take 3 years to be constructed, during which the annual development capex is 8.55 million USD as reported in Table 5.1. This is the baseline scenario for Maya. The cash flow and production time series are shown in Figure 5.2.

(a)

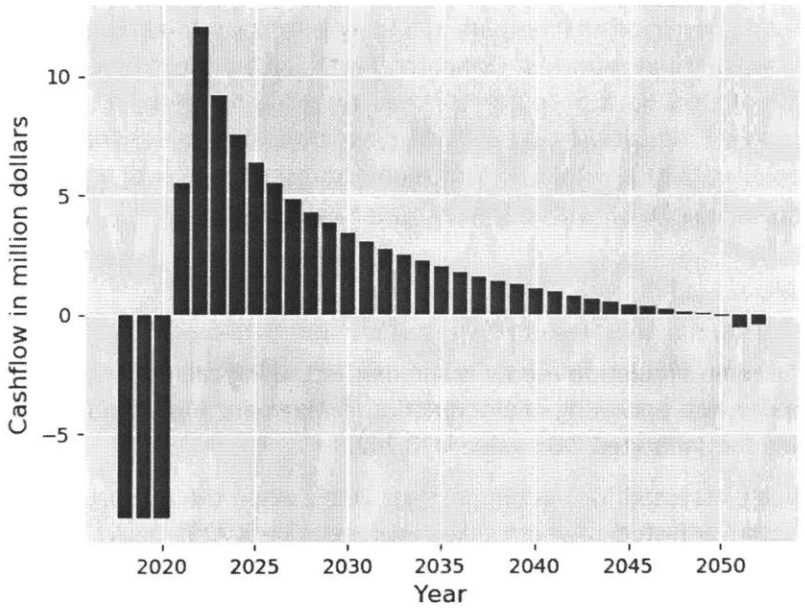

(b)

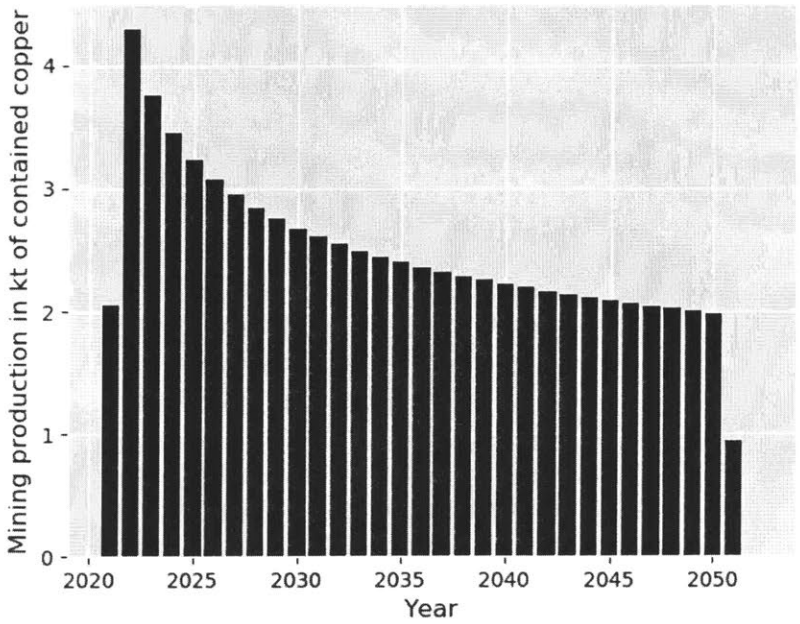

Figure 5. 2 (a) Simulated cash flow and (b) Mining production in Maya's mine life

It can be seen that during the first three years (2018 to 2020) of mining construction, the development capex is spent equally. Ore production reaches normal capacity in 2022 (CU=87.9%) after the ramp up stage in 2021. Since then, both cash flow and production gradually falls, due to ore grade decline and increase of mine site cost on a paid metal basis. Eventually, the low ore grade leads to negative cash flow

at 2050 and production ramps down at 2051. A relatively small reclamation cost is incurred at 2052 and Maya finishes all stages of its life.

The sensitivity of IRR to long-term price forecast is shown in Figure 5.3. If long-term price is expected to stay at the 2018 price level of 6372 USD/t, the expected IRR of the project would fall under the 15% cutoff, and Maya would not be decided to open.

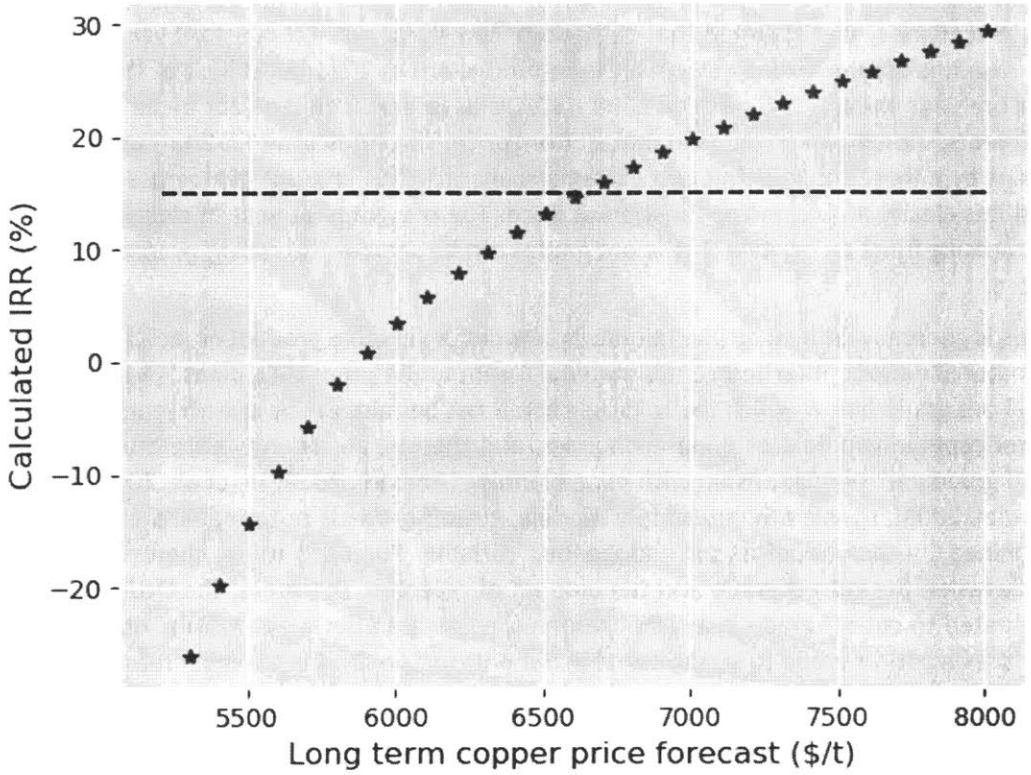

Figure 5. 3 Sensitivity of mine life IRR to long term copper price forecast. The blue dashed line represents the 15% cutoff.

The year of closure, and related mine properties, can be significantly affected by the cathode price in a mine's lifetime, as mentioned earlier. Table 5.3 compares several mine properties related to closure under five price scenarios:

Table 5. 3 Sensitivity of mine closure related mine properties to long term copper price forecasts

Copper cathode price in mine life (USD/t)	Simulated closure year	Cumulative copper production (kt)	Ore grade at closure year (%)	IRR (%)
6000	2034	39.30	0.72	3.40

6500	2040	53.40	0.66	13.15
7000	2050	74.68	0.59	19.71
7500	2062	98.12	0.55	24.85
8000	2078	126.96	0.50	29.28

In all five price scenarios, it is assumed that cathode price will stay at the constant value shown in the above table. Also it is assumed that Maya will begin production in 2021 regardless of the IRR. It can be seen that closure year under a low price of 6000 USD/t is different from the year under 8000 USD/t, by more than 40 years, showing the significant impact from price. The cumulative lifetime copper production is also different by a three times in the two extreme scenarios. This amount can be used as a proxy for reserves, and it is clearly an increasing function of price. The ore grade at year of closure, on the other hand, is a decreasing function of price. These ore grades can be seen as the *cut-off grades* of Maya under different prices.

A cut-off grade is generally defined as 'the minimum amount of valuable product or metal that one metric tonne (t) of material must contain before this material is sent to the processing plant.' (Rendu, 2014). This is the minimal ore grade below which the mineral should not be mined. The cut-off grade has been one of the core concepts in the field of mine economics, and there is an extensive literature studying the optimal cutoff grade and its relationship with mine planning (Ahmadi, 2018; He et al., 2009; Nieto, 2007; Osanloo & Ataei, 2003). In this primary supply module, cut-off grade is not modelled exogenously, but rather determined by the model as an endogenous variable. For each mine, there is a one-to-one relationship between the cut-off grade and the amount of reserves. Therefore, the OGEs for each mine could be calibrated to cut-off grade instead of reserves, to obtain equivalent results. However, there is not enough data on cut-off grade to support that in our dataset, and this is the main reason why the cut-off grade is not modeled explicitly here.

Extend the model to all operating mines and new mines

The example of Maya shows how the mine life simulation model works for a single mine. In the following, the model is extended to all operating mines and potential new mines in the future. The full model is scaled up and calibrated to total world copper production, which will be discussed in detail below.

Operating mines

Operating mines in this section refer to mines that are operating as of 2018. As mentioned earlier, SNL Mine Economics provides a detailed dataset on copper mine characteristics, including both operating mines and mines that are in the exploration stage. For 2018, the total copper production from the 374 mines that was covered is 17600 kt. Compared to ICSG reported world total mining production of 20500 kt, SNL's production coverage is about 86%. In order to match up total 2018 simulated production with ICSG reported world total, a random subsample is drawn from the pool of 374 operating mines and added to the same pool. The subsample size is 57 mines, and total 2018 production is 3100 kt, which fills the gap between SNL coverage and CISG reported total.

For each mine in the pool, most of the operating characteristics reported in Table 5.1 can be directly obtained. TCM of each mine is calculated based on Equation 5.4 and 2018 copper cathode price. Following

the calculated TCM value, CU can also be calculated based on Equation 5.6. Ore capacity of each mine can then be derived based on recovered metal production, 2018 ore grade and recovery rate. OGE can be calibrated using the algorithm described earlier.

It is assumed that the mine-specific minesite cost remains constant for per ton of ore treated, throughout the lifetime of each mine. Two other total cash cost components, including transport and offsite cost, and royalty, are assumed to remain constant for per ton of paid metal produced. It is worth mentioning that TCRC is a total cash cost component modeled in the price formation module, and is not assumed to be constant in the full system simulation. The two all-in-sustaining cost components, overhead cost and sustaining capex, are assumed to remain constant in total dollar terms since they are not linearly dependent on production volumes. The discount rate for NPV calculation is set as 10%, which is a value commonly used in mine planning (Ramboll IMS Ingenieurgesellschaft mbH, 2016; Runge, 1998; S&P Global Market Intelligence, 2019b).

One thing worth noting is that reclamation cost is modeled as a one-time closure cost in the simulation model. However, in major mining countries, mining companies usually have to pay incremental annual payments into an *environmental reclamation bond*. This bond exists so that if the company goes bankrupt or is in a parlous state and closes a mine, there is enough money to close the mine in a safe way and reclaim the land. By modeling reclamation simply as a one-time cost rather than a sustaining cost, I am essentially assuming that the total NPV of payment to and from the bond can be approximated by zero. This is a valid assumption if the discount rate used for the NPV calculation is on the same level with the percentage of interest payment from the bond. Due to limited data availability on reclamation bonds, the validity of this assumption could not yet be justified.

New mines

In order to simulate potential new mines opening into the future, the following two aspects need to be determined.

The first is the operating characteristics of potential new mines. It is assumed that potential new mines in the simulation will have operating characteristics that are similar to those of recently opened mines. Recently opened mines are selected from the operating mine pool based on the criterion $\frac{Cumulative\ ore\ production}{Ore\ capacity} < 3$. A total of 151 mines are selected from a pool of 374 mines. Following that, a pool of potential new mines is generated, by randomly subsampling from the 151 recently opened mines with perturbation. The size of this pool is 50,000 mines in our simulation. The characteristics below are perturbed by multiplying a random number following uniform distribution from 0.9 to 1.1 (i.e. perturbed by $\pm 10\%$): Ore capacity, initial ore grade, recovery rate, total cash cost components, all-in-sustaining cost components, development capex, reclamation cost and OGE. Since all the 151 mines have been operating, and I am generating characteristics of new mines, the initial ore grade of each operating mine is backcasted, using the current ore grade and the OGE value. TCRC is assumed to be not mine specific for new mines, and the 2018 annual TCRC value is used for all mines. Payable percent is not perturbed.

The second is the amount of mines opening each year. There are two major sources of uncertainty related to the amount of new mine opening in response to cathode price: the first is the uncertainty of price into the future, and the second is uncertainty regarding to the amount of mines and mining capacity expected to open under a certain price. For the first uncertainty, a baseline cathode price is set, assuming annual price from 2019 will stay constant at the 2018 level going on. For the second, a calibration process is performed, so that the total future production under the baseline price scenario from operating mines and new mines matches a benchmark. This benchmark, shown as the purple line in Figure 5.4, assumes

that world copper production will grow linearly between 2018 to 2040, and the amount of annual growth equals to the average growth between 2001 and 2011. This annual growth rate is much slower than the rate from last decade, and we assumed that this fast growth could not sustain in the future, due to slower demand growth that will be discussed in a later section. The amount of production from new mines opening post-2018 should match the gap between the future benchmark and production from the operating mines (blue line), under the baseline scenario.

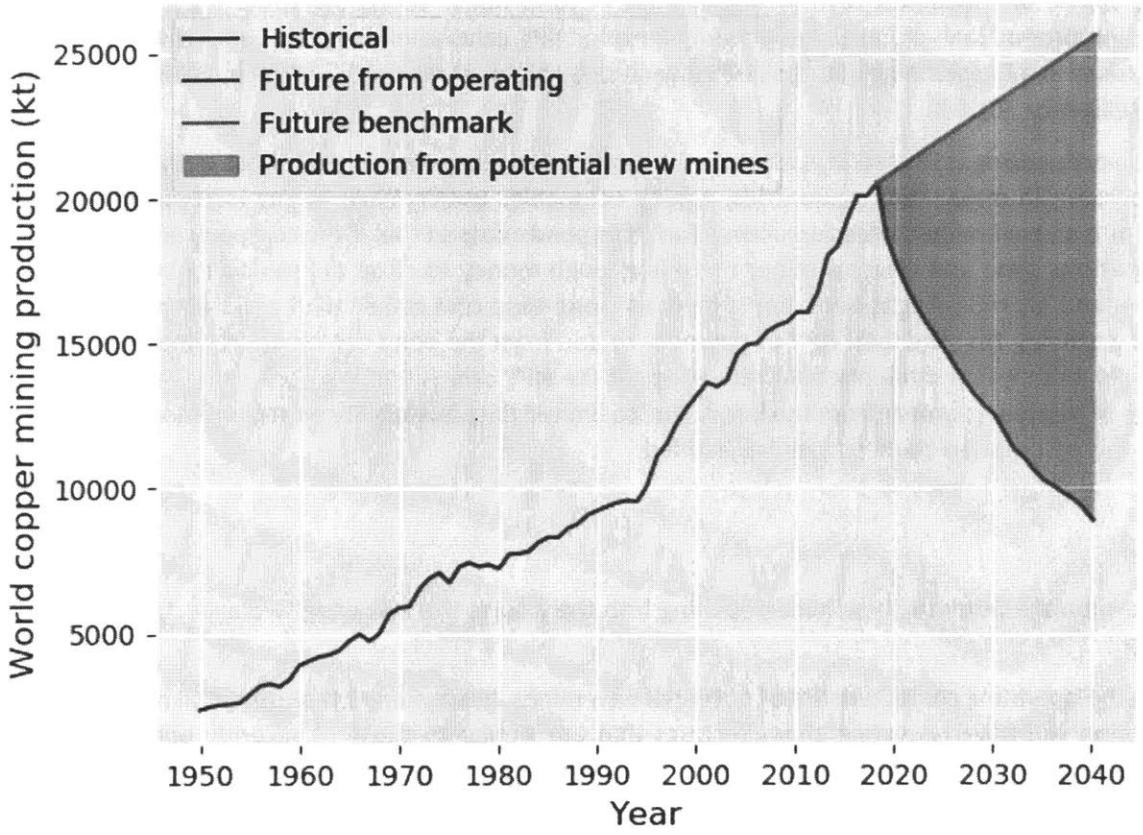

Figure 5. 4 Historical mining production and future simulated production

Calibration of future production for new mines is calibrated to the future benchmark up to 2040, following the process below.

1. The pool of potential new mines (size=50,000) is broken down into 25 blocks of 2,000 mines;
2. All new mines are assumed to take three years to complete construction, so the first set of mines opening in 2019 are being assessed and constructed starting 2016. A subsample of the first block of 2,000 mines is selected, and the IRRs of each mine are calculated based on the 10-year trailing average cathode price at 2016. This subsample size is tuned so that the amount of new mine production in 2019 approximately fills the gap (grey area in Figure 5.4);
3. Step 2 is repeated iteratively, moving one year ahead at a time. For each year, new mine opening is assessed based on a different block of 2,000 mines. The calibration is completed until new mine opening in 2040 is determined.

A time series of subsample size parameters for mines opening between 2019 and 2040 is recorded. These parameters are fixed for production forecasting under other price scenarios as well, but the amount of mines and mining production from new mine will vary based on copper cathode price and TCRC, due to change in IRRs.

Summary statistics under different cathode price scenarios

Five cathode price scenarios are defined here in order to explore high-level production responses to price. These prices are shown in Figure 5.5, where the baseline assumes that price stays constant between 2019 to 2040, at the 2018 price level of 6372 USD/t. The *high* and *low* price scenarios assume constant price that is 500 USD/t higher and lower than the 2018 level. The growing and shrinking price scenarios assumes price grows/shrinks at a rate of 100 USD/t per year. In all scenarios, TCRC is assumed to stay constant at the 2018 level.

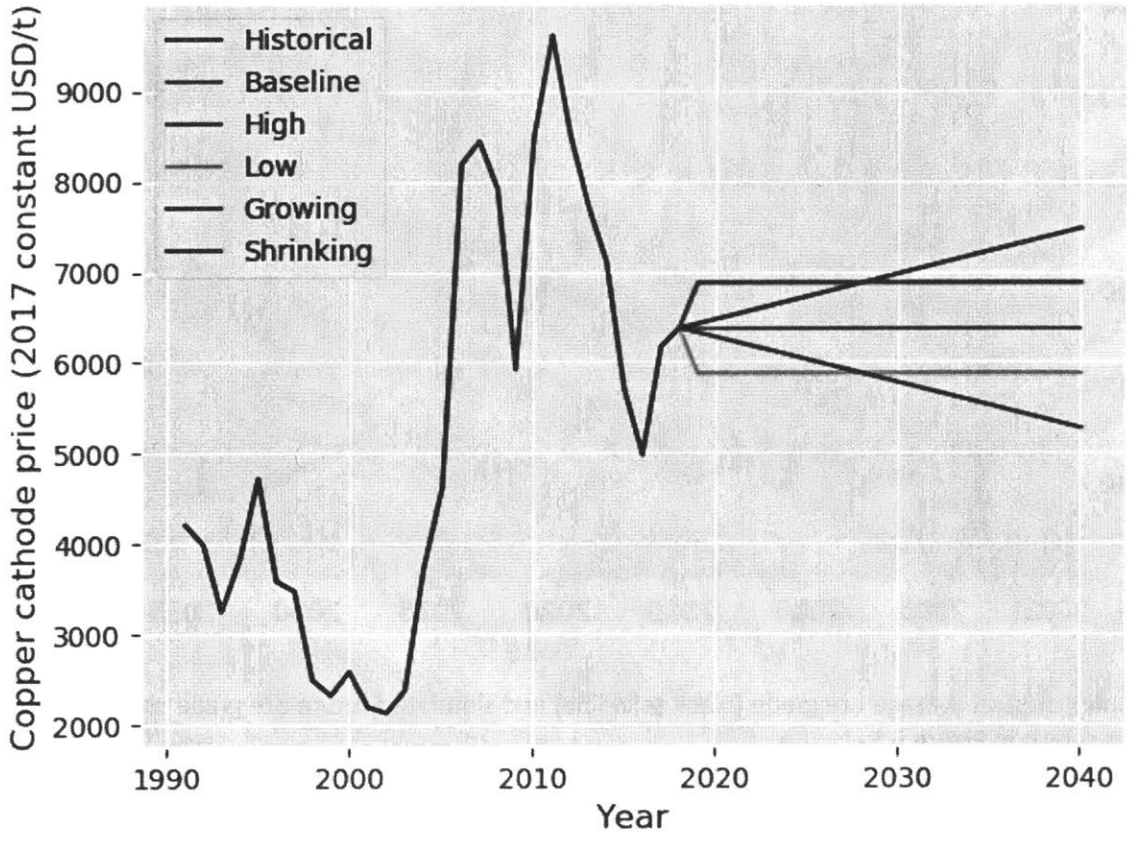

Figure 5. 5 Historical copper cathode price (black line) and future price scenarios, in 2017 constant USD/t

The average ore grade of all mines weighted by ore production, including operating mines and new mines, is shown in Figure 5.6. There are five ore grade evolution scenarios that corresponds to the five previously mentioned cathode price scenarios, and a final scenario shown by the dashed green line only includes operating mines under the baseline cathode price.

All of the series show a declining trend at a rate similar to historical ore grade decline. It can be seen that the time series of ore grade evolution under the five scenarios form a narrow band, and the impact of cathode price on average ore grade isn't significant. The series of operating mines only is significantly lower than the other five scenarios before 2035, indicating that new mines opening in the future should have ore grades higher than the currently operating mines. Also, the average ore grade in all scenarios begins to recover since 2037, which is a result of some of the large but low grade mines closing around that year.

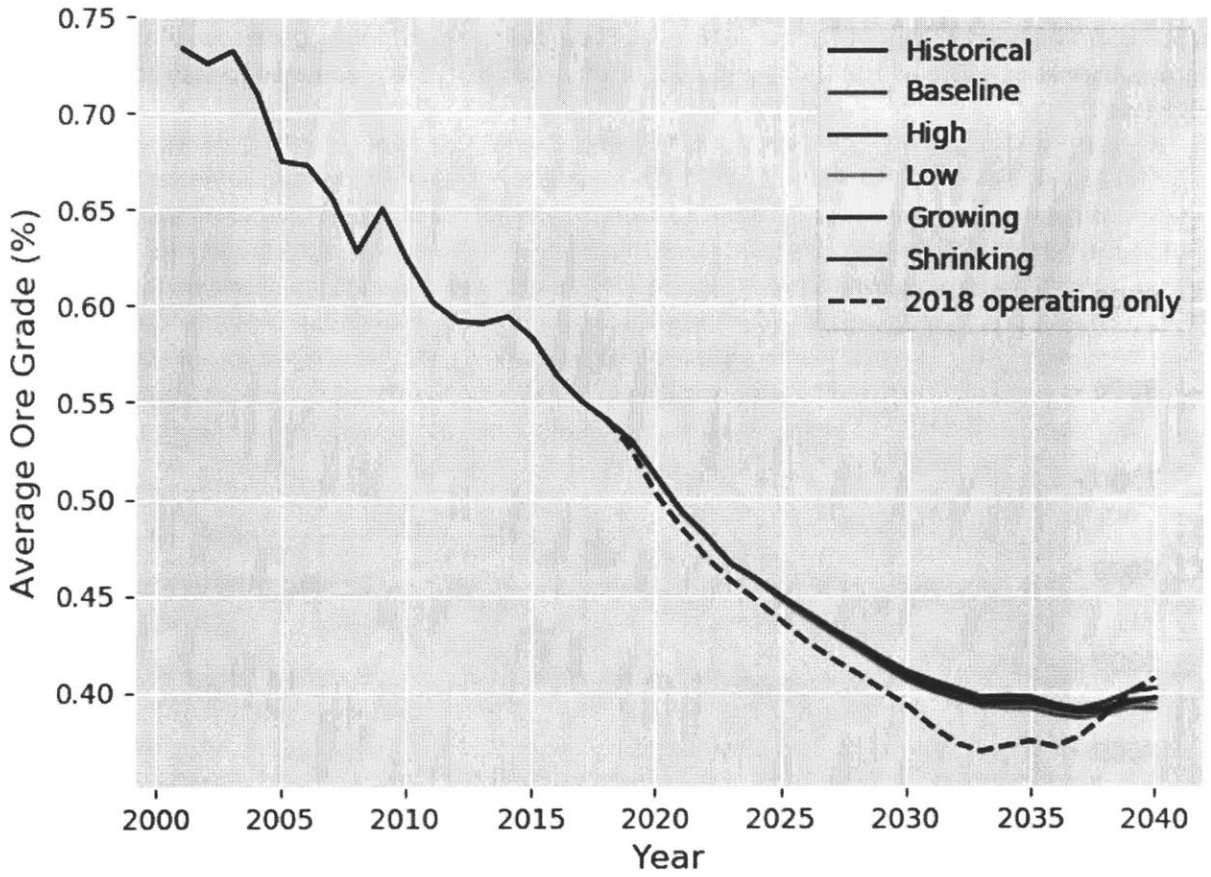

Figure 5. 6 Historical average ore grade (black solid line) and simulated future ore grade under five price scenarios shown in Figure 5.5.

Total mining production corresponding to the five scenarios is shown in Figure 5.7. The baseline scenario, represented by the grey line, is the one that was calibrated to future benchmark in Figure 5.4. It can be seen that total production varies significantly with cathode price, and the level of uncertainty in total production rises as forecast is done for a more distant future. The range of 2040 production is [16755, 30481] kt, where the high end is almost two times of the low end. This high sensitivity of mining production to cathode price is mostly result of the price effect on mine opening and closing, and the effect on short run production is very limited. The implications of this high sensitivity to the entire simulation system will be discussed further in later sections.

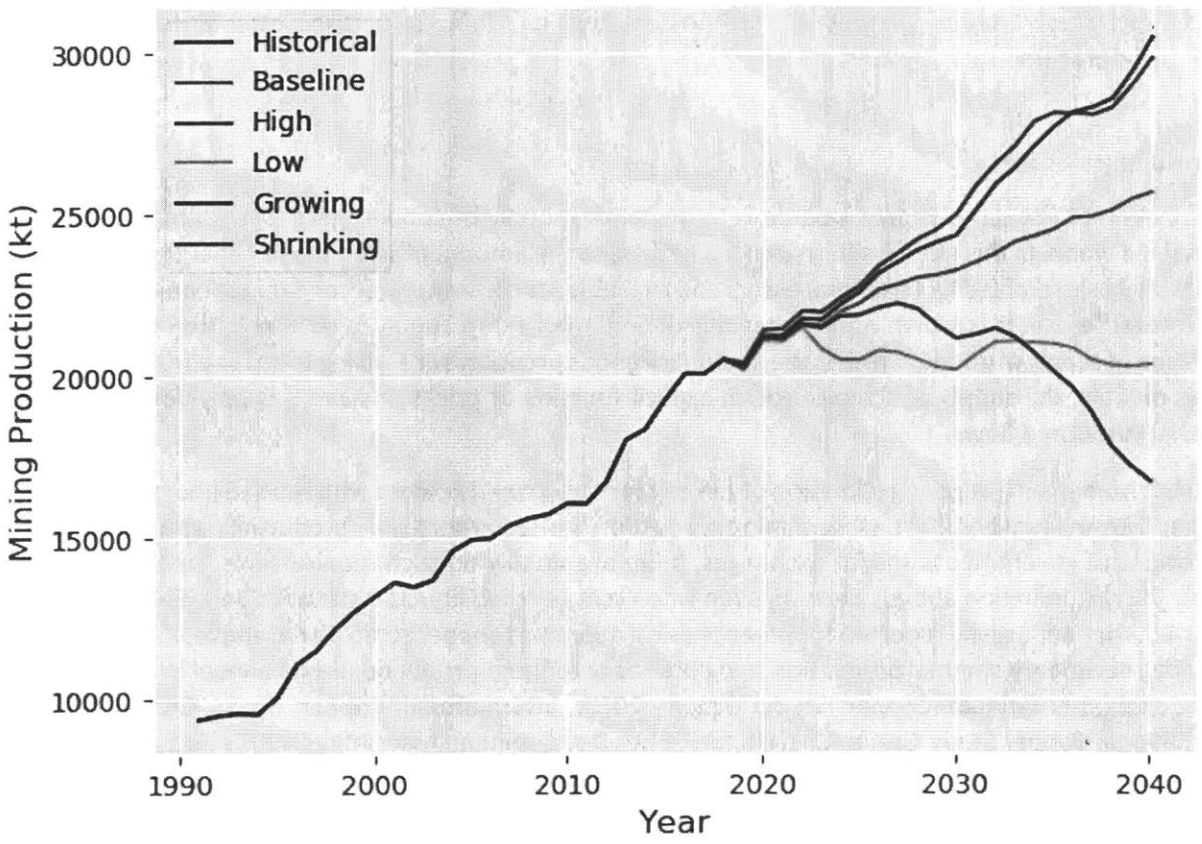

Figure 5. 7 Historical copper mining production (black solid line) and simulated future mining production under five price scenarios shown in Figure 5.5.

Summary of primary supply module

From a high level, the primary supply module is a sub-system which takes copper cathode price as the main input, and outputs copper mining production. This module is developed from a bottom-up perspective. The key component of the module is tool for mine life simulation, which tracks the four critical stages in the lifetime of a typical copper mine. The simulation model is calibrated to both historical data and a future production benchmark to reduce uncertainty.

Production responds to cathode price through three different mechanisms, and each of them is modeled in extensive details. This allows one to zoom in the copper mining industry from multiple dimensions. For example, one could

1. Investigate the characteristics of each operating mine and new mine during its lifetime, as a function of cathode price, total cash costs, speed of ore grade decline and other operating characteristics;
2. Explore sensitivity of total copper mining production to any operating characteristics. For example, the effect on production from an industry-wide minesite cost reduction can be estimated through this module;
3. Track the evolution of high-level industry characteristics, such as total production, average ore grade, average TCM and CU. These are important copper industry benchmarks that has been

extensively used by a variety of stakeholders, such as mining companies, exploration companies and traders.

Scrap supply module

The function of the scrap supply module is to model the supply of copper scrap from different sources around the world. In this model, scrap supply is defined as the amount of scrap that is generated, collected, separated/disassembled by scrap processers and available for consumers (secondary refineries and semis fabricators) to use. It is worth noting that this definition of scrap supply is different from the classical definition of supply of goods, which is the amount of goods producers are willing to sell at particular prices. In this module, the supply of scrap is not an explicit function of prices. Instead it is only determined by material stocks and flows.

Different from mining supply, estimation of the copper scrap supply comes with much higher uncertainty, for the following reasons. First, while mining production is often reported by producing companies due to regulations of governments and/or exchanges, there are usually no such requirements for copper scrap supply (by the definition above). Second, even when scrap availability/S&D statistics on a global level are reported, they are usually reported for other physical quantities copper scrap. For example, ICSG has been reporting secondary smelter production and secondary refinery production in its annual World Copper Factbooks (International Copper Study Group, 2017; International Copper Study Group, 2018b; International Copper Study Group, 2019b); In Copper Development Association's 2013 Technical Report (Jolly, 2013), it reported copper recovered from scrap and consumption of copper in direct melt scrap. All these statistics are in fact reported from scrap consumers' perspectives rather than scrap suppliers'. Thirdly, while world total copper scrap supply is not directly reported, it is modeled in many academic researches (T. E. Graedel et al., 2004; Gómez, Guzmán, & Tilton, 2007; Glöser et al., 2013; Fu, Ueland, & Olivetti, 2017). However, these models are usually based on highly uncertain parameters such as collection rate, fabrication efficiency and product lifetime distributions.

A material flow analysis (MFA) modeling approach is taken in order to estimate and simulate historical and future copper scrap. Some modeling parameters are calibrated to scrap demand/consumption statistics. Even after this calibration process, there is still considerable uncertainties in the set of parameters, and these uncertainties will be explored in a sensitivity analysis.

Many components of the scrap supply module developed here is based on a previous work from Fraunhofer Institute for Systems and Innovation Research (ISI) (Glöser et al., 2013), and the structure of their global copper flow model is illustrated in Figure 5.8. Here I briefly introduce this model, with a focus on estimating copper scrap supply. From a high level, this global copper flow model consists of five life stages: primary production (Mining + smelting and refining, or SX-EW); manufacturing (fabrication of semis and manufacturing of final products); use phase; waste management (scrap collection, sorting and copper recovery) and environment (material lost or end up in landfills). During the manufacturing stage, **new scrap**, or pre-consumer scrap is generated from fabrication residues. The amount of new scrap generated depends on the fabrication efficiencies of semis and final products. After the use stage, final products reach their end-of-life and **old scrap** is generated. Some amount of both new and old scrap has to be smelted/refined before re-entering semis fabrication, and this amount is called the **refined scrap**. Some other higher quality scrap can be directly used by semis fabricators, by simply being remelted, and this amount is called the **direct melt scrap**. It is worth noting that the breakdown of new and old scrap is from a scrap generation/supply perspective, while refined and direct melt scrap is from a scrap consumption/demand perspective. In what follows, I will introduce the models for estimating old and new scrap supply.

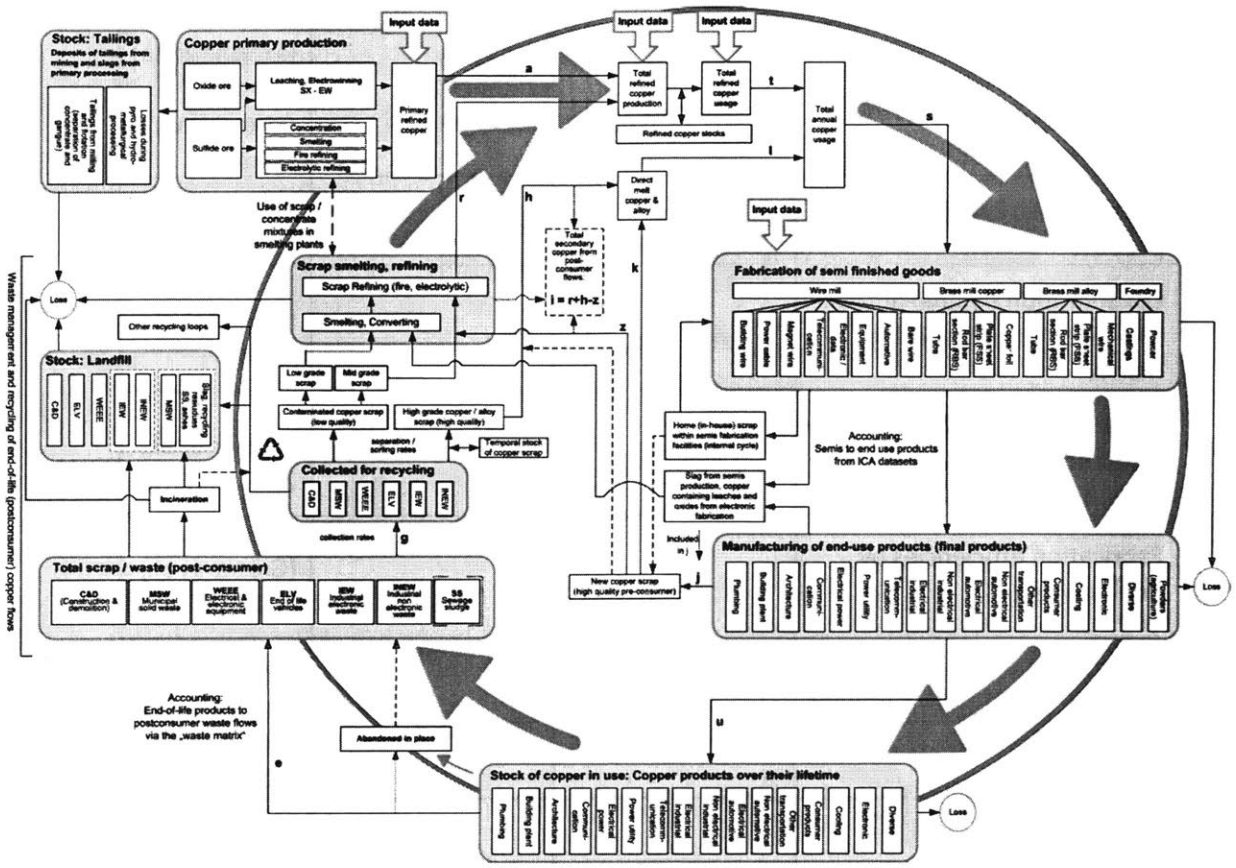

Figure 5. 8 Structure of the global copper flow model reproduced from (Glöser et al., 2013)

Old scrap

The variables and parameters used for the calculation of scrap supply is collected from different sources, as listed in Table 5.4.

Table 5. 4 Variables and parameters used in the scrap supply module, their symbols, timeframe and sources of data

Variable/parameter	Symbol	Timeframe	Source
Total consumption by end-use sector	$TC_{S_i,t}$	1912-1999	(International Copper Study Group, 2010)
		2000-2014	(Bhuwalka, Swei, Roth, & Kirchain, 2019)

Sector to final product accounting matrix	$AC1_{S_i,P_j}$	2006-2010 average	(International Copper Association, 2013)
Lifetime distribution by final product	$\{F_{P_i,\tau}\}_{\tau=0}^{\infty}$	NA	(Glöser et al., 2013)
Consumption by final product to waste type accounting matrix	$AC2_{P_i,W_j}$	NA	(Glöser et al., 2013)
Technical recycling efficiencies and collection rates by waste type	TE_{W_i}, CR_{W_i}	NA	(Glöser et al., 2013)
Fabrication efficiencies by final product	FE_{P_i}	NA	(Glöser et al., 2013)
World total secondary refined production	$P.Ref_{t,Sec}$	1960-2018	(International Copper Study Group, 2019b)
Direct melt scrap consumption	$C.Scrap_{t,DM}$	1960-2018	(International Copper Study Group, 2019b)

Old copper scrap enters the waste stream after the use stage of copper products. Therefore, the amount of old scrap supply is dependent on the lifetime (distribution) of these products, the historical consumption of these products and the recycling rates. The classification of final products is based on International Copper Association (ICA), and consistent with the classification in Figure 5.8. The high-resolution consumption by final products data is only available for years 2006-2010, from ICA. For years beyond those, the consumption breakdown is only available at the end-use sector level (Construction, electrical, industrial, transport and others). Therefore, I extrapolated the final product level consumption to 1912 to 2014, by assuming that the breakdown of final products within each end-use sector stays constant at the 2006-2010 average level during the entire timeframe. The amount of final products reaching end-of-life during each year can then be calculated as:

$$TC_{P_j,t} = TC_{S_i,t} AC1_{S_i,P_j}$$

$$EOL_{P_j,t} = \sum_{\tau=0}^{\infty} TC_{P_j,t-\tau} F_{P_j,\tau}$$

(Equations 5.12 and 5.13)

Where $TC_{S_i,t}$ is the amount of copper entering use in sector *i* at time *t*, $AC1_{S_i,P_j}$ is the (*i*, *j*) th element of the accounting matrix from sector to final products, and $U_{P_j,t}$ is the calculated amount of copper entering use from final product *j* at time *t*. $\{F_{P_j,\tau}\}_{\tau=0}^{\infty}$ is the lifetime distribution for product *j* in discrete frequencies, which satisfies $\sum_{\tau=0}^{\infty} F_{P_j,\tau} = 1$. $F_{P_i,\tau}$ is the fraction of final product *j* reaching end-of-life at year $t+\tau$ in the total amount of product entering use at year *t*. Therefore, $EOL_{P_j,t}$ is the total amount of product *j* reaching end of life at year *t*. In this module, I assumed that lifetime for all final products follow lognormal distributions $Lognormal(\mu, \sigma^2)$ with $\mu = 0.1\sigma$. The means of the distributions are taken from the average lifetime numbers from literature (Glöser et al., 2013). Then the continuous probability densities are transformed into discrete frequencies.

Once the products reach end-of-life and enters the waste management stage, they enter different waste streams to be collected, sorted, disassembled and become available to be recovered. The amount of waste generated by type can be calculated as,

$$G.OS_{W_j,t} = \sum_i EOL_{P_i,t}\, AC2_{P_i,W_j}$$

(Equations 5.14)

where $AC2_{P_i,W_j}$ is the fraction of final product *i* that ends up in waste stream *j*. Based on the definition of scrap supply, the total amount of old scrap supply is

$$S.OS_t = \sum_j G.OS_{W_j,t} TE_{W_j} CR_{W_j}$$

(Equations 5.15)

The technical recycling efficiency for waste type *j*, TE_{W_j}, is the efficiency for separating, sorting and disassembling, and CR_{W_j} is the collection rate for waste type *j*. These rates are shown in Table 5.5, and it is assumed that these rates will stay constant in the baseline scenario. Based on opinion from industry experts, the larger opportunity for improved recycling should be increasing collection rates rather than improving technical recycling efficiencies, which have been optimized for many waste streams already.

Table 5. 5 Technical recycling efficiency and collection rate by waste type

	C&D	MSW	WEEE	ELV	IEW	INEW
Technical recycling efficiency	90%	55%	55%	70%	75%	20%
Collection rate	72%	5%	63%	91%	66%	68%

The calculated historical old scrap supply by waste type is shown in Figure 5.9, in which consumption by sector values are based on reported historical data between 1912 and 2014, and based on projected data from the demand module between 2015 and 2018 (the details of demand projection will be discussed in the demand module section). As the consumption data started from 1912 as the initial year, the amount of old scrap might be underestimating reality, particularly for the first 40 years when a significant part of products used for the building and construction sector is still in the use stage. Later years are still underestimated, but to a much smaller extent.

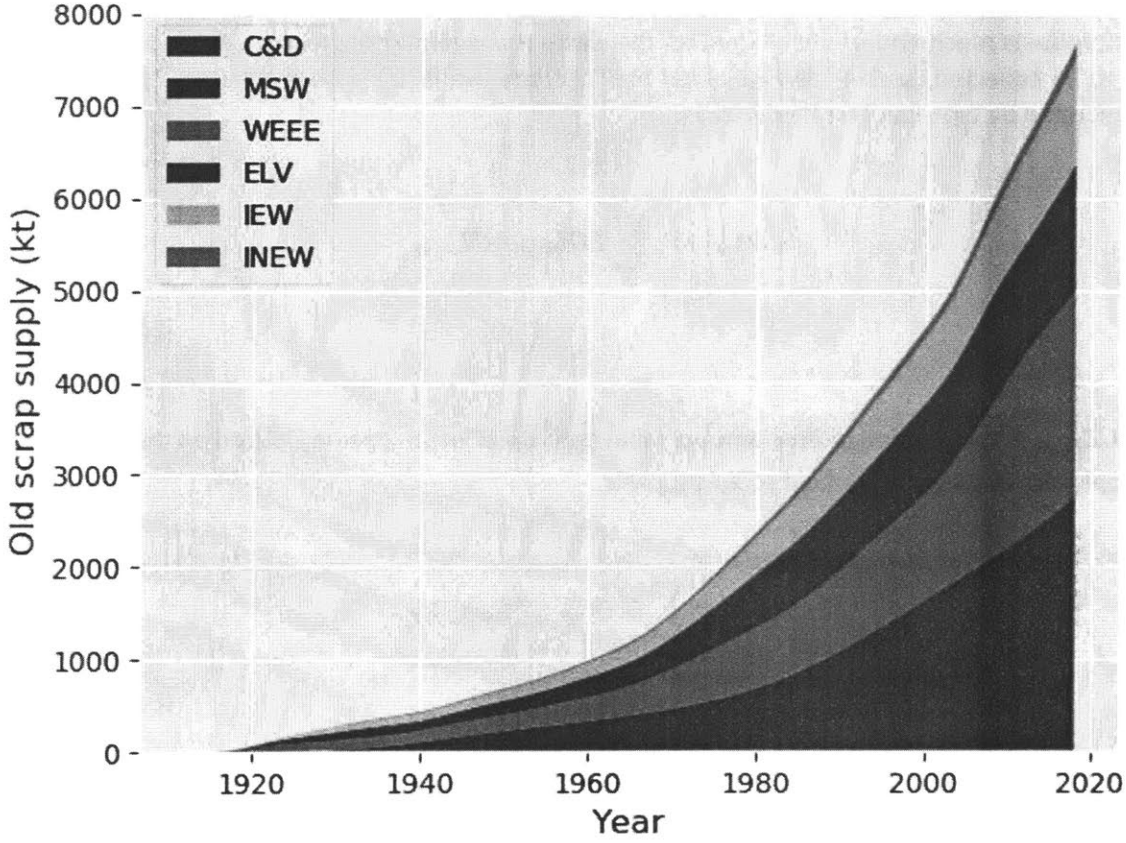

Figure 5. 9 Historical old scrap supply by waste type, calculated based on Equations 5.12 to 5.15

It can be seen from Figure 5.9 that old scrap from construction and demolition waste (C&D) and waste electrical and electronic equipment (WEEE) have accounted for 55% to 65% of total old scrap supplied historically. Industrial electrical equipment waste (IEW) and end-of-life vehicles (ELV) accounted for almost all of the rest, while industrial non-electrical equipment waste (INEW) and municipal solid waste (MSW) are almost negligible in total old scrap supply. In terms of actual quantities, C&D supplied 2750 kt of old scrap in 2018, followed by 2200 kt from WEEE, 1390 kt from ELV, 1140 kt from IEW, 160 kt from INEW and 27 kt from MSW. The extremely low value from MSW is a result of both low amount of scrap generated and low end-of-life collection rate.

For the projection of old scrap supplied after 2018, the copper consumption by sector data would be determined from the demand module, and it is assumed that all other accounting matrices, recycling rates and lifetime distributions stay constant in the future.

New scrap

New scrap, or pre-consumer scrap, is the scrap generated during the fabrication of semis and final copper products. However, unlike old scrap, not all new scrap ends up on the *scrap market* and is sold from scrap suppliers to scrap consumers. Therefore, we differentiate between three types of pre-consumer scrap:

1. **Home scrap**. This is sometimes also called *runaround scrap* or *in-house scrap*. It is generated and consumed by the same semis fabricator or final product manufacturer, and this physical quantity does not enter the scrap market. Instead, it is directly utilized within the fabrication facility in another production cycle. Because it is only used in-house and never leaves the fabrication facility, this amount is never included in any consumption statistics and the exact extend of home scrap is highly uncertain.
2. **Toll new scrap**. Many semis fabricators and final product manufacturers do not have the capability to directly utilize their fabrication residue in another production cycle, without further processing it. Instead of selling that residue to the market, some manufacturers may send their scrap to upstream scrap processors or other manufacturers who have the processing capability, and receive the processed scrap back after paying some processing fees. This process is called toll processing or toll manufacturing, and therefore I name this amount of pre-consumer scrap as *toll new scrap*. As an example, an air conditioner manufacturer that uses brass pipes as a raw material might produce copper alloy residues during the manufacturing process. It is incapable of processing the scrap on its own, so it sends the scrap to a brass mill for toll processing, and receive brass pipes in return made from the scrap.
3. **External new scrap.** Different from the previous two scrap types, external new scrap does not necessarily returns to the original facility where it is generated. It is sold to scrap dealers/processors who might then sell the scrap to any consumer that demanded it. Compared to using the fabrication residue internally or sending it to other processors for toll processing, selling the new scrap externally is undesirable, because it is usually less beneficial to do so from a cost/profit perspective. Scrap dealers' business model is based on earning the price difference between purchased scrap and sold scrap, so it is always more expensive to sell the scrap to the market and then buying from the market, than using the scrap internally.

As home scrap is not included in consumption statistics, it should also be excluded from the scrap supply module. This ensures that when the S&D of scrap is compared against each other, home scrap is taken out from both sides. Therefore, only the latter two types of pre-consumer scrap are included in the new scrap supply.

New scrap supply can be estimated as follows. First, the amount of copper consumed in different final products each year can be calculated from Equation 5.16. The total amount of new scrap generated at year t is

$$G.NS_t = \sum_i TC_{P_i,t}/(1 - FE_{P_i})$$

(Equations 5.16)

It is assumed that the ratio of home scrap, toll new scrap and external new scrap for product *i* in year *t* are $R.HS_{P_i,t}$, $R.TS_{P_i,t}$ and $R.ES_{P_i,t}$, respectively. By definition, $R.HS_{P_i,t} + R.TS_{P_i,t} + R.ES_{P_i,t} \equiv 1, \forall P_i$. Toll new scrap generated (G.TS) and external new scrap generated (G.ES) are

$$G.TS_{P_i,t} = TC_{P_i,t}/(1 - FE_{P_i}) \cdot R.TS_{P_i,t}$$
$$G.ES_{P_i,t} = U_{P_i,t}/(1 - FE_{P_i}) \cdot R.ES_{P_i,t}$$

(Equations 5.17 and 5.18)

Since toll new scrap does not involve in collection and separation of the scrap, it is assumed that the amount generated equals to the amount supplied. For external new scrap $G.ES_{P_i,t}$ generated from product *i*, it is assumed to enter different waste streams. Different from the accounting matrix used for old scrap, it is assumed that no scrap is lost to the environment, and the fractions of scrap entering different waste streams increase proportionally. Mathematically, the modified accounting matrix should satisfy $\sum_j AC2'_{P_i,W_j} = 1, \ \forall i$, and $\frac{AC2'_{P_i,W_j}}{AC2_{P_i,W_j}} = Constant_i, \forall i$. The collection rates for all waste types from external new scrap should be 100%, since it is directly sold to scrap dealers rather than being collected from end-of-life. Therefore, the total new scrap supply should be the sum of scrap supply from toll new scrap and external new scrap,

$$S.NS_t = \sum_i G.TS_{P_i,t} + \sum_j \left(TE_{W_j} \sum_i G.ES_{P_i,t} \, AC2'_{P_i,W_j} \right)$$

(Equations 5.19)

To the best of my knowledge, the ratios $R.HS_{P_i,t}$, $R.TS_{P_i,t}$ and $R.ES_{P_i,t}$ are not reported in any literature/industry reports. However, in several interviews that I have conducted with industry experts, it has been mentioned that the ratio for external new scrap should be very small, since the fabricating facilities still consider their own scrap as valuable material. Therefore, $R.ES_{P_i,t}$ is assumed to be 10% for all products and all years in the simulation. Also, for simplicity purpose, $R.HS_{P_i,t}$ and $R.TS_{P_i,t}$ are also assumed to be constant across products and only change over time. Therefore, $R.HS_t + R.TS_t \equiv 0.9$. To determine the values of $R.HS_t$ and $R.TS_t$, a calibration process is performed by matching total scrap supply with total scrap demand, described as follows.

First, world total copper scrap demand (copper content) is calculated as the sum of refined scrap consumption and direct melt scrap consumption,

$$C.Scrap_t = P.Ref_{t,Sec}/0.99 + C.Scrap_{t,DM}$$

(Equations 5.20)

It is assumed that refineries do not stock copper scrap, so secondary refined production $P.Ref_{t,Sec}$ is divided by an average scrap smelting and refining efficiency of 99% to get refined scrap consumption. Secondly, the gap between total scrap consumption $C.Scrap_t$ and old scrap supply $S.OS_t$ is calculated as a benchmark for new scrap supply, and a series of $R.HS_t$ is calculated so that $S.NS_t = C.Scrap_t - S.OS_t$. These are the 'equilibrium' home scrap ratio series that keep total scrap P&C in a perfect balance. Finally, to add a little imbalance, the home scrap ratios are smoothed by taking the average of the equilibrium values from [t-4, t+4] as the new value for year *t*.

The estimated amount of total scrap supply is shown in Figure 5.10, together with the series of total scrap demand. From a percentage perspective, the amount of new scrap has accounted for 25% to 50% of total scrap supply historically, and that number has been fluctuating around 30% for the last three decades. The total amount of new scrap supply for 2018 is 3260 kt.

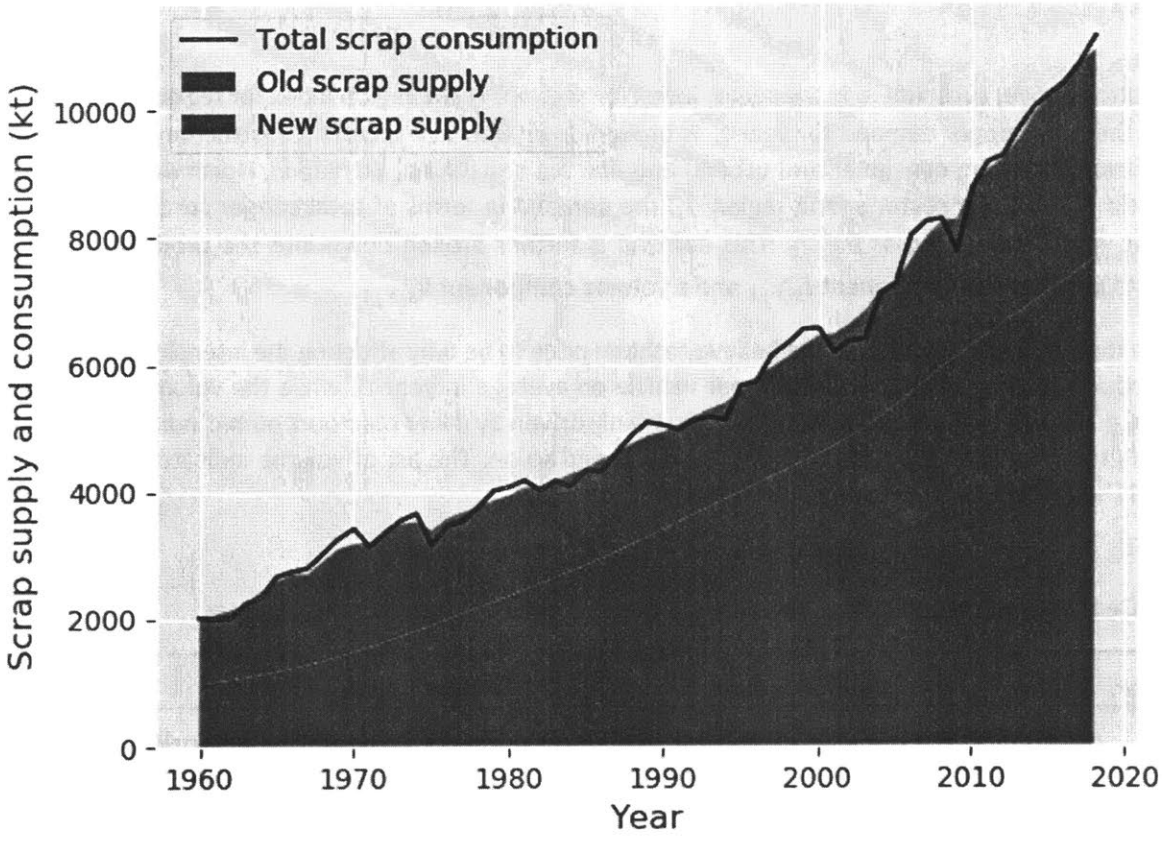

Figure 5. 10 Historical total scrap supply and consumption

Similar to the projection of old scrap supply after 2018, the consumption by sector data determined from the demand module is also used for new scrap supply simulation. In the next section, the demand module will be introduced in details.

Demand module

Acknowledgement: A part of this module is developed in collaboration Karan Bhuwalka, including selecting the appropriate volume indicators and projection of volume indicators. Karan estimated the demand elasticities with Bayesian regression models. A part of this model is being prepared for publication *'Estimating Copper Price Elasticity using Bayesian Hierarchical Modeling'* by Karan Bhuwalka, Omar Swei, Rich Roth and Randolph Kirchain (Bhuwalka et al., 2019).

The function of the demand module is mainly to forecast future world copper demand as function of cathode price. The basic form of the model is as follows:

$$D_{s_i,r_j,t} = I_{s_i,r_j,t} \cdot V_{s_i,r_j,t}$$

(Equations 5.21)

In the equation above, subscript s_i is the sector index for sector *i*, r_j the region index for region *j* and *t* for year *t*. D_t, the total copper demand for year *t*, is broken down into five sectors (construction, electrical, industrial, transportation, consumer and others) and five regions (China, EU, Japan, North America and rest of world (ROW)). For sector s_i and region r_j, the demand in terms of total copper content in final products at year t is denoted as $D_{s_i,r_j,t}$. This demand is further broken down into the product of two components, an intensity component $I_{s_i,r_j,t}$ and a volume component $V_{s_i,r_j,t}$.

The reason for this breakdown is that we believe cathode price to be only affecting the intensity of copper in final products (e.g. kg of copper used in per vehicle on average in year *t*), while the volume of those products (e.g. numbers of vehicles sold in year *t*) is mainly driven by other macroeconomic indicators such as regional gross domestic products (GDP), population and so on. The list of volume indicators for each sector, and the respective data sources, are listed in Table 5.6:

Table 5. 6 Demand volume indicators for each end-use sector and respective data sources

Sector	Volume indicator	Data source
Construction	Value added in construction sector	(OECD, 2019a; World Bank, 2019b)
Electrical	Total Grid Power capacity in GW	(Materials Systems Laboratory, 2019)
Industrial	Value added in manufacturing sector	(OECD, 2019b; World Bank, 2019b)

Transportation	Numbers of new vehicle produced	(Materials Systems Laboratory, 2019)
Consumer and others	GDP	(World Bank, 2019b)

All monetary values in Table 5.6 are in constant 2010 US dollars. The data for $D_{s_i,r_j,t}$ is also obtained from Mencer, the same data source shown in Table 5.4. The intensities $I_{s_i,r_j,t}$ can be calculated as the quotient of $D_{s_i,r_j,t}$ to $V_{s_i,r_j,t}$. We then model intensity growth using the model form below:

$$\Delta log\left(I_{s_i,r_j,t}\right) = \beta_{0,s_i} + \beta_{s_i}\,\Delta log(P'_t) + \beta_{r_j}\,\Delta log(P'_t) + \beta_{GDP}\,\Delta log\left(GDP_{r_j,t}\right)$$

(Equations 5.22)

The dependent variable modeled here is the log growth of $I_{s_i,r_j,t}$. β_{0,s_i} is a sector specific intercept that represents sector specific intensity reduction or dematerialization due to technology growth. It is expected to be negative. It is worth noting that we didn't include the symmetric term β_{0,r_j}. This is because we expect intensity reduction due to technology growth to be only sector specific, and once any manufacturer in the world adapts a new technology, the final products with less copper intensity will be available to all the regions in the world quickly. The second and the third term on the right hand side (RHS), $\beta_{s_i}\,\Delta log(P'_t)$ and $\beta_{r_j}\,\Delta log(P'_t)$, are the sector and regional specific price responses. The price used here, $P'_t = \frac{P_{t-1}+P_{t-2}}{2}$, is the first lag of trailing two year average cathode price. This price is used instead of cathode price at year *t* directly, because we believe that the price response on intensity growth is lagged (i.e. it takes time for manufacturers to cut material intensity in response to price), and the effect can live more than one year. These two terms are the *substitution effect* by microeconomics definition, since a rise in raw material price should cause manufacturers to use more substitute materials. Therefore, the price elasticities of demand β_{s_i} and β_{r_j}, are also expected to be negative under normal conditions. Finally, the last term on the RHS, $\beta_{GDP}\,\Delta log\left(GDP_{r_j,t}\right)$ is the intensity response to regional per capita real GDP. This term corresponds to the *income effect* by microeconomics definition. As income level increases, more material will be required based on per volume basis, especially for developing countries. The GDP elasticity β_{GDP} is therefore expected to be positive.

Bayesian regression models are used for model estimation. There are two main reason for using Bayesian regression. The first is that we have a relatively small number of data point (15 annual data) for each combination of sector and region (s_i, r_j), so using ordinary least square model could easily lead to insignificant results statistically. Bayesian regression models on the other hand, allow us to work with smaller data sets through hierarchical modeling (Vehtari, Gelman, & Gabry, 2017). Secondly, Bayesian models allow us to specify the prior distributions for parameters estimates. Since we already have expectations for at least the signs of these parameters, and price elasticities of copper demand have also been estimated in past literature, we have reasonable expectations for these prior distributions.

Details of the Bayesian regression can be found in the work by Bhuwalka et al. (Bhuwalka et al., 2019). The estimated results are the posterior distributions of parameters, and the they are assumed to be

normally distributed. Means and standard deviations of these normal distributions can be found in Table 5.7.

Table 5. 7 Mean and standard deviation of intercepts and elasticities estimated from Bayesian regression models

	Intercept mean	Intercept SD	Elasticity mean	Elasticity SD
Construction	-0.06	0.02	-0.1	0.07
Electrical	-0.1	0.02	-0.05	0.07
Industrial	-0.09	0.02	-0.08	0.07
Transportation	-0.02	0.02	0	0.07
Consumer and others	-0.08	0.02	-0.12	0.07
China	NA		-0.17	0.07
EU			-0.02	0.07
Japan			0.02	0.07
Nam			-0.16	0.07
ROW			-0.07	0.07
GDP			0.69	0.11

After parameter estimation, the intensity growth can be expressed as

$$\frac{\widetilde{I_{s_i,r_j,t}}}{I_{s_i,r_j,t-1}} = \int_{-\infty}^{+\infty} e^{\beta_{0,s_i}} pdf(\beta_{0,s_i})\, d\beta_{0,s_i} \cdot \int_{-\infty}^{+\infty} \left(\frac{P'_t}{P'_{t-1}}\right)^{\beta_{s_i}} pdf(\beta_{s_i})\, d\beta_{s_i} \cdot \int_{-\infty}^{+\infty} \left(\frac{P'_t}{P'_{t-1}}\right)^{\beta_{r_j}} pdf\left(\beta_{r_j}\right) d\beta_{r_j} \cdot \int_{-\infty}^{+\infty} \left(\frac{GDP_{r_{j,t}}}{GDP_{r_{j,t-1}}}\right)^{\beta_{GDP}} pdf(\beta_{GDP})\, d\beta_{GDP}$$

(Equations 5.23)

where $pdf()$ are the estimated posterior normal distributions on those parameters. Given price growth $\frac{P'_t}{P'_{t-1}}$ and regional GDP per capita growth $\frac{GDP_{r_{j,t}}}{GDP_{r_{j,t-1}}}$, the estimator of intensity $\widetilde{I_{s_i,r_j,t}}$ can be calculated.

In order to estimate $D_{s_i,r_j,t}$, we still need projection for $V_{s_i,r_j,t}$. A baseline projection is performed by using volume indicators from published reports, or extrapolating historical trend. The projection methods for these projections are listed in Table 5.8. GDP growth predictions baselines are based on OECD, World

Bank and US Congressional of Office Budget forecasts (OECD, 2014; U.S. Congressional Budget Office, 2019; World Bank, 2019a).

Table 5. 8 Projection methods for demand volume indicators for each end-use sector

Sector	Projection timeframe	Projection method
Construction	2018-2040	Extrapolated, assuming value added in construction equals GDP growth
Electrical	2018-2030	Modeled results from MIT MSL collaborators (Materials Systems Laboratory, 2019)
	2031-2040	Extrapolated, assuming constant regional growth rate
Industrial	2018-2040	Extrapolated, assuming linear relationship between value added in sector and GDP growth
Transportation	2018-2040	Modeled results from MIT MSL collaborators (Materials Systems Laboratory, 2019)
Consumer and others	2018-2040	Extrapolated, assuming growth equals GDP growth

Finally, total copper demand at year t can be calculated as $D_t = \sum_i \sum_j I_{s_i,r_j,t} \cdot V_{s_i,r_j,t}$. Following the same cathode price scenarios from Figure 5.5, we show the total copper demand response in Figure 5.11, where we also add the mining supply responses for comparison.

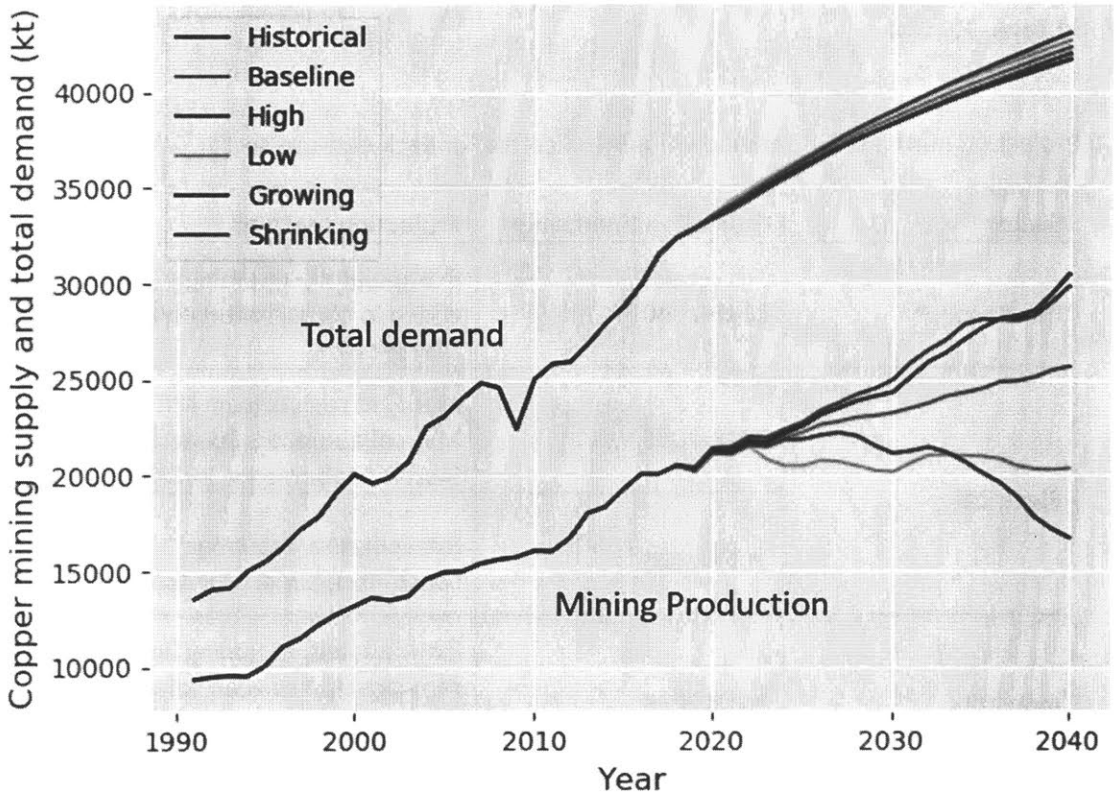

Figure 5. 11 Historical copper mining production and demand, and future simulated values under five price scenarios shown in Figure 5.5

It can be seen that while mining supply is very sensitive to price changes, total copper demand has a very low elasticity. The 2040 range of copper demand is [41669, 43060] kt, and the variation is less than 4%. The main reason for the low variation is that the mean of all price elasticities from the Bayesian model are very low (see Table 5.7). The GDP elasticity is much higher, and a higher/lower GDP scenario will be explored in the results section.

Refinery module

The function of the refinery module is to model cathode production from refineries, as a function of cathode price, TCRC and scrap price, and outputs the demand for both concentrate and refined copper scrap. It is worth noting that, while SX-EW mines also produce copper cathodes, they are not included in this module, and the SX-EW mining production is directly added to the total cathode production. Also, while concentrate is actually sent to smelters first to be smelted and then to be refined in refineries, this module essentially models smelters and refineries as integrated processors that produce cathode directly from concentrate.

A refinery level capacity and production data set from SNL metals and mining data (S&P Global Market Intelligence, 2019b) is investigated in detail. In order to estimate price sensitivities of cathode production. This dataset includes the annual production statistics from 378 refineries worldwide, between 1992 and

2016. For each year and each refinery, the refinery capacity, primary refinery production and secondary refinery production are reported. The total capacity and production time series are shown in Figure 5.12.

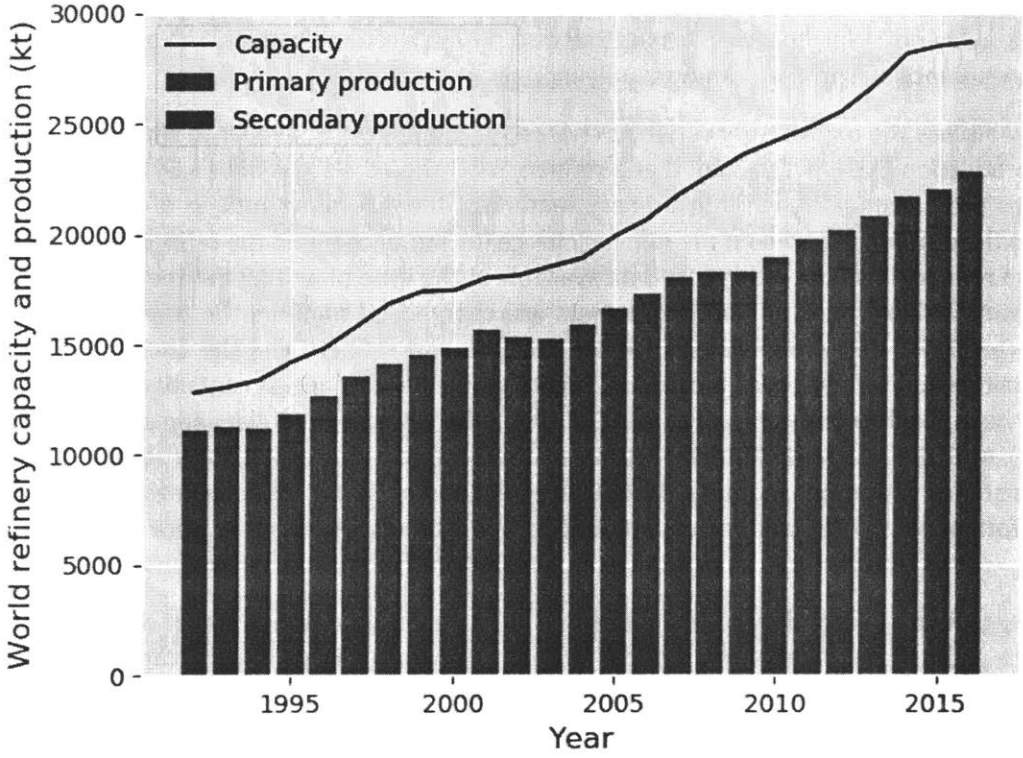

Figure 5. 12 World refinery capacity and production from 1992 to 2016 from SNL (S&P Global Market Intelligence, 2019b)

The average capacity utilization has been around 77% to 86% in the reported timeframe. In the 378 refineries from the SNL dataset, 104 refineries have been producing cathode from secondary materials, and the rest 274 refineries has been producing cathode from primary materials only. This former is called secondary refineries and the latter is called primary refineries in this chapter. 51 out of the 104 secondary refineries have also been producing cathode from primary materials. These are essentially refineries that are mixing raw materials from both primary and secondary sources, and the rest 53 are secondary only refineries. It is worth noting that, from an extraction process perspective, all refineries should have the capability to process both primary and secondary materials, for example, blister and anode board made from both concentrate and copper scrap. However, some refineries are using primary or secondary materials only, possibly because their source of supply has been limited to a few specific miners or scrap dealers.

Similar to how mining production is modeled in this chapter, production from a refinery should also be the product of its capacity and the rate of capacity utilization (CU). To model the changes in total refinery capacity, a simplistic approach is taken, instead of modeling the opening (addition of new refinery capacity) and closing (the removal of old refinery capacity) of refineries. It is assumed that the growth rate of total refinery capacity equals the growth of cathode consumption, with one-year lag. Essentially, I am assuming

that refineries' capacity can respond to changes in demand after one year, which is a much smaller lag than the opening and closing response of mining production. This assumption agrees with the opinion from a few industry experts I interviewed, who believed that adding new refinery capacity is easier than adding new mining capacity, because of smaller initial capital constraint and shorter construction period. Therefore, price responses are modeled explicitly only for CU. It is worth mentioning that, this one year lag assumption doe not apply to SX-EW mines that also produce refined copper. The production changes in SX-EW mines is modeled in the primary supply module.

Here I briefly discuss the explanatory variables chosen for modeling CU. Similar to the model developed for mining production CU, it is assumed that a refinery's CU should also be driven by its level of margin. For refineries producing cathode from primary materials, the operating margin of a refinery can be calculated as the difference between the refining charge (RC) to miners and the refinery's operating cost. As there is no refinery level operating cost data available at the time of writing this thesis, RC is chosen as the explanatory variable here. Historically, miners are charged by smelters the treatment charge and refining charge (TCRC) to have their concentrate smelted and refined, and the charge is then shared between smelters and refineries. As a baseline, the RC global benchmark (in cents per pound of payable copper) has been fixed to one-tenth of total TCRC global benchmark (in dollars per dry metric tonne of concentrate). As RC is linear with TCRC, the latter can also be used as the explanatory variable equivalently. For the consistency with other modules, TCRC is used instead of RC for modeling refineries' CU. Details around the formation of TCRC and factors influencing it will be discussed in the price formation module section.

For a refinery producing secondary cathode, the level of margin is determined by the difference between cathode price and its raw material scrap price (neglecting operating cost). Most scrap sent to refineries are either No.1 copper scrap (high grade unalloyed copper scrap with 99% nominal copper content) or No.2 copper scrap (unalloyed copper scrap with 96% nominal copper content, Institute of Scrap Recycling Industries code Birch), although most No.1 scrap is directly sent to semis fabricators to be directly melted without being first refined. Therefore, the difference between cathode price and No.1/No.2 scrap prices (also called spread) are used as explanatory variables for modeling secondary refineries' CU. The data sources used in this module are listed in Table 5.9.

Table 5. 9 Data used in the refinery module, time frame and data sources

Data description	Timeframe	Source
Refinery capacity utilization panel data	1992-2016	(S&P Global Market Intelligence, 2019b)
Annual TCRC		
COMEX cathode price		(Fastmarkets AMM, 2019)
No.1 scrap price		
No.2 scrap price		

The dynamic panel regression model is used for estimation. The SNL dataset is broken down into two subsets, one for the primary only refineries and the other subset for the secondary refineries. Models are estimated on both datasets, respectively. For primary refineries, the model for CU is

$$log(PCU_{i,t}) = \alpha + \rho log(PCU_{i,t-1}) + \beta log(TCRC_t) + \mu_i + \varepsilon_{i,t}$$

(Equations 5.24)

where PCU is the individual specific CU for primary only refineries. There isn't data available for the refinery specific RC, so the global TCRC benchmark series is used instead. The estimated elasticities are shown in Table 5.10, and the long run elasticity to TCRC is calculated to be 0.057.

Table 5. 10 Summary statistics for regression in Equation 5.24

	Dependent variable: $log(PCU_{i,t})$
$log(PCU_{i,t-1})$	0.313***
	(0.061)
$log(TCRC_t)$	0.039***
	(0.020)
Observations	n=130, T=24, N=1671
Notes:	*p<0.1; **p<0.05; ***p<0.01

Similarly, the model for secondary refineries' CU is

$$log(SCU_{i,t}) = \alpha + \rho log(SCU_{i,t-1}) + \beta log(TCRC_t) + \mu_i + \varepsilon_{i,t}$$

(Equations 5.25)

where SCU is the individual specific CU for all secondary refineries (including secondary only refineries and refineries mixing both primary and secondary raw materials). The No.1 and No.2 spread series are not found to be statistically significant. The estimated elasticities are shown in Table 5.11, and the long run elasticity to TCRC is 0.153. Although this is still a low elasticity, it is about three times the size of elasticity for PCU. A possible reason for the higher elasticity is that secondary refineries have more flexibility in sourcing raw materials, compared to primary refineries whose supply are usually locked in with long term contracts with miners and smelters.

Table 5. 11 Summary statistics for regression in Equation 5.25

	Dependent variable: $log(SCU_{i,t})$
$log(SCU_{i,t-1})$	0.508***
	(0.087)

$log(TCRC_t)$	0.075***
	(0.018)
Observations	n=97, T=24, N=1158
Notes:	*p<0.1; **p<0.05; ***p<0.01

The total refinery production can be determined by the capacity growth mechanism and the two models above. However, not all production from secondary refineries are secondary refined production, because some secondary refineries also have the capability to produce from primary sources. The ratio of secondary refined production in a secondary refinery is referred to as *secondary ratio* (SR), and a panel regression model is developed for it similarly. Conceptually, SR should depend on both TCRC and scrap spread: If TCRC increases, then it becomes more profitable for some secondary refineries to consume primary materials, and SR should decrease; If scrap spread increases, then consuming scrap becomes cheaper and SR should increase. The model form for SR is as follows:

$$log(SR_{i,t}) = \alpha + \rho log(SR_{i,t-1}) + \beta_1 log(TCRC_t) + \beta_2 log(Birch.Spread_t) + \mu_i + \varepsilon_{i,t}$$

(Equations 5.26)

Only the No.2/Birch scrap spread is found to be statistically significant. The coefficients are estimated in Table 5.12, and the long run elasticities to TCRC and No.2/Birch scrap spread are -0.197 and 0.316, respectively. These are higher elasticities and reflects the flexibility of secondary refineries substituting primary for secondary materials, or vice versa.

Table 5. 12 Summary statistics for regression in Equation 5.26

	Dependent variable: $log(SR_{i,t})$
$log(SR_{i,t-1})$	0.361***
	(0.077)
$log(TCRC_t)$	-0.126***
	(0.047)
$log(Birch.Spread_t)$	0.202***
	(0.073)
Observations	n=97, T=24, N=849
Notes:	*p<0.1; **p<0.05; ***p<0.01

Putting these models together, the total primary and secondary refined production can be expressed as

$$PRP_t = PC_t \cdot PCU_t + SC_t \cdot SCU_t \cdot (1 - SR_t)$$

$$SRP_t = SC_t \cdot SCU_t \cdot SR_t$$

(Equations 5.27 and 5.28)

Where the variables PRP_t, SRP_t, PC_t, SC_t are the total primary refined production, total secondary refined production, primary refinery capacity and secondary refinery capacity for year *t*, respectively. The two CU's and SR are determined by

$$PCU_t = PCU_{t-1} \cdot \left(\frac{TCRC_t}{TCRC_{t-1}}\right)^{0.057}$$

$$SCU_t = SCU_{t-1} \cdot \left(\frac{TCRC_t}{TCRC_{t-1}}\right)^{0.153}$$

$$SR_t = SR_{t-1} \cdot \left(\frac{TCRC_t}{TCRC_{t-1}}\right)^{-0.197} \cdot \left(\frac{Spread_t}{Spread_{t-1}}\right)^{0.316}$$

(Equations 5.29 to 5.31)

Note that all the subscripts *i* are taken out in the equations above. This is because the elasticities estimated from all panel regressions above are not individual specific, so I can equivalently model total refinery production as if there are only two large refineries in the world, one for primary and one for secondary.

While the total refined production numbers from SNL matches the reported total production from other data sources, such as USGS, ICSG and Copper Development Association (CDA), the secondary refined production from SNL is significantly lower than others. As a comparison, the 2010 total refined production is 18940 kt from SNL, 19100 kt from USGS, 18980 kt from ICSG, and 18970 kt from CDA, which are fairly close to each other. However, the secondary refined production from SNL is 1610 kt, which is 50% lower than the three other data sources. I believe that SNL significantly underestimated total secondary refined production, due to some refineries only reporting total refined production. However, it is assumed that SR_t of 2016 calculated from SNL data (the last year reported), based on the quotient of total secondary production to total secondary refineries' production (including production from primary sources), is representative for all secondary production including the missing production from SNL. In other words, there should be more refineries producing from secondary raw material than those shown in SNL, but the distribution of SS for those secondary refineries should be the same as those reported from SNL.

In order to determine the initial values (for 2018) of variables in Equations 5.27 and 5.28 that are consistent with other global production benchmarks, a final calibration process is performed. These initial values will be used as initial system conditions for the full simulation. First of all, the SR_{2018} is determined by predicting SR_t two years ahead into the future, using SR_{2016} as the initial value and the actual price history for TCRC and No.2 spread between 2016 to 2018. Secondly, both PCU_{2018} and SCU_{2018} are fixed at 86%, the 2018 annual refinery CU reported from ICSG (International Copper Study Group, 2018a). Thirdly, PC_{2018} and SC_{2018} are calculated so that the resulting PRP_{2018} and SRP_{2018} matches the world total numbers from ICSG (International Copper Study Group, 2018a).

Finally, PRP_t and SRP_t can be directly converted to the concentrate consumption and refined scrap consumption at year t, by dividing them with the concentrate to cathode efficiency and scrap to cathode efficiency respectively. Both efficiencies are set at 99% based on values from literature (Glöser et al., 2013).

Semis module

The function of the semis module is to output semis fabricators' demand for copper cathode and demand for direct melt copper scrap. It is assumed that semis fabricators do not change the stock of semis products, and therefore the amount of copper in semis production always equals the copper content in semis consumption, which is the result from the demand module. Also, I assume that the scrap directly used by semis fabricators is all direct melt scrap. While semis fabricators also indirectly consume scrap by using secondary copper cathode, this is included in the refined scrap demand. Together with the refinery module, the total demand for copper scrap can be calculated, as the sum of refined scrap demand and direct melt scrap demand.

Semi-finished products (semis) are classified based on ICA classification. 17 types of semis from 3 types of semis fabricators (wire mill, brass mill and foundry) are considered in this classification, shown in Table 5.13.

Table 5. 13 Semis classified based on ICA classification, by fabricator and alloyed/unalloyed

Semis fabricator	Alloyed/Unalloyed	Semis product
Wire Mill	Unalloyed	Building wire
		Power cable
		Magnet wire
		Telecommunications
		Electronic/data
		Equipment
		Automotive
		Bare wire
Brass Mill	Unalloyed	Tube
		Rod bar section (RBS)
		Plate sheet strip (PSS)
		Copper foil
	Alloyed	Tube
		RBS
		PSS
		Mechanical wire

Foundry	Alloyed	Castings

The second column in Table 5.13 indicates whether the semis product is made from unalloyed copper (cathode) or alloyed copper. In reality, copper alloys with designated copper content more than 93.3% but less than 96% for wrought alloys (or 94% for cast alloys) is called high copper alloys, and they are widely used by wire mills for making cables, wires and electrical contacts. However, it is assumed that these high copper alloys consumed by wire mills are only manufactured from copper cathode, and wire mills do not consume old scrap or external new scrap purchased from the market. In fact, based on CDA's 2013 scrap report (Jolly, 2013), even for the wire mill's own home scrap, it still requires a fire-refining step before re-entering the fabrication process. Therefore, while high copper alloys are actually consumed by wire mills, it is reasonable to assume that there is no direct melt scrap consumption and that all the wire mill consumption is coming from cathode. For brass mills, the ICA classification is already differentiating semis products made from copper and those made from copper alloys, and the former represents cathode consumption only.

The total semis production in copper content by semis is reported for 2006-2010 by the ICA dataset from Table 5.4. Based on this dataset, the accounting matrix for copper consumption by end-use sector to consumption by semis can be calculated (from 2006-2010 average), and copper demand by semis can be expressed as

$$U_{SM_j,t} = \sum_i U_{S_i,t} AC3_{S_i,SM_j}$$

(Equations 5.32)

where $U_{SM_j,t}$ is the consumption of copper for semis product j at year t, $U_{S_i,t}$ is the total consumption of copper in sector i and $AC3_{S_i,SM_j}$ is (i,j)th element for the accounting matrix mentioned above. The sum is over all sectors, since a certain type of semis can be consumed in multiple sectors. While this accounting matrix should in reality have changed over time, there is not enough high-resolution data to determine what the historical trend might have been. Therefore, it is assumed to be constant at the 2006-2010 average level in this module.

Based on Equation 5.32 above and using a constant accounting matrix, the total copper cathode consumption from the 12 unalloyed semis in Table 5.13 is calculated and compared with ICSG world refined copper consumption. The mean absolute percentage difference between the two series from 1960-2014 is only 5.1%, and this can be seen as a great fit given the inconsistencies between different data sources and the shift in the accounting matrix. It is therefore reasonable to assume that all copper cathode consumption is coming from the 12 unalloyed semis mentioned above, while all direct melt scrap consumption is attributed to the other 5 alloyed semis. This assumption agrees with the response from industry interviews that brass mills and foundries rarely consume copper cathode, and always prefer No.1 copper scrap when available, because of the cheaper price compared to cathode.

As a sanity check, the modeled cathode consumption is compared against historical total cathode production, including the SX-EW production and the primary/secondary refined production. Cathode consumption is calculated based on

$$CC_t = \sum_{j \epsilon USM} \sum_{i} U_{S_i,t} AC3_{S_i,SM_j}$$

(Equations 5.33)

where USM is the set containing indices for the 12 unalloyed semis. The results are shown in Figure 5.13, and it can be seen that production and consumption has been tracking each other in the last five decades, and the 2018 production/consumption is around 24000 kt.

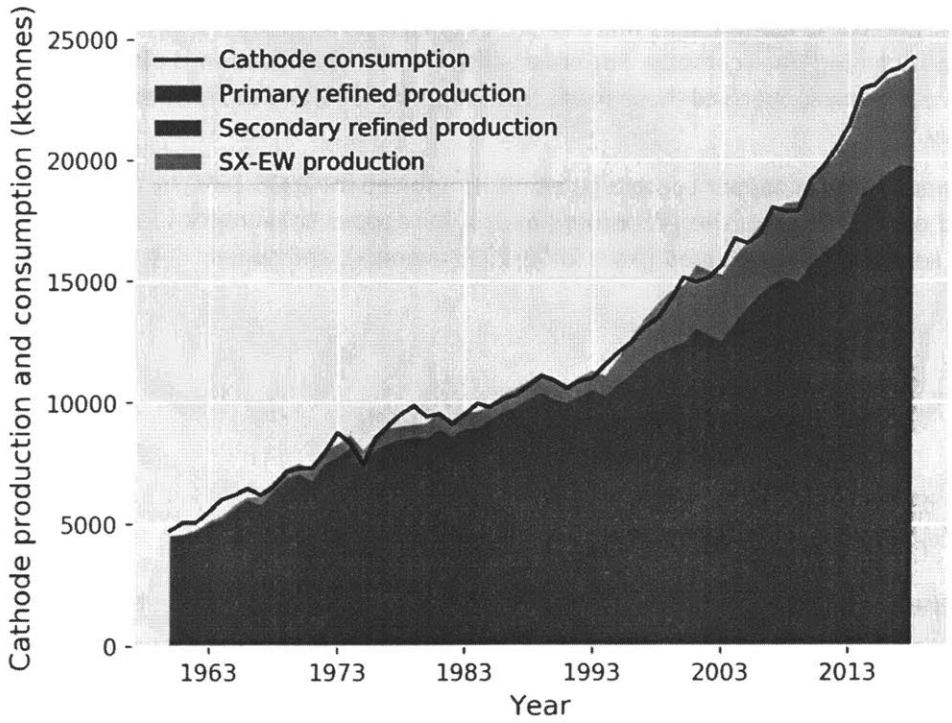

Figure 5. 13 Historical cathode production and consumption data

While the consumption for copper cathode is just for this one commodity, consumption for direct melt scrap includes various grades of copper scrap, including both alloyed and unalloyed scrap. The demand for a specific grade of scrap is dependent on many factors such as the price and availability of that grade of scrap, the quality of the scrap in terms of both chemical compositions and physical properties, the quality constraint of brass mills and foundries consuming direct melt scrap, and the demand for different grades of alloys of these fabricators. An attempt is made on modeling the breakdown of direct melt scrap demand. For reasons that will be discussed in a following section, this model does not affect the results on estimating copper displacement. Rather, the evolution of prices determined from the simulation can be used as inputs to this model. Here I briefly introduce the methodology, and the results on direct melt scrap breakdown will be shown at the end of this chapter.

Direct melt breakdown model

Acknowledgement: A part of this module is developed in collaboration with John Ryter, who is currently a PhD student in the Department of Materials Science and Engineering at MIT.

It is assumed previously that all the direct melt scrap is consumed by alloyed semis fabricators including brass mills and foundries, which produce different grades of alloyed products. For each grade of alloy, some specific scrap grades are preferred, for example, those scrap grade that have similar chemical compositions with the alloy. Therefore, the breakdown of direct melt scrap consumption depends on the grades and amount of alloy produced. Mathematically, consumption by alloy grade can be calculated for each alloyed semis as

$$U_{AL_j,t} = \sum_{i \epsilon ASM} U_{SM_i,t} AC4_{SM_i,AL_j}$$

(Equations 5.34)

$U_{AL_j,t}$ represents consumption of alloy grade AL_j at year t, and $AC4_{SM_i,AL_j}$ is an accounting matrix to calculate the fraction of alloy AL_j consumed for semis SM_i. The sum is over ASM, a set containing the five alloyed semis (Alloyed tube, alloyed RBS, alloyed PSS, mechanical wire and castings).

In total, 154 alloy grades are found that has been mentioned to be used in the five alloyed semis, based on several industry specifications (Davis, 2001; Copper Development Association, 2004; European Committee for Standardization, 2015). While no reported data is readily available for the accounting matrix $AC4$, it is modeled based on a supplier database from CDA (Copper Development Association, 2019a). The CDA copper alloy supplier database provided supplier counts for each alloy in a given semis in the US. For example, 19 suppliers produce alloy C93200 as tube, but only 4 suppliers produce it as a casting. Based on interviews with industry experts, we believe that alloys with more suppliers should make up a larger fraction of the consumption for each specific alloyed semis, compared to those with fewer suppliers. It is also assumed that these fractions do not simply follow the supplier counts linearly, but rather determined by the formula below.

$$Group\ Fraction_n = \begin{cases} 0.7, \ if\ n > mean(n) + 2 * stdev(n) \\ 0.2, \ if\ n > mean(n) + \frac{1}{2} * stdev(n) \\ 0.1, \ else \end{cases}$$

(Equations 5.35)

These group fractions were determined based generally on the 80-20 rule, which states that 80% of the market for each alloyed semis will be dominated by 20% of the alloys, though in this case modified to account for the large number of alloys with either no suppliers listed by the CDA or with a small number of suppliers. This large quantity of alloys with few or no suppliers produced a highly-skewed distribution,

hence both group fraction cutoffs being above the mean, and is representative of the large number of specialty alloys that introduce trace amounts of less common elements to the eventual scrap stream. Equation 5.35 is applied to each of the five alloyed semis, where n is the number of suppliers for each grade of alloy, $mean(n)$ is the arithmetic mean of the number of suppliers for each alloy, and $stdev(n)$ is the standard deviation of the same.

Within each group fraction, alloy fractions were determined based on the weight of each n in that group. For example, if only two alloys, A and B, for a given semis had sufficient suppliers to be in the 0.7 group fraction, where $n_A = 30$ and $n_B = 20$, the fraction assigned to alloy A would be 0.42, while the fraction assigned to alloy B would be 0.28. The resultant fractions for each alloy were then perturbed and renormalized iteratively until the average copper content of an alloyed semis matched that from the ICA data.

Once the accounting matrix $AC4$ is calculated, consumption for each of the 154 alloys can be calculated based on Equation 5.34. Then, the breakdown of direct melt scrap is based on a blending optimization model. The major model assumptions are

1. Alloyed semis fabricators (brass mills and foundries) have the capability to directly melt/blend different raw materials including refined metals, Barley and other grades of alloyed copper scraps into alloys. It is assumed that there is no loss of materials during the blending process, and the chemical composition of the final blended product is the weighted average of all raw materials.
2. The only quality constraint on the blended alloy product is the compositional specifications of elements in the alloy. In reality, there could be other quality constraints in the fabrication processes, such as requirements for mechanical properties and durability that might prohibit specific scrap grades into entering the melt. These other constraints are essentially neglected in this model.
3. It is assumed that raw materials costs only come from scraps and refined metals purchased. Other costs such as energy, labor, fixed costs, etc. are considered as constant. As long as compositional requirements are met, fabricators seek to minimize raw materials cost by purchasing the cheapest mix of raw materials as possible.
4. Fabricators allow for the possibility that some products could be out of the compositional requirements. Rather they control for the success rate, or the fraction of products that meet compositional requirements.
5. All grades of raw materials are assumed to be infinitely available.

Based on these assumptions, a blending optimization model is formulated mathematically as follows:

Objective:

$$\min(RMC) = \sum_i M_i P_i$$

Subject to:

1. Compositional constraints:

$$\forall j, Pr\left\{\sum_i M_i X_{ij} \leq c_j^U Q\right\} > \lambda$$

$$\forall j, Pr\left\{\sum_i M_i X_{ij} \geq c_j^L Q\right\} > \lambda$$

2. Mass balance:

$$\sum_i M_i = Q$$

(Equations 5.36 to 5.39)

The description of each variable/symbol can be found in Table 5.14. 23 grades of raw materials are used in this model, including 8 refined metals, 1 grade of unalloyed scrap (Barley) and 13 grades of alloyed scrap. The complete list of these grades and their compositional ranges are shown in Table A.1. Due to limited data availability for both scrap compositions and scrap prices, the 14 scrap grades used here represent groups of scrap grades rather than specific ISRI grades. For example, the *nickel-silver* scrap grade in this model corresponds to six ISRI grades (Maize, Major, Malar, Malic, Naggy, Niece). Also note that, this optimization should be applied to each specific alloy and to all years in the simulation. A chance constrained formulation is used here, i.e., the compositional constraints are probabilistic instead of deterministic. This formulation corresponds to assumption 4 mentioned above. In order to find the optimal solution, the compositional constraints are represented through the fuzzy number approach, following what is used in a previous study (Noshadravan, Gaustad, Kirchain, & Olivetti, 2017).

Table 5. 14 Description of variables used in the blending optimization model

Symbol	Description
RMC	Total raw material cost
M_i	Mass of raw material grade i consumed
P_i	Price of raw material grade i
X_{ij}	Mass fraction of element j in material i
$c_j^{U/L}$	Upper/lower limit for element j in alloy based on its specification
Q	Mass of alloy produced
λ	Confidence level of product meeting specification

In summary, the direct melt scrap breakdown model described above takes alloyed semis consumption and raw material prices as input, and outputs the amount of direct melt scrap consumption for each scrap grade. These inputs can be obtained from the full simulation model, and I will discuss the results at the end of this chapter.

Price formation module

Cathode price, TCRC and various scrap prices are key inputs to other modules including the primary supply, refinery and demand modules. Therefore, the function of the price formation module is to project prices one year ahead based on the imbalance between P&C of different commodities. Together with the other five modules that model supply and demand of copper ore/concentrate, cathode and scrap, the dynamic relationships between S&D and price can be simulated for the entire copper market. The models for each price is introduced in details below.

Cathode price

Copper cathode is traded between cathode producers (refineries and SX-EW mines) and semis fabricators, and cathode price is an important indicator for the S&D of the commodity. The trading of copper can be based on either spot contract if delivery is immediate upon transaction, or based on futures contract if delivery takes place at a future date specified by the contract. Only the spot contract price, or spot price in short, is modeled here, because spot price is believed to be a better indicator for current S&D than futures price (Turnovsky, 1983; Silvapulle & Moosa, 1999; R. K. Kaufmann & Ullman, 2009).

The trading of copper cathode can take place directly between a producer and a consumer, or indirectly with the facilitation of an exchange. In the former case, cathode price on exchanges is also used as a benchmark, and the two parties of the transaction can add a small premium or discount to the exchange price depending on the specific conditions of the two parties. Currently, three major commodity exchanges have provided marketplaces for copper spot and futures trading: the London Metal Exchange (LME), the commodity exchange owned and operated by CME Group (COMEX), and the Shanghai Futures Exchange (SHFE). The copper cathode spot prices on these three exchanges are often no more than 0.5% different from each other, after adjusting for currency exchange rates. This is because if there was a larger difference, then a trader could potentially buy low on one exchange and sell high on the other and use part of the profit to cover costs for the transactions. Such a process is called arbitraging, and the act of arbitrages decreases the price difference between exchanges and ensures price equality (Ross, 2012). Therefore, these price differences are neglected in the price formation module, and only LME cathode price is modeled. LME is selected from the three exchanges because it has been providing more liquidity than the other two exchanges, historically.

Factors influencing copper cathode price have been intensively studied by economists, commodity researchers and industry practitioners (W. C. Labys, Rees, & Elliott, 1971; Svedberg & Tilton, 2006; Mikesell, 2013; Sverdrup, Ragnarsdottir, & Koca, 2014). For mining companies in particular, cathode price is one of the most important factor determining short term profits, and the volatility in price has been a major source of risk to them. Fundamentally, all commodity prices should be determined by supply and demand, and the price at supply demand equilibrium should be the real value of the commodity (Baumol & Blinder, 2015). In reality however, the formation of price is much more complicated than the fundamental S&D indicates. Besides producers and consumers that trade physical copper in the market, an important part of market participants are speculators that trade either spot contracts or futures contracts in the expectation of earning monetary profit. Their buy (long)/sell (short) decisions can be based on various factors, including expectation of S&D, the level of inventory, monetary policies, general economic conditions, currency exchange rates, prices of other metals/commodities, and market sentiment, etc. For example, LME copper cathode price gained 11% following the week Donald Trump was elected the President of the United States. That gain was due to the expectation of increased copper

demand for infrastructure and construction, but in no way reflected an actual change in P&C level. It is worth pointing out that it is not the goal of this price formation model to estimate the impact of all the possible factors influencing cathode price mentioned above. Instead, an attempt is made to capture only the effect from the fundamental S&D.

Regression model

An autoregressive distributed lag (ARDL) model is constructed to estimate the S&D effect, shown in Equation 5.40.

$$\Delta P.Cat_t = \rho \Delta P.Cat_{t-1} + \beta_1 \Delta P.Oil_t + \beta_2 \Delta Inv.Cat_{t-1} + \varepsilon_t$$

(Equations 5.40)

$P.Cat_t$ is LME cathode price for time t in USD per tonned of copper, $P.Oil_t$ is the New York Mercantile Exchange (NYMEX) West Texas Intermediate (WTI) oil price in USD per barrel, and $Inv.Cat_t$ is a term for world cathode inventory in kt. The first lag of inventory, $Inv.Cat_{t-1}$, is selected because of higher statistical significance than $Inv.Cat_t$. All prices are in 2017 constant USD and all variables are first-differenced to be stationary. On the RHS, the first autoregressive term of cathode price is included to capture the effect of the most recent price trend. The second term, price of oil, is included in the regression in order to control for the various effects that are beyond the S&D of copper. Historically, the linear correlation between and LME copper cathode price and NYMEX WTI oil price has been 0.87 from 1990 to 2018. This high correlation suggests that many price influencing factors mentioned above, such as general economic conditions and market sentiment, affect the commodities market as a whole. Therefore, by including oil price in the regression, at least part of those effects which are beyond just the S&D of copper should be accounted for.

Finally, $Inv.Cat_t$, the ICSG World Refined Stock End of Period (International Copper Study Group, 2019a) is used as an explanatory variable in the regression. It is widely believed that stock/inventory data is used by market participants to inform their trading decisions. Inventory decrease may indicate a supply deficit and signals potential upward price movement, and increase in inventory may indicate the opposite. It is also a better indicator than refined P&C to signal changes in S&D, because the reporting frequency is usually higher. For example, while both refined production and consumption are reported by ICSG monthly (International Copper Study Group, 2019a), with two months of lag, inventory data is reported from LME and COMEX in a daily frequency and SHFE with a weekly frequency.

The inventory of copper is known to exhibit significant seasonality, mostly due to demand cycles. A major driver in world copper demand in the last two decades has been the use of copper in the construction sector from the Northern hemisphere, particularly from China. Production in the construction sector usually slows down before the Chinese New Year and warms up again in the spring, based on information from industry interviews. This seasonality component of the inventory needs to be filtered for the regression in Equation 5.40, because this kind of seasonality is well known to all market participants and should not influence the formation of price. The seasonality component for inventory data (monthly frequency between Jan 2005 and Dec 2018) can be filtered as follows:

1. For each month in a calendar year, calculate the average value of inventory for that month, across all the years. For example, the January average inventory is the average of all January inventory values from 2005 to 2018;
2. Replicate the twelve values calculated from step 1, for Jan 2005 to Dec 2018;
3. Remove the mean of the time series from step 2, by subtracting the mean of the series from it. This is the demeaned seasonality component of inventory;
4. Subtract the seasonality component from the time series of inventory. The remaining part is the deseasonalized inventory time series.

The result of seasonality filtering is shown in Figure 5.14.

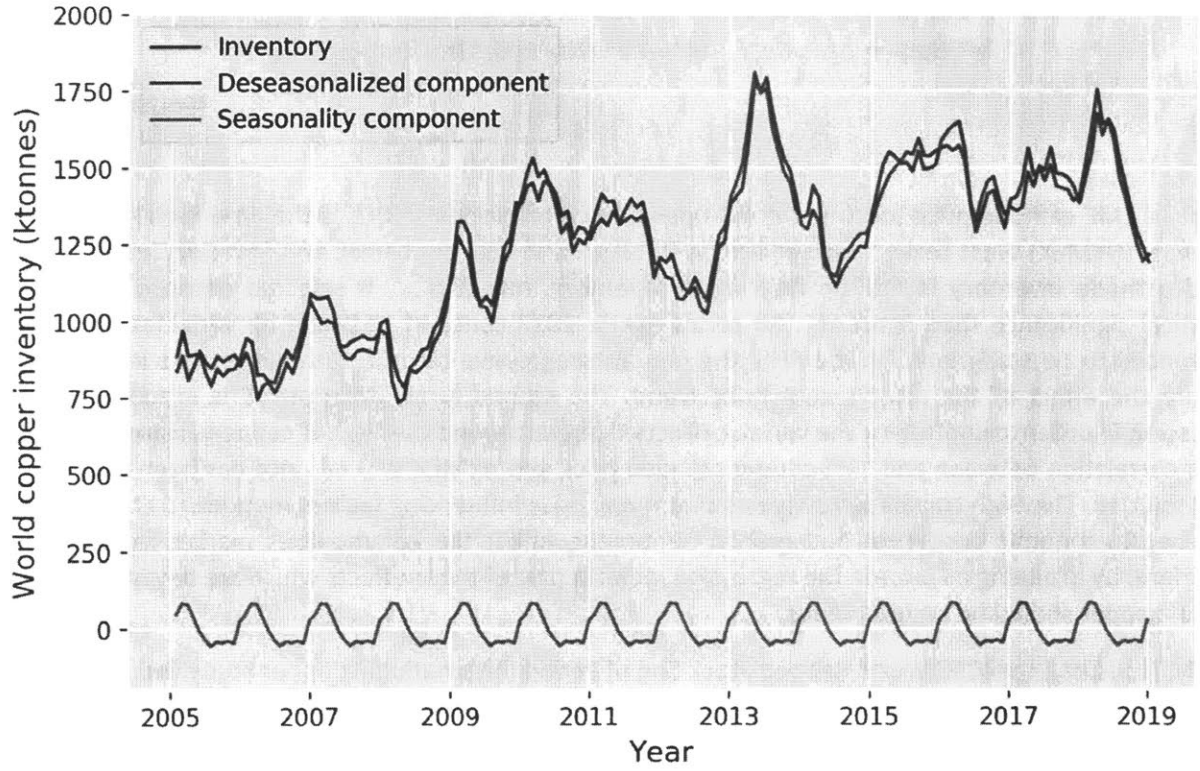

Figure 5. 14 World copper inventory from ICSG and its seasonal decomposition

The model in Equation 5.40 is estimated on a dataset with monthly frequency. While cathode price and oil price can be traced back to a longer history, inventory data is only available between Jan 2005 and Dec 2018. The coefficients estimated are shown in Table 5.15, and the long-run elasticity is calculated to be -1.356. Notice that this elasticity is not based on the Cobb-Douglas form between supply/demand and price, and the interpretation on this elasticity is that each kt of increase in world copper inventory should cause cathode price to move down 1.356 USD/t in the long run.

Table 5. 15 Summary statistics for regression in Equation 5.40

	Dependent variable: $\Delta P.Cat_t$

$\Delta P.Cat_{t-1}$	0.213***
	(0.067)
$\Delta P.Oil_t$	30.973***
	(5.030)
$\Delta Inv.Cat_{t-1}$	-1.068*
	(0.558)
Observations	n=166
Adjusted R2	0.291
F statistic	23.74***
Notes:	*p<0.1; **p<0.05; ***p<0.01

One thing worth pointing out is that, while inventory is used as the explanatory variable in the cathode price formation model, its future values cannot be directly simulated from other modules. Cathode production can be determined endogenously from the SX-EW portion of the primary supply module and the refinery module, and consumption can be obtained from the demand module and the semis module. However, the difference between P&C doesn't entirely explain the changes in inventory. The inventory variable used in the regression include not only stock from producers (SX-EW mines and refineries) and consumers (semis fabricators) but also stock from merchants, governments and exchanges. Together these consist the *visible inventory* of copper. However, there is also a large amount of unreported copper stock, or *invisible inventory*, most notably from those held in China's bonded areas. Recent surveys from Metal Bulletin (Metal Bulletin, 2019) indicate that the bonded copper stock in Shanghai alone is 30%-40% of the visible inventory, between 2016 and 2018. Based on the information from an anonymous copper trader in China, a significant portion of the copper in the bonded area is used by various merchants and individuals as collateral to borrow from banks, and this stock can be released back to exchanges, producers and consumers once the financing process is completed. The transferring of physical copper between visible inventory and invisible inventory is driven largely by the financial demand for copper rather than the physical demand.

Due to the existence of this financial demand and other unreported stocks, there is a mismatch between the P&C difference and the visible inventory used in the regression. The exact extent of financial demand is not modeled in here, due to lack of transparent data. Instead, the relationship between P&C difference and visible inventory is modeled with another simple linear regression, and it is found that P&C difference explains 46.7% of the changes in visible inventory. Therefore, the long-run elasticity from Equation 5.40 is multiplied by this factor to be used in the full simulation.

TCRC

From a high level, TCRC is a cash cost component to a miner producing concentrate and a source of revenue to a smelter/refinery. Similar to cathode price, TCRC is an indicator for the S&D of a commodity, copper concentrate. The level of TCRC influences mining production to some extent, and I have also shown in the refinery module that TCRC influences both the primary and the secondary refined production levels. However, different from the price of copper cathode, TCRC is not the price of a commodity, and also not

traded on major exchanges. Therefore, it is reasonable to assume that TCRC is driven mainly by physical producers (concentrate miners) and consumers (refineries). Speculators play a much lesser role in the TCRC market, and there is little hedging activities.

It is worth reviewing how concentrate is charged and TCRC is determined here in this section. When a transaction of concentrate takes place between a miner and a smelter, the buyer pays the seller value of the concentrate, minus TCRC and sometimes adjust for the metal content of the concentrate and the value of byproducts. This is equivalent to saying that miners pay smelters the TCRC, but in reality the payment is taken as a deduction to the selling price of the concentrate. Depending on the copper content of the concentrate, the buyer usually pay 93% to 97% of the copper content. This percentage is the *payable amount* mentioned in the primary supply module. For example, based on the specifications from Boliden (Söderström, 2008), a 96.65% payable amount is applied to concentrate with 30% or higher copper content. For concentrate with exactly 30% copper content, this is equivalent to 29% payable copper content in the concentrate. If the smelter and refinery processing the concentrate can do so with a recovery rate higher than the payable amount, they can essentially earn the value of *free metal*.

The treatment charge, TC, is priced based on per dry metric tonne (DMT) of concentrate. A 145 USD/DMT of TC is equivalent to 500 USD/t of payable copper, assuming 29% payable amount. The refining charge, RC, is priced based on payable copper and usually presented in US cents/lb. Although the units are different, it has been the custom of the copper industry to always set the value of RC as 1/10 of the value of TC. For example, 145 USD/DMT of TC indicates 14.5 US cents/lb of RC. Converted to the same unit, this RC is 319.67 USD/t of payable copper, about 64% of the TC above. The exact ratio of RC to TC depends on the copper content of the concentrate, but on average it is reasonable to assume that RC is linear with TC and therefore also linear with total TCRC. Historically, there has been a *price participation* (PP) agreement on long-term concentrate contracts, which specifies that RC shall be increased/decreased by 0.1 US cents/lb of payable copper for each 1 US cents/lb increase/decrease in LME cathode price, for each US cents/lb of LME cathode price above/below 90 US cents/lb. For example, if LME cathode price is at 190 US cents/lb, PP should be (190-90)*0.1=10 US cents/lb. However, miners have stopped to participate in the PP agreement since 2007. In addition to TCRC charged for copper in the concentrate, refineries can also charge for RC of precious by-product metals such as gold and silver, as long as the concentrate is sold for those metal contents. A copper concentrate can also be penalized for metals that are harmful to the smelting and refining processes, such as zinc.

The copper TCRC between a buyer and seller is negotiated between the two participating parties, and similar to cathode trading, there are spot contracts and long-term contracts. Long-term contracts are mostly negotiated on an annual basis, and they are preferred by smelters because long-term contracts provide stability to their revenue streams. At the end of each year, a group of some of the world's largest smelters and another group of large miners would sit together and negotiate a benchmark for long-term/annual TCRC that is used within these two groups for the next year. Other smaller smelters and miners would follow the benchmark or use it as a reference in their own negotiations. Since 2003, the China Smelters Purchase Team (CSPT), consisted of the 10 largest copper smelters in China, has been setting the annual TCRC benchmark with oligarch miners like BHP, Rio-Tinto and Freeport-McMoran. Different from long-term/annual contracts, spot contracts are negotiated throughout the whole year between miners, smelters and some traders. Spot TCRC is much more volatile than annual TCRC, and it depends on short term concentrate supply and demand conditions, among other factors. Based on a dataset including annual TCRC and spot TCRC (annual average) from 1982 to 2018 (S&P Global Market Intelligence, 2019b), it is found that spot TCRC is highly correlated with annual TCRC, with a linear correlation of 0.73. Based on the reasons described above, only the annual TCRC is modeled in the price formation module.

An ordinary least square (OLS) regression model is constructed as follows and estimated on the TCRC dataset mentioned above,

$$\Delta TCRC_t = \beta(P.Conc - C.Conc)_{t-1} + \varepsilon_t$$

(Equations 5.41)

where $TCRC_t$ is the annual TCRC of year *t* (in USD/t payable copper) and $(P.Conc - C.Conc)_{t-1}$ is the world concentrate production and consumption difference at year *t-1* (in kt), from ICSG data (International Copper Study Group, 2019b). TCRC is in 2017 constant USD it is first-differenced to be stationary. The index on P&C difference is *t-1*, because P&C at year *t* is in fact future information when $TCRC_t$ is determined at yearend *t-1*. A few factors are also tested for, but excluded from this regression model because of lack of statistical significance:

1. The autoregressive term of TCRC;
2. Copper cathode price. Higher cathode price indicate that smelters can earn higher profit from free metal, and therefore could potentially sacrifice for lower TCRC;
3. Oil price. This can be used as a proxy for the energy cost of smelters and refineries. Qualitatively, higher smelting/refining cost should lead to smelters/refineries charging more TCRC from miners;
4. Sulfuric acid price. Sulfuric acid is a major byproduct from copper smelting and an important revenue source for smelters. Similar to the reasoning on cathode price, higher sulfuric acid price means that smelters could compromise for lower TCRC.

The estimated result of the above regression model is shown in Table 5.16. This result can be interpreted as each kt production surplus at year *t-1* will cause TCRC to rise 0.164 USD/t of payable copper.

Table 5. 16 Summary statistics for regression in Equation 5.41

	Dependent variable: $\Delta TCRC_t$
$(P.Conc - C.Conc)_{t-1}$	0.164*
	(0.084)
Observations	n=36
Adjusted R2	0.073
F statistic	3.824*
Notes:	*p<0.1; **p<0.05; ***p<0.01

Scrap prices/spreads

Copper scrap is generated and collected from both pre-consumer and post-consumer sources. Due to variation in semis products and final products, copper scrap collected from both sources also vary in copper content, alloyed metal content, shapes, sizes, etc. Copper scrap is not traded on major exchanges,

but many scrap yards/dealers/traders are essentially acting as the marketplace for scrap sellers and scrap buyers, and prices are negotiated between the buyers, sellers and dealers.

The scrap price/spread formation model developed here is based on both qualitative and quantitative information learned from industry interviews and historical data. Below I briefly describe the value chain of copper scrap from generation to consumption. This value chain can be illustrated by the schematic in Figure 5.15. First, scrap that is sent to the market is generated either from in-use stock (old scrap) or the semis/final product fabrication residue (external new scrap). Then these scrap is collected by various scrap collecting individuals and/or local scrap yards. These individuals and yards are usually small in size and have limited direct connections with end consumers such as refineries and brass mills. Instead they can sell their scrap to wholesale scrap yards and scrap dealers that are connected with consumers. These wholesale yards/dealers have more capability to meet the requirement to consumers, and often they have facilities to sort/disassemble scrap they obtained from upstream.

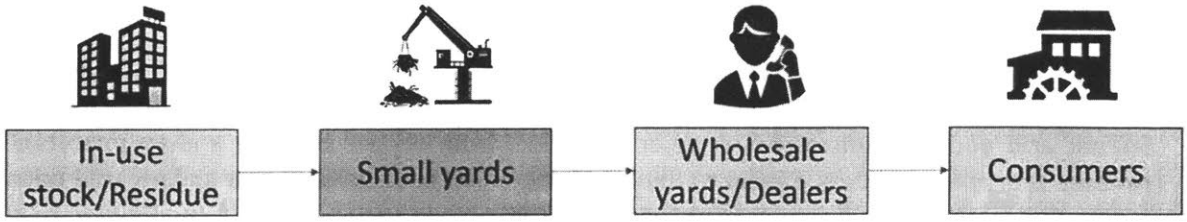

Figure 5. 15 Simplified old scrap supply chain structure. Small yards are highlighted because it is believed to be the bottleneck for old scrap supply

The value chain described above is a simplification of the complex scrap trading network in reality. Between scrap generation and scrap reaching end consumers, there could be just one middleman or multiple middlemen, but essentially all of the scrappers/yards/dealers are acting the market place to facilitate scrap buying and selling. However, small yards and wholesale yards/dealers in Figure 5.15 are still differentiated due to one key distinction. Historically, changes in copper scrap prices have closely followed changes in copper cathode price, especially for unalloyed copper scrap such as No.1 and No.2 scrap. Due to small yards limited financial capability, they usually cannot hedge the risk of price variations. Therefore, their business model is often based on speculating cathode price: when price is going down, small yards would hoard more copper; And when price is rising, they would release their inventory to the market. This type of behavior has created mismatch between the supply and demand of copper scrap: even when scrap demand and generated old scrap amount is high, small yards would not make much scrap available to consumers, as long as scrap prices are dropping. Therefore, small yards are essentially the bottleneck of scrap supply, and the box standing for small yards is highlighted in Figure 5.15 for this reason. Wholesale yards/dealers on the other hand, are usually more financially capable and aware than small yards. They usually hedge against variation in copper price, and build their business based on earning the buying/selling price difference. Based on industry sources, many of these yards are public companies that are required by government/exchange regulations to not speculate. Therefore, it is reasonable to assume that the amount of scrap purchased and sold by wholesale yards/dealers are not the function of copper scrap prices.

Based on the qualitative description of the copper scrap value chain above, the scrap price formation model can be constructed as follows. Assume that for a particular grade of scrap, the recoverable amount

of old scrap plus external new scrap reaching small yards during period [t, t+1] is SS_t. During this period, small yards adjust their inventory from $I_{S,t}$ to $I_{S,t+1}$ and the difference $\Delta I_{S,t+1} = I_{S,t+1} - I_{S,t}$ is can be modeled as a function of change in cathode price

$$\Delta I_{S,t+1} = -\beta \Delta P.Cat_{t+1} + \varepsilon_t$$

(Equations 5.42)

Coefficient β is expected to be positive. The recoverable amount of scrap reaching wholesale yards/dealers during period [t, t+1] is therefore $SS_t - \Delta I_{S,t+1}$. If the scrap consumption during the same period is SC_t, then the inventory change at wholesale yards/dealers $\Delta I_{W,t+1} = I_{W,t+1} - I_{W,t}$ can be expressed as

$$\Delta I_{W,t+1} = SS_t - SC_t - \Delta I_{S,t+1}$$

(Equations 5.43)

Similar to the model for cathode price, the inventory change at wholesale yards/dealers should be an indicator for scrap price changes. However, it is assumed that inventory change only affects scrap spread, the difference between cathode price and scrap price. This is because the intrinsic value of copper scrap is still based on the value of copper cathode, and changes in S&D should only move the spread. Conceptually, this is similar to how concentrate is priced between miners and smelters: the value of copper content in the concentrate is always based on cathode price, but S&D of concentrate would influence the level of TCRC. Putting everything together, the first difference of scrap spread can therefore be expressed as

$$\Delta Spread_t = \gamma \Delta I_{W,t} + e_t = \gamma(SS_{t-1} - SC_{t-1}) + \gamma\beta \Delta P.Cat_t + u_t$$

(Equations 5.44)

The first term on the RHS, $\gamma(SS_{t-1} - SC_{t-1})$, is the *scrap S&D effect* that captures impact from scrap S&D conditions. The second term, $\gamma\beta \Delta P.Cat_t$ is the *cathode price effect* that affects scrap spread due to speculation activities at the small yards. Both γ and β are expected to be positive.

The model in Equation 5.44 should in theory be estimated for each different grade of copper scrap, since each grade of scrap should be priced differently. However, to the best of my knowledge, no data is available for the global supply and consumption for any specific copper scrap grade. Therefore, the total scrap supply and consumption statistics is used to estimate scrap S&D effect.

Before describing the estimation process, I first briefly describe the different grades of copper scrap. The Institute of Scrap Recycling Industries (ISRI) has been classifying copper scrap grades in its annual *Scrap Specifications Circular*, and it recognizes 52 copper scrap grades in its latest publication (Institute of Scrap Recycling Industries, 2018). These grades have been used as industry standards for scrap trading

participants. Generally speaking, these grades can be broken down into two buckets, one for unalloyed copper scrap and the other for alloyed copper scrap. For unalloyed copper scrap, the industry differentiates between No.1 scrap (copper content > 99%) and No.2 scrap (copper content between 94% to 99%). The ISRI grades provide more granularity, and further classifies a few different grades for both No.1 and No.2 scrap. The highest ISRI grade of unalloyed copper scrap is coded as *Barley*, also commonly known as No.1 Bare Bright or Brass mill's No.1. It consists of only No. 1 bare, uncoated, unalloyed copper wire. Due to its high quality, Barley is used by brass mills as direct melt scrap and is rarely used by refineries. Refineries can use slightly lower grades of unalloyed scrap such as *Berry* (also known as Refinery's No.1) and *Birch* (No.2 copper wire). As a reminder, the price of Berry and Birch are used in the refinery module to model the response of CU and secondary ratio but only Birch is included in the final model due to statistical significance. The price of Barley shall be used in a blending optimization model to determine the breakdown of direct melt scrap. Therefore, only the prices of Barley and Birch are considered in the price formation module, as they are the only two unalloyed copper scrap prices to be used in the full simulation.

The monthly average prices of copper cathode, brass mill buying price of Barley and refinery buying price of Birch are shown in Figure 5.16, between 1995 to end of 2018. The prices of Barley and Birch are obtained from American Metal Market (AMM) (Fastmarkets AMM, 2019). All prices are shown in 2017 constant USD.

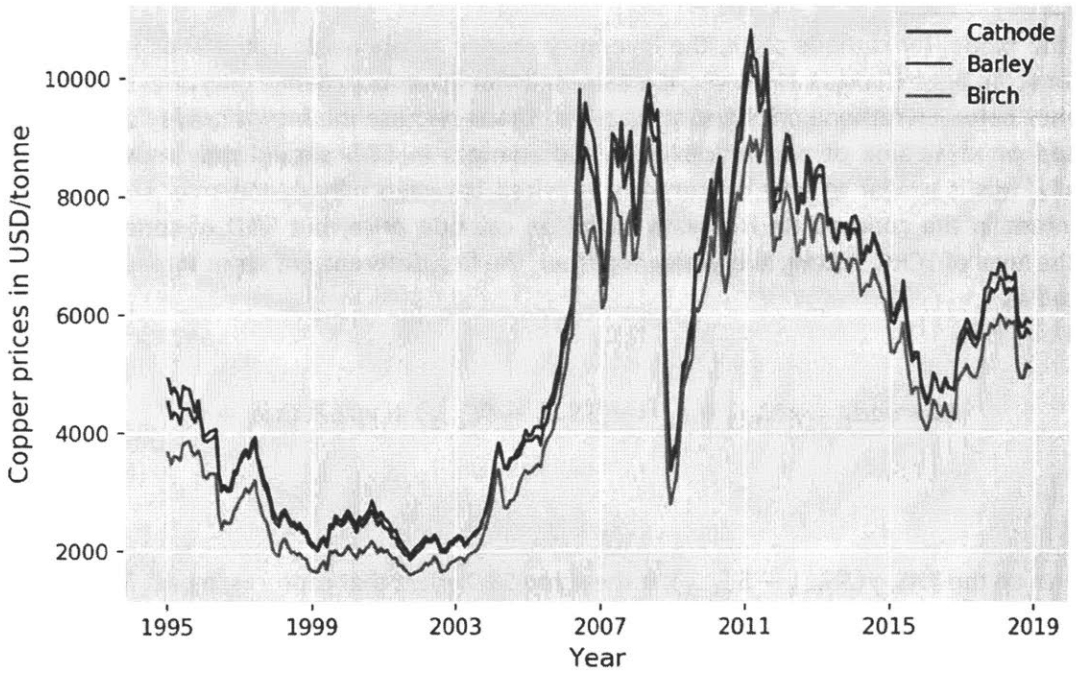

Figure 5. 16 Historical prices of copper cathode, Barley and Birch

It can be seen that cathode price is almost consistently higher than both Barley and Birch, and the spread of Barley is only 3% of cathode price on average. This low spread is an indicator of Birch's high quality. The spread of Barley has even been negative for three short periods during the entire timeframe presented in Figure 5.16, possibly due to brass mills not capable of getting enough cathode under extremely tight

cathode supply. The price of Birch has been consistently lower than cathode, and the Birch spread has been 15% of cathode price on average.

Two regression models are constructed to estimate the cathode effect on the spread of Barley and Birch. Lag terms and lag orders selection are based on BIC and statistical significance of variables. The two models are expressed as follows, and the estimated coefficients are shown in Table 5.17 and Table 5.18, respectively.

$$\Delta Barley.Spread_t = \beta \Delta P.Cat_t + \varepsilon_t$$

$$\Delta Birch.Spread_t = \rho \Delta Birch.Spread_{t-1} + \beta \Delta P.Cat_t + \varepsilon_t$$

(Equations 5.45 and 5.46)

Table 5. 17 Summary statistics for regression in Equation 5.45

	Dependent variable: $\Delta Barley.Spread_t$
$\Delta P.Cat_t$	0.064***
	(0.007)
Observations	n=309
Adjusted R2	0.190
F statistic	73.62***
Notes:	*p<0.1; **p<0.05; ***p<0.01

Table 5. 18 Summary statistics for regression in Equation 5.46

	Dependent variable: $\Delta Birch.Spread_t$
$\Delta Birch.Spread_{t-1}$	0.205***
	(0.049)
$\Delta P.Cat_t$	0.146***
	(0.016)
Observations	n=309
Adjusted R2	0.252
F statistic	52.97***
Notes:	*p<0.1; **p<0.05; ***p<0.01

The long-run cathode effect for Barley and Birch spread calculated based on Equation 5.45 and 5.46 are 0.064 and 0.184, respectively. These coefficients can be interpreted as: a 1 USD/t of increase in cathode price will cause Barley spread and Birch spread to increase 6.4 US cents/t and 18.4 US cents/t, respectively.

Alloyed copper scraps, on the other hand, are priced differently from unalloyed scraps. Besides copper, there are various other metal contents in alloyed scraps, such as zinc, lead, tin, nickel, aluminum, manganese, iron, etc. Zinc is widely used in brasses and bronzes and is the most common alloying elements in these scraps. The value of zinc in alloyed scraps is usually accounted for during scrap trading. This can be done, for example, by multiplying the zinc content by the LME zinc spot price on the day of transaction. Other alloying elements, however, are not always credited for their values. For example, tin is a valuable alloying element, and LME tin price has been around 20k USD/t in recent years, about three times the price of copper. Therefore, semis fabricators that produce tin bronze products can directly melt tin bronze scraps to fabricate new products, and they would pay for the tin content in alloyed scraps. However, fabricators of red brass semis usually need to control the tin content in semis under 0.3% (cite CDA), so a high tin content in the scrap causes problem for them and they would need to dilute this scrap with other purer scraps or refined metals in order to meet the product specifications. In short, *quod ali cibus est aliis fuat acre venenum* (one man's meat is another man's poison). What is valuable to one fabricator might be the problem of another. Furthermore, according to an industry expert, the alloyed scrap market has been very illiquid, and a scrap seller often cannot find a buyer who would pay for all the elements in an alloyed scrap.

Based on the information above, the *nominal value* of alloyed scraps is calculated as 100% the value of copper and zinc and s% of all other alloying elements. s is a tuning parameter here and is set to be 50% as a baseline. The spread of a grade of alloyed scrap is calculated as the difference between the nominal value and its consumer buying price. In the scrap price dataset from AMM, only four grades (ISRI codes: Ocean, Honey, Enerv, Ebony) of alloyed scrap are collected, and data collection only started from 2011. Their spreads are calculated respectively and presented in Figure 5.17.

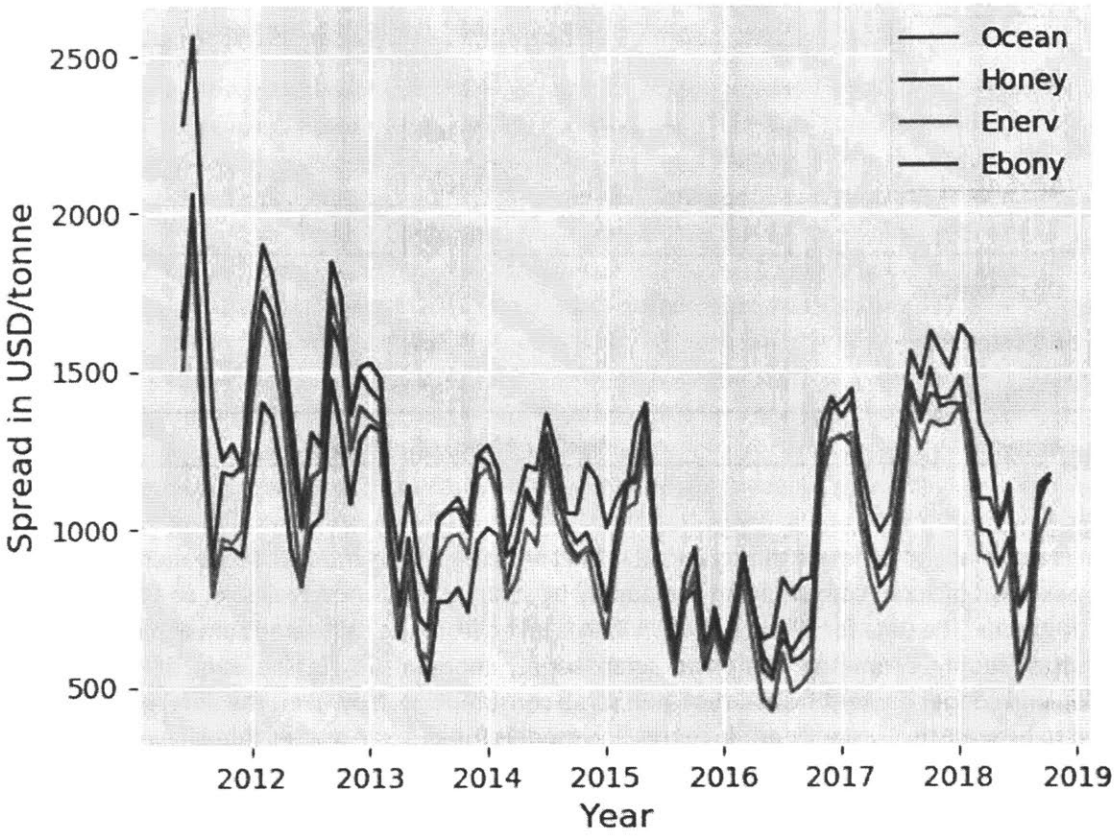

Figure 5. 17 Historical spread calculated as difference between nominal value and consumer buying price, for four grades of alloyed scrap

All these spreads show very similar trends. The first differences of these four series of spreads are highly correlated with each other, with the lowest correlation being 0.94. Therefore, it is assumed that $\Delta Alloyed.Spread_t$ is essentially the same for all grades of alloyed scraps, and the average $\Delta Spread_t$ of the four grades above is used as an outcome variable in the regression model to estimate the cathode effect. The model form after lag orders and terms selection can be expressed as

$$\Delta Alloyed.Spread_t = \beta_1 \Delta P.Cat_t + \beta_2 \Delta P.Cat_t + \varepsilon_t$$

(Equations 5.47)

The estimated coefficients are shown in Table 5.19, and the long-run elasticity on cathode effect is 0.412. The interpretation is that a 1 USD/t of increase in cathode price will cause all alloyed scrap spreads to increase 41.2 US cents/t.

Table 5. 19 Summary statistics for regression in Equation 5.47

	Dependent variable: $\Delta Alloyed.Spread_t$
$\Delta P.Cat_t$	0.599***
	(0.036)
$\Delta P.Cat_{t-1}$	-0.187***
	(0.035)
Observations	n=87
Adjusted R2	0.764
F statistic	141.5***
Notes:	*p<0.1; **p<0.05; ***p<0.01

An attempt is also made to estimate the scrap S&D effect with regression models. I have mentioned earlier that the breakdown of scrap consumption and supply by scrap grade is not available, so total scrap data is used for all grades. The data for SS_t in Equation 5.44 is taken from the calibrated sum of old scrap supply and new scrap supply estimated from the scrap supply module. SC_t is the sum of refined scrap consumption and copper content from direct melt scrap consumption. However, the difference $SS_t - SC_t$ is not found to be statistically significant in regression models for all scrap grades that I have data for. One possible reason for the lack of statistical significance is that SS_t is based on modeled result from the scrap supply module rather than from actual data from survey. Nevertheless, based on the qualitative understanding of the copper scrap value chain and opinions from industry experts, I still believe that scrap S&D effect does exist for all scrap spreads.

A different coefficient γ in Equation 5.44 is assigned to each different grade of scrap. This coefficient represents the elasticity of spread to scrap S&D effect, and is termed the SSDE coefficient in this chapter. For all the scrap grades considered, the first difference of scrap spreads $\Delta Spread_t$ are all highly correlated with the cathode effect term $\Delta P.Cat_t$ (the coefficient $\gamma\beta$ does not affect the strength of the correlation). The linear correlation coefficient between the annual $\Delta Spread_t$ and $\Delta P.Cat_t$ is 0.64 for Barley, 0.85 for Birch and 0.91 for alloyed scraps. These high correlations indicate that cathode effect alone explained a majority of the variation in $\Delta Spread_t$, and the size of scrap S&D effect should be much smaller than the cathode effect. Therefore, the baseline values for SSDE coefficients are set so that the mean of absolute for scrap S&D effect is 10% of the mean of absolute for cathode effect, for each grade of scrap. As there is still some arbitrariness in assigning these SSDE coefficients, the response of the simulation system to the variation in these parameters will be examined in a sensitivity analysis later.

System evolution

The six modules introduced above compose the full simulation system for estimating displacement. The initial year is set as 2018 in the simulation, because all the information on prices, production and consumption in 2018 is available from historical data. The future changes in price are then determined by the price formation module, and these modeled changes can then be used to calculate prices in 2019. The price formation equations used in the simulation are described as follows:

$$\Delta P.Cat_t = -0.461(P.Ref_{t-1} - C.Ref_{t-1})$$

$$\Delta TCRC_t = 0.164(P.Conc_{t-1} - C.Conc_{t-1})$$

$$\Delta Birch.Spread_t = 0.184\Delta P.Cat_t + 0.0845(S.Scrap_{t-1} - C.Scrap_{t-1})$$

$$\Delta Barley.Spread_t = 0.0643\Delta P.Cat_t + 0.0296(S.Scrap_{t-1} - C.Scrap_{t-1})$$

$$\Delta Alloyed.Spread_t = 0.412\Delta P.Cat_t + 0.190(S.Scrap_{t-1} - C.Scrap_{t-1})$$

(Equations 5.48 to 5.52)

The description of variables can be found in Table 5.20. Only the Birch (No.2) spread is used for the simulation of displacement, while the spread for Barley and alloyed scraps are used in the simulation for direct melt scrap breakdown. Following the above set of equations, the prices of cathode, TCRC and spreads can be projected for 2019. These prices are then used to simulate production and consumption of concentrate, copper scraps and cathode in 2019:

Primary supply module:

$$P.Conc_t = f_{PS,Conc}(\{P.Cat_\tau\}_{t-9}^{t}, TCRC_t)$$

$$P.SXEW_t = f_{PS,SXEW}(\{P.Cat_\tau\}_{t-9}^{t}, TCRC_t)$$

$$P.Mine_t = P.Conc_t + P.SXEW_t$$

(Equations 5.53 to 5.55)

Scrap supply module:

$$S.Scrap_t = f_{SS}(Material\ Flows)$$

(Equations 5.56)

Demand module:

$$D_{s_i,r_j,t} = f_D(P.Cat_{t-2}, P.Cat_{t-1})$$

(Equations 5.57)

Refinery module:

$$P.Ref_{t,Pri} = f_{R,Pri}(TCRC_t, Birch.Spread_t)$$

$$P.Ref_{t,Sec} = f_{R,Sec}(TCRC_t, Birch.Spread_t)$$

$$P.Ref_t = P.Ref_{t,Pri} + P.Ref_{t,Sec} + P.SXEW_t$$

$$C.Conc_t = P.Ref_{t,Pri}/0.99$$

$$C.Scrap_{t,Ref} = P.Ref_{t,Sec}/0.99$$

(Equations 5.58 to 5.62)

Semis module:

$$C.Ref_t = f_{S,Ref}\left(\left\{D_{s_i,r_j,t}\right\}\right)$$

$$C.Scrap_{t,DM} = f_{S,DM}\left(\left\{D_{s_i,r_j,t}\right\}\right)$$

$$C.Scrap_t = C.Scrap_{t,Ref} + C.Scrap_{t,DM}$$

(Equations 5.63 to 5.65)

The description of all variables and functions can also be found in Table 5.20. All the production and consumption values for 2019 can be calculated from Equation 5.53 to 5.65. These values can then be fed into the price formation equations again in order to project prices in 2020. As long as the initial conditions are provided for 2018, the system can evolve based on these equations without inputting prices exogenously.

Table 5. 20 Description of all variables and functions used in the evolution of the system

Variable	Description
$P.Cat_t$	Copper cathode price
$TCRC_t$	Annual TCRC benchmark
$Barley.Spread_t$	Difference/spread between brass mill buying price of Barley and cathode price
$Birch.Spread_t$	Difference/spread between refinery buying price of Birch and cathode price
$Alloyed.Spread_t$	Difference/spread between consumer buying price of alloyed scrap and its nominal value
$P.Ref_t$	World total production of refined copper/cathode
$P.Ref_{t,Pri}$	World total production of refined copper/cathode from primary materials
$P.Ref_{t,Sec}$	World total production of refined copper/cathode from secondary materials
$P.SXEW_t$	World total production of refined copper/cathode from SX-EW mines

$C.Ref_t$	World total consumption of refined copper/cathode
$P.Conc_t$	World total production of copper concentrate
$C.Conc_t$	World total consumption of copper concentrate
$P.Mine_t$	World total mining production
$S.Scrap_t$	World total supply of copper scrap, in recoverable amount of copper content
$C.Scrap_t$	World total consumption of copper scrap, in copper content
$C.Scrap_{t,Ref}$	World total consumption of refined copper scrap, in copper content
$C.Scrap_{t,DM}$	World total consumption of direct melt scrap, in copper content
$D_{s_i,r_j,t}$	Copper demand for sector i, region j
Functions	**Description**
$f_{PS,Conc}$	Output concentrate production from the primary supply module, as a function of cathode price history in last ten years and current year TCRC
$f_{PS,SXEW}$	Output SXEW production from the primary supply module, as a function of cathode price history in last ten years and current year TCRC
f_{SS}	Output total scrap supply in recoverable amount of copper content from old scrap and external new scrap, as a function of material flows
f_D	Output sectorial and regional copper demand, as a function of last two year cathode prices
$f_{R,Pri}$	Output primary refined production, as a function of TCRC and Birch (No.2) scrap spread
$f_{R,Sec}$	Output secondary refined production, as a function of TCRC and Birch (No.2) scrap spread
$f_{S,Ref}$	Output refined scrap consumption, as a function of copper demand
$f_{S,DM}$	Output direct melt scrap consumption, as a function of copper demand

Results from baseline scenario

As I mentioned earlier, this simulation system can evolve spontaneously under a set of initial conditions and system parameters. With more than 100 system parameters, I have a huge parameter space within which many scenarios can be explored. At the origin of the parameter space, all system parameters are kept in their baseline values. This corresponds to the baseline scenario of the simulation, and the results from this scenario are presented below.

Prices

All scenarios are simulated up to 2040. The evolution of cathode price, annual TCRC and Birch spread are shown in Figure 5.18 to 5.20, and the black dashed lines in all figures represent the year of 2018, the initial

year for the simulation. Historical prices before 2018 are also shown in each figure for comparison. All prices are shown in 2017 constant USD, both for historical prices and projected prices.

Two patterns can be noticed for the projection of cathode price. First, while the historical price volatility from 1960 to 2018 is calculated to be 22.5%, the price volatility in the projection from 2018 to 2040 is merely 3.6%. As cathode price in the simulation is only driven by the production and consumption difference of cathode, the difference in historical and projected volatility can be explained by other factors such as market sentiment, price of other commodities, general economic conditions, etc. These other factors are essentially held as constant in the simulation. Second, it can be noticed that projected cathode price roughly follows a sinusoid, with two peaks and valleys in the projection. This observation matches the prediction from commodity cycle theories: both production and consumption of a commodity responds to its price, but there are imbalances and lags in the two responses, which causes surplus or deficit in supply for temporary periods. Price will eventually balance S&D by pushing one up to pressing the other down. Therefore, commodity price in reality should oscillate around the value/equilibrium price of that commodity, and the length of cycles are dependent on multiple factors such as speed of production and consumption response, price elasticities and so on.

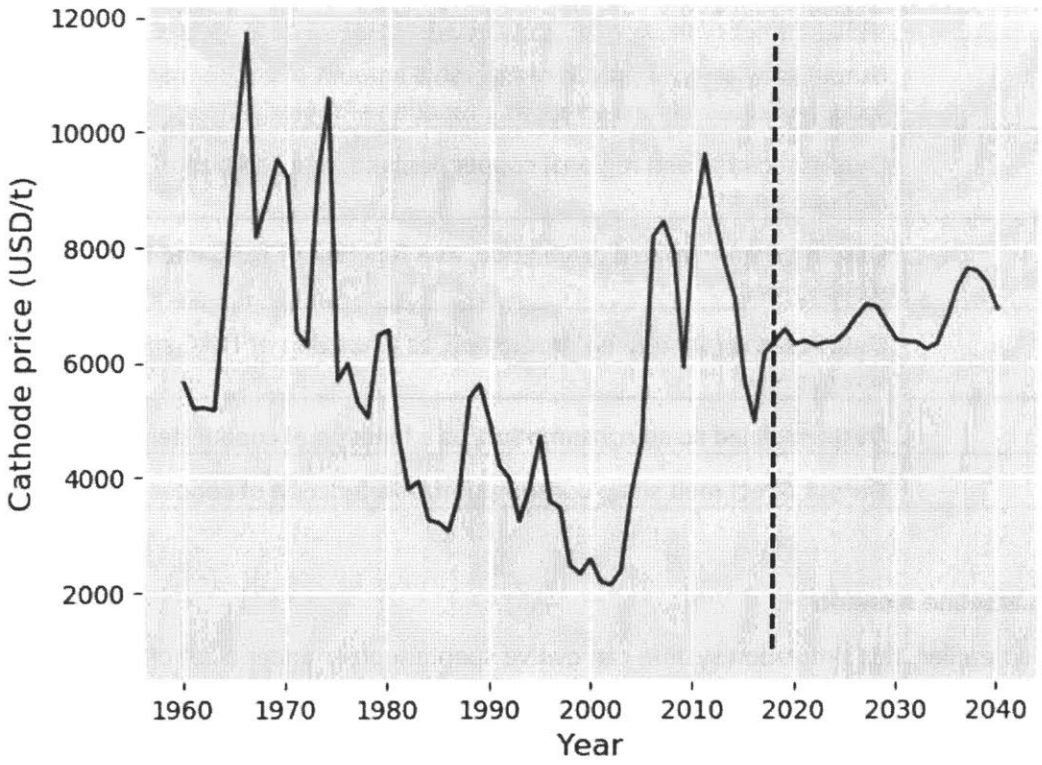

Figure 5. 18 Historical and simulated copper cathode price in 2017 constant USD/t

The evolution of TCRC is shown in Figure 5.19. While the projected volatility (7.3%) is also significantly smaller than historical volatility (24.8%), there are not obvious signs of cycles, and TCRC has been increasing almost every year since 2031. This pattern is the result of a cascade of system responses, but it is most likely mainly affected by the mining supply's behavior. In the primary supply module, mine

opening decision is based on the ten year moving averaged cathode prices. The peaks of cathode price around 2027 and 2037 might have shifted the moving average significantly so that many new mines are opening. Once these mines open, production will last for many years before the depletion of resources, and the short run elasticity is very low. Therefore, surplus in mining production (and therefore concentrate production) will sustain for a relatively long period, which will cause TCRC to rise. Eventually TCRC should fall down and follow its own cycles, but these cycles might be longer than the simulation timeframe.

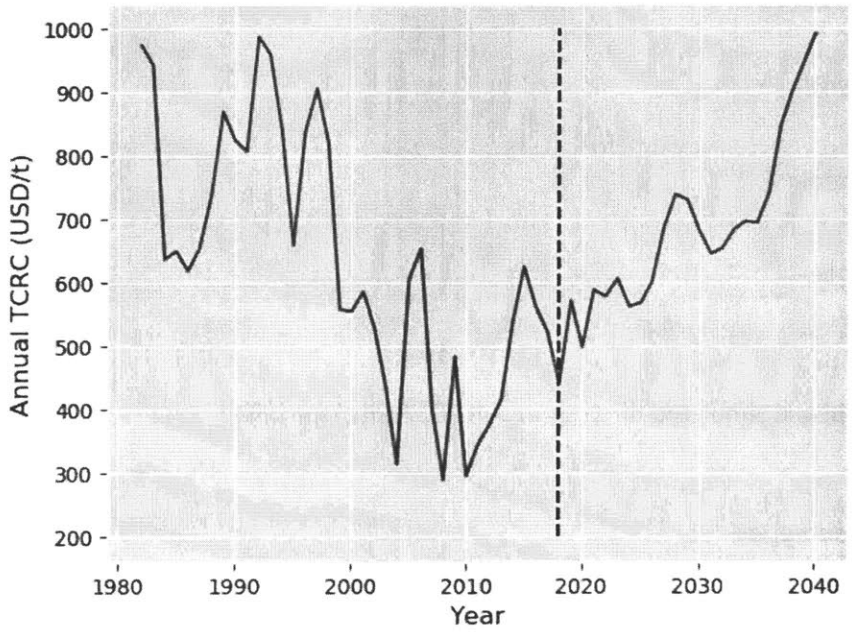

Figure 5. 19 Historical and simulated annual TCRC price in 2017 constant USD/t

The price of Birch spread has been closely following the trend of cathode price, for both historical data and projected data. The historical linear correlation between $\Delta Birch.Spread_t$ and $\Delta P.Cat_t$ is 0.85 between 1992 and 2018, and 0.97 between 2018 and 2040. As I mentioned in the price formation module, the historical high correlation indicates that cathode effect explains the majority of variation in $\Delta Birch.Spread_t$ and the scrap S&D effect should be much less significant in size.

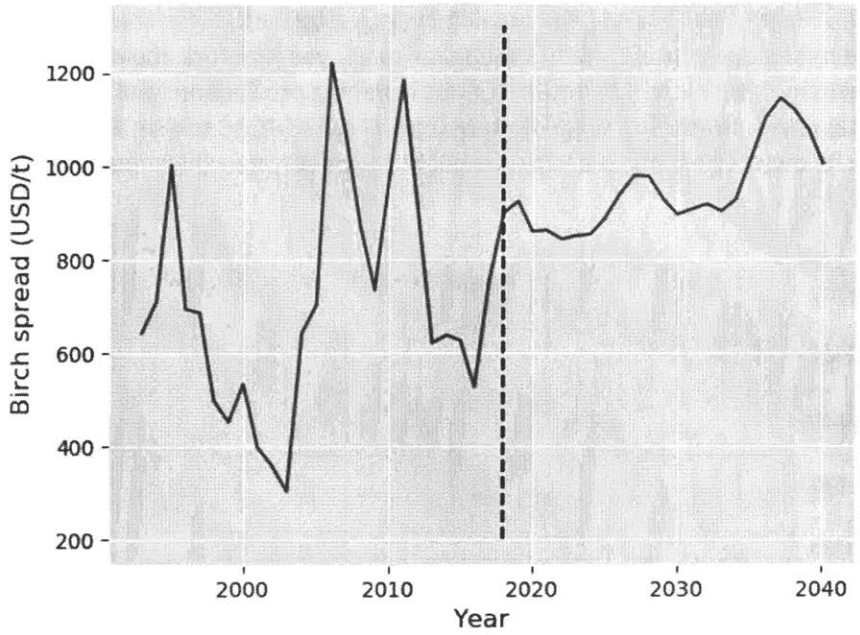

Figure 5. 20 Historical and simulated Birch spread in 2017 constant USD/t

Production and consumption

The production/supply and consumption for concentrate, cathode and scrap is shown in Figure 5.21 to Figure 5.23. Likewise, the black dashed lines in all figures represent the year of 2018, the initial year for the simulation.

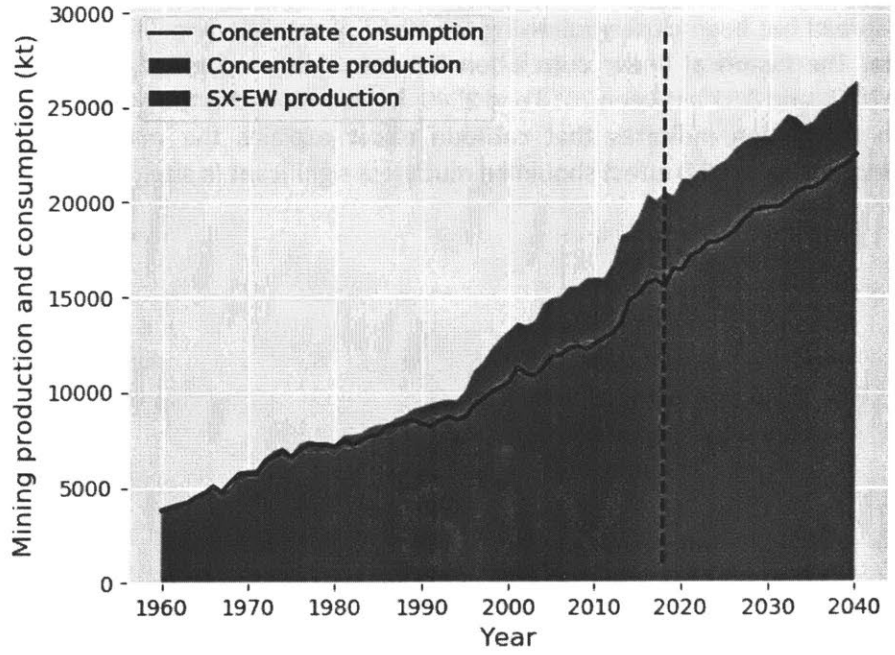

Figure 5. 21 Historical and simulated copper mining production and consumption in kt

The total annual mining production has grown from 20500 kt in 2018 to 26300 kt in 2040. This represents an annual growth of 264 kt, assuming production growth is linear. Recall that, a future mining benchmark is set in the primary supply module, in which the production in 2040 is 25700 kt. The simulated number is slightly higher than that benchmark, due to cathode prices higher than 2018 on average. While concentrate production have been growing pretty steadily in the simulation timeframe, mining production from SX-EW is more volatile. Historically, the fraction of world total copper mining production coming from SX-EW has been growing from 0 in 1960 to about 20% in early 2000's, and that fraction has been fluctuating around 20% since. This fraction is still fluctuating in the simulation, but with a slight decrease to about 16% in 2040. Since the properties of new mines are resampled from recently opened operating mines in the simulation, this decrease indicates that SX-EW mines are not more profitable than concentrate mines opened in the last few years. In other words, SX-EW mines won't be favored in new mine opening, if the costs of new mines are similar to recently opened mines. In terms of production and consumption balance, there has been a consistent production surplus of concentrate between 2035 and 2039, for about 350 kt each year. This surplus explains the sharp increase in TCRC during the same period.

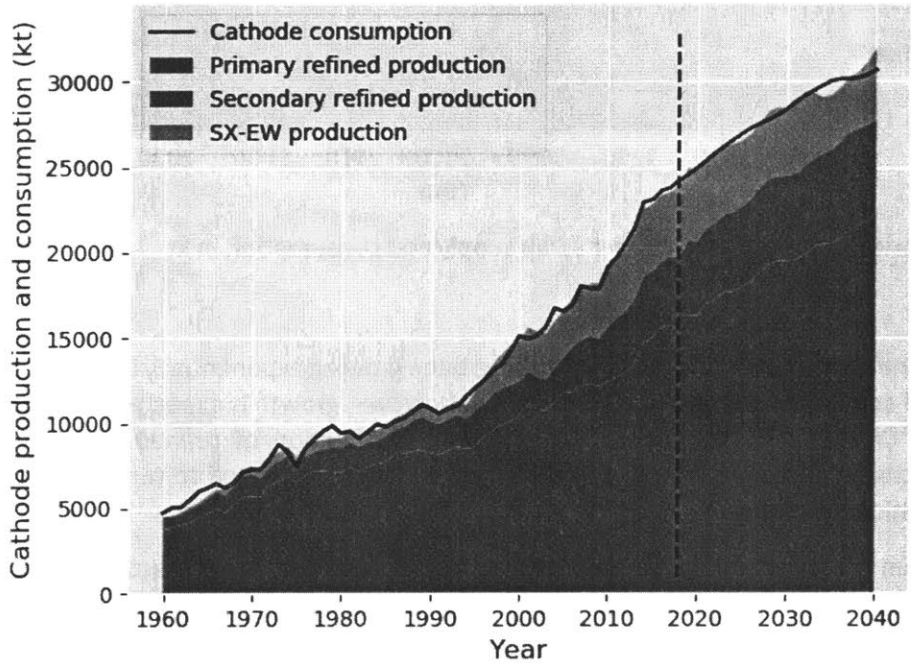

Figure 5. 22 Historical and simulated copper cathode production and consumption in kt

Simulated cathode production and consumption is shown in Figure 5.22. The projected annual growth of cathode consumption is 351 kt between 2018 and 2040, about 10% faster than the growth between 2014 to 2018. Cathode production from both primary and secondary refineries has been growing steadily, and the only volatile component has been refined production from SX-EW mines. The fraction of total cathode

production from secondary refined production has been fluctuating around 12% to 18% historically, and stays around 17% to 19% in the simulation. The temporary stalling of SX-EW production starting 2033 has lead to consumption to exceed production between 2033 and 2036, and the total supply deficit between this period has been 2200 kt. This deficit drives cathode price to rise from 6330 USD/t in 2034 to 7640 USD/t in 2037.

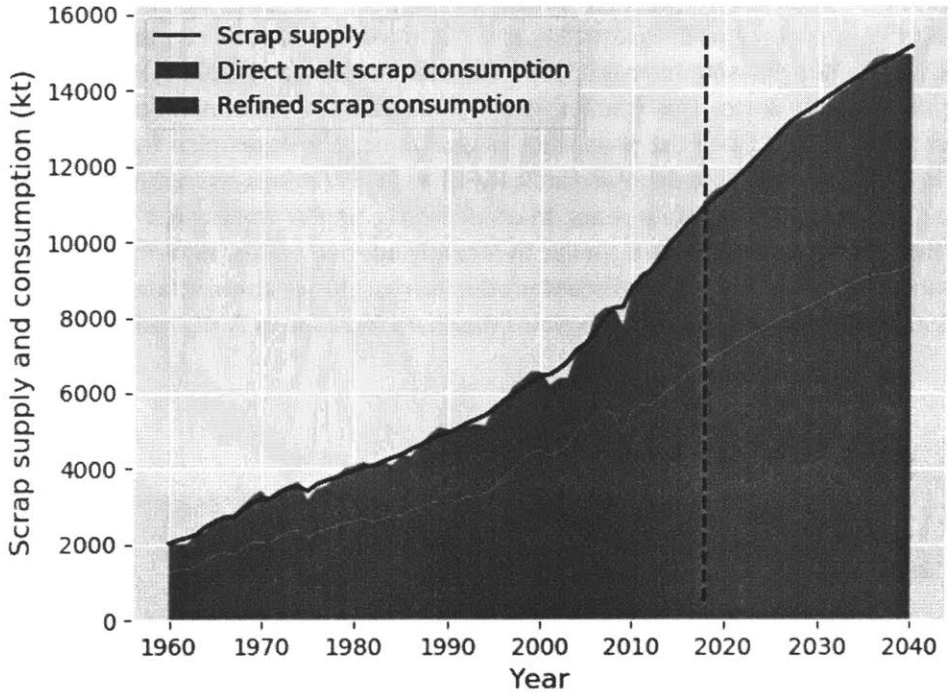

Figure 5. 23 Historical and simulated copper scrap supply and consumption in kt

Both the supply and consumption of copper scrap have been growing exponentially in the last five decades, with a compound annual growth rate (CAGR) of 2.96%. However, growth is expected to slow down in the simulation, with CAGR=1.48% between 2018 to 2040. The fraction of refined scrap in total scrap consumption fluctuates between 39% and 67% historically, and is expected to remain between 59% to 65% in the simulation timeframe.

Lastly, results from the direct melt scrap model are briefly presented here. Recall that the direct melt scrap breakdown model takes alloyed semis consumption and raw material prices as inputs, and outputs the amount of direct melt scrap consumption for each scrap grade. These two inputs can be obtained from the baseline scenario directly. Below the breakdown between 2018 and 2040 is shown in Figure 5.24. Several scrap grades share the majority of direct melt scrap consumption, including Barley, yellow brass, red brass, leaded red brass, Ocean, and Cartridge brass. Barley is essentially used as pure copper by semis fabricators, and its large volume of consumption can be explained by brass mills and foundries using it to dilute the concentration of other alloying elements. Cartridge brass is also extensively used because it contains very little amount of alloying elements (other than zinc, see Table A.1). The other alloyed scrap grades that show significant consumption levels are mostly due to their compositional similarity to alloyed semis products. It is worth noting that, while the amounts in Figure 5.24 are simulated as consumption

levels, they actually reflect demand for those materials because I assumed all scrap grades to be infinitely available.

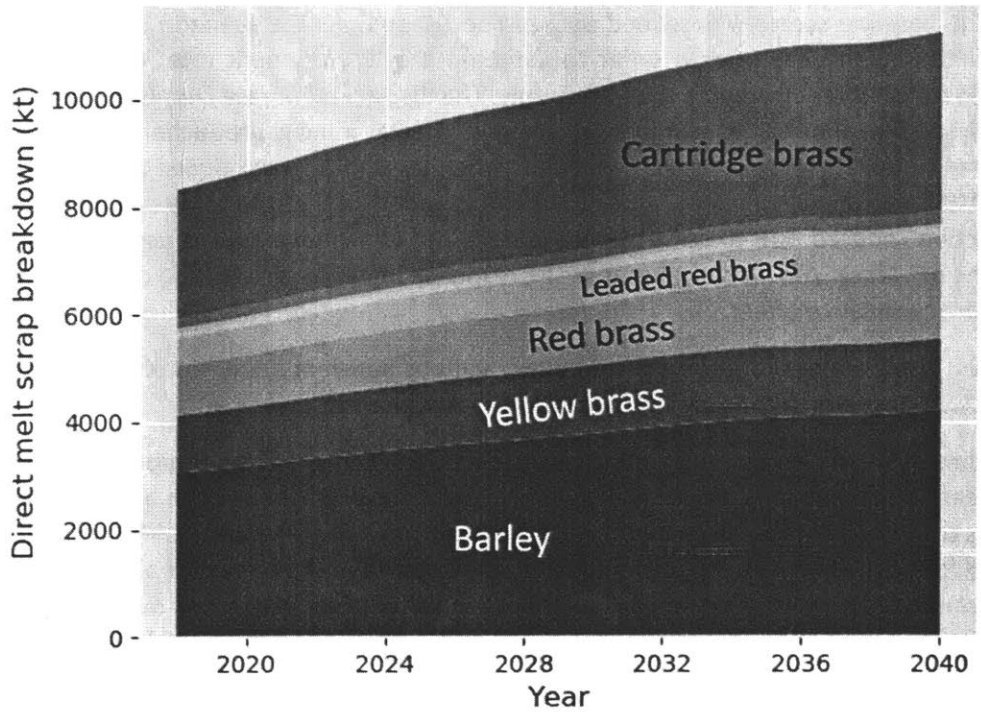

Figure 5. 24 Simulated direct melt scrap consumption breakdown in kt

Estimating displacement

The prices, production and consumption projections shown in the section above are all based on the baseline scenario. Once any parameter is deviated from the baseline, the system will be perturbed and responds differently. For example, if the collection rate for MSW is improved by 10% starting from 2019, then the 2019 total scrap supply should increase, followed by responses in all other parts of the system.

An important motivation for this simulation model is to estimate and understand the response in mining production following an increase in scrap supply. From an environmental perspective, recycling will lead to greater environmental benefit if an increased recycling leads to more mining production being displaced or avoided. In this thesis, secondary copper's displacement of primary copper is estimated by comparing the system responses under two scenarios, which is expressed as follows:

$$\delta P.Mine_t = P.Mine_{t,AS} - P.Mine_{t,BS}$$

$$\delta S.Scrap_t = S.Scrap_{t,AS} - S.Scrap_{t,BS}$$

$$Displacement_t = -\frac{\sum_{\tau=t_0}^{t} \delta P.Mine_\tau}{\sum_{\tau=t_0}^{t} \delta S.Scrap_\tau}$$

(Equation 5.66 to 5.68)

In the set of equations above, $P.Mine_{t,BS}$ and $S.Scrap_{t,BS}$ are the total mining production and scrap supply from the baseline scenario described above. The *AS* denotes the scenario *after shock*, and the shocks are relative to the baseline. In order to estimate the displacement rate, these shocks to the baseline should reflect direct increases to scrap supply. The displacement rate $Displacement_t$ is defined mathematically as the quotient of cumulative changes in total mining production to the cumulative changes in scrap supply. t_0 represents the initial year when the shock is introduced to the system, and it is set to be 2019 for all shock scenarios. A negative sign is added so that the value can be interpreted as mining production *reduced* due to scrap supply *added*. The cumulative sum is used in Equation 5.68 instead of using $\delta P.Mine_\tau/\delta S.Scrap_\tau$, because the response in mining production can be slow and I am interested in the cumulative effect.

In what follows, displacement rate is estimated under various different scenarios of scrap supply shock. Below are a few factors worth considering about the shock scenarios:

1. **Duration of shock**. Scrap supply shocks to the baseline can either be temporary (shock last for one year or a few years) or permanent. A permanent shock can be seen as a series of temporary shocks to the baseline, each perturbing the system from its original status. The impact on mining supply from a permanent shock should be much larger than the impact of a temporary shock of the same size. However, the impact of shocks introduced in later years during the simulation timeframe might not have manifested yet, and displacement of mining production can still occur beyond end of the simulation timeframe.
2. **Size of shock**. The size of change in mining supply, $\delta P.Mine_t$, is apparently related to the size of scrap supply shock, $\delta S.Scrap_t$. The displacement rate should also depend on the size of scrap supply shock. While an extremely small shock may not be enough to change the opening and closing of mines and only impact short run production, a large enough shock can. Larger shocks can also significantly change copper consumption by shifting the S&D balance of copper cathode.
3. **Directness of shock.** Many different types of shocks can cause scrap supply to increase. For example, increase in recycling through improving collection rate and technical recycling efficiencies can cause old scrap supply to increase; Increased consumption of copper in all semis can also cause external new scrap supply to increase, other things equal. However, only the former shock is a *direct scrap supply shock*, as the immediate system response is increase in $S.Scrap_t$ from the baseline. The latter is an *indirect scrap supply shock*, because the immediate system response is increase in cathode consumption $C.Ref_t$ and direct melt scrap consumption $C.Scrap_{t,DM}$, rather than an increase in scrap supply. Only direct scrap supply shock scenarios are considered in the estimation for displacement rate.

When an infinitesimal shock, or a *marginal shock*, is introduced on top of the baseline scenario, the change in all prices, production and consumption should also be infinitesimal. Mining production is only affected because of change in short run production, and mine opening/closing could not have been affected. The displacement rate estimated from a marginal shock is called *marginal displacement*, and it represents the mining production that would be displaced for each infinitesimally more amount of copper that is recycled. Such a marginal shock can be simulated by increasing the technical recycling efficiencies for all waste types by 1e-7 from the baseline efficiencies.

In what follows, the impact from duration of shock and size of shock is investigated in details. For the investigation of duration, the size of shock is kept constant at the marginal level. The results on displacement rate are shown in Figure 5.21 below:

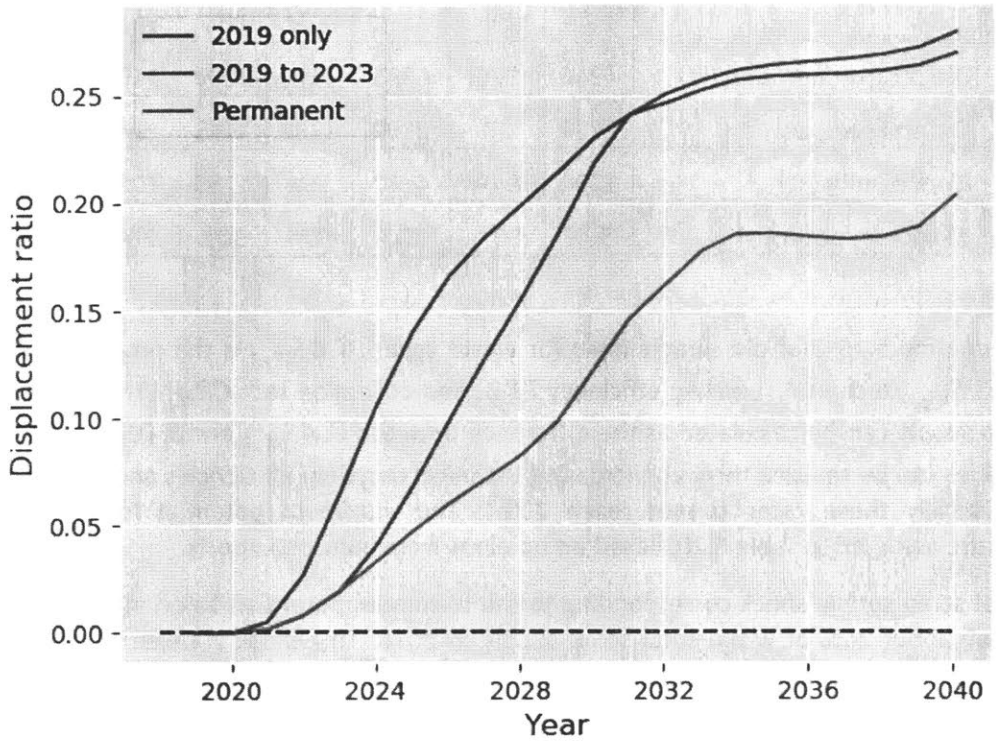

Figure 5. 25 Displacement rate under different duration of marginal shocks

The red curve in Figure 5.25 represents a temporary marginal shock that is introduced in 2019 only. After 2019, the baseline technical recycling efficiencies are used. It can be seen that displacement rate gradually increases from 0 in 2020 to about 0.26 in 2033. Then displacement starts to asymptote at this level, with a slight jump in 2040. The blue curve represents another temporary shock that lasts for 5 years between 2019 and 2023. It can be seen that displacement rate also asymptote to a similar level of 0.27, but the initial speed of growth is much lower than the 2019 only scenario. As I briefly mentioned previously, this is due to the slow response in mining supply: it can take more than 10 years for marginal displacement to reach its full potential, and the initial response in the first couple of years after the shock can be pretty low. While the cumulative size of shock $\sum_{\tau=t_0}^{t} \delta S.Scrap_{\tau}$ from the five year shock scenario is approximately five times of that from the 2019 only scenario, the mining response before 2030 has yet to catch up with the growth in shock size. Finally, displacement rate estimated from the permanent shock scenario is consistently lower than the 2019 only, again due to shocks introduced in later years not reaching full potential yet.

To explore the impact from size of shock, duration of shock is kept constant at 2019 only. Larger shocks should in theory lead to greater responses in mining production, but displacement rate is not necessarily monotonic with size of shock. The amount of end-of-life old scrap and opportunities in increasing recycling is used to estimate reasonable sizes for shocks that could occur in the real world. These amounts are shown in Table 5.21.

Table 5. 21 Opportunity for increase in old scrap supply by waste type

	C&D	MSW	WEEE	ELV	IEW	INEW
Old scrap generation (kt)	4246	976	6345	2179	2309	1167
Old scrap supply (kt)	2751	27	2199	1388	1143	159
Opportunity (kt)	1494	949	4147	791	1166	1008
Maximum potential	50%	50%	10%	50%	30%	20%

Recall from Equation 5.15 that old scrap supply for waste type j, $S.OS_{W_{j,t}}$ is the product of old scrap generation $G.OS_{W_{j,t}}$, technical recycling efficiency TE_{W_j} and collection rate CR_{W_j}. The opportunity to increase scrap supply can be calculated as the difference between $G.OS_{W_{j,t}}$ and $S.OS_{W_{j,t}}$. Only part of the opportunities can be realized through increasing technical recycling efficiencies and collection rates, because realistically these rates cannot reach 100%. The maximum potential for utilizing these opportunities are assumed in Table 5.20, based on opinions from industry experts.

The amount of scrap supply shock corresponding to the maximum potentials listed above is 2583 kt of copper in total, about 24% of world total scrap supply in 2018. This shock is taken as the maximum recycling potential scenario in the simulation. Three other shock scenarios are also tested, corresponding to 10%, 20% and 50% of the maximum potential. All these shocks can be simulated by increasing the values of TE_{W_j} and CR_{W_j} from the baseline in 2019. The results on displacement rate are shown in Figure 5.26, and the marginal displacement rate (with shock in 2019 only) is also shown for comparison.

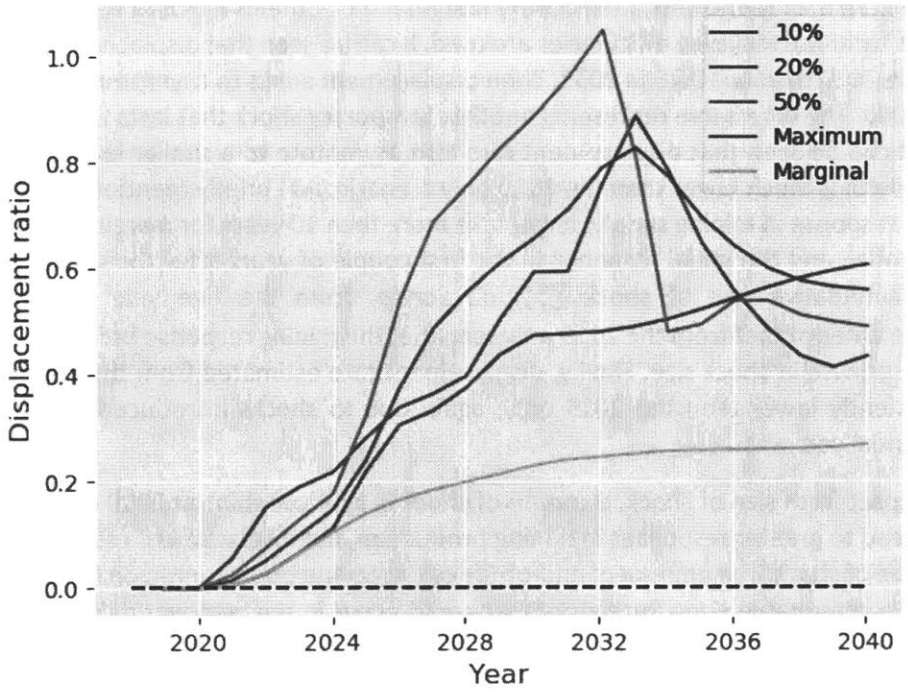

Figure 5. 26 Displacement rate under different size of shocks

There are a few interesting phenomena from this figure. First, it can be observed that all displacement rates in Figure 5.26 are consistently higher than the marginal displacement rate. While the marginal displacement rate asymptotes to 0.26, their values fall between 0.4 to 0.6 at 2040, for all other shock scenarios. This is because larger shocks not only causes mining production to shift in the short run, but also advances mine closing or delays new mine opening. Secondly, only the 50% scenario has seen displacement rate going above 1 at 2032, while other displacement rate values in all other scenarios and all other years are smaller than 1. This is in part of a result from *rebound in demand*: with more secondary copper supplied to the market, cathode price will drop and demand of copper in both cathode and direct melt scrap will eventually catch up, therefore offsetting part of the potential to reduce mining production. Thirdly, for shocks above 10% of maximum potential, there are periods during which displacement rates significantly fall down. This recoil in displacement rate can be explained by the recoil in cathode price, shown in Figure 5.27. When cathode price initially becomes lower than the baseline in all after shock scenarios for a few years, it causes various system responses including rebound in demand and reduction in mining production. If it eventually causes a more significant cathode supply deficit than the baseline, cathode price will then bounce back to levels higher than the baseline. If this bouncing back is significant enough, it could actually raise mining production for a certain period of time. This is exactly what happened for the 20%, 50% and maximum shock scenarios shown in Figure 5.26. I call this behavior the *rebound of mining production*. Both rebound in demand and rebound in mining production offsets part of the environmental benefit of recycling, and prevent displacement rate from reaching levels above 1.

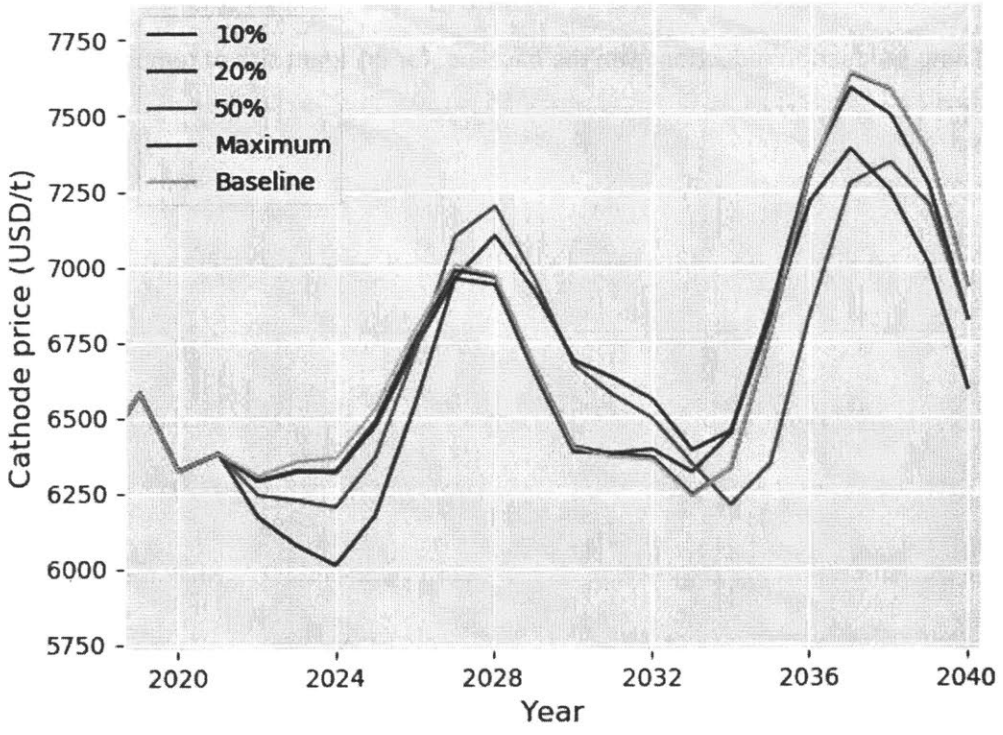

Figure 5. 27 Cathode price evolution under different size of temporary shocks (2019 only)

To get a better understanding of the actual size of system responses in tonnages, the reduction in mining production from the baseline is shown for the 10%, 20%, 50% and maximum recycling potential level. This is shown for both temporary shocks at 2019 only and for permanent shocks, in Figure 5.28 and Figure 5.29.

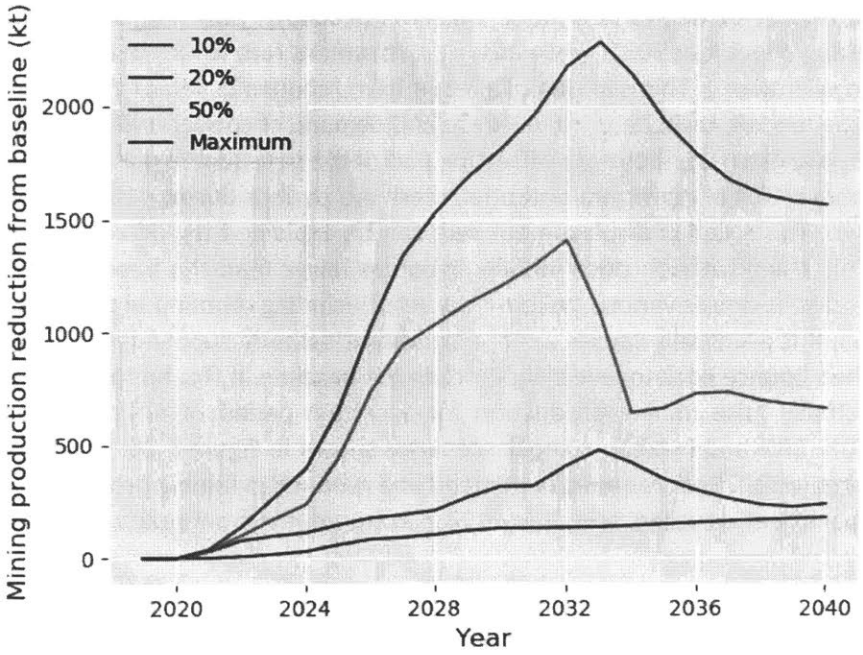

Figure 5. 28 Mining production reduction from the baseline, for different size of temporary shocks (2019 only)

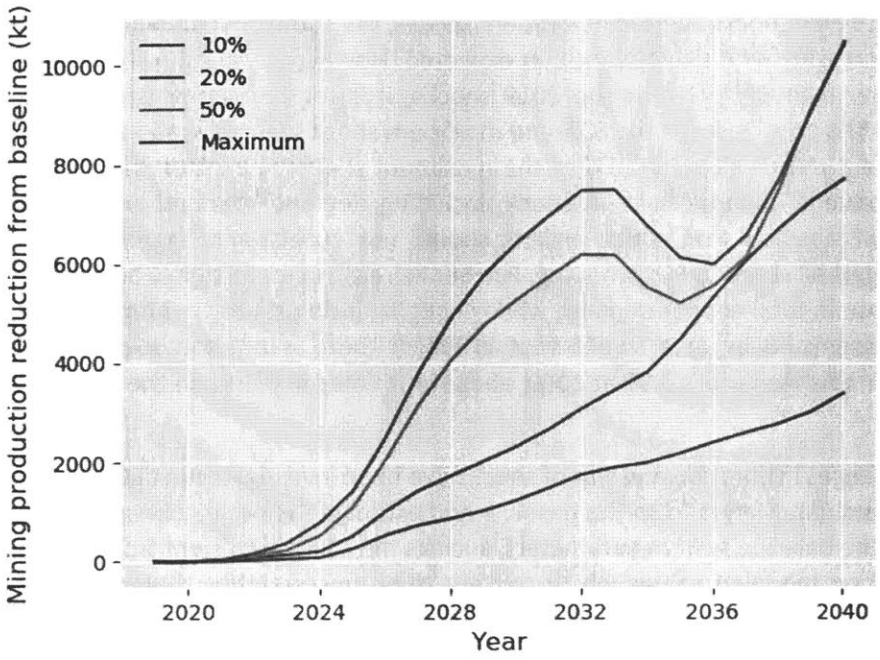

Figure 5. 29 Mining production reduction from the baseline, for different size of permanent shocks (2019 only)

The cumulative scrap supply increase and displaced mining production between 2019 and 2040, and displacement rates at 2040 are shown in Table 5.22 for all 8 scenarios.

Table 5. 22 Comparison of cumulative scrap supply increase, cumulative mining production reduction and displacement rate at 2040 for shocks with different durations and sizes

Duration of shock	Size of shock as percent of maximum	Cumulative scrap supply increase (kt)	Cumulative mining production reduction (kt)	Displacement rate at 2040
2019 only	10%	293	178	0.61
	20%	548	238	0.43
	50%	1352	664	0.49
	100%	2795	1565	0.56
Permanent	10%	8019	3387	0.42
	20%	15442	7697	0.50
	50%	39790	10403	0.26
	100%	79612	10467	0.13

Within both the 2019 only shocks and the permanent shocks, the cumulative mining production displaced is monotonically increasing with size of shock, as expected. However, while the size of displaced mining production is not far from 1:2:5:10 for the 2019 shocks, it is for permanent shocks. The cumulative displacement at 2040 is very close for the 50% and maximum shock scenarios, and even the 20% scenario leads to displacement that is close to 75% of the maximum shock. The latter is a strong indication of various system rebounds under maximum shock, including demand rebound and mining production rebound. This result suggests that policy makers should not expect that aggressive improvement in recycling leads to aggressive reduction in mining. Further increase in scrap supply beyond some threshold only leads to increase in total copper demand while changing little primary mining production. The 20% permanent shock seems to be at a sweet spot in which there is not too much rebound, and the displacement rate in this scenario is 0.50 at 2040, about four times higher than the ratio under maximum shock scenario.

The impact from changes in duration and size of shock have been investigated in detail above. This is done by shifting the system parameters from the baseline and estimate system response in the new scenario. However, many of the baseline system parameters, such as the ESSD coefficient from the price formation module, are based on modeled values which contain some uncertainties themselves. Therefore, the sensitivity of displacement rate to the changes of baseline system parameters is investigated next.

Sensitivity of displacement rate to baseline system parameters

The sensitivity to baseline parameters is investigated by a series of controlled experiments, shifting one baseline parameter at a time. Two scenarios are set up for all parameters, including a high scenario where the baseline parameters are doubled and a low scenario where they are halved, unless otherwise specified. The duration and size of the shock are kept at 2019 only and marginal, respectively. Below is the list of parameters investigated.

1. **Mining production elasticity (MPE).** This is the mining CU short run elasticity to TCM estimated in the primary supply module, and the baseline value is 0.024. This short run elasticity is responsible for the marginal displacement, and I would like to see how the shift in this parameter will affect marginal displacement rate.
2. **Secondary ratio elasticities (SREs).** In the refinery module, the secondary ratio for secondary refinery is also responding to both TCRC and Birch spread. These are essentially the substitution elasticities between concentrate and refined scrap. When these elasticities are higher, substitution between primary and secondary raw materials should be more sensitive to prices at the secondary refinery.
3. **Scrap S&D elasticity (SSDE).** While all other coefficients in the price formation module are estimated from regression models based on historical production and consumption data, SSDE is assigned semi-quantitatively. It is therefore also explored in the sensitivity analysis here.
4. **Demand elasticities (DEs).** It is shown in Figure 5.11 that overall copper demand elasticity to cathode price is much lower that of the mining supply elasticity. Therefore, two high-than-baseline scenarios are explored here, corresponding to 200% and 400% of the baseline DEs. Only the price elasticity means from the demand module are changed, while the standard deviation for elasticity, intercepts and GDP elasticity are all kept constant at the baseline level.

Results of the sensitivity analysis are shown in Figure 5.30 to Figure 5.33.

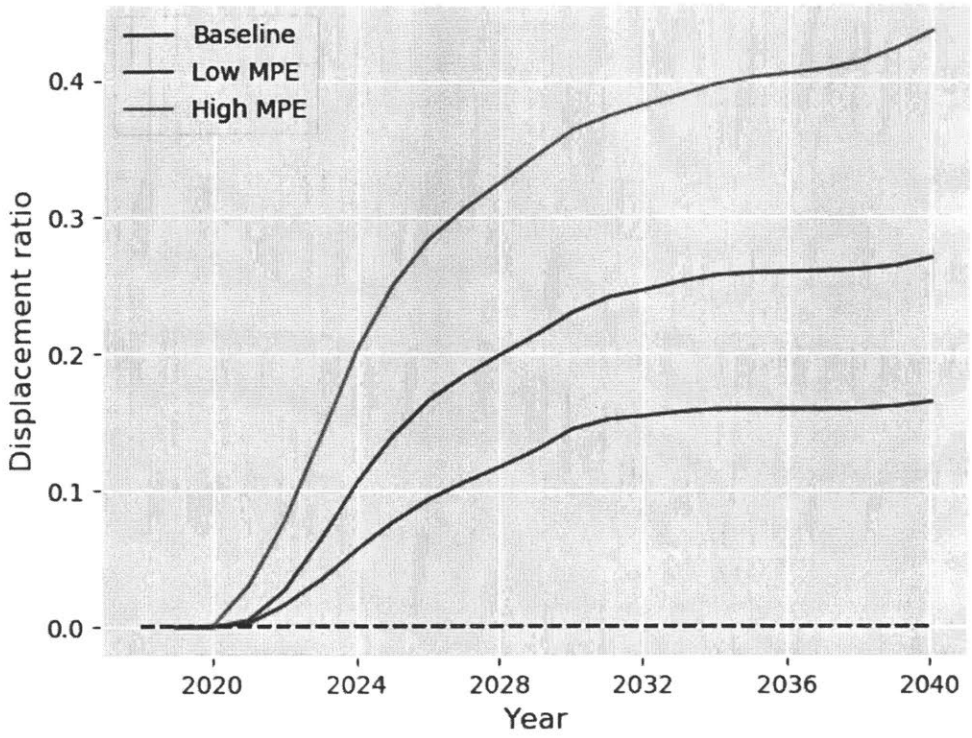

Figure 5. 30 Sensitivity of displacement rate to MPE

The changes in MPE have a significant impact on displacement. Marginal displacement at 2040 for the low MPE, baseline and high MPE scenarios are 0.16, 0.27 and 0.44, respectively. Higher MPE leads to consistently higher displacement, because mining production is more responsive to the same change in cathode price, compared to a lower MPE.

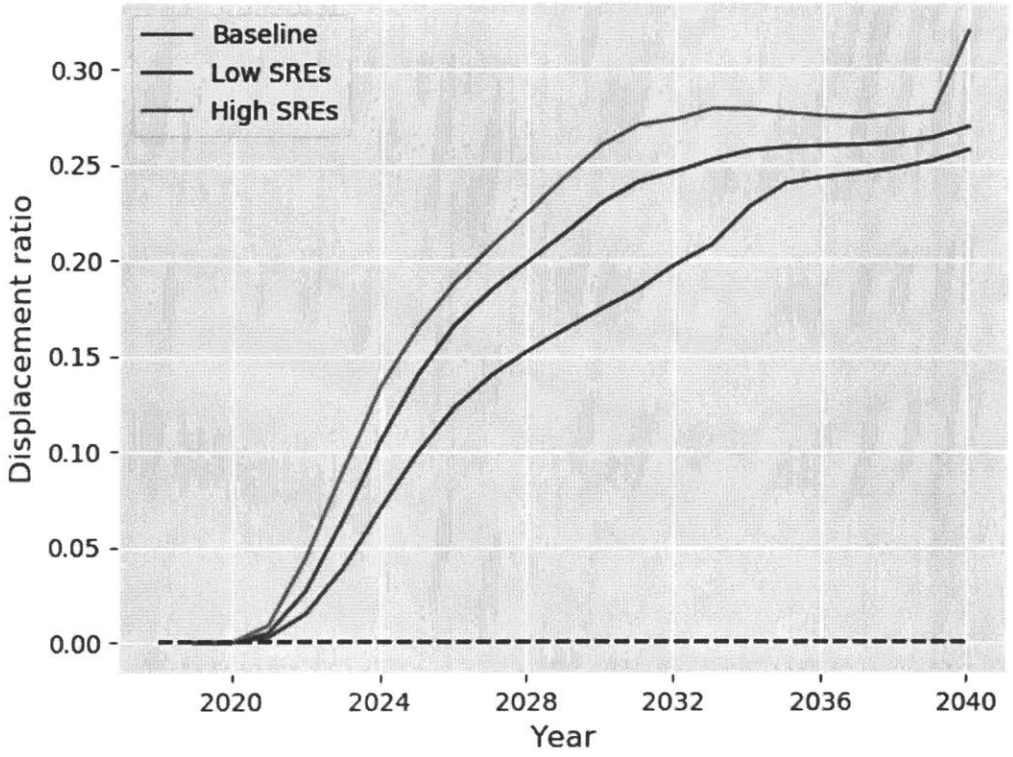

Figure 5. 31 Sensitivity of displacement rate to SREs

Similar to MPE, higher SRE leads to consistently higher marginal displacement, because secondary refineries will substitute more primary materials with scrap with higher SRE. However, changes in SREs have less significant impact on displacement rate than MPE. This is likely because that shifts in the refinery are less 'direct' than shifts in the mines. While MPE being higher directly means more reduction in mining production all other things equal, higher SRE impacts only the consumption of concentrate and refined scrap directly. These changes then affect TCRC, scrap spread and finally affect cathode price with a delay. Therefore, miners only indirectly respond to SRE changes, and displacement rate does not change much due to changing SRE.

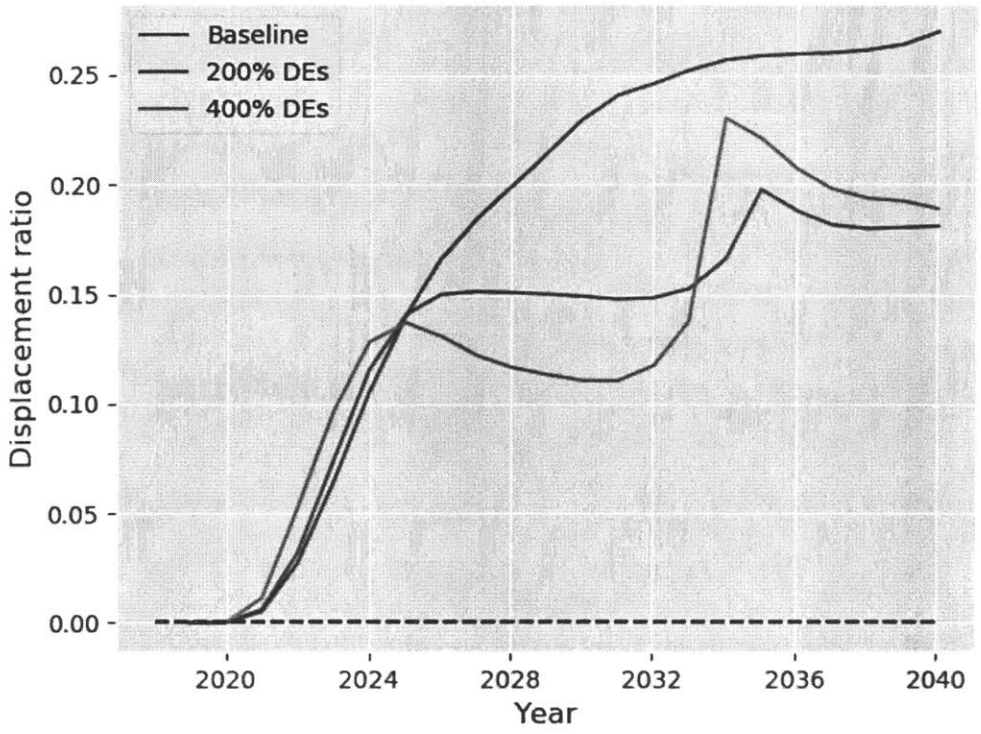

Figure 5. 32 Sensitivity of displacement rate to DEs

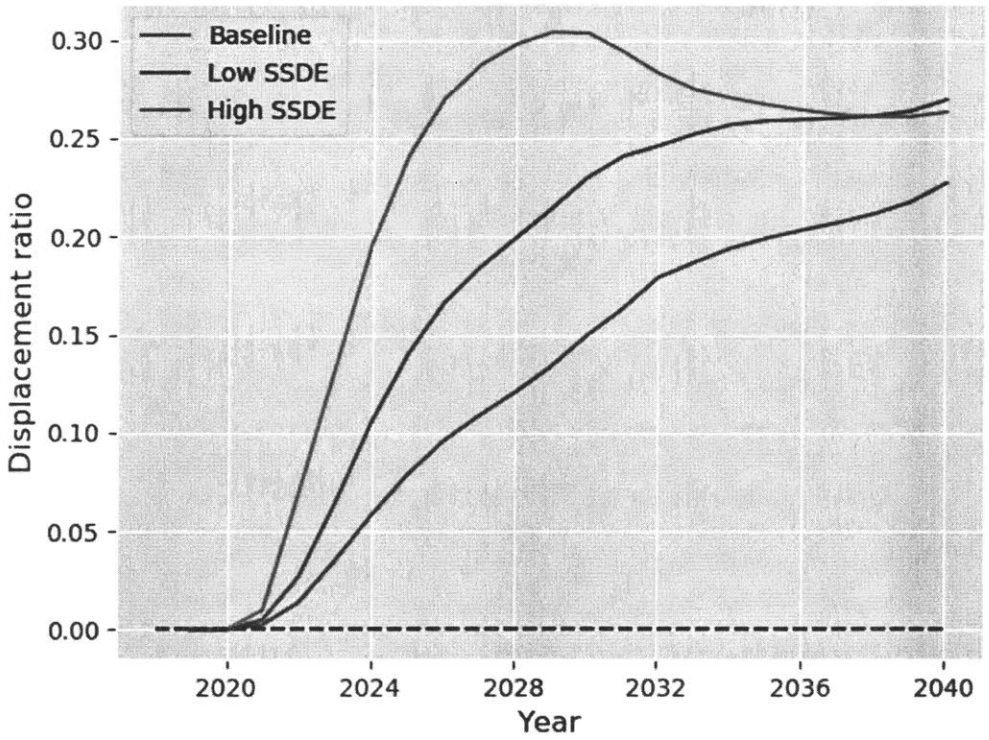

Figure 5. 33 Sensitivity of displacement rate to SSDE

The impact from changing DEs and SSDE is more complicated than the two previous parameters, as rebound effects play major roles here. For the DE scenarios, higher DEs mean that both cathode consumption and direct melt scrap consumption should increase more if cathode price drops. Initially, the higher direct melt scrap consumption seems to dominate, leading to slightly higher displacement rate before 2025. However, as higher cathode consumption gradually shifted the P&C imbalance, cathode price becomes much higher, leading to increase in mining production and decrease in displacement rate. This rebound manifests in the 400% DEs scenario most significantly.

The scenarios around SSDE also shows some rebound in displacement rate, for the high SSDE scenario. As a reminder, SSDE represents the speed of scrap spread responding to difference in scrap supply and consumption. Higher SSDE should lead to higher increase in scrap spread, and therefore higher substitution of primary materials at the secondary refinery. In Figure 5.33, it can be seen that displacement rate initially increases monotonically as a function of SSDE. However, substitution can go both ways, so higher SSDE also leads to more consumption of concentrate when scrap spread begins to decrease. This substitution appears as the rebound in displacement rate in the high SSDE scenario. At 2040, both the high SSDE and baseline scenarios asymptote to similar levels. The low SSDE scenario does not reach that level yet in the simulation timeframe, but may asymptote too if the simulation was extended. Therefore, while SSDE is the only parameter in the price formation module that is not estimated from historical data, it does not significantly impact the final potential of displacement rate.

So far, the copper mining production response from many different scenarios have been investigated in detail. However, as a result of copper scrap supply shocks introduced to the simulation system, changes in the copper system will also cause changes in other metal systems that are co-products or by-products in copper production. In what follows, an attempt is made to quantify the impact of increased copper recycling on the supply of its byproducts, particularly for cobalt, tellurium and selenium.

Impact on byproducts

Acknowledgement: Portions of this section is based on a work by Fu et al. submitted to Environmental Science and Technology in 2019, titled *Supply Perspectives on Cobalt in the Face of Changing Demand* (Fu et al., 2019)

Impact on cobalt

Cobalt is an essential metal for a wide variety of uses, particularly technical applications, often with limited ability to substitute with another element with matched performance. Primary demand of cobalt is based on end uses in lithium ion batteries (LIB), superalloys, hard materials/cutting tools, and catalysts (U.S. Geological Survey, 2019b). LIB uses, concentrated in consumer electronics and electric vehicles (EVs), are currently the largest end use of cobalt (accounting for 50% of the global cobalt demand) (U.S. Geological Survey, 2019b). While, consumer electronics and superalloy demand for cobalt are projected to remain constant in the coming years, the market for EVs is expected to increase exponentially after 2020, as costs for EVs equalize with those for traditional ICE vehicles (Darton Commodities, 2018). Along with cost, country-specific policy decisions are limiting the production and sale of traditional vehicles in favor of a more sustainable alternative, such as EVs. These regulations, along with increased EV demand, will likely give a huge boost to cobalt demand in the coming years.

On the supply side, cobalt ranks highly along various potential supply chain disruption factors including by-product production dependence, geographically concentrated production, sociopolitical instability and unrest, and (N. T. Nassar et al., 2015; Shedd, 2017) Primary supply of cobalt is heavily geographically concentrated, both for mining/production and processing of the mined materials. Current estimates put approximately 60% of all mined cobalt production in the Democratic Republic of Congo (DRC); This value is expected to reach upwards of 65% before 2030 (Hamilton & Kamal, 2017). cobalt processing is also heavily concentrated; 2017 numbers indicate that China is responsible for 58% of refined cobalt, 91% of which originates in the DRC (Darton Commodities, 2018).

Apart from problems directly related to supply chain concentration, this heavy concentration in the DRC raises additional questions of materials availability: cobalt is mined primarily as a by-product of copper in DRC, and the fraction of cobalt coming from copper primary mines is 56% in 2018. Based on estimates from a working paper that I co-authored, this fraction is projected to stay above 45% before 2030 (See Figure 5.34). As these copper primary mines are more likely to be driven by copper prices (cathode price, TCRC and scrap prices) rather than cobalt prices, a significant part of world cobalt supply is reliant on the dynamics of copper supply from these mines. The implication of carrier supply constraint on the supply of the byproduct have been discussed in details in Chapter 3 and 4, and the focus of this chapter is to estimate the impact from increased recycling of the carrier.

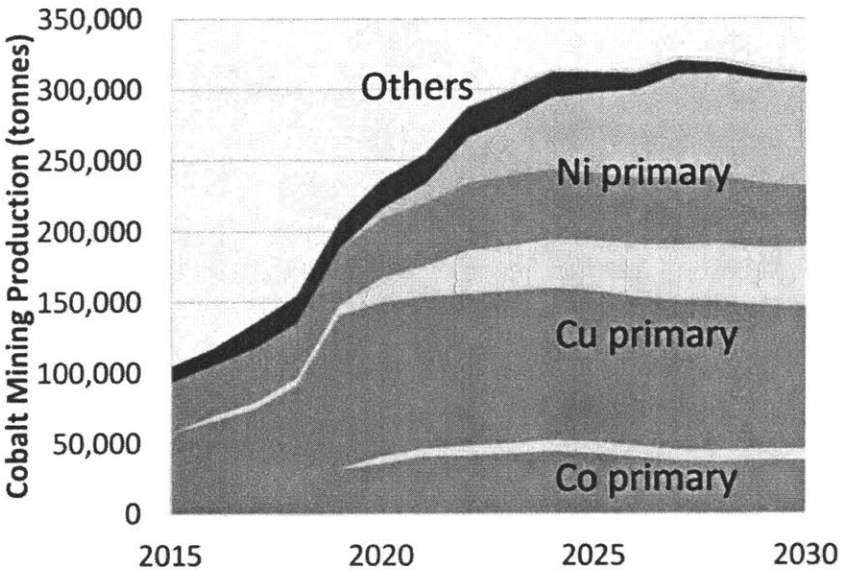

Figure 5. 34 Modeled cobalt mining production between 2015 and 2030 by primary metals, reproduced from (Fu et al., 2019)

Several modeling assumptions are made in order to quantify such an impact, listed below. A differentiation is made between cobalt mines that are operating in 2018, and potential new cobalt mines that will start after 2018.

1. No amount of cobalt is recovered from copper scrap. The small amount of cobalt contained in alloyed copper scraps is essentially neglected.

2. The prices of other metals, such as nickel and cobalt, are assumed to be constant in the simulation timeframe.
3. Out of all mines producing cobalt, assume that only copper primary mines are affected by increased copper recycling. While other mines still have some copper production in reality, it is assumed that mining production only responds to the price of their primary metals.
4. **For cobalt mines that are operating in 2018**:
    a. The copper production of each mine is determined by the primary module.
    b. Assume that the copper-to-cobalt production ratio of each mine will stay constant at the 2018 level.
5. **For new cobalt mines that start after 2018:**
    a. **Calibrating total production:** assume that total future cobalt production from copper primary mines will follow the projection from Fu et al. (Fu et al., 2019), as shown in Figure 5.34. Beyond 2030, assume that annual cobalt production stays constant at the 2026-2030 average level.
    b. Assume that all new mines are copper primary mines, and for each year the copper-to-cobalt production ratio is the same across all mines.

Following the above assumption, a baseline cobalt production from new mine can be calculated: the baseline system parameters are used to simulate mine level copper production between 2018 and 2040, for both operating mines and new mines. Since the 2018 copper-to-cobalt production ratios are known for each operating mine, the baseline future cobalt production from these mines can be calculated. This series of production is then subtracted from the projection benchmark from assumption 5, to get the baseline future cobalt production for new mines. Then, the mine-invariant copper-to-cobalt production ratio is calculated for each year so that total cobalt production from new mines matches the baseline.

For each scenario in the copper system, a series of future cobalt production can be simulated, following the approach mentioned above. The impact from a shock can be estimated as the cumulative difference between the after shock scenario and the baseline scenario,

$$\delta CM.P.Co_{\tau} = \sum_{\tau=t_0}^{t} \left(P.Co_{\tau,AS} - P.Co_{\tau,BS}\right)$$

(Equation 5.66)

where $P.Co_{\tau,AS}$ and $P.Co_{\tau,BS}$ are the cobalt production for year τ under the after shock scenario and the baseline scenario, respectively. The four shocks shown in Figure 5.29 are used here as well, corresponding to 10%, 20%, 50% and 100% of the maximum recycling improvement potential. Only the permanent shocks are used, because these shocks resemble those in real life: increase in technical recycling efficiencies and collection rates due to technology improvement and/or policies are likely permanent to the system. The results are shown in Figure 5.35 below.

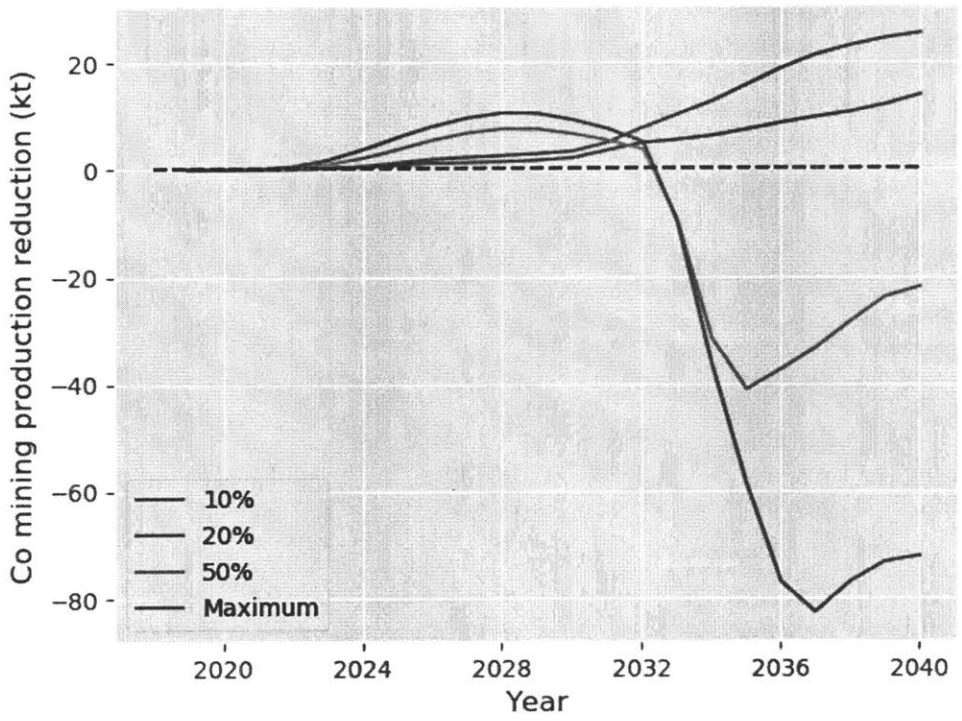

Figure 5. 35 Cobalt mining production reduction from the baseline, under four different scenarios described in Figure 5.29

To be consistent with the copper mining response, responses in cobalt mining production are also shown in terms of reduction, i.e., the negative of $\delta CM.P.Co_{\tau}$. The cumulative cobalt production reduction under the 10% and 20% scenarios are 13.9 kt and 25.5 kt, respectively, roughly following a 1:2 relationship. As a comparison, the projected cumulative cobalt mining production is 6673 kt between 2019 and 2040, based on previous work (Fu et al., 2019). Production reduction under the 20% scenario is less than 0.4% of total cobalt production during the same period, representing a relatively insignificant reduction.

Interestingly, mining reduction becomes negative at 2040, under the 50% and maximum scrap supply shock scenarios. In other words, cobalt mining production increased instead of decreased. After a careful mine level investigation, I have found that this increase is mainly due to two large cobalt mines (in terms of cobalt production size) delaying mine closing for five years, in response to the rebound of cathode price. The cathode prices evolution under these four permanent shock scenarios are shown in Figure 5.36, and it can be clearly seen that cathode prices under the 50% and maximum shock scenarios start to rise significantly higher than the baseline starting 2028. While these rebounds have not caused 2040 cumulative copper mining production to increase from the baseline, two large copper primary cobalt mines happen to be benefited significantly from the rebounds, and are able to extend production for five more years from the baseline. The cumulative increases in cobalt mining are 22 kt and 72 kt for 2040, respectively.

In summary, cobalt mining production is not significantly impacted by increased copper recycling activities, for the baseline and scenarios explored here. One reason is that cobalt mining production from copper primary mines is very small compared to production (~70 kt in 2018) is very small compared to total copper mining production (~20000 kt in 2018). Therefore, if maximum displacement potential in copper mining production is about 10000 kt up to 2040 cumulatively (value based on the last row in Table 5.22),

this roughly means about 35 kt reduction in cobalt mining production, which is still very small compared to cumulative cobalt production of about 6700 kt. In addition, significant cathode price rebounds further prevent reduction in cobalt production to even reach that level, and even leads to cobalt production increase under two scenarios.

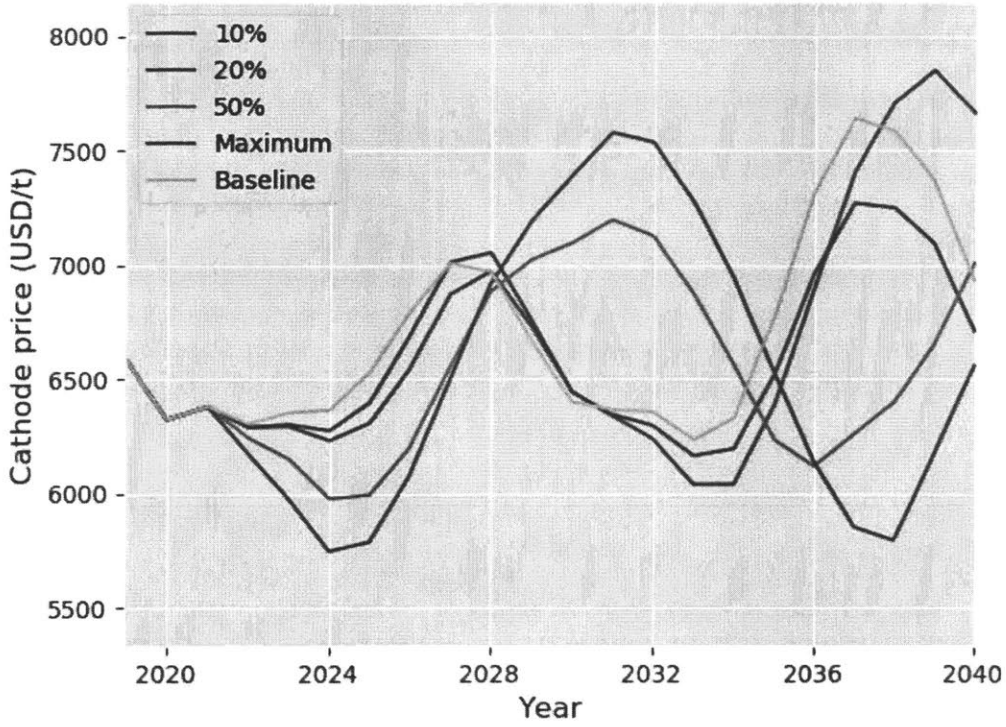

Figure 5. 36 Copper cathode price evolution under different size of permanent shocks

Impact on selenium and tellurium

Selenium and tellurium are both semiconductor elements in the same chemical family as oxygen, sulfur and polonium. The major application of selenium has been the metallurgical use as an additive (selenium dioxide) for electrolytic manganese production. Other applications include use in glass manufacturing, agriculture, and use as pigments. Demand of selenium for copper-indium-gallium-diselenide (CIGS) solar cells has been increasing in recent years (Blewais, 2010; C. Schuyler Anderson, 2018). The use in solar sell has also been a significant application for tellurium, where the element is used in the production of cadmium telluride (CdTe) thin-film solar cells. Other uses of tellurium include additive in various copper alloys, steel and lead alloys, and also use as pigments.

In terms of production, both selenium and tellurium are produced as byproducts of copper. They are recovered from the anode slimes during the electrolytic refining of copper. Note that the production of selenium and tellurium are only associated with primary refined production, while secondary refined production and SX-EW does not lead to these two byproducts being extracted. Based on data collected in Chapter 3, selenium is produced 100% as byproduct of copper, while the byproduct fraction of tellurium from copper is slightly less than 80%.

In the previous section, I estimated the response of cobalt production to scrap supply shocks in the copper system, by assuming that the ratio of copper and cobalt production reduced/increased follows the copper-to-cobalt production ratio of each mine. However, for the cases of selenium and tellurium, these two byproducts are separated from copper at the copper refineries rather than at mine sites. Therefore, selenium and tellurium production are directly influenced by changes in primary refined production rather than mining production. Below, the response of primary refined production from the baseline are shown in Figure 5.37, for the four permanent shock scenarios used for cobalt earlier.

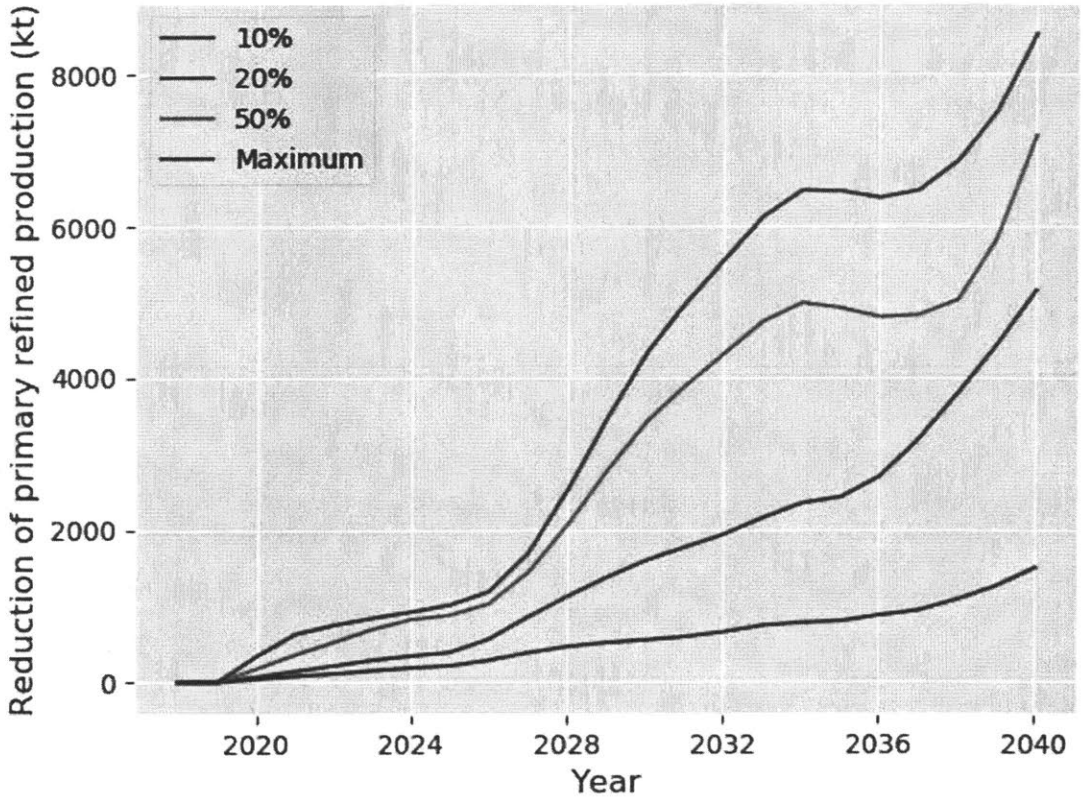

Figure 5. 37 Primary copper refined production reduction from the baseline, for different size of permanent shocks

Compared to the mining production response under the same four scenarios (shown in Figure 5.29), response in primary refined production show similar trends, in which the 50% and maximum shock scenarios see greater rebounds than the other two. However, the sizes of primary refined production reduced/displaced are significantly lower than those of mining production, shown in Table 5.23. This is in part due to primary refined production only corresponds to the concentrate part of mining production and SX-EW is not accounted for. The equivalence of displacement rates, i.e. the quotient of cumulative reduction in primary refined production to cumulative scrap supply increase, are also shown in Table 5.23 and it can be found that these ratios are consistently smaller than the values for mining production displacement.

Table 5. 23 Comparison of cumulative scrap supply increase, cumulative mining production/primary refined production reduction and displacement rate at 2040 for permanent shocks with different sizes

Production affected	Size of shock as percent of maximum	Cumulative scrap supply increase (kt)	Cumulative production reduction (kt)	Displacement rate at 2040
Mining production	10%	8019	3387	0.42
	20%	15442	7697	0.50
	50%	39790	10403	0.26
	100%	79612	10467	0.13
Primary refined production	10%	8019	1495	0.19
	20%	15442	5150	0.33
	50%	39790	7193	0.18
	100%	79612	8531	0.11

The impact on selenium and tellurium can be estimated based on reduction of primary refined production. Similar to the treatment in Chapter 4, these impacts are shown for the supply potential of the byproducts, assuming 100% recovery efficiency from anode slimes. A 2006 study estimates that for each tonne of copper anode processed in refineries, there are 400 grams of selenium and 105 grams of tellurium on average (Green, 2006). Here I use these numbers for estimating impacts, assuming that for each tonne of primary refined production displaced, 400 grams of selenium and 105 grams of tellurium are deducted from the supply potential of these two metals. The impact on selenium and tellurium are shown in Figure 5.38 and 5.39, respectively.

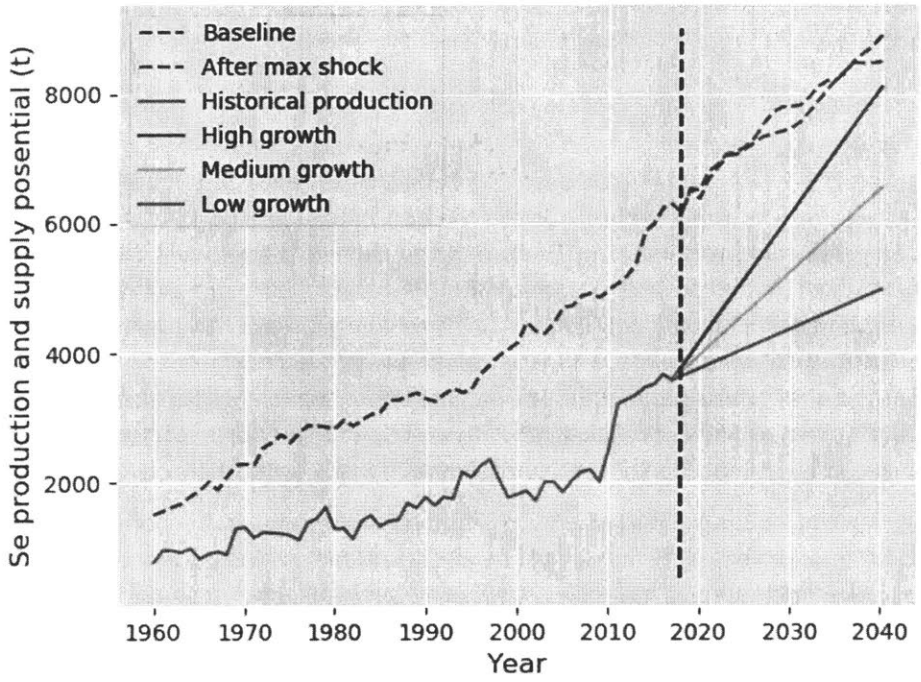

Figure 5. 38 Selenium production and supply potential history and future scenarios

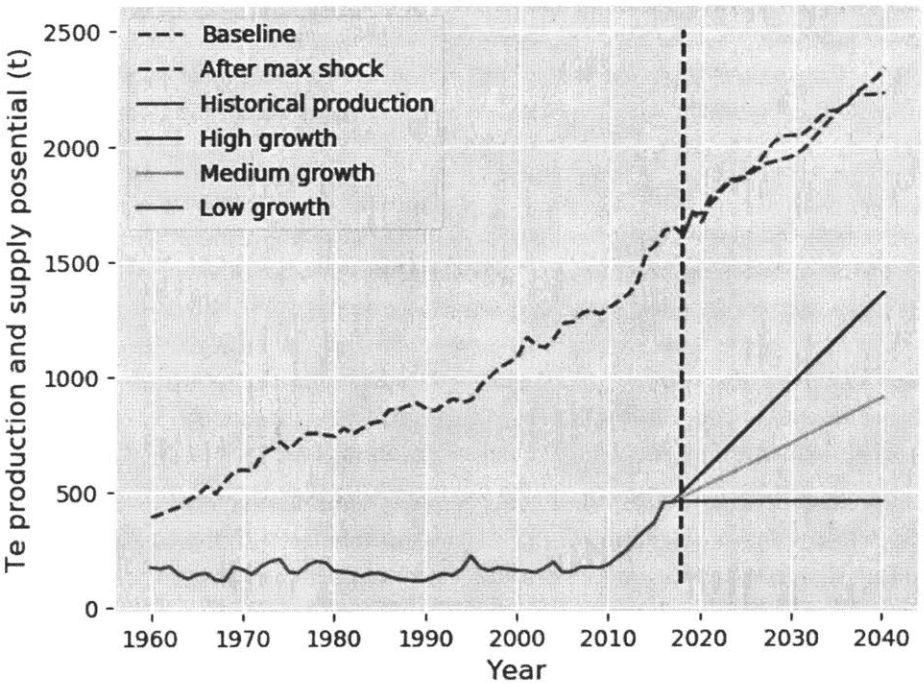

Figure 5. 39 Tellurium production and supply potential history and future scenarios

The dashed lines in the two figures above represent the supply potential of selenium and tellurium, for both the baseline and the after-shock scenarios. Only the maximum scrap supply shock scenario is shown here, as I am interested in the maximum extent of supply potential shifts and the other three scenarios cause less shift in supply potentials. Furthermore, the historical production and projected production scenarios of both metals are shown. The projections of future production are simply based on extrapolating historical trends linearly.

Qualitatively speaking, the impacts from the maximum shock scenario have not significantly shifted supply potentials of both metals. These shifts are not significantly changing whether the supply potential is constraining production of the byproduct. Except for the high growth future projection scenario for selenium, there is plenty of distance between production and supply potential projections. Further increase of selenium and tellurium production can be realized by sending more copper anode slimes to refineries capable of extracting the byproducts, and increasing recovery efficiencies. Quantitatively, the maximum shock has cumulatively reduced 3.4 kt of selenium supply potential from a total of 170 kt, and reduced 0.9 kt of tellurium supply potential from a total of 45 kt. Both reduction is about 2% of the total amount.

Conclusion

In calculating the environmental of recycling activities, it is often implicitly assumed that products made from secondary materials displace those made from primary materials on a one-to-one basis. This assumption is unrealistic given the existence of market interactions and various rebound effects. Attempts have been made in past studies to quantify the exact extent of secondary products displacing primary products. However, the behavior of market participants such as producers, consumers and broker-dealers are not explicitly modeled in these studies, hence leading to possibly biased estimates of displacement rate.

In this chapter, a bottom-up copper market simulation tool is built to mimic the behavior of major market participants. Production and consumption of different copper commodities (concentrate, cathode and copper scraps) from these participants/agents are modeled as function of copper prices. The imbalances between production and consumption then determine the evolution of copper prices in return, leading to spontaneous evolution of the system giving a specific set of initial conditions. Displacement rate is estimated by introducing scrap supply shocks to the simulation system, by shifting the system parameters from the baseline and then estimating the resulting changes in mining production. It is found that 1) displacement rate under a marginal shock asymptotes to levels around 0.25, and is most sensitive to MPE compared to other system elasticities; 2) Displacement under other larger shocks can be more volatile. It may reach levels above one for some period of time, but will eventually drop down to a much lower level as rebound in copper demand, cathode prices, etc. offset the initial displacement. Results on mining production response show that a maximum scrap supply shock (corresponding to 3600 kt scrap supply increase on annual average) only leads to 467 kt of average reduction in mining production annually. By contrast, if scrap supply shock is only 20% of the maximum, it will lead to 702 kt scrap supply increase while reducing 350 kt mining production annually. Therefore, resources policy makers should not expect that mining production reduction is linear with the level of improvement in recycling activates, and aggressive improvements cannot ensure much greater environmental benefits beyond some threshold.

The impacts of copper recycling on the availability of its byproducts are also investigated quantitatively in this chapter. For the three case studies on cobalt, selenium and tellurium, it is found that copper recycling do not change their availability significantly, even under the maximum scrap supply shock scenario. The

future production of cobalt can be reduced by at most 0.5% cumulatively, and the supply potential of selenium and tellurium can be reduced by 2% at most. These should be considered as relatively insignificant changes, compared to other possible supply and demand shocks that might disturb these byproduct metal systems dramatically.

Despite the promising capabilities this simulation model has shown, opportunities exist to further augment the model developed here in this thesis. There are a few areas where the model could be further improved on a module level:

1. In the primary supply module, new mine opening is modeled by selecting a different pool of incentive mines each year, and calculate the expected lifetime IRR of each mine. The real world mine opening mechanism should be more complicated, and some mines can be assessed multiple times for its profitability before a final decision is made on opening. Therefore, a more sophisticated model on mine opening can be developed to better reflect this reality.
2. While smelters and refineries are modeled as a whole in the refinery module, there should be differentiation in market behaviors in reality. There are markets of copper matte, blisters and anode boards, within the network of smelters, refineries and some dealers. Due to lack of transparent data for these markets, more in-depth industry surveys and interviews should be conducted in order to enhance the model in this aspect.
3. Copper demand intensities are modeled as function to cathode price and regional GDPs, and a universal baseline is used for demand volume predictions. Both volumes and intensities can be explored further in scenario analysis.
4. In the price formation module, I have used relatively simplistic approaches to model the relationship between price and S&D. Future researches could explore other approaches of price forecasting, such as using non-linear frameworks (e.g. regression trees, support vector machine, ensemble methods) or using text mining to understand the relationship between market sentiment and price.

Furthermore, future research could explore various supply and demand scenarios under this simulation framework by changing the initial values of system parameters. A few of these system parameters are shown in Table 5.24, including many parameters investigated in the sensitivity analysis in this chapter. Changes in these parameters can lead to a chain of effects within the simulation, and their direct impacts on the system are also shown in Table 5.24.

The effect of many supply risk mitigation strategies can be quantified using this simulation. As an interesting example, one could estimate how much copper mining production would be avoided following the lifetime extension of copper wires used in the building and construction sector. The extension of product lifetime has been frequently discussed as a supply risk mitigation strategy in material criticality studies (Buchert et al., 2009; Moss et al., 2011, 2013). However, while longer product lifetime does mean less demand for new product, it also means less old scrap generated from end-of-life products. Therefore, the net effect on reducing total copper demand needs to be quantitatively demonstrated. Similarly, other supply risk mitigation scenarios, such as increasing fabrication efficiency, material substitution, product re-use, and dematerialization can be quantified under the simulation framework presented in this thesis. Results from these scenario analyses could help decision makers prioritize mitigation strategies for particular materials in particular locations on a supply chain.

Table 5. 24 Example system parameters and their respective direct impacts on the system if the initial values are higher than baseline

Module	Parameters	Direct impact on the system if the initial values are higher than baseline
Primary supply	Reclamation cost	Mines become less profitable, and more operating mines will postpone closing
	Ore grade elasticity	Lifetime of mines will be shorter
	IRR cutoff	New mines are more difficult to open
	Mining production elasticity	Mining production become more responsive to cathode price
Scrap supply	Product lifetime	Less old scrap generated, and less new product demand
	Collection rate	More scrap supply
	Technical recycling efficiency	More scrap supply
	Semis fabrication efficiency	Less new scrap generated, and less raw material demand
Refinery	Secondary ratio long run elasticity to TCRC	See discussion in the sensitivity analysis section
	Secondary ratio long run elasticity to No.2 spread	
Demand	GDP growth prediction	Higher copper demand for all end-use sectors
	Volume growth prediction	Higher copper demand for specific end-use sectors
Price formation	Scrap S&D elasticity	See discussion in the sensitivity analysis section

Chapter 6: Concluding Remarks

Conclusions and contributions

The concerns over the future availability of materials have motivated a variety of material criticality studies. However, after more than ten years of development in this field, 'material criticality' now has a much broader meaning: based on Graedel and Reck (T.E. Graedel & Reck, 2019), criticality can be defined as 'the quality, state, or degree of being the highest importance'. However, how to understand what is meant by 'the highest importance'? Studies have offered answers to this question from geological, geopolitical, social, economic, environmental, and technological perspectives. This thesis focuses on two aspects related of criticality: 1) the status of a metal being produced as a byproduct; 2) The market impact of increased recycling.

Chapter 1 provided an overview to material availability concerns and supply risk mitigation strategies. Material availability concerns can be either short-term or long-term in nature. Long-term concerns, which are most frequently related to the ultimate depletion of a material, have yet to show significant impact on the production and consumption patterns in human society. Although the long-term scarcity of many metal elements has been perceived to increase due to ore grade decline, cost decrease due to technology improvement seem to have dominated or at least offset ore grade decline in many cases. Short-term perturbations to the availability of materials, on the other hand, can take place wherein some end consumers might suffer due to lack of raw material supply or high raw material costs. From another dimension, availability concerns can either be supply side or demand side in nature. The byproduct status of metals is a highly considered short-term supply side concern, and many people fear that there would be inadequate supply of these metals in the near future, particularly for metals used in clean-energy applications. Correspondingly, supply risk mitigation strategies can also initiate from suppliers or consumers. Recycling is considered as an important mitigation strategy, as increased recycling provides additional secondary supply to the material market.

A literature review of material criticality is performed in **Chapter 2**, in which I summarized supply risk indicators used in 25 criticality studies between 2006 and 2018. I found that, while byproduct dependency and recyclability are among the most frequently reported supply risk indicators, understanding these two indicators lacks quantitative rigor and consistency. This observation provides a fundamental motivation for this thesis. For byproduct dependence, this thesis provides a quantitative framework and explores metrics that are more robust than state-of-the-art approaches. However, for recycling the focus is specifically on secondary material displacement of primary material, which has been recognized as a critical component for understanding the environmental benefits of recycling.

In Chapter 3, a classification for over 40 carrier-byproduct pairs is performed, based on two market characteristics essential to byproduct metals. By employing clustering analysis, metal pairs are categorized into five groups with distinct byproduct characteristics. Such an analysis allows one to quickly identify the type of major risk associated with a byproduct metal of interest. Following this analysis, case studies are performed on three byproduct metals from the group with high-byproduct status. Contrary to conventional views for byproduct metals in many criticality studies, these case studies provide new quantitative evidence that, byproduct metals' availability may not be directly limited by carrier supply. Results suggest that rather than limited primary production of carrier, lack of incentive for improving recovery efficiency may limit availability of the byproduct. This behavior is found in the zinc-indium and copper-selenium systems. For germanium, on the other hand, we instead propose influence from the byproduct market itself leading to price inelasticity of supply.

Following the discovery in **Chapter 3** that a byproduct metal's availability can be seriously limited by low recovery efficiency, a corresponding supply risk mitigation strategy is explored in **Chapter 4**: Developing alternative extraction processes with high recovery rate. Using the ratio between byproduct metal value in ore and minesite cost as a screening indicator, indium and germanium were isolated. An extraction process is proposed to phase separate indium from its carrier metal zinc at a mine sites, potentially increasing the overall indium recovery efficiency from 15%~20% in the conventional process to 55% under the alternative process. The alternative process is also found to be highly favorable from a total cash margin perspective, because the additional revenue from indium is significant enough to cover extra processing costs for most deposits investigated. Results from the deposit level analysis also shows that global indium supply could increase by around 10%, if all economically feasible deposits switch to using the new process. This result demonstrates the significant opportunity to increase byproduct metal availability under processing technology improvements. In addition, results from sensitivity analysis suggest that byproduct metal producers should pay attention to risk management associated with metal prices, because metal prices have been highly volatile historically.

In **Chapter 5**, a bottom-up copper market simulation model is developed to provide an estimate for how much primary production is offset by increased recycling (which is then linked to the subsequent influence on the availability of a byproduct, discussed below). While the primary goal is displacement estimation, this model also allows various scenarios to be investigated under the context of primary copper market interacting with secondary market. Compared to previous studies that try to quantify displacement, the methodology developed in this thesis is much more granular: instead of just modeling total primary/secondary supply and demand, the specific behavior of major market agents (miners, refineries, scrap dealers, manufacturers) are quantified and mimicked. In addition to scenarios on recycling increase, this model is also capable of simulating other supply risk mitigation strategies, such as product lifetime extension, dematerialization in specific end-use sectors, and so on. Results on displacement estimation show that, displacement rate is dependent on the size of secondary supply shocks, as larger shocks lead to larger system rebounds. Due to various rebound effects that incentivize mining production, policy makers should not expect that aggressive improvement in recycling leads to aggressive reduction in mining.

The two foci of this thesis, 1) the status of a metal being produced as a byproduct and 2) the market impact of increased recycling, have been investigated independently in the above. Finally, in the second part of **Chapter 5**, a connection is made between the two foci, by estimating the impact of carrier metal recycling on the availability of its byproduct metals. Three case studies are carried out, focusing on cobalt, selenium and tellurium as byproducts of copper. It is found in all three cases that, even the most aggressive copper recycling scenario does not bring significant impact to the supply/supply potential of these byproducts. Therefore, recycling as a risk mitigation strategy for a carrier metal does not bring additional supply risk to the byproduct in the cases investigated.

Based on results presented in this thesis, I provide several suggestions to decision makers managing critical materials' supply risk: First, decision makers should not feel panic by the statement that 'byproduct metals have problematic supply'. In fact, not all byproduct metals have problematic supply. The degree of risk varies by byproduct and carrier, and one could refer to the clusters in Figure 3.2 to identify the major type of risk for a certain carrier-byproduct metal pair. Second, in a case where supply limitations are identified for a specific byproduct metal, policies and research efforts should focus on developing appropriate supply risk mitigation strategies that break the major bottleneck in supply. For example, alternative extraction processes (and improved recovery) can be developed for metals that suffer from low recovery efficiencies. Third, as various suppliers, dealers, and consumers interact within commodity markets, any mitigation strategy would inevitably cause rebound effects that offset potential benefits.

Therefore, decision makers should use analytical tools to quantify the net effect of mitigation strategies, and prioritize ones that are more effective from a market perspective.

Limitations and future work

While this thesis provides novel approaches to assessing material criticality, there are inevitably limitations in these approaches, and opportunities exist for future research to further improve the models developed in this thesis.

First, as described in **Chapter 3** and **Chapter 4,** limited data availability on byproduct metals restricts how quantitative the conclusions can be. Due to the larger size of market, data on common base metals are often collected and summarized by industry associations and market participants with great amount of effort, while data on many minor metals are limited. The high country level and company level production concentration for several byproduct metals worsen this situation, as production data is often withheld by major producers. For indium, a global deposit level metal concentration dataset is utilized in both **Chapter 3** and **Chapter 4**, which greatly enhances the depth of analyses. Therefore, I suggest that future work should investigate similar high-resolution datasets. In cases where such datasets are not available, researchers could characterize deposit level information with statistical approaches, and analyze the statistical uncertainties. For the indium case study in particular, it is worth noting that the goal of this study is to provide a framework for assessing deposit level economic feasibility of alternative extraction processes, instead of proposing the process to replace all current extraction processes. Practical feasibility of this process, including reaction kinetics and the morphology of indium-containing ores, should be examined experimentally in future work.

Second, econometric models are used in **Chapter 3** and **Chapter 5** for the estimation of various supply/demand responses to price. As these regression-based models are designed to capture the linear relationships between the independent variables and the dependent variables, non-linearities have been neglected. For future research, one could augment linear methods with non-linear approaches such as regression trees, support vector machine and ensemble learning methods to improve the predictive power of supply/demand/price forecast models. Specifically, the price formation models developed in **Chapter 5** could be more complex, and many other price influencing factors should be investigated more systematically. Furthermore, this thesis only explores system responses under a few simulation scenarios, while there are about 100 additional parameters in the whole simulation system. Many more supply and demand scenarios, and system sensitivities, could be investigated by changing these parameters, such as the ones shown in Table 5.24.

Third, models developed in this thesis focused on a pair of carrier-byproduct metals, while all metal cycles are ultimately connected. For example, although the simulation model developed in **Chapter 5** incorporates all major participants on the copper market, the model does not explicitly include metal producers whose primary commodity is not copper. All the mines are assumed to only respond to copper market prices, although a subset of these mines can be driven by the prices of other coproducts such as nickel, cobalt, PGMs, and so on. A multi-metal simulation system could in part solve this problem, by expanding the copper model to the supply/demand/price responses of coproduct metals similarly. Such a multi-metal market simulation tool could help researchers to investigate market response under policy impacts, technology shifts and market events.

References

Achzet, B., & Helbig, C. (2013). How to evaluate raw material supply risks—An overview. *Resources Policy*, *38*(4), 435–447. https://doi.org/10.1016/j.resourpol.2013.06.003

Ahmadi, M. R. (2018). Cutoff grade optimization based on maximizing net present value using a computer model. *Journal of Sustainable Mining*, *17*(2), 68–75. https://doi.org/10.1016/j.jsm.2018.04.002

Alfantazi, A. M., & Moskalyk, R. R. (2003). Processing of indium: A review. *Minerals Engineering*, *16*(8), 687–694. https://doi.org/10.1016/S0892-6875(03)00168-7

Allwood, J. M., Ashby, M. F., Gutowski, T. G., & Worrell, E. (2011). Material efficiency: A white paper. *Resources, Conservation and Recycling*, *55*(3), 362–381. https://doi.org/10.1016/j.resconrec.2010.11.002

Alonso, E. (2010). *Material scarcity from the perspective of manufacturing firms: Case studies of platinum and cobalt*. Massachusetts Institute of Technology.

Anderson, C. S. (2015). *Selenium, in U.S. Geological Survey Minerals Information: Mineral Commodity Summaries*. U.S. Geological Survey.

Anderson, C. S. (2017). *Selenium and Tellurirum, in U.S. Geological Survey Minerals 2015 Minerals Yearbook*. U.S. Geological Survey.

Anderson, C. Schuyler. (2018). *Selenium and Tellurium, in 2016 Minerals Yearbook*. Retrieved from U.S. Geological Survey website: https://www.usgs.gov/centers/nmic/selenium-and-tellurium-statistics-and-information

Andersson, B. A. (2000). Materials availability for large-scale thin-film photovoltaics. *Progress in Photovoltaics: Research and Applications*, *8*(1), 61–76. https://doi.org/10.1002/(SICI)1099-159X(200001/02)8:1<61::AID-PIP301>3.0.CO;2-6

Angerer, G., Marscheider-Weidemann, F., Lüllmann, A., Erdmann, L., Scharp, M., Handke, V., & Marwede, M. (2009). *Raw materials for emerging technologies*. Retrieved from Fraunhofer ISI, Institute for Futures Studies and Technology Assessment IZT website: http://publica.fraunhofer.de/eprints/urn_nbn_de_0011-n-1115143.pdf

Arellano, M., & Bond, S. (1991). Some Tests of Specification for Panel Data: Monte Carlo Evidence and an Application to Employment Equations. *The Review of Economic Studies*, *58*(2), 277–297. https://doi.org/10.2307/2297968

Arrobas, D. L. P., Hund, K. L., Mccormick, M. S., Ningthoujam, J., & Drexhage, J. R. (2017). *The Growing Role of Minerals and Metals for a Low Carbon Future* (No. 117581; pp. 1–0). Retrieved from The World Bank website: http://documents.worldbank.org/curated/en/207371500386458722/The-Growing-Role-of-Minerals-and-Metals-for-a-Low-Carbon-Future

Asad, M. W. A. (2007). Optimum cut-off grade policy for open pit mining operations through net present value algorithm considering metal price and cost escalation. *Engineering Computations*. https://doi.org/10.1108/02644400710817961

Asad, M. W. A., & Topal, E. (2011). Net present value maximization model for optimum cut-off grade policy of open pit mining operations. *Journal of the Southern African Institute of Mining and Metallurgy*, *111*(11), 741–750.

Atherton, J. (2007). Declaration by the Metals Industry on Recycling Principles. *The International Journal of Life Cycle Assessment*, *12*(1), 59–60. https://doi.org/10.1065/lca2006.11.283

Ayres, R. U., & Peiro, L. T. (2013). Material efficiency: Rare and critical metals. *Philosophical Transactions of the Royal Society A: Mathematical, Physical and Engineering Sciences*, *371*(1986), 20110563–20110563.

Ayres, Robert U. (1997). Metals recycling: Economic and environmental implications. *Resources, Conservation and Recycling*, *21*(3), 145–173.

Bandara, H. D., Darcy, J. W., Apelian, D., & Emmert, M. H. (2014). Value analysis of neodymium content in shredder feed: Toward enabling the feasibility of rare earth magnet recycling. *Environmental Science & Technology*, *48*(12), 6553–6560.

Barin, I. (1995). *Thermochemical Data of Pure Substances*. Retrieved from https://ci.nii.ac.jp/naid/10006949556/

Barnett, D. F., & Crandall, R. W. (2002). Steel: Decline and Renewal. In *Industry studies* (3rd ed., pp. 134–135). New York: M. E. Sharpe, Inc.

Bauer, D., Diamond, D., Li, J., McKittrick, M., Sandalow, D., & Telleen, P. (2011). *Critical Materials Strategy*. Retrieved from U.S. Department of Energy website: https://www.osti.gov/biblio/1000846-department-energy-critical-materials-strategy

Bauer, D., Diamond, D., Li, J., Sandalow, D., Telleen, P., & Wanner, B. (2010). *Critical Materials Strategy*. Retrieved from U.S. Department of Energy website: https://www.osti.gov/biblio/1000846-department-energy-critical-materials-strategy

Baumol, W. J., & Blinder, A. S. (2015). *Microeconomics: Principles and policy*. Nelson Education.

Behrendt, S., Scharp, M., Kahlenborn, W., Feil, M., Dereje, C., Bleischwitz, R., & Delzeit, R. (2007). *Seltene Metalle: Mabnahmen und Konzepte zur Lösung des Problems konfliktverschärfender Rohstoffausbeutung am Beispiel Coltan*. Retrieved from Umwelt Bundes Amt website: https://d-nb.info/990406679/34

Bhuwalka, K., Swei, O., Roth, R., & Kirchain, R. (2019). *Estimating Copper Price Elasticity using Bayesian Hierarchical Modeling*.

Blewais, D. I. (2010). *Byproduct Mineral Commodities Used for the Production of Photovoltaic Cells*. Retrieved from U.S. Geological Survey website: https://pubs.usgs.gov/circ/1365/

British Geological Survey. (2011). *Risk List 2011*. Retrieved from https://www.bgs.ac.uk/downloads/start.cfm?id=2063

British Geological Survey. (2012). *Risk List 2012*. Retrieved from https://www.bgs.ac.uk/downloads/start.cfm?id=2643

British Geological Survey. (2015). *Risk List 2015*. Retrieved from https://www.bgs.ac.uk/downloads/start.cfm?id=3075

Buchert, M., Schüler, D., & Bleher, D. (2009). *Critical metals for future sustainable technologies and their recycling potential*. Retrieved from UNEP DTIE; Öko-Institut website: http://www.unep.fr/shared/publications/pdf/DTIx1202xPA-Critical%20Metals%20and%20their%20Recycling%20Potential.pdf

Buchholz, P., & Brandenburg, T. (2018). Demand, Supply, and Price Trends for Mineral Raw Materials Relevant to the Renewable Energy Transition Wind Energy, Solar Photovoltaic Energy, and

Energy Storage. *Chemie Ingenieur Technik*, *90*(1–2), 141–153. https://doi.org/10.1002/cite.201700098

Bustamante, M. L., & Gaustad, G. (2014). Challenges in assessment of clean energy supply-chains based on byproduct minerals: A case study of tellurium use in thin film photovoltaics. *Applied Energy*, *123*, 397–414. https://doi.org/10.1016/j.apenergy.2014.01.065

Cargill, S. M., Root, D. H., & Bailey, E. H. (1980). Resource estimation from historical data: Mercury, a test case. *Journal of the International Association for Mathematical Geology*, *12*(5), 489–522. https://doi.org/10.1007/BF01028882

Cargill, S. M., Root, D. H., & Bailey, E. H. (1981). Estimating usable resources from historical industry data. *Economic Geology*, *76*(5), 1081–1095. https://doi.org/10.2113/gsecongeo.76.5.1081

Chagnon, M. J. (1995). Indium and indium compounds. In *Kirk-Othmer Encyclopedia of Chemical Technology*. New York: John Wiley & Sons.

Cobb, C. W., & Douglas, P. H. (1928). A theory of production. *The American Economic Review*, *18*(1), 139–165.

Cook, N. J., Ciobanu, C. L., Pring, A., Skinner, W., Shimizu, M., Danyushevsky, L., … Melcher, F. (2009). Trace and minor elements in sphalerite: A LA-ICPMS study. *Geochimica et Cosmochimica Acta*, *73*(16), 4761–4791. https://doi.org/10.1016/j.gca.2009.05.045

Cooper, J. C. (2003). Price elasticity of demand for crude oil: Estimates for 23 countries. *OPEC Energy Review*, *27*(1), 1–8.

Copper Development Association. (2004). *Copper and Copper Alloys: Compositions, Applications and Properties*. Retrieved from https://copperalliance.org.uk/knowledge-base/resource-library/coppers-copper-alloys-designations-standards/

Copper Development Association. (2019a). Copper Alloy Supplier Database. Retrieved July 24, 2019, from https://www.copper.org/resources/suppliers/CDAFabricatorSearch.php

Copper Development Association. (2019b). Copper Timeline. Retrieved July 23, 2019, from Copper Timeline website: https://www.copper.org/education/history/timeline/timeline.html

Croissant, Y., & Millo, G. (2008). Panel Data Econometrics in R: The plm Package. *Journal of Statistical Software*, *27*(1), 1–43. https://doi.org/10.18637/jss.v027.i02

Dahmus, J. B., & Gutowski, T. G. (2007). What gets recycled: An information theory based model for product recycling. *Environmental Science & Technology*, *41*(21), 7543–7550.

Darton Commodities. (2018). *Cobalt Market Review 2017-2018*.

Davis, J. R. (2001). *Copper and Copper Alloys*. ASM International.

Dewulf, J., Van der Vorst, G., Denturck, K., Van Langenhove, H., Ghyoot, W., Tytgat, J., & Vandeputte, K. (2010). Recycling rechargeable lithium ion batteries: Critical analysis of natural resource savings. *Resources, Conservation and Recycling*, *54*(4), 229–234. https://doi.org/10.1016/j.resconrec.2009.08.004

Drozdov, A. (2007). *Aluminium: The Thirteenth Element*. Russia: The RUSAL Library.

Duclos, S. J., Otto, J. P., & Konitzer, D. G. (2010). Design in an era of Constrained Resources. *Mechanical Engineering Magazine Select Articles*, *132*(09), 36–40. https://doi.org/10.1115/1.2010-Sep-3

Ekvall, T. (2000). A market-based approach to allocation at open-loop recycling. *Resources, Conservation and Recycling*, *29*(1), 91–109. https://doi.org/10.1016/S0921-3449(99)00057-9

Ekvall, T., & Weidema, B. P. (2004). System boundaries and input data in consequential life cycle inventory analysis. *The International Journal of Life Cycle Assessment*, *9*(3), 161–171. https://doi.org/10.1007/BF02994190

Erdmann, L., Behrendt, S., & Feil, M. (2011). *Kritische Rohstoffe für Deutschland*. KfW Bankengruppe.

European Commission. (2010). *Critical raw materials for the EU*. Retrieved from https://ec.europa.eu/growth/sectors/raw-materials/specific-interest/critical_en

European Commission. (2014). *Report on Critical Raw Materials for the EU*. Retrieved from https://ec.europa.eu/growth/sectors/raw-materials/specific-interest/critical_en

European Commission. (2017). *Study on the review of the list of Critical Raw Materials*. Retrieved from https://ec.europa.eu/growth/sectors/raw-materials/specific-interest/critical_en

European Committee for Standardization. (2015). *Copper and copper alloys: Compendium of compositions and products*.

Fastmarkets AMM. (2019). *AMM Scrap Metal Prices*. Retrieved from https://www.amm.com/Pricing/ScrapPrices_FullList.html?stubid=14220

Federal Reserve Bank of St. Louis. (2016). Federal Reserve Economic data. Retrieved November 30, 2016, from FRED, Federal Reserve Bank of St. Louis website: https://fred.stlouisfed.org/

Fisher, F. M., Cootner, P. H., & Baily, M. N. (1972). An econometric model of the world copper industry. *The Bell Journal of Economics and Management Science*, 568–609.

Fisher, L. A., & Owen, A. D. (1981). An economic model of the US aluminium market. *Resources Policy*, *7*(3), 150–160.

Fizaine, F. (2013). Byproduct production of minor metals: Threat or opportunity for the development of clean technologies? The PV sector as an illustration. *Resources Policy*, *38*(3), 373–383.

Fortier, S. M., Nassar, N. T., Lederer, G. W., Brainard, J., Gambogi, J., & McCullough, E. A. (2016). *Draft Critical Mineral List—Summary of Methodology and Background Information—U.S. Geological Survey Technical Input Document in Response to Secretarial Order No. 3359*. Retrieved from U.S. Geological Survey website: https://pubs.usgs.gov/of/2018/1021/ofr20181021.pdf

Frees, N. (2007). Crediting aluminium recycling in LCA by demand or by disposal. *The International Journal of Life Cycle Assessment*, *13*(3), 212. https://doi.org/10.1065/lca2007.06.348

Frenzel, M., Kullik, J., Reuter, M. A., & Gutzmer, J. (2017). Raw material 'criticality'—Sense or nonsense? *Journal of Physics D: Applied Physics*, *50*(12), 123002.

Frenzel, Max, Ketris, M. P., & Gutzmer, J. (2014). On the geological availability of germanium. *Mineralium Deposita*, *49*(4), 471–486. https://doi.org/10.1007/s00126-013-0506-z

Frenzel, Max, Ketris, M. P., Seifert, T., & Gutzmer, J. (2016). On the current and future availability of gallium. *Resources Policy*, *47*, 38–50.

Frenzel, Max, Tolosana-Delgado, R., & Gutzmer, J. (2015). Assessing the supply potential of high-tech metals–A general method. *Resources Policy*, *46*, 45–58.

Friedman, J., Hastie, T., & Tibshirani, R. (2008). Unsupervised Learning. In *The elements of statistical learning* (2nd ed.). New York: Springer Series in Statistics.

Frondel, M., Grösche, P., Huchtemann, D., Oberheitmann, A., Peters, J., Angerer, G., ... Wagner, M. (2007). *Trends der Angebots-und Nachfragesituation bei mineralischen Rohstoffen*. Retrieved from Rheinisch-Westfälisches Institut für Wirtschaftsforschung (RWI Essen), Fraunhofer-Institut für System-und Innovationsforschung (ISI), Bundesanstalt für Geowissenschaften und Rohstoffe (BGR) website: https://www.econstor.eu/handle/10419/70880

Fu, X., Beatty, D., Gaustad, G., Ceder, G., Roth, R., Kirchain, R., ... Olivetti, E. (2019). *High Resolution Insights into Co Supply in the Face of Changing Demand*.

Fu, X., Ladd, J., Osmundsen, R., & Glerum, J. A. (2017). *Indium Extraction as a Byproduct of Zinc, MIT 3.19 Class Project Report*.

Fu, X., Polli, A., & Olivetti, E. (2018). High-Resolution Insight into Materials Criticality: Quantifying Risk for By-Product Metals from Primary Production. *Journal of Industrial Ecology*.

Fu, X., Ueland, S. M., & Olivetti, E. (2017). Econometric modeling of recycled copper supply. *Resources, Conservation and Recycling*, *122*, 219–226.

Gaustad, G., Li, P., & Kirchain, R. (2007). Modeling methods for managing raw material compositional uncertainty in alloy production. *Resources, Conservation and Recycling*, *52*(2), 180–207. https://doi.org/10.1016/j.resconrec.2007.03.005

George, M. W. (2004). *Selenium and Tellurirum, in U.S. Geological Survey Minerals 2004 Minerals Yearbook*. U.S. Geological Survey.

Glöser, S., Soulier, M., & Tercero Espinoza, L. A. (2013). Dynamic Analysis of Global Copper Flows. Global Stocks, Postconsumer Material Flows, Recycling Indicators, and Uncertainty Evaluation. *Environmental Science & Technology*, *47*(12), 6564–6572. https://doi.org/10.1021/es400069b

Glöser, S., Tercero Espinoza, L., Gandenberger, C., & Faulstich, M. (2015). Raw material criticality in the context of classical risk assessment. *Resources Policy*, *44*, 35–46. https://doi.org/10.1016/j.resourpol.2014.12.003

Gómez, F., Guzmán, J. I., & Tilton, J. E. (2007). Copper recycling and scrap availability. *Resources Policy*, *32*(4), 183–190. https://doi.org/10.1016/j.resourpol.2007.08.002

Graedel, T. E. (2002). Material substitution: A resource supply perspective. *Resources, Conservation and Recycling*, *34*(2), 107–115. https://doi.org/10.1016/S0921-3449(01)00097-0

Graedel, T. E., Allwood, J., Birat, J.-P., Buchert, M., Hagelüken, C., Reck, B. K., ... Sonnemann, G. (2011a). What Do We Know About Metal Recycling Rates? *Journal of Industrial Ecology*, *15*(3), 355–366. https://doi.org/10.1111/j.1530-9290.2011.00342.x

Graedel, T. E., Allwood, J., Birat, J.-P., Buchert, M., Hagelüken, C., Reck, B. K., ... Sonnemann, G. (2011b). What do we know about metal recycling rates? *Journal of Industrial Ecology*, *15*(3), 355–366.

Graedel, T. E., Barr, R., Chandler, C., Chase, T., Choi, J., Christoffersen, L., ... Zhu, C. (2012). Methodology of Metal Criticality Determination. *Environmental Science & Technology*, *46*(2), 1063–1070. https://doi.org/10.1021/es203534z

Graedel, T. E., & Cao, J. (2010). Metal spectra as indicators of development. *Proceedings of the National Academy of Sciences*, *107*(49), 20905–20910. https://doi.org/10.1073/pnas.1011019107

Graedel, T. E., Harper, E. M., Nassar, N. T., Nuss, P., & Reck, B. K. (2015). Criticality of metals and metalloids. *Proceedings of the National Academy of Sciences*, *112*(14), 4257–4262. https://doi.org/10.1073/pnas.1500415112

Graedel, T. E., van Beers, D., Bertram, M., Fuse, K., Gordon, R. B., Gritsinin, A., ... Vexler, D. (2004). Multilevel Cycle of Anthropogenic Copper. *Environmental Science & Technology*, *38*(4), 1242–1252. https://doi.org/10.1021/es030433c

Graedel, T.E., & Reck, B. K. (2019). Defining the Criticality of Materials. In *Critical Materials: Underlying Causes And Sustainable Mitigation Strategies* (p. 103). World Scientific.

Graedel, Thomas E., Barr, R., Chandler, C., Chase, T., Choi, J., Christoffersen, L., ... others. (2012). Methodology of metal criticality determination. *Environmental Science & Technology*, *46*(2), 1063–1070.

Gramatyka, P., Nowosielski, R., & Sakiewicz, P. (2007). Recycling of waste electrical and electronic equipment. *Journal of Achievements in Materials and Manufacturing Engineering*, *20*(1–2), 535–538.

Green, M. A. (2006). Improved estimates for Te and Se availability from Cu anode slimes and recent price trends. *Progress in Photovoltaics: Research and Applications*, *14*(8), 743–751. https://doi.org/10.1002/pip.703

Guberman, D. E. (2016). *Germanium, in U.S. Geological Survey Minerals Information: Mineral Commodity Summaries*. U.S. Geological Survey.

Habashi, F. (2017). *Principles of Extractive Metallurgy*. https://doi.org/10.1201/9780203742112

Hagelüken, C., & Meskers, C. E. (2010). Complex life cycles of precious and special metals. *Linkages of Sustainability*, *4*.

Hamilton, C., & Kamal, K. (2017). *Cobalt: Solving for a Supply-Constrained Market*. BMO Capital Markets.

Hatayama, H., & Tahara, K. (2015). Criticality Assessment of Metals for Japan's Resource Strategy. *Materials Transactions*, *56*(2), 229–235. https://doi.org/10.2320/matertrans.M2014380

He, Y., Zhu, K., Gao, S., Liu, T., & Li, Y. (2009). Theory and method of genetic-neural optimizing cut-off grade and grade of crude ore. *Expert Systems with Applications*, *36*(4), 7617–7623. https://doi.org/10.1016/j.eswa.2008.09.018

Herrera, A. M., Lagalo, L. G., & Wada, T. (2011). Oil price shocks and industrial production: Is the relationship linear? *Macroeconomic Dynamics*, *15*(S3), 472–497.

Hiraki, T., Takeda, O., Nakajima, K., Matsubae, K., Nakamura, S., & Nagasaka, T. (2011). Thermodynamic criteria for the removal of impurities from end-of-life magnesium alloys by evaporation and flux treatment. *Science and Technology of Advanced Materials*, *12*(3), 035003.

Holtz-Eakin, D., Newey, W., & Rosen, H. S. (1988). Estimating Vector Autoregressions with Panel Data. *Econometrica*, *56*(6), 1371–1395. https://doi.org/10.2307/1913103

Hotelling, H. (1931). The economics of exhaustible resources. *The Journal of Political Economy*, 137–175.

Huang, C. H., Lin, C. I., & Chen, H. K. (2005). Carbothermic reduction of zinc sulfide in the presence of calcium oxide. *Journal of Materials Science*, *40*(16), 4299–4306. https://doi.org/10.1007/s10853-005-2805-y

Huang, K. J., Li, L., & Olivetti, E. A. (2018). Designing for Manufacturing Scalability in Clean Energy Research. *Joule*, *2*(9), 1642–1647. https://doi.org/10.1016/j.joule.2018.07.020

Human Development Reports. (2019). Retrieved July 23, 2019, from http://hdr.undp.org/en/content/human-development-index-hdi

Institute of Scrap Recycling Industries. (2018). *Scrap Specifications Circular*. Retrieved from https://www.isri.org/recycling-commodities/scrap-specifications-circular

International Copper Association. (2013). *World total semis production data, 2006-2010, (from Glöser et al. 2013, Dynamic Analysis of Global Copper Flows. Global Stocks, Postconsumer Material Flows, Recycling Indicators, and Uncertainty Evaluation)*.

International Copper Study Group. (2010). *Copper Scrap Market Issues and Developments in the Semi-Fabricators Industry*. Presented at the Joint ICSG Statistical, Environmental and Economic Committee Meeting, Antofagasta, Chile.

International Copper Study Group. (2017). *The World Copper Factbook 2016*. Lisbon, Portugal.

International Copper Study Group. (2018a). *ICSG 2018 Statistical Yearbook*.

International Copper Study Group. (2018b). *The World Copper Factbook 2017*. Lisbon, Portugal.

International Copper Study Group. (2019a). *ICSG World Copper Production Data, from Refinitiv Datastream*. Refinitiv Datastream.

International Copper Study Group. (2019b). *The World Copper Factbook 2018*. Lisbon, Portugal.

International Monetary Fund. (2019). Global price of Coal, Australia. Retrieved July 24, 2019, from FRED, Federal Reserve Bank of St. Louis website: https://fred.stlouisfed.org/series/PCOALAUUSDM

Ishihara, S., Murakami, H., & Li, X. (2011). Indium concentration in zinc ores in plutonic and volcanic environments: Examples at the Dulong and Dachang mines, South China. *Bulletin of the Geological Survey of Japan*, *62*(7–8), 259–272.

Ishihara, S., Murakami, H., & Marquez-Zavalia, M. F. (2011). Inferred Indium Resources of the Bolivian Tin-Polymetallic Deposits. *Resource Geology*, *61*(2), 174–191.

Jensen, N. L. (1985). Tellurium. In *Mineral Facts and Problems* (1985 Edition). UNT Digital Library.

Jiang, K., Wang, Y., Zou, X., Zhang, L., & Liu, S. (2012). Extraction of Molybdenum from Molybdenite Concentrates with Hydrometallurgical Processing. *JOM*, *64*(11), 1285–1289. https://doi.org/10.1007/s11837-012-0457-3

Johnson, J., Reck, B. K., Wang, T., & Graedel, T. E. (2008). The energy benefit of stainless steel recycling. *Energy Policy*, *36*(1), 181–192.

Johnson, J. X., McMillan, C. A., & Keoleian, G. A. (2013). Evaluation of Life Cycle Assessment Recycling Allocation Methods. *Journal of Industrial Ecology*, *17*(5), 700–711. https://doi.org/10.1111/jiec.12050

Jolly, J. L. (2013). *2013 Technical Report: The U.S. Copper-base Scrap Industry and Its By-products*. Retrieved from Copper Development Association website: https://trends2008.copper.org/publications/pub_list/pdf/scrap_report.pdf

Jorgenson, J. D., & George, M. W. (2005). *Indium, Mineral Commodity Profile*. U. S. Geological Survey.

Kagawa, S., Tasaki, T., & Moriguchi, Y. (2006). The environmental and economic consequences of product lifetime extension: Empirical analysis for automobile use. *Ecological Economics*, *58*(1), 108–118. https://doi.org/10.1016/j.ecolecon.2005.06.003

Kapur, A., & Graedel, T. E. (2006). *Copper mines above and below the ground*. ACS Publications.

Kaufmann, D., Kraay, A., & Mastruzzi, M. (2011). The Worldwide Governance Indicators: Methodology and Analytical Issues1. *Hague Journal on the Rule of Law*, *3*(2), 220–246. https://doi.org/10.1017/S1876404511200046

Kaufmann, R. K., & Ullman, B. (2009). Oil prices, speculation, and fundamentals: Interpreting causal relations among spot and futures prices. *Energy Economics*, *31*(4), 550–558. https://doi.org/10.1016/j.eneco.2009.01.013

Kavlak, G., & Graedel, T. E. (2013a). Global anthropogenic selenium cycles for 1940–2010. *Resources, Conservation and Recycling*, *73*, 17–22. https://doi.org/10.1016/j.resconrec.2013.01.013

Kavlak, G., & Graedel, T. E. (2013b). Global anthropogenic tellurium cycles for 1940–2010. *Resources, Conservation and Recycling*, *76*, 21–26. https://doi.org/10.1016/j.resconrec.2013.04.007

Kelly, J. C., Sullivan, J. L., Burnham, A., & Elgowainy, A. (2015). Impacts of Vehicle Weight Reduction via Material Substitution on Life-Cycle Greenhouse Gas Emissions. *Environmental Science & Technology*, *49*(20), 12535–12542. https://doi.org/10.1021/acs.est.5b03192

Kelly, T. D., & Matos, G. R. (2015). *Cobalt statistics, in Historical statistics for mineral and material commodities in the United States (2015 version)*. Retrieved from U.S. Geological Survey website: https://www.usgs.gov/centers/nmic/historical-statistics-mineral-and-material-commodities-united-states

Klöpffer, W. (1996). Allocation rule for open-loop recycling in life cycle assessment. *The International Journal of Life Cycle Assessment*, *1*(1), 27–31. https://doi.org/10.1007/BF02978629

Krausmann, F., Gingrich, S., Eisenmenger, N., Erb, K.-H., Haberl, H., & Fischer-Kowalski, M. (2009). Growth in global materials use, GDP and population during the 20th century. *Ecological Economics*, *68*(10), 2696–2705.

Labys, W. C., Rees, H. J. B., & Elliott, C. M. (1971). Copper Price Behaviour and the London Metal Exchange. *Applied Economics*, *3*(2), 99–113. https://doi.org/10.1080/00036847100000032

Labys, Walter C., Achouch, A., & Terraza, M. (1999). Metal prices and the business cycle. *Resources Policy*, *25*(4), 229–238.

Laner, D., Rechberger, H., & Astrup, T. (2014). Systematic evaluation of uncertainty in material flow analysis. *Journal of Industrial Ecology*, *18*(6), 859–870.

Lasky, S. (1950). How tonnage and grade relations help predict ore reserves. *Engineering and Mining Journal*, *151*(4), 81–85.

Licht, C., Peiró, L. T., & Villalba, G. (2015). Global Substance Flow Analysis of Gallium, Germanium, and Indium: Quantification of Extraction, Uses, and Dissipative Losses within their Anthropogenic Cycles. *Journal of Industrial Ecology*, *19*(5), 890–903. https://doi.org/10.1111/jiec.12287

Liu, G., Bangs, C. E., & Müller, D. B. (2013). Stock dynamics and emission pathways of the global aluminium cycle. *Nature Climate Change*, *3*(4), 338–342. https://doi.org/10.1038/nclimate1698

Lloyd, S. M., & Ries, R. (2007). Characterizing, Propagating, and Analyzing Uncertainty in Life-Cycle Assessment: A Survey of Quantitative Approaches. *Journal of Industrial Ecology*, *11*(1), 161–179. https://doi.org/10.1162/jiec.2007.1136

Lokanc, M., Eggert, R., & Redlinger, M. (2015). *The availability of indium: The present, medium term, and long term*. National Renewable Energy Lab.(NREL), Golden, CO (United States).

London Metal Exchange: LME Cobalt. (n.d.). Retrieved July 23, 2019, from https://www.lme.com/en-GB/Metals/Minor-metals/Cobalt#tabIndex=0

Løvik, A. N., Restrepo, E., & Müller, D. B. (2016). Byproduct Metal Availability Constrained by Dynamics of Carrier Metal Cycle: The Gallium–Aluminum Example. *Environmental Science & Technology*, *50*(16), 8453–8461. https://doi.org/10.1021/acs.est.6b02396

Madlener, R., Bernstein, R., & González, M. A. A. A. (2011). *Econometric estimation of energy demand elasticities*. E.ON Energy Research Center, RWTH Aachen University.

Massari, S., & Ruberti, M. (2013). Rare earth elements as critical raw materials: Focus on international markets and future strategies. *Resources Policy*, *38*(1), 36–43.

Materials Systems Laboratory. (2019). *Commodity Model (unpublished)*. Massachusetts Institute of Technology.

McMillan, C. A., Skerlos, S. J., & Keoleian, G. A. (2012). Evaluation of the Metals Industry's Position on Recycling and its Implications for Environmental Emissions. *Journal of Industrial Ecology*, *16*(3), 324–333. https://doi.org/10.1111/j.1530-9290.2012.00483.x

Metal Bulletin. (2019). *Shanghai bonded copper stocks*. Retrieved from https://www.metalbulletin.com/My-price-book.html?price=43138

Mikesell, R. F. (2013). *The World Copper Industry: Structure and Economic Analysis*. https://doi.org/10.4324/9781315064437

Milisauskas, S. (2002). *European Prehistory: A Survey*. Springer Science & Business Media.

Morley, N., & Eatherley, D. (2008). *Material Security: Ensuring resource availability for the UK economy*. C-Tech Innovation Limited.

Moss, R., Tzimas, E., Kara, H., Willis, P., & Kooroshy, J. (2011). Critical metals in strategic energy technologies. *JRC-Scientific and Strategic Reports, European Commission Joint Research Centre Institute for Energy and Transport*.

Moss, R., Tzimas, E., Willis, P., Arendorf, J., Thompson, P., Chapman, A., ... others. (2013). Critical metals in the path towards the decarbonisation of the EU energy sector. *Assessing Rare Metals as Supply-Chain Bottlenecks in Low-Carbon Energy Technologies. JRC Report EUR, 25994*.

Mudd, G. M. (2007). Global trends in gold mining: Towards quantifying environmental and resource sustainability. *Resources Policy*, *32*(1–2), 42–56.

Mudd, G. M. (2012). Key trends in the resource sustainability of platinum group elements. *Ore Geology Reviews*, *46*, 106–117.

Mudd, G. M. (2014). The future of Yellowcake: A global assessment of uranium resources and mining. *Science of the Total Environment*, *472*, 590–607.

Mudd, G. M., Jowitt, S. M., & Werner, T. T. (2017). The world's lead-zinc mineral resources: Scarcity, data, issues and opportunities. *Ore Geology Reviews*, *80*, 1160–1190. https://doi.org/10.1016/j.oregeorev.2016.08.010

Nadler, H. G. (2000). Rhenium and Rhenium Compounds. In *Ullmann's Encyclopedia of Industrial Chemistry*. https://doi.org/10.1002/14356007.a23_199

Nadler, H. G., & Starck, H. C. (2012). Rhenium and rhenium compounds. In *Rhenium and Rhenium Compounds, in Ullmann's Encyclopedia of Industrial Chemistry* (5th ed.). Weinheim: Wiley-VCH Verlag GmbH & Co. KGaA.

Nakajima, K., Takeda, O., Miki, T., Matsubae, K., & Nagasaka, T. (2011). Thermodynamic analysis for the controllability of elements in the recycling process of metals. *Environmental Science & Technology*, *45*(11), 4929–4936.

Nakajima, K., Takeda, O., Miki, T., Matsubae, K., Nakamura, S., & Nagasaka, T. (2010). Thermodynamic analysis of contamination by alloying elements in aluminum recycling. *Environmental Science & Technology*, *44*(14), 5594–5600.

Nakajima, K., Yokoyama, K., Nakano, K., & Nagasaka, T. (2007). Substance Flow Analysis of Indium for Flat Panel Displays in Japan. *Materials Transactions*, *48*(9), 2365–2369. https://doi.org/10.2320/matertrans.MAW200702

Nansai, K., Nakajima, K., Kagawa, S., Kondo, Y., Suh, S., Shigetomi, Y., & Oshita, Y. (2014). Global flows of critical metals necessary for low-carbon technologies: The case of neodymium, cobalt, and platinum. *Environmental Science & Technology*, *48*(3), 1391–1400.

Nassar, N. T., Graedel, T. E., & Harper, E. M. (2015). By-product metals are technologically essential but have problematic supply. *Science Advances*, *1*(3), e1400180. https://doi.org/10.1126/sciadv.1400180

Nassar, Nedal T., Du, X., & Graedel, T. E. (2015). Criticality of the rare earth elements. *Journal of Industrial Ecology*, *19*(6), 1044–1054.

Nassar, Nedal T., Wilburn, D. R., & Goonan, T. G. (2016). Byproduct metal requirements for U.S. wind and solar photovoltaic electricity generation up to the year 2040 under various Clean Power Plan scenarios. *Applied Energy*, *183*, 1209–1226. https://doi.org/10.1016/j.apenergy.2016.08.062

National Science and Technology Council. (2016). *Assessment of Critical Minerals: Screening Methodology and Initial Application*. Retrieved from https://www.whitehouse.gov/sites/whitehouse.gov/files/images/CSMSC%20Assessment%20of%20Critical%20Minerals%20Report%202016-03-16%20FINAL.pdf

Naumov, A. V., & Grinberg, E. E. (2009). Several peculiarities in the analysis of the markets of rare and scattered metals after 2004. *Russian Journal of Non-Ferrous Metals*, *50*(1), 61–68. https://doi.org/10.3103/S1067821209010131

Nes, N. V., Cramer, J., & Stevels, A. (1999). A practical approach to the ecological lifetime optimization of electronic products. *Proceedings First International Symposium on Environmentally Conscious Design and Inverse Manufacturing*, 108–111. https://doi.org/10.1109/ECODIM.1999.747592

Nieto, A. ** B. A. * &. (2007). Determination of optimal cut-off grade policy to optimize NPV using a new approach with optimization factor. *Journal of the Southern African Institute of Mining and Metallurgy*, *107*(2), 87–94.

Northey, S., Mohr, S., Mudd, G. M., Weng, Z., & Giurco, D. (2014). Modelling future copper ore grade decline based on a detailed assessment of copper resources and mining. *Resources, Conservation and Recycling*, *83*, 190–201.

Noshadravan, A., Gaustad, G., Kirchain, R., & Olivetti, E. (2017). Operational Strategies for Increasing Secondary Materials in Metals Production Under Uncertainty. *Journal of Sustainable Metallurgy*, *3*(2), 350–361. https://doi.org/10.1007/s40831-016-0100-6

Nyrstar. (2009). *Introduction to Zinc and Lead Smelting Business*. Retrieved from https://www.nyrstar.com/~/media/Files/N/Nyrstar/results-reports-and-presentations/english/2009/zincleadsmelting.pdf

OECD. (2014). Long-term baseline projections, No. 95 (Edition 2014). *OECD Economic Outlook: Statistics and Projections (Database)*. https://doi.org/10.1787/data-00690-en

OECD. (2019a). National Accounts at a Glance. *OECD National Accounts Statistics (Database)*. https://doi.org/10.1787/data-00369-en

OECD. (2019b). National income, value added by activity. Retrieved July 24, 2019, from http://data.oecd.org/natincome/value-added-by-activity.htm

Olivetti, E. A., Gaustad, G. G., Field, F. R., & Kirchain, R. E. (2011). Increasing secondary and renewable material use: A chance constrained modeling approach to manage feedstock quality variation. *Environmental Science & Technology*, *45*(9), 4118–4126.

Osanloo, M., & Ataei, M. (2003). Using equivalent grade factors to find the optimum cut-off grades of multiple metal deposits. *Minerals Engineering*, *16*(8), 771–776. https://doi.org/10.1016/S0892-6875(03)00163-8

Patzek, Tad W. (2004). Thermodynamics of the Corn-Ethanol Biofuel Cycle. *Critical Reviews in Plant Sciences*, *23*(6), 519–567. https://doi.org/10.1080/07352680490886905

Patzek, Tadeusz W., & Croft, G. D. (2010). A global coal production forecast with multi-Hubbert cycle analysis. *Energy*, *35*(8), 3109–3122.

Polinares. (2012). *Fact Sheet: Indium*. Polinares, EU policy on Natural Resources.

Prior, T., Giurco, D., Mudd, G., Mason, L., & Behrisch, J. (2012). Resource depletion, peak minerals and the implications for sustainable resource management. *Global Environmental Change*, *22*(3), 577–587. https://doi.org/10.1016/j.gloenvcha.2011.08.009

Ramboll IMS Ingenieurgesellschaft mbH. (2016). *Analysis of the Economic Benefits of Developing Commercial Deep Sea Mining Operations in Regions where Germany has Exploration Licences of the International Seabed Authority, as well as Compilation and Evaluation of Implementation Options with a Focus on the Performance of a Pilot Mining Test*.

Rao, Y. K., & El-Rahaiby, S. K. (1985). Direct reduction of lead sulfide with carbon and lime; Effect of catalysts:Part i. Experimental. *Metallurgical Transactions B*, *16*(3), 465–475. https://doi.org/10.1007/BF02654845

Reck, B. K., & Graedel, T. E. (2012). Challenges in Metal Recycling. *Science*, *337*(6095), 690–695. https://doi.org/10.1126/science.1217501

Redlinger, M., & Eggert, R. (2016). Volatility of by-product metal and mineral prices. *Resources Policy*, *47*, 69–77. https://doi.org/10.1016/j.resourpol.2015.12.002

Reller, A. (2009). *Rohstoffsituation Bayern: Keine Zukunft ohne Rohstoffe: Strategien und Handlungsoptionen*. Retrieved from IW Consult GmbH website: https://www.energieatlas.bayern.de/file/pdf/691/studie

Rendu, J.-M. (2014). *An Introduction to Cut-off Grade Estimation, Second Edition*. Society for Mining, Metallurgy, and Exploration.

Rosenau-Tornow, D., Buchholz, P., Riemann, A., & Wagner, M. (2009). Assessing the long-term supply risks for mineral raw materials—A combined evaluation of past and future trends. *Resources Policy*, *34*(4), 161–175. https://doi.org/10.1016/j.resourpol.2009.07.001

Roskill. (2010). *Indium: Global industry markets and outlook*. Roskill Information Services.

Ross, S. A. (2012). The Arbitrage Theory of Capital Asset Pricing. In *World Scientific Handbook in Financial Economics Series*: *Vol. Volume 4. Handbook of the Fundamentals of Financial Decision Making* (pp. 11–30). https://doi.org/10.1142/9789814417358_0001

Runge, I. C. (1998). *Mining Economics and Strategy*. SME.

Rutledge, D. (2011). Estimating long-term world coal production with logit and probit transforms. *International Journal of Coal Geology*, *85*(1), 23–33.

Sahu, S. K., Chmielowiec, B., & Allanore, A. (2017). Electrolytic Extraction of Copper, Molybdenum and Rhenium from Molten Sulfide Electrolyte. *Electrochimica Acta*, *243*, 382–389.

Schulte-Schrepping, K.-H., & Piscator, M. (2000). Cadmium and Cadmium Compounds. In *Ullmann's Encyclopedia of Industrial Chemistry*. https://doi.org/10.1002/14356007.a04_499

Schwartz, M. (2015). *Base Metal Pricing & Concentrate Contracts*. Presented at the Teck Modeling Workshop. Retrieved from https://www.teck.com/media/Investors-Presentations-Webcasts-20151104-modelling-workshop.pdf

Schwarz-Schampera, U. (2013). Indium. In *Critical Metals Handbook* (pp. 204–229). https://doi.org/10.1002/9781118755341.ch9

Shamsuddin, M. (2016). *Physical Chemistry of Metallurgical Processes* (1st ed.). https://doi.org/10.1002/9781119078326

Shedd, K. (2017). *Cobalt, in 2015 Minerals Yearbook*. Retrieved from U.S. Geological Survey website: https://www.usgs.gov/centers/nmic/cobalt-statistics-and-information

Shinjoh, H. (2006). Rare earth metals for automotive exhaust catalysts. *Journal of Alloys and Compounds*, *408*, 1061–1064.

Silvapulle, P., & Moosa, I. A. (1999). The relationship between spot and futures prices: Evidence from the crude oil market. *Journal of Futures Markets*, *19*(2), 175–193. https://doi.org/10.1002/(SICI)1096-9934(199904)19:2<175::AID-FUT3>3.0.CO;2-H

Smith, C. S., & Forbes, R. J. (1957). Metallurgy and assaying. In *A history of technology* (Vol. 3, p. 29).

Söderström, U. (2008). *Copper smelter revenue stream*. Retrieved from https://www.boliden.com/globalassets/investor-relations/reports-and-presentations/capital-markets-day/2008/cmd/13-copper-smelters-revenue-stream-ulf-soderstrom-president-ba-market.pdf

S&P Global Market Intelligence. (2019a). *Mine Economics Methodology, Market Intelligence Metals & Mining Database*. Retrieved from S&P Global Market Intelligence website: https://www.snl.com//help/Mine_Economics_Methodology.htm

S&P Global Market Intelligence. (2019b). *SNL Metals & Mining Data*.

Stock, J. H., & Watson, M. W. (2003). *Introduction to Econometrics*. Boston: Addison Wesley.

Summers, L. H. (1987). Investment incentives and the discounting of depreciation allowances. In *The effects of taxation on capital accumulation* (pp. 295–304). University of Chicago Press.

Svedberg, P., & Tilton, J. E. (2006). The real, real price of nonrenewable resources: Copper 1870–2000. *World Development*, *34*(3), 501–519. https://doi.org/10.1016/j.worlddev.2005.07.018

Sverdrup, H. U., Ragnarsdottir, K. V., & Koca, D. (2014). On modelling the global copper mining rates, market supply, copper price and the end of copper reserves. *Resources, Conservation and Recycling*, *87*, 158–174. https://doi.org/10.1016/j.resconrec.2014.03.007

Thibault, J. D., McKeen, T. R., Scott, S. M., Boyd, T., & Hara, A. (2010). *NI 43-101 Independent Technical Report Mount Pleasant North Zone Preliminary Assessment*. Retrieved from http://www.adexmining.com/financial/pdf/Adex%2043-101%20Technical%20Report%20for%20NZ%20Jan.%2025,%202010.pdf

Thomas, V. M. (2003). Demand and Dematerialization Impacts of Second-Hand Markets. *Journal of Industrial Ecology*, *7*(2), 65–78. https://doi.org/10.1162/108819803322564352

Thomason, J. S., Atwell, R. J., Bajraktari, Y., Bell, J. P., Barnett, D. S., Karvonides, N. S., … Schwartz, E. L. (2010). *From National Defense Stockpile (NDS) to Strategic Materials Security Program (SMSP): Evidence and analytic support. Volume 1*. Retrieved from Institute for Defense Anslyses website: https://apps.dtic.mil/dtic/tr/fulltext/u2/a527258.pdf

Tolcin, A. C. (2016). *Indium, in U.S. Geological Survey Minerals Information: Mineral Commodity Summaries*. U. S. Geological Survey.

Tolcin, A. C. (2017). *Zinc, in U.S. Geological Survey 2015 Minerals Yearbook*. U.S. Geological Survey.

Turnovsky, S. J. (1983). The Determination of Spot and Futures Prices with Storable Commodities. *Econometrica*, *51*(5), 1363–1387. https://doi.org/10.2307/1912279

U. S. Geological Survey. (2016). Historical Statistics for Mineral Commodities in the United States (2016 version): U.S. Geological Survey Data Series 140. Retrieved November 29, 2016, from http://minerals.usgs.gov/minerals/pubs/historical-statistics/

U.S. Congressional Budget Office. (2019). Budget and Economic Data. Retrieved July 24, 2019, from https://www.cbo.gov/about/products/budget-economic-data

U.S. Geological Survey,. (1980). *Principles of a resource/reserve classification for minerals* (USGS Numbered Series No. 831). Retrieved from http://pubs.er.usgs.gov/publication/cir831

U.S. Geological Survey. (2000). *Copper, In Mineral Commodity Summaries 2000* (p. 57) [USGS Unnumbered Series]. Retrieved from http://pubs.er.usgs.gov/publication/70202434

U.S. Geological Survey. (2009). *Cobalt, In Mineral Commodity Summaries 2009* (p. 49) [USGS Unnumbered Series]. Retrieved from http://pubs.er.usgs.gov/publication/70202434

U.S. Geological Survey. (2019a). *Cadmium, In Mineral Commodity Summaries 2019* (p. 40) [USGS Unnumbered Series]. Retrieved from http://pubs.er.usgs.gov/publication/70202434

U.S. Geological Survey. (2019b). *Cobalt, In Mineral Commodity Summaries 2019* (p. 51) [USGS Unnumbered Series]. Retrieved from http://pubs.er.usgs.gov/publication/70202434

U.S. Geological Survey. (2019c). *Copper, In Mineral Commodity Summaries 2019* (p. 53) [USGS Unnumbered Series]. Retrieved from http://pubs.er.usgs.gov/publication/70202434

U.S. Geological Survey. (2019d). *Gallium, In Mineral Commodity Summaries 2019* (p. 62) [USGS Unnumbered Series]. Retrieved from http://pubs.er.usgs.gov/publication/70202434

U.S. Geological Survey. (2019e). *Germanium, In Mineral Commodity Summaries 2019* (p. 68) [USGS Unnumbered Series]. Retrieved from http://pubs.er.usgs.gov/publication/70202434

U.S. Geological Survey. (2019f). *Indium, In Mineral Commodity Summaries 2019* (p. 78) [USGS Unnumbered Series]. Retrieved from http://pubs.er.usgs.gov/publication/70202434

U.S. Geological Survey. (2019g). *Zinc, In Mineral Commodity Summaries 2019* (p. 190) [USGS Unnumbered Series]. Retrieved from http://pubs.er.usgs.gov/publication/70202434

U.S. National Research Council. (2008). *Minerals, critical minerals, and the US economy*. National Academies Press.

Vehtari, A., Gelman, A., & Gabry, J. (2017). Practical Bayesian model evaluation using leave-one-out cross-validation and WAIC. *Statistics and Computing*, *27*(5), 1413–1432. https://doi.org/10.1007/s11222-016-9696-4

Venetski, S. (1969). "Silver" from clay. *Metallurgist*, *13*(7), 451–453.

Vieira, M. D., Goedkoop, M. J., Storm, P., & Huijbregts, M. A. (2012). Ore grade decrease as life cycle impact indicator for metal scarcity: The case of copper. *Environmental Science & Technology*, *46*(23), 12772–12778.

Von Erdberg, E. (1993). *Ancient Chinese bronzes: Terminology and iconology*. Siebenberg-Verlag.

Weidema, B. P. (2003). *Market information in life cycle assessment* (Vol. 863). Miljøstyrelsen.

Weidema, B. P., & Wesnæs, M. S. (1996). Data quality management for life cycle inventories—An example of using data quality indicators. *Journal of Cleaner Production*, *4*(3), 167–174. https://doi.org/10.1016/S0959-6526(96)00043-1

Werner, T. T., Mudd, G. M., & Jowitt, S. M. (2017). The world's by-product and critical metal resources part III: A global assessment of indium. *Ore Geology Reviews*, *86*, 939–956. https://doi.org/10.1016/j.oregeorev.2017.01.015

Wilburn, D. R. (2012). *Byproduct Metals and Rare-earth Elements Used in the Production of Light-emitting Diodes: Overview of Principal Sources of Supply and Material Requirements for Selected Markets*. Retrieved from U.S. Geological Survey website: https://pubs.usgs.gov/sir/2012/5215/

Wilhelm, W. B. (2012). Encouraging sustainable consumption through product lifetime extension: The case of mobile phones. *International Journal of Business and Social Science*, *3*(3).

World Bank. (2019a). Global Economic Prospects. Retrieved July 24, 2019, from https://datacatalog.worldbank.org/dataset/global-economic-prospects

World Bank. (2019b). National GDP in current US$. Retrieved July 24, 2019, from https://data.worldbank.org/indicator/ny.gdp.mktp.cd

Worrell, E., & Reuter, M. (2014). *Handbook of Recycling: State-of-the-art for Practitioners, Analysts, and Scientists*. Retrieved from https://books.google.com/books?hl=zh-CN&lr=&id=gQfUAgAAQBAJ&oi=fnd&pg=PP1&dq=reuter+handbook+of+recycling&ots=mn0OJT4lvw&sig=2DMn2Ow8jg3i0xxbqSVKoNCFjkc

Xiarchos, I. M., & Fletcher, J. J. (2009). Price and volatility transmission between primary and scrap metal markets. *Resources, Conservation and Recycling*, *53*(12), 664–673.

Yaksic, A., & Tilton, J. E. (2009). Using the cumulative availability curve to assess the threat of mineral depletion: The case of lithium. *Resources Policy*, *34*(4), 185–194. https://doi.org/10.1016/j.resourpol.2009.05.002

Yellishetty, M., Mudd, G. M., Ranjith, P. G., & Tharumarajah, A. (2011). Environmental life-cycle comparisons of steel production and recycling: Sustainability issues, problems and prospects. *Environmental Science & Policy*, *14*(6), 650–663. https://doi.org/10.1016/j.envsci.2011.04.008

Yoshimura, A., Daigo, I., & Matsuno, Y. (2013). Global Substance Flow Analysis of Indium. *Materials Transactions*, *54*(1), 102–109. https://doi.org/10.2320/matertrans.M2012279

Zabalza Bribián, I., Valero Capilla, A., & Aranda Usón, A. (2011). Life cycle assessment of building materials: Comparative analysis of energy and environmental impacts and evaluation of the eco-efficiency improvement potential. *Building and Environment*, *46*(5), 1133–1140. https://doi.org/10.1016/j.buildenv.2010.12.002

Zhang, J., Everson, M. P., Wallington, T. J., Field III, F. R., Roth, R., & Kirchain, R. E. (2016). Assessing Economic Modulation of Future Critical Materials Use: The Case of Automotive-Related Platinum Group Metals. *Environmental Science & Technology*, *50*(14), 7687–7695.

Zink, T., Geyer, R., & Startz, R. (2016). A Market-Based Framework for Quantifying Displaced Production from Recycling or Reuse. *Journal of Industrial Ecology*, *20*(4), 719–729. https://doi.org/10.1111/jiec.12317

Zink, T., Geyer, R., & Startz, R. (2018). Toward Estimating Displaced Primary Production from Recycling: A Case Study of U.S. Aluminum. *Journal of Industrial Ecology*, *22*(2), 314–326. https://doi.org/10.1111/jiec.12557

Appendices

Table A. 1 Composition of raw materials used in the direct melt breakdown model. The high and low limits for each element are shown for each raw material (Hi=high, Lo=low)

Raw material	Cu		Zn		Pb		Sn		Ni		Al		Mn		Fe	
	Hi	Lo	Hi	Lo	Hi	Lo	Hi	Lo	Hi	Lo	Hi	Lo	Hi	Lo	Hi	Lo
Cu	100	100	0	0	0	0	0	0	0	0	0	0	0	0	0	0
Zn	0	0	100	100	0	0	0	0	0	0	0	0	0	0	0	0
Pb	0	0	0	0	100	100	0	0	0	0	0	0	0	0	0	0
Sn	0	0	0	0	0	0	100	100	0	0	0	0	0	0	0	0
Ni	0	0	0	0	0	0	0	0	100	100	0	0	0	0	0	0
Al	0	0	0	0	0	0	0	0	0	0	100	100	0	0	0	0
Mn	0	0	0	0	0	0	0	0	0	0	0	0	100	100	0	0
Fe	0	0	0	0	0	0	0	0	0	0	0	0	0	0	100	100
No.1	99	99	0	0	0	0	0	0	0	0	0	0	0	0	0	0
No.2	98	94	0	0	0	0	0	0	0	0	0	0	0	0	0	0
Yellow brass	68.5	63	37	31.3	0.15	0	0	0	0	0	0	0	0	0	0.07	0
Leaded yellow brass	74	58	40	20	3.8	0.8	2	0.5	1	0	0.55	0	0.25	0	0.7	0
Low brass	81.5	78.5	20	20	0.2	0.05	0	0	0	0	0	0	0	0	0.2	0.05
Red brass	86	84	16	14	0.2	0.06	0	0	0	0	0	0	0	0	0.2	0.05
Leaded red brass	86	84	6	4	6	4	6	4	1	0	0	0	0	0	0.3	0
Manganese bronze	68	35.6	42	22	0.4	0.2	1.5	0.5	4	0	7.5	0.5	5	0.1	4	0
Aluminum bronze	88	71	0	0	0.05	0	0	0	5.5	0	13.5	6	14	0	5	0
Tin bronze	93	71.2	5	0	5	0	20	6	2	0	0	0	0.1	0	1.2	0
Leaded tin bronze	86	68.5	4	0	25	6	11	4.5	1	0	0	0	0	0	0.2	0
Nickel-silver	68.5	53.5	27	17	0.1	0	0	0	19.5	9	0	0	0.5	0	0.25	0
Ocean	70	68	15	10	12	7	5	3	0	0	0	0	0	0	0	0
Cartridge	71.5	68.5	31.5	28.4	0.07	0	0	0	0	0	0	0	0	0	0.05	0
Grape	77	65	33	15	6	2	2	0	0	0	0	0	0	0	0	0